

Processing and Interpretation of Multichannel Seismic Data from Van Mijenfjorden, Svalbard

Eric Willgohs Knudsen



Master of Science Thesis

Department of Earth Science

University of Bergen

June 2015

Abstract

This work was done based on 10 multichannel seismic lines from Van Mijenfjorden, collected during Svalex in 2013 and 2014-.

The objective of the thesis is twofold:

1. In the first part processing is done where emphasis has been in removing multiples and noise from the data.
2. Interpretation of the data is done in the second part. Here identification of seismic structures as well as correlation with the Ishøgda well is done.

A problem in the processing are high velocities in seabed and shallow water depth, which causes strong multiples. Multiple removals were performed by applying deconvolution and f-k filtering. Velocity filtering is performed on the CDP position of both shot and receiver collection. This allows the collections that are shot in opposite direction to be simulated. Collections shot in opposite directions will have different apparent velocity since they are shot either “up-dip” or “down-dip”.

Furthermore, surface consistent deconvolution was used to attenuate remaining multiples after f-k filtering. This process computes a filter for shot, receiver position and offset. In addition different modules are used for improving signal to noise ratio, amplitude recovery, amplitude smoothing and spherical spreading correction etc. The data is interpreted based on data from the Ishøgda well, which was drilled in 1965-66. The well is located 77°50'22''N, 15°58'00''E and reaches down to Lower Permian.

The reflectors under Van Mijenfjorden depict a wide, asymmetric syncline, -(the central Spitsbergen Basin) which has deposits of Tertiary age. Upper Cretaceous rocks are missing on Svalbard; which makes base Tertiary an unconformity.

The underlying formation within the Lower Cretaceous has thickness estimates near the thickness of the same formations adjacent to the fjord.

Within the Janusfjellet subgroup there exists large thickness variations, which is caused by folding and is related to the Tertiary compressional tectonics. There exists small anticline structures in the syncline, which is likely caused by mobilization of the shales from the Agardfjellet formation (Upper Jurassic).

A reflector in middle Triassic at ca 1400 ms stands out as the strongest amplitude in the seismic. This reflector is interpreted to be a dolerite. It is also very likely that there exists a

dolerite in the Kapp Toscana formation. The depth of the Permian /Triassic boundary is found to be at approximately 3.8 km depth and corresponds to an impedance contrast between the highly silicified carbonates of the Kapp Starostin Formation and overlying shales in the Sassendalen formation. An unconformity is interpreted at 2200 ms twt and is thought to represent an unconformity at base Gipsdalen. Furthermore, the top of the Hecla Hoek is interpreted to be located at 2800 ms twt because it represents the strongest reflector under 1400 ms twt. Below this depth, reflectors have much higher dips and do not follow the geometries of above lying reflectors. The area in the western part of the seismic is part of the West Spitsbergen Fold and Thrust belt. This is an area hard to migrate because the area constitutes complex structures. However a rough interpretation of the area is done and asymmetrical folds is interpreted in the area.

Further north in Van Mijenfjorden more symmetrical folds are found, a reason for this could be that the stress induced into this area was lower. These structures most likely formed in response to the opening in the North Atlantic Ocean. No normal faults are interpreted in the area. Such faults could exist due to the spreading of Oligocene seafloor between Greenland and Svalbard causing oblique extension.

Acknowledgement

I would like to express appreciation to Professor Rolf Mjelde (at Institute for Geoscience, University of Bergen), for his guidance and support throughout the development of this thesis. The help provided by Bent Ole Ruud (at Institute for Geoscience, University of Bergen) has been very valuable. His insight, knowledge and especially his patience and tolerance with regard to all my questions is greatly valued. I would also like to acknowledge Rolf Mjelde and Bent Ole Ruud for the time used to go through the thesis and pointing out errors and parts to improve. I am also thankful to Statoil for giving permission to having access to well information from the Ishøgda well. Furthermore would I like to thank my family and fellow students for their care and motivation.

Bergen, 31'st May 2015

Eric Willgohs Knudsen

Table of Contents

Abstract.....	
Acknowledgement.....	III
Chapter 1- Introduction.....	1
Chapter 2- Geological background of Svalbard.....	3
2.1 Introduction	4
2.2 Svalbard Continental Margin	4
2.2.1 Margin Main Fault Systems	5
2.2.2 Geology of the Continental Margin.....	6
2.3 Svalbard Tectonic History	6
2.3.1 Precambrian and Lower Devonian.....	6
2.3.2 Devonian	7
2.3.3 Late Paleozoic	7
2.3.4 Mesozoic	8
2.3.5 North Atlantic Evolution	8
2.3.6 Cenozoic	10
2.4 Central Spitsbergen Basin.....	11
2.5 West Spitsbergen Fold and Thrust Belt	12
2.6 Stratigraphic setting	14
2.6.1 Pre- Caledonian Sequence	15
2.6.2 Post-Caledonian	15
Chapter3-Processing/Seismic interpretation theory.	21
3.1.1 Seismic Source.....	21
3.1.2 Seismic Receivers	22
3.2.1 Reformatting and editing.....	23
3.2.2 Designature	23
3.2.3 Gain Recovery.....	23
3.2.4 Filtering of seismic data.....	23
3.2.5 Velocity filtering.....	24

3.2.6 Inverse filtering (De-convolution)	24
3.2.7 Velocity analysis	25
3.2.8 NMO correction.....	26
3.2.9 Muting.....	27
3.2.10 Stacking.....	27
3.2.11 Migration	27
3.2.12 Seismic velocities.....	29
3.3 Principles for seismic interpretation.....	30
3.3.1 Seismic facies	30
3.3.2 Seismic interpretation of structures.....	32
3.3.3 Compressional Deformations structures	32
3.3.4 Seismic Resolution in the data acquired in Van Mijenfjorden.....	33
Chapter 4-Data Acquisition Parameters	34
Chapter 5-Processing	36
5.1 Geoclusteran and Geopad (CGGVeritas)	36
5.1.1 XJOB.....	37
5.1.2ChronoVista.....	38
5.1.3 XPS	38
5.1.4 Modules used in the processing	39
5.2 Reformatting.....	43
5.2.1 BANDPASS FILTER	45
5.2.2 Removing Noise Burst	46
5.3 Filter 1.....	47
5.3.1 Removing incoherent noise	47
5.3.2 Signature Deconvolution.....	48
5.3.3 Spherical Spreading Correction.....	49
5.3.4 Spatial Amplitude Smoothing.....	50
5.3.5 Velocity Filtering (F-K) Filtering.	51
5.4 Filter 2.....	53
5.4.1 RESULTS OF FK FILTERING IN FILTER 2 JOB	54

5.4.2 Amplitude Recovery	55
5.5 Velocity Analysis	56
5.6 Migration	58
5.6.1 Kirchhoff Time Migration	60
5.6.2 Processing the problematic area in the west	61
5.6.3 Time Variant Bandpass filter	63
5.6.4 Adjusted velocities	63
5.7 Poststack Processing	64
Chapter 6-Seismic interpretation	69
6.1 Introduction	69
6.1.1 Data Quality	72
6.1.2 Correlation map	73
6.1.3 Interpretation tool	74
6.1.4 Time Depth Conversion	74
6.2 Interpretation of Seismic Lines	75
6.2.1 Seabed	76
6.2.2 Tertiary unit	76
6.2.3 Carolinefjellet and Helvetiafjellet formation	79
6.2.4 Base Rurikfjellet-Base Cretaceous	81
6.2.5 Base Agdarfjellet Formation-Base Upper Jurassic	83
6.2.6 Upper Triassic	85
6.2.7 Middle Triassic	87
6.2.8 Top Permian	88
6.2.9 Lower Permian	89
6.2.10 Upper Carboniferous	90
6.3 Complex area part of the Westspitsbergen Fold and Thrust Belt.....	91
6.4 Hecla Hoek	94
Chapter 7-Discussion	96
7.2 Tertiary unit.....	97

7.3 Cretaceous unit.....	101
7.4 Triassic unit.....	107
7.5 Permian unit.....	111
7.6 Carboniferous unit.....	114
7.7 Hecla Hoek	115
7.8 West Spitsbergen Fold and Thrust belt.....	116
Chapter 8-Conclusion	121
REFERENCES.....	124
APPENDIX.....	A1

1-Introduction

The Svalbard Archipelago is located 700 km north of Norway, between 76° and 80° N and is bordered by the Arctic Ocean to the north, the Barents Sea to the south and east, and the Greenland Sea to the west. Van Mijenfjorden is the second largest fjord in western Svalbard, 50 km long and ca.10 km wide and constitutes the study area. The geology in the study area is dominated by a large syncline, the Spitsbergen central basin, and more complex structures in the Spitsbergen fold and thrust belt in the western part (Fig.1.1).

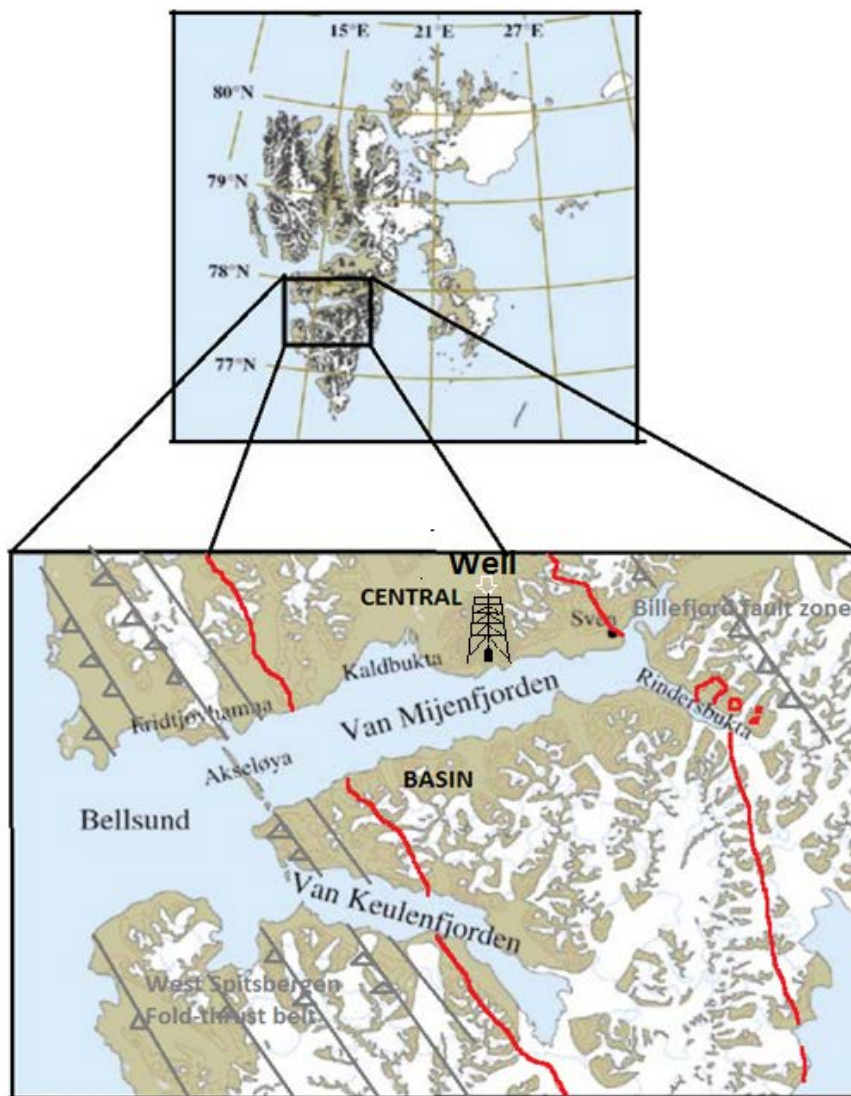


Fig 1.1: The figure shows Van Mijenfjorden and the location of the Central Basin and West Spitsbergen Fold-thrust belt. The source of the figure is from Lydersen et al, (2012). The structures in the figure are drawn in red are based on information from Blinova et al, (2009).

The thesis is based on seismic data acquired during Svalex 2013 and 2014(Mjelde,2013;2014). The lines cover an area of 28.9*5.5 km(Fig.1.2).

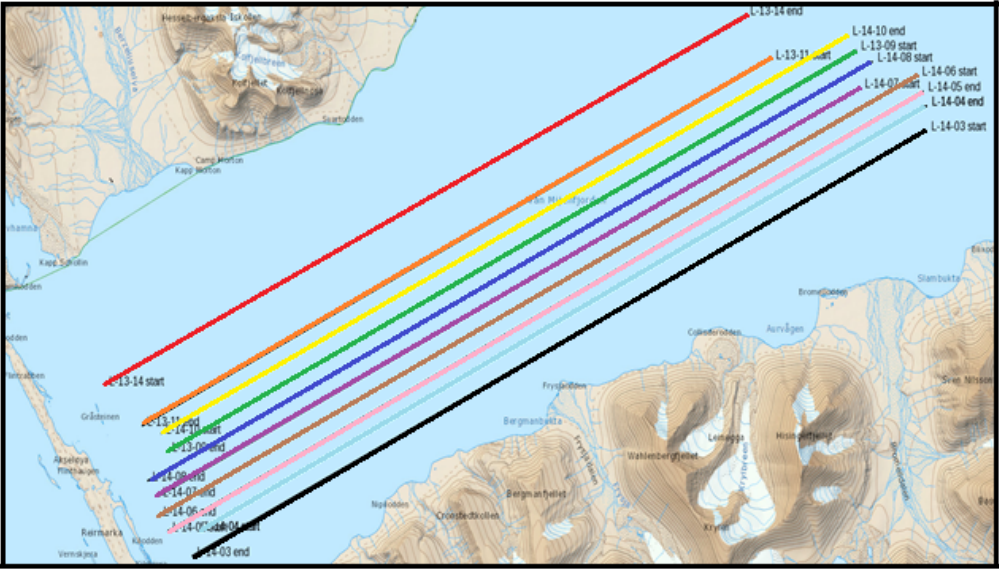
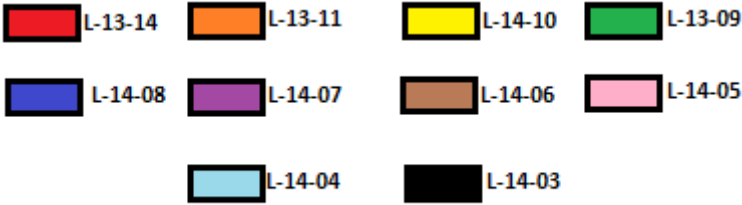


Fig 1.2: The figure shows the seismic lines acquired during Svalex in 2013 and 2014. The figure is from www.toposvalbard.npolar.no and later modified by colors.



The main objective of this thesis is to process the seismic data from Van Mijenfjorden in order to obtain the best possible imaging of the geological structures, by checking the effect of various seismic processing modules.

The purpose of processing is to manipulate the acquired data into an image that can be used to infer the sub-surface structures. Increasing signal/noise ratio, replacing dipping events to their true subsurface locations (migration), increasing the resolution and attenuating unwanted signals are some of the most common processing goals. The main challenge with data is attenuation of strong multiples caused by the area’s hard seafloor.

After processing the data are fit for seismic interpretation. The seismic lines are interpreted based on a well located at 77°50’22’’N, 15°58’00’’E, see fig 1.1. Furthermore, the interpreted seismic data are correlated with previous seismic studies in Van Mijenfjorden. The thickness of the formations in the sub-surface are also correlated with known thicknesses of formations

on land close to Van Mijenfjorden. This thesis represents the first interpretation of seismic data in Van Mijenfjorden directly correlated with the Ishøgda well since 1985. Since that time processing techniques have had significant progress. The thesis also gives an alternative interpretation of the westernmost part of the fjord compared to other studies in the area. However this area is noisy due to very complex geology making it hard to migrate traces to its correct place.

2. GEOLOGICAL BACKGROUND OF SVALBARD

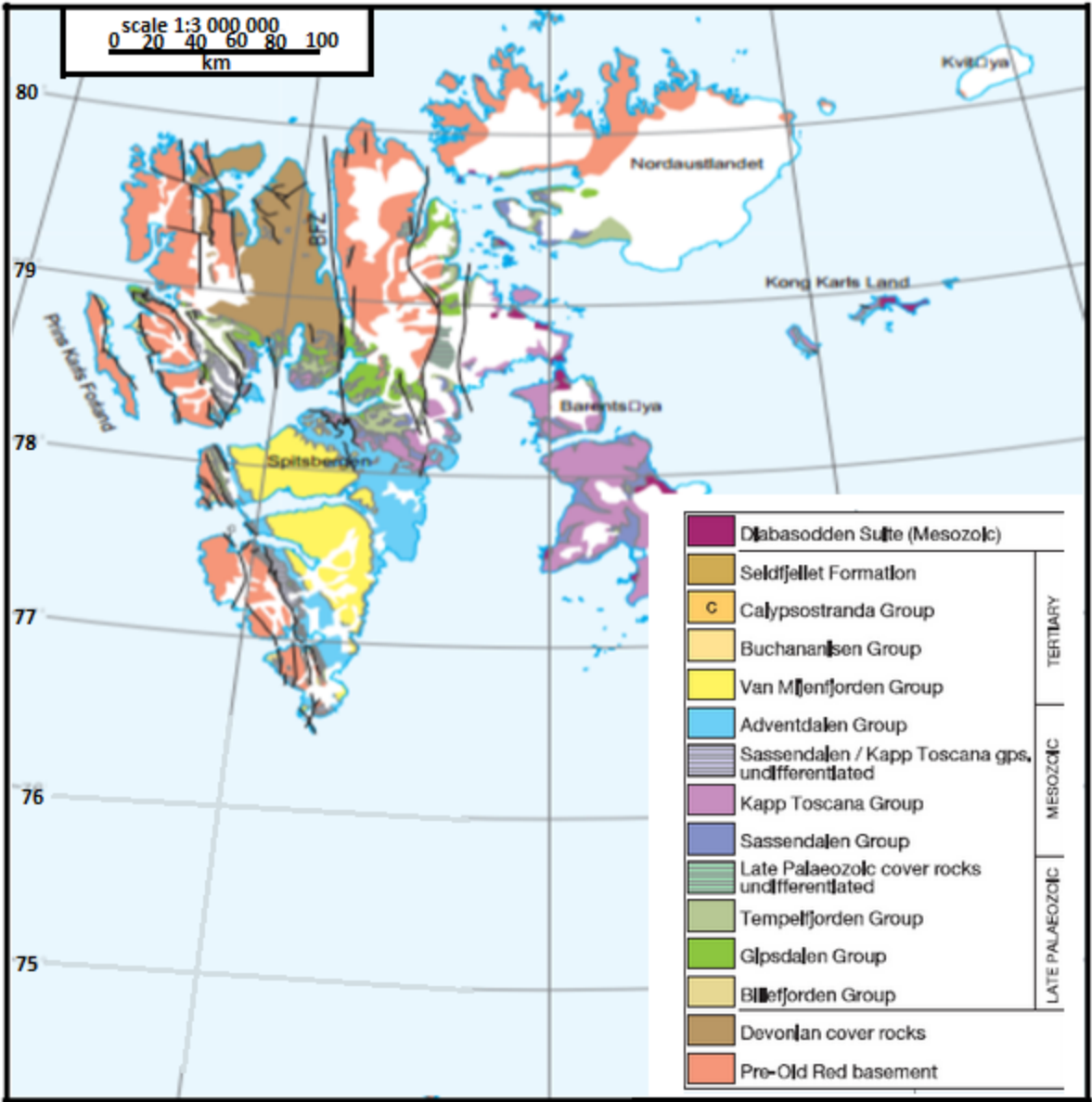


Fig 2.1: Simplified geological map of Svalbard (Dallmann 1999)

2.1 Introduction

Svalbard is situated at the uplifted north western corner of the Barents shelf. Svalbard has been beneath sea level throughout the greater part of its geological history and is called a paradise for geologist. Almost unbroken deposition of sand, gravel, clay, carbonate, etc. has taken place here. This material has subsequently been transformed into stratified rocks. Svalbard has rocks from every part of the history of the planet which can be seen from the almost complete stratigraphical column. Often well-preserved fossils of animals and plants from the past can be seen.

2.2 Svalbard Continental Margin

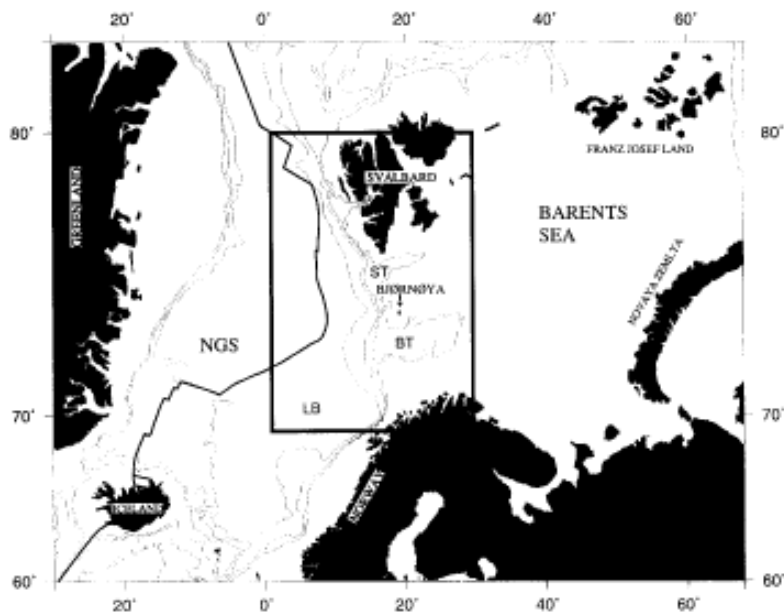


Figure 2.2: .Location of western Barents Sea-Svalbard continental margin. BT= Bjørnøya Through, LB=Lofoten Basin, NGS=Norwegian-Greenland Sea, ST=Storfjorden Trough (Faleide, Solheim et al. 1996)

The western Barents Sea and Svalbard continental margin extends about 1000 km in a north-south direction (Fig 2.2).The continent-ocean boundary is restricted to a narrow faulted zone beneath the continental shelf south of Spitsbergen and a limited region of unknown crust further north (Myhre and Eldholm 1988)-. Investigations have suggested that areas further north was fed by sediments from the Barents Sea region (Faleide, Solheim et al. 1996).

The western Svalbard continental margin began to develop at the Paleocene-Eocene transition. At that time major plate reorganization took place in the North Atlantic and Arctic.

Greenland commenced with relatively northward movements as a separate plate (Talwani and Eldhom 1977).

The outer part of the continental shelf consists of thick sequences of low velocity sediments, which is assumed to be deposited after a change in plate motion from shear to oblique rifting in the lower Oligocene (Eiken and Austegard 1994). The margin consists of three main structural segments:

- (1) a southern sheared margin along the Senja Fracture Zone
 - (2) a central rift complex associated with volcanism
 - (3) a northern initially sheared and later rifted margin along the Hornsund Fault Zone
- (Faleide, Solheim et al. 1996)

2.2.1 Margin Main Fault Systems

The two main structural features in this region are Forlandsundet Graben and the Hornsund Fault Zone.

“The Hornsund Fault Zone is defined as a zone of downfaulted blocks that extend along the central and outer continental shelf in a NNW-SSE direction. These blocks are covered by the Tertiary sedimentary wedge. The eastern boundary is interpreted as the start of the westward-dipping down-faulted blocks of basement. The location of this fault is located just landward of the continent-ocean boundary, forming a transitional area separating the young oceanic crust from the old platform on the inner shelf” quote (Myhre and Eldholm 1988). The Hornsund fault zone probably represents deep-rooted zones of weakness since early Carboniferous times (Bergh and Grogan 2003).

The Forlandsundet Graben extends in a NNW-SSE direction along the Spitsbergen continental shelf bordered by Prins Karls Forland to the west and the coastline of Spitsbergen to the East. The faults of the Graben are NNE-SSE striking and steeply dipping (Blinova, Thorsen et al. 2009). It contains a sedimentary sequence with a total stratigraphic thickness of 5 km. The basin covers less than 100 square km, most of it is below the shallow water of the Forlandssundet area (Worsley, Aga et al. 1986). This basin is presumed to be transtensional (Bergh and Grogan 2003).

2.2.2 Geology of the Continental Margin

The southwestern Barents Sea is composed of a series of regional basins and structural highs. The sediments range mainly from Late Paleozoic to Cretaceous in age having maximum thickness of at least 10-12 km. Rapid erosion has increased sedimentary load along the Svalbard western margin and turned the epicontinental basin of central Spitsbergen into a rapidly subsiding foreland basin (Czuba, Ritzmann et al. 2004).

Seismic surveys in the western Barents Sea and Svalbard margin reveals the existence of chaotic seismic sequences with discontinuous internal reflections and frequent diffraction hyperbolae. This is interpreted as a result of rapid build-up of unstable sediment masses from grounded. Glacial sediments can be transported by different mechanism including meltwater, glacial transport or within a subglacial layer of deformation. Subglacial deformation has the highest transport capacity and is considered the most important mechanism here (Faleide, Solheim et al. 1996).

2.3 Svalbard Tectonic History

In this subsection a brief review of the Svalbard's geological history from Precambrian to Devonian is presented.

2.3.1 Precambrian and Lower Devonian

Hecla Hoek represents the oldest rock successions on Svalbard and is interpreted to represent a local branch of the Caledonian fold belt. This branch has a E-W width of 400 km and extends 700 km N-S from northern Spitsbergen to Bjørnøya (Worsley, Aga et al. 1986). Hecla Hoek is considered to be the product of the Caledonian orogeny, however distinct unconformities have been reported from southern Spitsbergen and Nordaustlandet (Dallmann 1999). There exists some disagreement about the origin of the Lower Hecla Hoek. Some authors interpret it to be volcano sedimentary rocks of Late Proterozoic age. Others have interpreted it to be of basement origin of Early Proterozoic or earlier age (Gee, Björklund et al. 1994). The same authors concluded in their studies that the Lower Hecla Hoek is a stack of thrust sheets, intercalating basement and cover. The Caledonian orogeny was a result of collision between two continental plates, the Canadian-Greenland Plate (Laurentia) and the

Fennoscandian Plate, (Hjelle 1993). Caledonian rocks on Svalbard occur in at least three terrains separated by Old Red Sandstone and younger basins. Eastern areas have much in common with East Greenland, while some of the western areas seem to have similarities with North Greenland and Ellesmere Island (Gee, Björklund et al. 1994). Since late 1980s, U-Pb zircon isotopic age determination has revealed several Precambrian events.

Some of these events are: Baikalian movements (600-650 Ma), the Grenvillian tectonothermal event (950-1000 Ma), and indications of earlier events are recognized in several areas (ca.1400 Ma, 1700-1800 Ma, and two or three older ones), (Ohta 1994). These mountain chains have long since been eroded away and the rocks we now see are from their deeper, inner parts (Hjelle1993).

2.3.2 Devonian

The main Caledonian Orogeny ended at the transition from Silurian to Devonian (Hjelle 1993). During the Late Devonian Svalbardian phase, the sediments were faulted and partly folded in a tectonic regime characterized by lateral shear movements. Lower to Middle Devonian sediments were down faulted into N-S trending grabens where they are preserved. These sequences of coarse -grained Devonian sandstones rest on the metamorphic Hecla Hoek (Faleide and Gudlaugsson 1985). This graben unit separates Nordaustlandet plus Ny Friesland and northwestern Spitsbergen. These two structures and western Spitsbergen make up the pre-Devonian basement of Svalbard (Hjelle 1993). The basement formed is a down-faulted crustal block, bounded by the northwestern and eastern basement provinces (Dallmann 1999). The Devonian is called the age of fishes. Fossils of primitive fish and primitive plants have been found on Svalbard. The first terrestrial plants evolved at this time (Hjelle 1993).

2.3.3 Late Paleozoic

The Early Carboniferous was characterized by rapid subsidence. A mid Carboniferous tectonic episode renewed faulting activity and contributed to maintaining the Horst and Graben setting and sedimentation (Faleide and Gudlaugsson 1985).

During the Carboniferous Period, Svalbard developed from a site of fault block tectonism with differential sedimentation to a stable shelf that experienced overall subsidence (except

for southern Spitsbergen (Dallmann1999). Salt water periodically flooded the land in this period. This salt reacted with calcareous beds and when the sea retreated again and evaporation set in, gypsum, anhydrite and dolomite were formed. Svalbard rapidly drifted from a damp, sub -tropical area to a dry temperate area, subsequently the climate changed from wet to desert-like. (Hjelle1993).

2.3.4 Mesozoic

The portion of the crust that is now the Svalbard region drifted from about 45°N to 60°N, (Hjelle 1993).The Mesozoic stratigraphic record consists of repeated clastic sedimentary successions mainly delta and shallow shelf sediments (Dallmann1999). The Mesozoic sediments were deposited in an increasingly stable platform environment. Gradual tectonic uplift in the northern areas during Cretaceous times resulted in strong erosion all over Svalbard (Faleide and Gudlaugsson 1985). Many of the fossils which could have shown today are therefore gone, but there are lots of fossils from Mesozoic sediments left in Svalbard. Common fossils in the Triassic deposits are bivalves and ammonites.

. The sedimentary rocks in Jurassic contains fossil like ammonites, belemnites and bivalves. Volcanic activity and faulting interrupted the stable conditions in Svalbard during the end of Jurassic and the beginning of Cretaceous. Magma intruded and crystallized as a dark igneous rock called dolerite (Hjelle1993). Intrusions occur predominantly as sills, up to 100 m thick and laterally continuous for up to 30 km. Dykes range in thickness from <10 m up to 100 m. Published geochemical data reveals that the vast majority of samples have a basaltic geochemical signature (Senger, Tveranger et al. 2014).

2.3.5 North Atlantic Evolution

The north Atlantic evolution can be divided into three stages,

- the Paleocene,
- Eocene
- Oligocene.

Below is a brief summarizing of what happened in the different stages.

The initiation of sea-floor spreading on the western side of Greenland took place in early Paleocene along the Reykjanes, Aegir, and Mohns Ridge. The opening was generally steady without ridge axis jumps along the Mohns and Reykjanes Ridges (Talwani and Eldholm 1977).

Before this time Greenland belonged to the Eurasian plate and a land bridge existed between North Greenland and Svalbard. “Between Early Eocene (Chron 24b, 53.7 Ma) and earliest Oligocene (Chron 13, ~35 Ma), seafloor spreading in the Norwegian Sea along the Reykjanes-Aegir-Mohns spreading axes was connected to the Gakkel spreading axis in the Arctic-Eurasia Basin through a right lateral continental transform consisting of the Senja Fracture Zone, Hornsund Fault Zone, and Greenland Fracture Zone” quote (Lundin and Doré 2002).

This phase was characterized by major plate reorganization, and started with seafloor spreading in the Norwegian-Greenland Sea in Eocene. Greenland became separate plate and started to move northward obliquely to western Spitsbergen along a huge shear zone. The movement between the Greenland and Eurasian plates caused transpressional deformation along western Spitsbergen and subsequently formed the Western Spitsbergen Fold and Thrust Belt (Blinova 2011). Spreading in the Labrador Sea finished in early Oligocene (Chron 13, 35 Ma). Greenland then became part of the North American plate and a counter-clockwise rotation of the opening direction took place in the Norwegian Sea, changing from NNW-SSE to NW-SE (Lundin and Doré 2002). At this time Greenland moved to WNW relative to Eurasia, and seafloor spreading started between Greenland and Svalbard (Blinova). The West Spitsbergen Fold belt thus became inactive (Blinova, Thorsen et al. 2009).

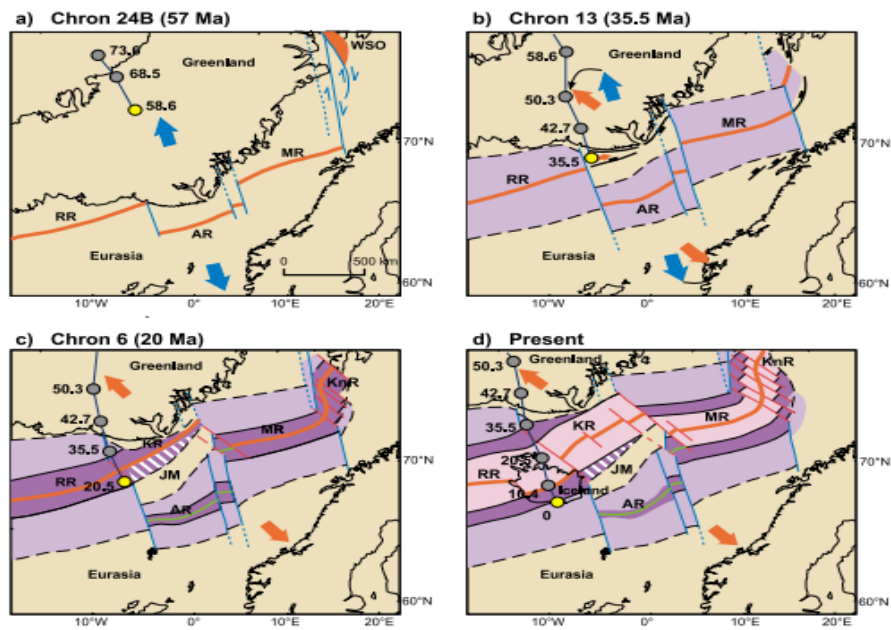


Fig 2.3: Plate tectonic evolution of the Norwegian-Greenland Sea. Grey and yellow dots mark the position of the Iceland Plume center. Major plate reorganization and change in direction of relative plate separation (from blue to red arrows), (Lundin and Doré 2002).

2.3.6 Cenozoic

Svalbard has probably been covered by a massive ice sheet at least once during the Quaternary (Hjelle1993). Overview of the Quaternary is found in the deep sea sediments where over 30 glacial episodes have been recognized through the last 1.6 million years. Today Svalbard is still in an "ice age" with glaciers coverage of about 60 %. Approximately 2100 glaciers range from small glaciers, less than 1 km^2 to the largest ice-cap in Europe, Austfonna on Nordaustlandet , 8100 km^2 (Worsley, Aga et al. 1986). Volcanic activity of both Tertiary and Quaternary age occurred in NW Spitsbergen , overlying Devonian and Pre Cambrian rocks. The Tertiary volcanites are plateau basalts of mainly Miocene to Pliocene age, while the Quaternary volcanites are mainly alkali basalts (Dallmann 1999).

2.4 Central Spitsbergen Basin

This basin was formed in the Early Paleocene during a right-lateral strike-slip phase, after the plate boundary between Greenland and Svalbard had jumped eastward to the Hornsund Fault Zone (Müller and Spielhagen 1990). The Tertiary Central Basin of Spitsbergen is 200 km long and 60 km wide and contains 2,3 km of clastic deposits, referred to as the Van Mijenfjorden Group, see fig 2.4.

The lower part of the succession (Firkanten, Basilika and Grumantbyen formations) is of early to mid-Paleocene age.

The upper part of the succession is more than 1,5 km thick and consist of the Hollenderdalen Gilsonryggen Battfjellet and Aspelintoppen Formations(Steel 1985). The basin forms an elongated syncline with it thickest parts near the western margin where it is bounded by, and partly incorporated in the early Tertiary fold belt (Worsely 1986).

The early to mid-Paleocene Central basin is extensional. Furthermore the beginning of seafloor spreading between Greenland and Eurasia and a major counterclockwise change in spreading direction between Greenland and North America after induced compression-dominated transpression between Greenland and Svalbard until Lower Eocene (Müller and Spielhagen 1990). There was a significant change in the tectonic setting of the central basin during the late Paleocene. From this time the central basin was analogous to a foreland basin depressed by flexural loading of the thrust sheets (Steel 1985).

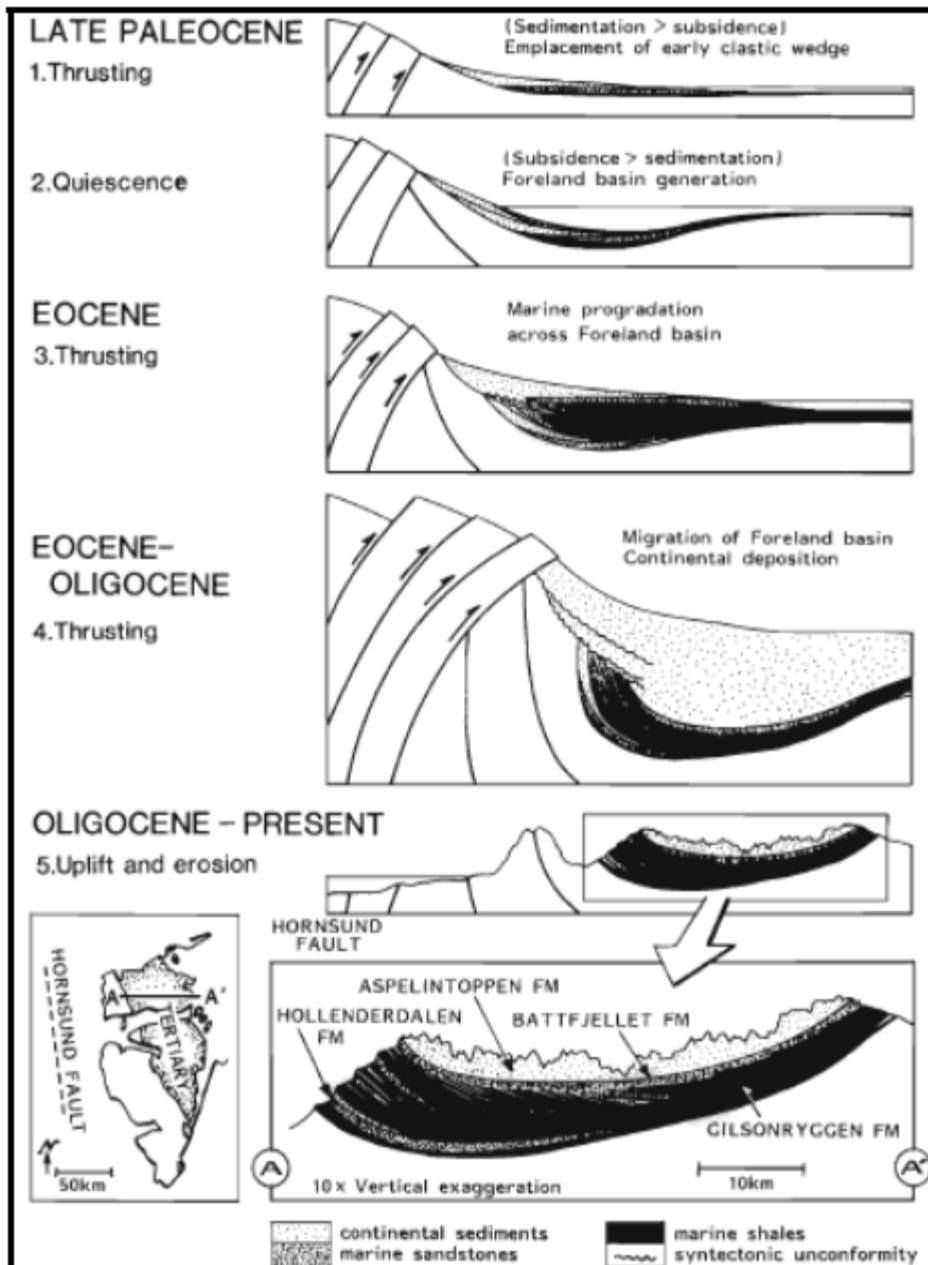


Fig 2.4: Series of diagram showing the suggested relationship of the late Paleocene -Oligocene development of the Central Basin and tectonic movements in the fold and thrust belt of western Spitsbergen (Steel 1985).

2.5 West Spitsbergen Fold and Thrust Belt

The west Spitsbergen fold and thrust belt formed along the transform plate boundary between Greenland and the western Barents Sea during Paleocene Eocene breakup (Leever, Gabrielsen et al. 2011). The fold and thrust belt of western Spitsbergen is 300 km long and less than 50 km wide (Steel 1985). This belt extends from Sørkapp in the south to Kongsfjorden in the north (Saalman and Thiedig 2000). It is situated on the western part of the island of

Spitsbergen and its adjacent to the narrow continental shelf on the NW corner of the Barents Sea, (Leever, Gabrielsen et al.2011). It is characterized by wrench faults, thrust faults and asymmetric folds.

Most of the faults of Western Spitsbergen are of Tertiary age or were reactivated in Tertiary time. The deformation along the fold belt has been a subject of study for a long time. And it is now suggested that it is related to the opening of the Norwegian Greenland Sea. The deformation is interpreted in terms of compression generated by the northward movement of Greenland against Spitsbergen (Steel 1985). From west to east, the WSFTB can be subdivided in to four distinct zones, see fig 2.5:

- (1) The western hinterland zone (zone 1) was affected by Oligocene extensional deformation.
- (2) On land toward the east, a basement involved fold thrust complex (zone 2) is recognized.
- (3) The central zone (zone 3) is a thin skinned fold and thrust unit.
- (4) In the eastern foreland province (zone 4), thick skinned structural inversion of the Billefjorden and Lomfjorden fault zones bounding Carboniferous / Devonian grabens caused folding of the strata above the overlying decollement, (Leever, Gabrielsen et al. 2011)

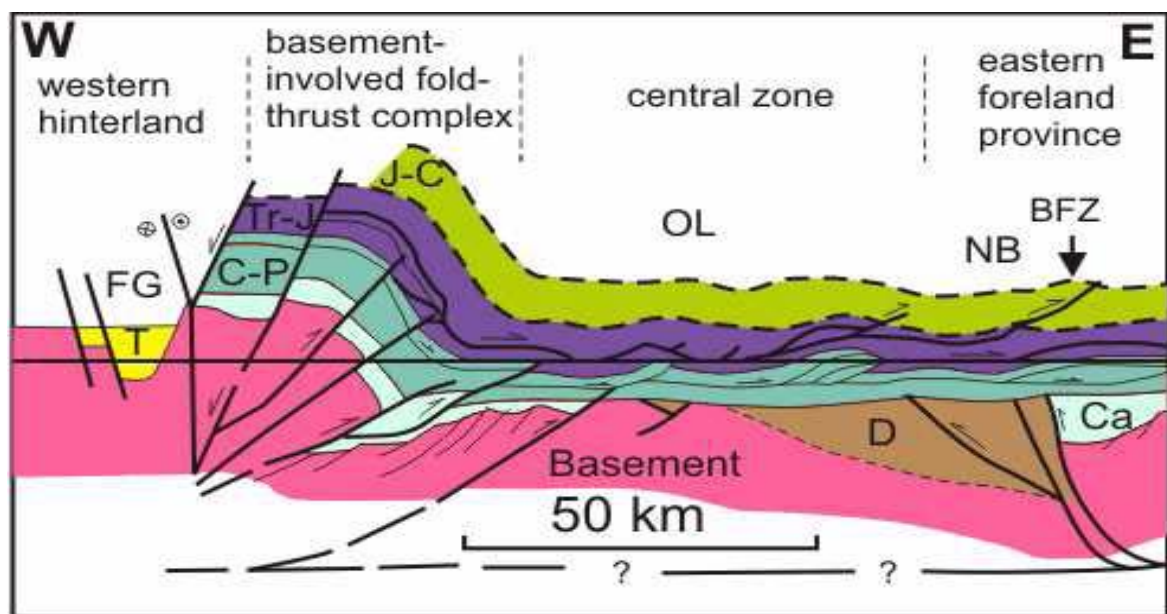


Fig 2.5: The generalized cross section of the WSFTB in Isfjorden. J-C Jurassic and Cretaceous, Tr-J- Triassic and lowermost Jurassic, C-P Carboniferous and Permian, Ca-Lower-Middle Carboniferous), D- Devonian (Blinova, Faleide et al. 2012).

2.6 Stratigraphic setting

The Svalbard area displays a nearly complete stratigraphical succession ranging from the late Precambrian through to the Palaeogene. The history can be divided into different phases.

Figure 2.6 explain the main characteristics of the stratigraphic setting. Climatic changes seem to be linked to a general northwards movement of the entire area-from equatorial regimes around Devonian/Carboniferous boundary to high northern temperate latitudes by the Paleogene. The entire sequence is clastic-dominated , and the only significant carbonates were deposited in late Carboniferous and early Permian times when Svalbard may have lain in the northern arid climatic belt (Worsley, Aga et al. 1986).

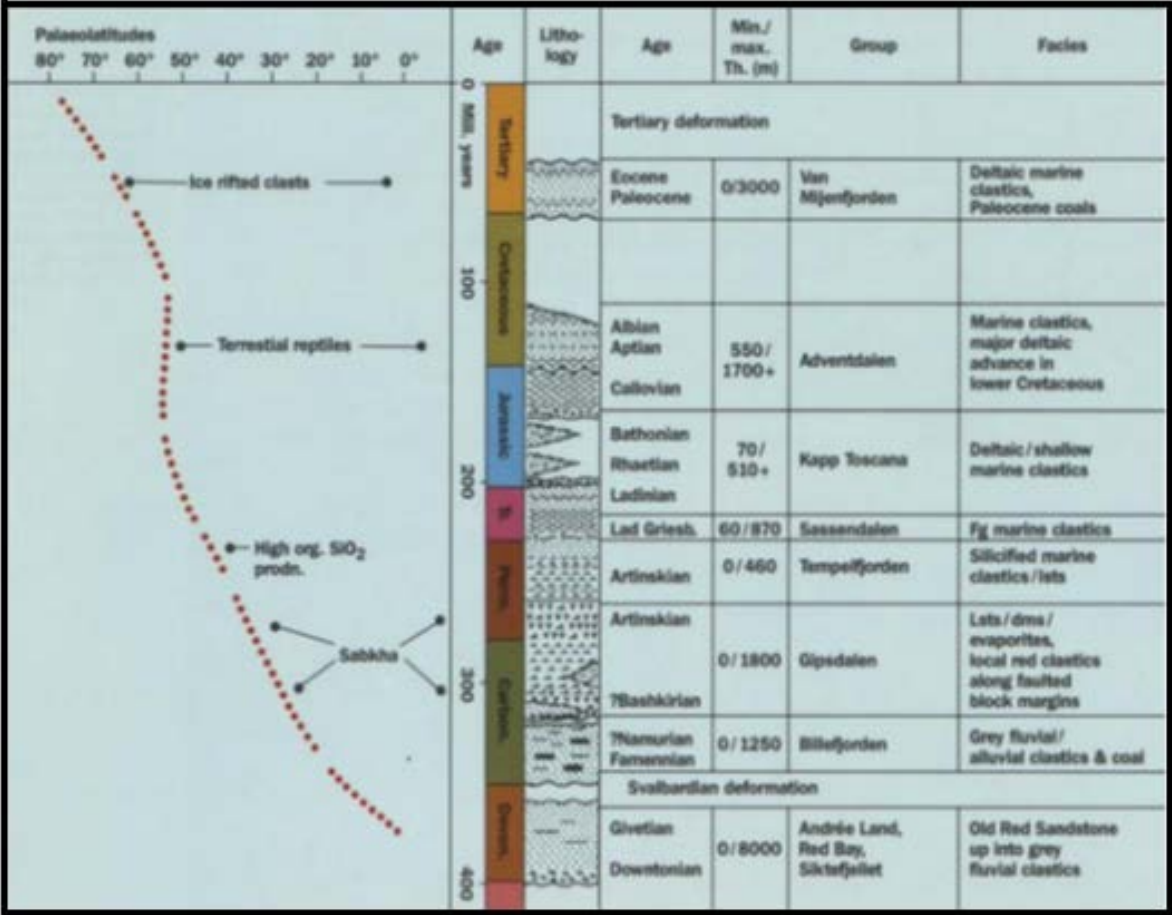


Fig.2.6:Shows the Correlation between the Paleo latitude of Svalbard through time and lithology (Worsley, Aga et al. 1986).

2.6.1 Pre- Caledonian Sequence

Hecla Hoek-Pre Caledonian Group:

The term Hecla Hoek is generally used for sediments, meta sediments and related igneous rocks of late Riphean to Silurian age. These were tectonised and metamorphosed during the major Caledonian, and possibly older-orogenic phases (Worsley, Aga et al. 1986).

2.6.2 Post-Caledonian

Billefjord group

This group consist of conglomerates, sandstones and coals. It represent palaeoenvironments dominated by large alluvial fans (Johnsen, Mørk et al. 2001) .

Gypsdalen group

Gypsdalen includes marine carbonates and evaporates (Johnsen, Mørk et al. 2001).This group have two subgroups called Gipshuken formation and Nordenskiöldbreen formation.

Gipshuken Formation

Gipshuken formation comprises interbedded evaporates and dolomites. Sulphatic beds dominate the lower part of the unit, passing up into a dolomite dominated section. The sediments was deposited in arid lagoonal to tidal environments (Lauritzen 1981).

Nordenskiöldbreen Formation

This formation is dominated by bio clastic limestone (Shen, Tazawa et al. 2005).

The Tempelfjorden group overly the Gypsdalen group and contains mainly carbonate and siltstone which is silica cemented. One of the main characteristic of this group is the high organic production. Sequences of extensive silica cemented reservoirs often show extremely low porosity and permeability and display a high seismic velocity. This late Permian cap may obscure seismic identification of older structures (Worsley, Aga et al. 1986).

Sassendalen (Early-Middle Triassic) and Kapp-Toscana group (Late Triassic-Middle Jurassic)

In western Spitsbergen the Sassendalen group comprises deltaic to shallow shelf deposits. The upper part is highly organic and phosphatic and consists of sandstones, siltstones and shales representing shallow shelf deposition. (Johnsen, Mørk et al. 2001).

Sassendalen contain the following subgroups:

Botneheia Formation

This succession contains bituminous marine shales. In eastern Svalbard this formation contain up to 12 wt.% organic carbon and occurs at the oil window maturity level (Krajewski 2008). At Svalbard the best source rock lie within the Triassic Botneheia Formation (Abay, Karlsen et al.).

Tvillingodden Formation

The outcrop of this formation found on land is from the Lower Triassic black shale and contain dead algae organism. The total organic contain (TOC) is 6-8 %. The rock is a source rock for oil and contain kerogen type tree, because its origin is marine carbon (Rasmussen 2006).

Vardebukta Formation

In this formation sediments are softer, and coarsening upwards from mud/silt to sand occurs. It is reported sills within this formation in Svalbard. Sills is intrusive igneous rock horizontal with the beds. These Basaltic intrusive comes from volcanic activities at the end of Jurassic, a major rift phase prior to the opening of the Atlantic Ocean started to open (Rasmussen 2006).

Kapp Toscana Group

The lower part of this formation consists of grey shales, upwards grading into sandstones. The uppermost part forms a condensed clastic sedimentary succession containing thin phosphatic nodule layers. This group was on Svalbard deposited in a generally nearshore, deltaic environment (Johnsen, Mørk et al. 2001).

Kapp Toscana contain the following subgroups :

Willhelmøya Formation

This group contains mature sandstone, shale, mudstone and conglomerate. Typical characteristics are phosphate nodular beds(Mørk, Elvebakk et al. 1999).

De Geerdalen Formation

The formation consists of repeated coarsening-upwards successions, fine sandstone and shale constitutes the main lithology(Hynne 2010).



Figure 2.7: Outcrop of the Botneheia, De Geerdalen Fm from Edgeøya. (Hynne 2010).

Adventdalen group (Middle Jurassic-Early Cretaceous)

This Group is widely exposed along the margins of the Central Basin, as well as in eastern Spitsbergen. It is dominated by dark, marine mudstones, but also include deltaic and shelf sandstones and thin condensed carbonate beds(Johnsen, Mørk et al. 2001).

This group contains the following subgroups:

Carolinefjellet formation

This formation consists of marine sandstones, silts and shales. Suggested deposition is on a shallow marine shelf due to; thin upward coarsening beds, storm related deposits and oscillation ripple marks (Dallmann 1999).

Helvetiafjell formation

This formation consists of fluvial generated sandstone unit in the lower part and shallow marine sediments in the upper part. It indicates an overall transgressive trend, and consist mainly of sandstone, shale, stiltstone and thin coal seams (Gjelberg and Steel 1995). A graditional boundary is found between the terrestrial Helvetiafjellet and the overlying

marine Carolinefjellet Formation(Maher Jr 2001).

Janusfjellet subgroup of the Adventdalen group

Organic rich shales and silts comprise the Janusfjellet subgroup of the Jurassic to Cretaceous Adventdalen group and is further subdivided in Agardhfjellet Formation and Rurikfjellet Formation (Maher Jr 2001). These two units are divided by a thin interval (usually <2 m) of yellowish weathering clays. “The lower part of the Agardhfjellet Formation is dominated by siltstone and sandstone beds grading upwards into dominating black and grey shales. This formation represents deposition in oxygen-deficient shelf environments characterized by sedimentation of fine -grained material such as clay and organic matter. The dominant lithology’s of the Rurikfjellet Formation are shales, siltstones and sandstones composing several coarsening-upward sequences deposited in marine shelf to prodeltaic environments “ quote (Dypvik, Eikeland et al. 1991).

Tertiary succession

The Tertiary succession comprises the Van Mijenfjorden group. In Van Mijenfjorden rocks of Tertiary age are deposited in Central Spitsbergen Basin.

Van Mijenfjorden group:

The formation consists of continental sandstones, siltstones and shales with plant beds and coal seams. Marine beds with molluscs, conglomerates and slumped beds are less frequent (Croxtton and Pickton 1976). This group can be divided into the following subgroups.

Gilsonryggen formation

This formation comprises soft shales and siltstones. It also contains some clay-ironstone, commonly with well-rounded chert pebbles. Two sandstone bands are present, which are coarse grained and poorly sorted. Plant fragments does also occur (Croxtton and Pickton 1976).

Grumantbyen Formation

This formation consist of highly bioturbated sandstone rich in chlorite and glauconi(Dypvik, Riber et al. 2011).



Fig 2.8: Map shows various groups along the Van Mijenfjorden (Svalbardkartet.npolar.no)



Basilika Formation

This formation contains a series of soft grey shales and siltstones. Pebbles, quartzite and chert up to a diameter of about 10 cm are common. (Croxtan and Pickton 1976).

Firkanten Formation

This formation can be subdivided into two members. The lower part is coal bearing (Croxtan and Pickton 1976). These sediments contains delta-plain and shore face sediments deposited in a transgressive basin infilling phase (Dypvik, Riber et al. 2011). There is an unconformity at the base of the Tertiary Van Mijenfjorden Group, marked by a conglomerate (Croxtan and Pickton 1976).Upper cretaceous rocks are missing on Svalbard.

Age		Group	Formation
Tertiary	Lower	Van Mijen- Fjorden Gr.	Gilsonryggen Fm
			Grumantbyen Fm
			Basilika Fm
			Firkanten Fm
Cretaceous	Lower	Advent- dalen Gr.	Carolinefjellet Fm
			Helvetiafjellet Fm
Jurassic	Upper	Kapp Toscana Gr.	Janusfjellet sub-group Rurikfjellet Fm
			Agardh- fjellet Fm
Triassic	Lower/Middle	Sassen- dalen Gr.	Willhelmøya Fm
	Upper		De Geerdalen Fm
	Middle		Botneheia Fm
Permian	Upper	Tempel- Fjorden Gr.	Tvillingodden Fm
	Lower	Gipsdalen Gr.	Vardebukta Fm
Car- bon- ifer- ous	Upper		Kapp Starostin Fm
			Gipshuken Fm
			Nordenskiold- breen Fm
Pre Old Red/ Devonian			

Fig 2.9: Modified stratigraphic subdivisions of the formations in Van Mijenfjorden (Nøttvedt 1994)

3-Processing Theory.

3.1.1 Seismic Source

The air-gun is activated by sending an electrical signal to the solenoid located at the top of the gun. The major air volume is initially in the lower air chamber, as the shuttle moves upward after the solenoid has been activated, the high pressure air escapes into the water creating a seismic pulse.(Landrø, Amundsen et al. 2011). The released air creates a bubble in the surrounding water. The bubble increases in the beginning but after a while the pressure from outside, the hydrostatic pressure, is larger than the pressure from inside of the bubble and the expansion slows down. The bubble will collapse, and oscillate around equilibrium position. The collapses and expansions will not go on because of the heat dissipation into the water. The result from this behavior is a damped oscillatory pressure signal (Drijkoningen and Verschuur 2003)

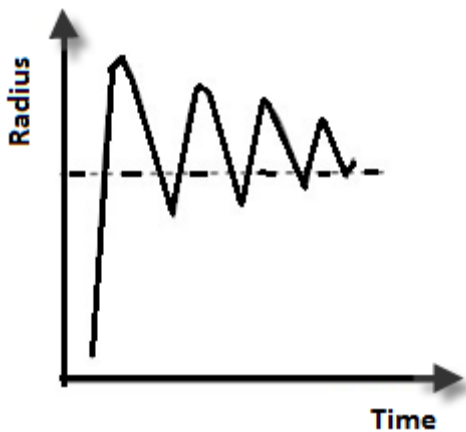


Fig 3.1: Schematic section of radius versus time of a released bubble. Modified from (Drijkoningen and Verschuur 2003)

The Signal from a single air gun has typically a length of 200 ms. Common pressures is 2000 psi. Assuming an incompressible fluid, it can be derived that the bubble Period T amounts to:

$$T = \frac{K(P_{In}^{\frac{1}{3}} V_{In}^{\frac{1}{3}})}{P_H^{5/6}}$$

P_{In} =pressure inside the air gun, V_{In} =volume of the chamber, P_H =hydrostatic pressure, K is some constant.

This formula is known as the modified Rayleigh -Willis formula, which means that the air gun bubble period scales as the 1/3 power of the pressure and the volume (Drijkoningen and Verschuur 2003).

To tune the air-gun array a large number of air guns with different volumes are arranged over a small area. This produce bubble-pulse free pressure signatures because it reinforces the initial pulse (first peak) and reduces or cancel the bubble pulse (second largest peak). The advantages of using an array is that a sharp signature can be produced.(Landrø, Amundsen et al. 2011). In Van Mijenfjorden four Bolt air guns 300+240+136+90 *inch*³ were used for exactly this purpose to reinforce the initial pulse (first peak) and reduce the bubble pulse. As seen on the seismic lines little information is seen under 2000 ms twt because this technique lowers the low frequency energy contained in the pressure signature.

3.1.2 Seismic Receivers

The hydrophone consists of two plates of piezo-electric ceramic placed on an elastic electrode. The active element is deformed by pressure variations in the surrounding water and it produces voltage .The active element produces a voltage not only under a variation of pressure but also when it is subject to acceleration. The hydrophone is constructed such that voltage produced by an acceleration cancel each other whereas those created by a pressure wave add (Drijkoningen and Verschuur 2003) The type of streamer used to gather the seismic lines in Van Mijenfjorden is a 3.0 km digital streamer (Western Geco, Nessie 3). Some of the characteristic main features of this streamer are low system noise (100 dB dynamic range), spare transmission channels for increased reliability; it also applies digital production filters.

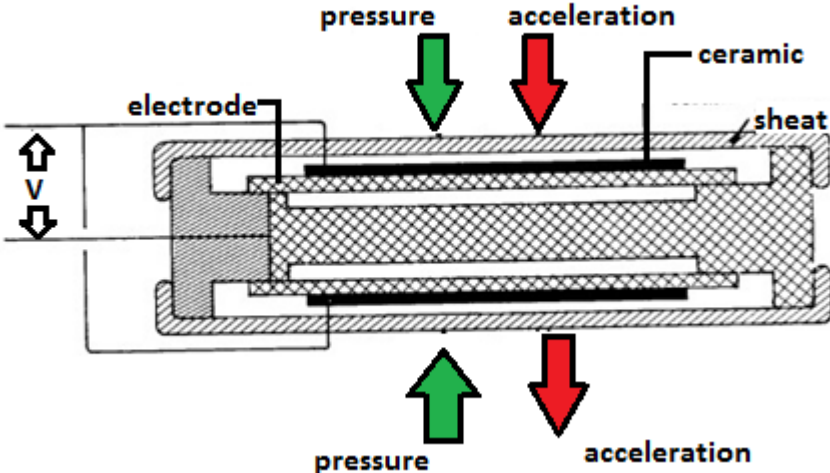


Fig 3.2: Schematic cross-section of a piezoelectric hydrophone modified from (Drijkoningen and Verschuur 2003)

3.2.1 Reformatting and editing

Reformatting includes converting the data from standard industry format into the format the processing system uses. Editing is to remove traces that appear noisy. (Bacon, Simm et al. 2007)

3.2.2 Designature

Air guns output a signal with a main peak, followed by a smaller secondary peak .A secondary signal is unwanted since every reflection would be followed by a smaller repetition of itself. Designature removes the second peak. At this stage of the processing a decision is made whether the output should be zero or minimum phase. A zero-phase wavelet is one that is symmetrical about its center, while a minimum -phase wavelet is one that starts at time zero and has much energy near the start as physically possible. (Bacon, Simm et al. 2007)

3.2.3 Gain Recovery

Energy is “lost” as a seismic wave travels away from its source because of geometric spreading .The rate of energy loss can be calculated; subsequently it can be compensated for by applying a gain function to the data in order to restore the signal amplitudes with depth. A drawback is that not only reflection signals are amplified-, but also noise.(Reynolds 2011)

3.2.4 Filtering of seismic data

Frequency filters differentiate against frequency components of an input waveform and can be low-pass, high pass, band pass or band rejected. Frequency filters are employed when the signal and noise components of a waveform have different frequency characteristics and can therefore be separated on this basis (Kearey, Brooks et al. 2013)

3.2.5 Velocity filtering

“A 2D Fourier transform from time-offset domain to the frequency-wavenumber domain is the basic for this analysis” quote (Hautus 1980). The purpose of velocity filtering is to remove coherent noise from seismic records on the basis of the angles at which the events dip. The angle of the dip is determined from the apparent velocity. The apparent velocity is given by:

$$V_a = \frac{V}{\sin \alpha}$$

V_a is the apparent velocity, α is the angle the wavefront makes with the surface

Along the spread direction, each component of the pulse will have an apparent wavenumber k_a related to its individual frequencies f , where

$$f = V_a K_a$$

A plot of frequency against apparent wavenumber k_a for the pulse will yield a straight line with a gradient of v_a . Different types of seismic events fall within different zones of the f - k plot, such that unwanted areas in the f - k domain can be attenuated (Kearey, Brooks et al. 2013)

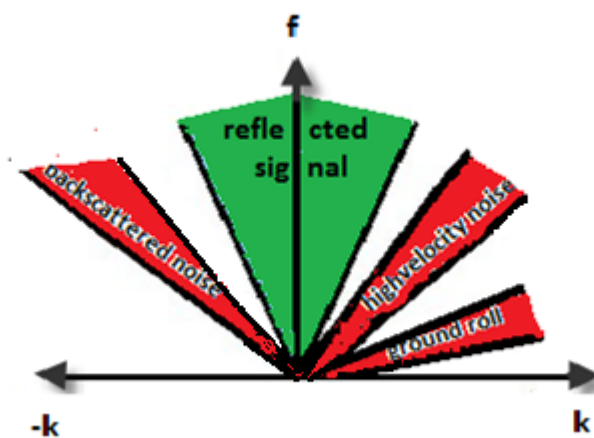


Fig 3.3: Principal mapping of different events in the f - k domain. The reflected energy surrounds the center ($k=0$) (green colored triangle), whereas noisy signal is clearly separated from the center. Modified from (Kearey, Brooks et al. 2013)

3.2.6 Inverse filtering (De-convolution)

Inverse filters are able to suppress noise that has the same frequency as the reflected signal. Deconvolution involves convolution with an inverse filter. The idea is that it will undo the effects of a previous filter. Deconvolution improves the resolution of seismic. This is done by compressing the seismic wavelet. (Kearey, Brooks et al. 2013)

3.2.7 Velocity analysis

Velocity analysis is performed using the normal move out (NMO) equation which is based on the assumption of flat, horizontal reflectors (Al-Yahya 1989).

The aim of the velocity analysis is to determine the stacking velocity as a function of reflection time. This is done by picking the peaks or anomalies in the contoured semblance values in a velocity spectrum window. The semblance is defined as the ratio of the stacked trace energy to the input trace energy within a time gate across several seismic traces. The stacked trace energy is the energy in the trace formed by stacking (summing) the input traces, while the input traces energy is the energy within the time gate in all of the input traces. (Al-Shuhail 2013)

When correct stacking velocity has been picked, NMO is removed (Kearey, Brooks et al. 2013).

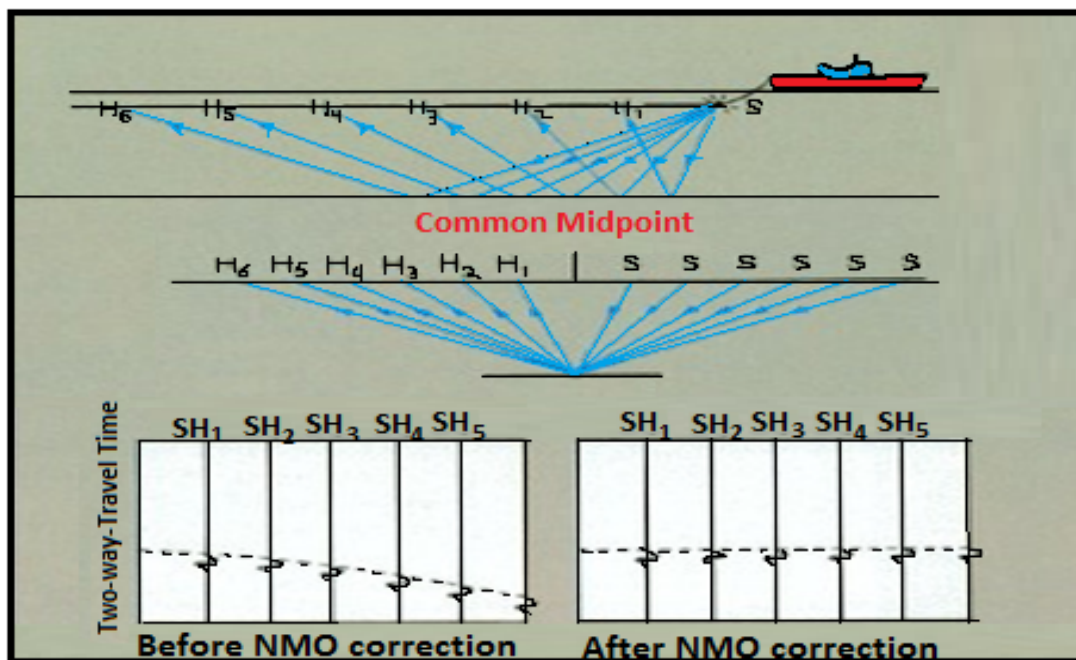


Fig 3.4: Shows the definition on CMP and seismic traces before and after NMO Correction, modified from (Schlumberger glossary)

3.2.8 NMO correction

“The difference between the two-way time at a given offset and the two-way zero-offset time is called normal moveout(NMO)” quote (Yilmaz 2001). According to the same author reflection traveltimes must be modified for NMO before summing the traces in the CMP gather. NMO is dependent on many factor including velocity, offset, two-way zero-offset time, and dip of the reflector

An expression for a simplified approximation of the difference in traveltime for reflected arrivals at x and at zero offset is given by:

$$\Delta T_{nmo} = T_x - T_0 \approx \frac{x^2}{2T_0} * \frac{1}{v^2}$$

T_x is the two way reflection time for a trace of offset distance x. Basically NMO correction involves the subtraction of a time increment ΔT_{NMO} from each record time T_x . This converts a trace of offset x into a zero-offset trace(Robinson and Treitel 1980)

NMO stretching occurs after NMO correction. A frequency distortion occurs, mainly for shallow events and at large offsets. The waveform with a dominant period T is stretched so that its period T_0 after NMO correction is greater than T. Stretching is a frequency distortion in which events are shifted to lower frequencies.

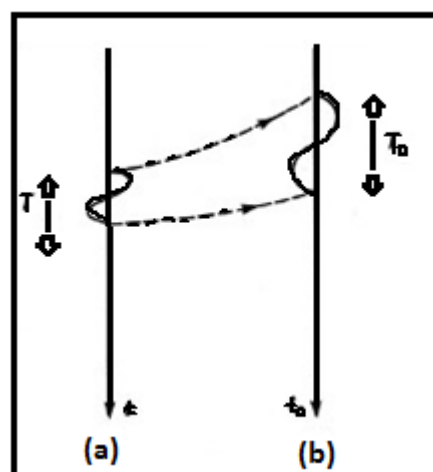


Fig 3.5 A signal (a) with a period of T is stretched to a signal (b) with a period of $T_0 > T$ after NMO correction. The figure is modified from (Yilmaz 2001)

3.2.9 Muting

Muting is used to suppress undesirable portions of the data (Claerbout 1985). It is usually applied in the early part of the traces that contains first arrivals of body waves. Mute can be performed over a time interval to keep airwaves, ground roll, and noise out of the stack section. This process is called surgical mute (Gadallah and Fisher 2005). Stretching changes the frequency spectrum of the wavelet, which results in attenuation of higher frequencies in subsequent stacking. Therefore, long offset traces are normally muted before the stretching reaches 25% (Sheriff and Geldart 1995). Improper NMO stretch mute can degrade the amplitude and spectral characteristics of reflection wavelets.

Far-offset information, near critical-angle reflection information is most sensitive to stretch. A correct NMO stretch mute stabilizes the spectral properties of shallow reflections, allowing for effective use of wavelet and multiple suppression routines (Miller 1992). If the signal-to-noise ratio is good, muting more than stretch mute requirements is applied to preserve signal bandwidth. When the signal-to-noise ratio is poor, accepting a large amount of stretch may be necessary to get any events on the stack. Muting is also a tool for elevating the small move out discrimination between primaries and multiples at small offsets (Yilmaz 2001).

3.2.10 Stacking

Stacking means summing the traces contained in a CDP gather to produce a single composited trace. When summing the primary reflections are in phase and add constructively, whereas noise and other seismic signals not in phase tend to cancel. The signal to noise ratio thus increases, by factors approaching \sqrt{N} . Where N is the number (fold) of the CDP traces summed (Robinson and Treitel 1980).

3.2.11 Migration

Moving the reflections to their proper places with their correct amount of dips is called migration. Even though the travel paths are normal to dipping reflectors, the traces are presented on the record section as if the travel paths were vertical. Migration moves them back up-dip. This results in a more accurately cross-section of the earth. Migration also collapses diffraction (Gadallah and Fisher 2005).

Many migration techniques have been developed, three methods are generally applied to data after it has been stacked: Kirchoff migration, finite difference migration and the Frequency-domain technique. The common idea behind all three methods is that the stacked section can be considered as the upcoming wave recorded at the Earth's surface. Using the scalar wave equation it is possible to trace this wavefield back to any depth, finding the origin of the waves-the reflected position.

This is called the downward continuation technique(Badley and Gibson 1987).

Kirchoff Migration

The Kirchoff method migrates the data by searching for diffractions and moving all energy along the diffraction curve to its apex(Badley and Gibson 1987).

The advantage of this method is the good performance in case of steep-dip structures. The method does not perform well when the signal to -noise ratio is low(Gadallah and Fisher 2005).

Finite Difference Migration

“The main idea behind the FD method is to compute the wavefield u at a discrete set of closely-spaced grid points by approximating the derivatives occurring in the equation of motion with finite difference formulas, and recursively solving the resulting difference equation “ quote (Krebes). One advantage of the finite difference method is the capability to perform good under low signal-to-noise ratio conditions. Its drawbacks include long computing time and difficulties in handling steep dips(Gadallah and Fisher 2005).

Frequency-domain migration

This migration transforms the data into a frequency versus wave-number domain (Badley).

Both Stolt and Phase shift migration operates here, phase shift migration is considered to be the most accurate. It is a deterministic approach via the wave equation as an alternative of using the finite difference approximation (Gadallah and Fisher 2005). The technique uses less computer time, has good performance with steep dips and good performance under low signal to noise ratio. Disadvantages of this method include difficulties with widely varying velocities. (Badley and Gibson 1987, Gadallah and Fisher 2005).

3.2.12 Seismic velocities

Root mean square velocity

The root-mean square velocity of the section of ground to the nth interface is given by

$$V_{rms,n} = [\sum_{i=1}^n V_i^2 t_i / \sum_{i=1}^n t_i]^{1/2}$$

V_i is the internal velocity of the ith layer and t_i is the one way travel time of the reflected ray through the ith layer (Kearey, Brooks et al. 2013)

Average Velocity

The average velocity is defined as

$$V_{avg} = \frac{\sum_f V_f \Delta t_f}{\sum_f \Delta t_f} = \frac{\sum_f \Delta z_f}{\sum_f \Delta t_f}$$

Δt_f is the travel time through layer f, Δz_f is the thickness through layer z and V_f velocity in layer f. (Sheriff and Geldart 1995)

Interval Velocity

Interval velocity can be found by using values of V_{rms} down to different reflectors.

To compute the interval velocity v_n for the nth interval:

$$V_n = \left[\frac{V_{rms,n}^2 t_n - V_{rms,n-1}^2 t_{n-1}}{t_{n-1}} \right]^{1/2}$$

$V_{rms,n}^2, t_{n-1}$ and $V_{rms,n}, t_n$ are respectively the root mean-square velocity and reflected travel times to the (n-1)th and nth reflectors (Kearey, Brooks et al. 2013)

Stacking Velocity

Stacking velocity is defined as the velocity which produces the maximum amplitude of the reflection event in the stack of traces. Stacking velocity is that which removes NMO, it is given by: $V_{st}=[x^2/t^2 - t_0^2]^{1/2}$ (Kearey, Brooks et al. 2013)

3.3 Principles for seismic interpretation

In seismic interpretation the aim is to extract subsurface geological information from seismic data. It generally assumes (1) that the coherent events seen on seismic records are reflections from acoustic impedance contrast in the earth, and (2) that these contrasts are associated with formations with their unique structures and geometries. (Sheriff and Geldart 1995). However the danger in seismic interpretation is interpreting everything perceived as geology. The data could have defects due to acquisition problems and processing problems (Brown 2013)

3.3.1 Seismic facies

Seismic facies analysis use different seismic parameters in order to get more than structural information; a seismic facies unit can be defined as a sedimentary unit which is different from neighboring units in its seismic characteristic. Essential parameters in seismic facies analysis is reflection amplitude, reflection frequency, reflection polarity, reflection continuity, reflection configuration, geometry of seismic facies units, interval velocity (Roksandić 1978).

Reflection Amplitude

Amplitude is the height of a seismic reflection peak (or trough) and is dependent on the reflection coefficient. Vertical changes in amplitude can be used to help discover unconformities, lateral changes can be used to help distinguish different seismic facies (Badley and Gibson 1987).

Reflection Polarity

In a seismic section presented with SEG normal polarity a reflection boundary appear as a trough in the seismic trace if $Z_2 > Z_1$. The reflection boundary appear as a peak in the seismic trace if $Z_2 < Z_1$ (Badley and Gibson 1987)

Reflection Spacing

Reflection spacing or frequency refers to the number of reflections per unit time. It is affected by both interference effects and the frequency of the seismic signal. Vertical variations in reflector gaps can be used as a guide to detect boundaries between depositional sequences, but should not be used as the only criterion. The gradual loss of higher frequency with depth has a noticeable effect on reflector spacing. Also multiples can often produce false increases in reflection spacing (Badley and Gibson 1987).

Reflection Continuity

Reflection continuity refers to the lateral persistence of a reflection. A discontinuous reflection is one where its alignment is clear but the continuous parts of the reflection are separated by spaces. Continuous reflectors are characteristic of depositional environments where uniform conditions are laterally extensive (deep-water environments). Discontinuous reflectors are characteristic of environments where rapid lateral facies change dominates (e.g., fluvial, alluvial environments) (Badley and Gibson 1987).

Table 3.1: shows seismic characteristics and its interpretations (Sheriff and Geldart 1995)

Interpretation	Characteristics	Other characteristics
Generally marine deposits alternating neritic shale/limestone, interbedded high/low energy deposits, or shallow marine clastics transported mainly by wave action.	High Continuity, high amplitude.	
Fluvial or near shore clastics, fluvial/wave transport process (delta platform), or low energy turbidity.	Variable continuity, low amplitude, occasional high amplitude	
Non marine clastics, fluvial or marginal marine	Low continuity, variable amplitude.	Occasional high amplitude and high continuity from coal member

Delta complex	Variable continuity and amplitude	Internal reflections gently sigmoid to divergent
Low energy , deep marine clay and silt	Variable continuity and amplitude. Fan-shaped to extensive along slope.	
reef	Reflection free configuration	

3.3 2 Seismic interpretation of structures.

Folds and faults are the two main features when interpreting structures. Folds are recognizable from the dip changes of reflectors. They are found on all scales and develop under many conditions-from regional compression, to down bending associated with subsidence, to frictional drag associated with faulting, etc. Folds can be described in terms of their amplitude, wavelength, plunge, axial trace, etc.

In seismic there are generally two types of faults namely normal faults and reverse faults. A normal fault is a fault where the hanging wall has moved down relative to the footwall. A reverse fault is a dip-slip fault, on which the hanging wall has moved up relative to the footwall (Badley and Gibson 1987).

3.3.3 Compressional Deformations structures

When rocks are shortened by tectonic or gravitational forces are contractional deformation structures formed. These faults and folds are in all parts of a collision zone. Contractional faults are solely reverse faults and thrust faults. Reverse faults are steeper than thrust faults (steeper than 30 degree) and do not have the large displacements seen in thrust. Contractional faults can arise at any scale , from the micro scale to regional mountain belts and subduction zone (Fossen 2010). The western part of the Van Mijenfjorden is a part of the west Spitsbergen fold and thrust belt. In fold and thrust belt large scale asymmetric folds are often found associated with contractional faults (Ghosh and Saha 2005). Asymmetric fold is one whose limbs are unequal in length and axial plane is inclined , dipping in the same direction as that of the gently dipping limb. These folds can have S or Z shapes depending on their sense of asymmetry and these can in turn give rise to complex like shapes. (Fossen 2010).

3.3.4 Seismic Resolution in the data acquired in Van Mijenfjorden

Resolution relates to how close two points can be, and still be perceived as two separate points. There are two types of resolution, vertical and horizontal resolution. The benchmark for vertical resolution is the dominant wavelength. The benchmark for lateral resolution is the Fresnel Zone, a circular area on a reflector whose size depends on the velocity above the reflector, depth to the reflector, and the dominant frequency.

Vertical Resolution

“For two reflections, one from the top and one from the bottom of a layer, there is a limit of how close they can be, and still be separable. This is known as vertical resolution. The acceptable threshold for vertical resolution generally is a quarter of the dominant wavelength.” quote (Sheriff and Geldart 1995)

$$\lambda = \frac{v}{f}$$

Here v is the velocity and f is the dominant frequency(Yilmaz 2001).

The velocity varies between 4000m/s in the shallowest part in our area and for deeper parts around 5000m/s. From figure 5.28 the dominant frequency is 50 Hz. This could be the case especially for reflectors deeper than 900 ms since this frequency is not filtered by the band pass. Then for reflectors under 900 ms the vertical resolution would be $5000/50/4=25$ meter. This means that it is possible to distinguish structures down to 25 meters, and structures under 25 will not be seen. Down to 900 ms is the dominant frequency 80 Hz since it is allowed by the band pass and figure 5.28 also show that these frequencies are present. The vertical resolution for the upper 900 ms is then be $4000/ 80/4=12.5$ meter. From Fig 5.29 a frequency of 50 Hz corresponds to approximately 12 dB meaning it represents $\frac{1}{4}$ of the maximum amplitude in the seismic. A frequency of 80 hz corresponds to 42 db. The vertical resolution down to 900 ms could be computed more exact by using velocity information from Fig 6.7. The mean velocity down to 900 ms is then 4100 m/s this gives a vertical resolution of 12.8 meter. Small differences is also seen for velocities under 900 ms using the well information and taking -12 dB as a basis from Fig 5.29 a vertical resolution of 23.6 meter is obtained. Since same types of result are obtained using two different approaches, the vertical resolution is considered accurate.

4- DATA ACQUISITION AND PARAMETERS

The following chapter describes briefly the collection parameters and technical information about the seismic

data . The data consists of 10 seismic multichannels

2D profiles, collected in Van Mijenfjorden during studies courses in 2013 and 2014.

Table 4.1: shows the geophysical acquisitions parameters used in the survey Mjelde(2013-2014) Cruise Report.

Digital streamer (WesternGeco,Nessie3)	3 km
Four bolt air guns	300+240+136+90inch3
Shot interval	5.0 km
Recording length	12 s
Air-gun depth	6 m
Streamer depth	8 m
Group Length	12.5 meter
Distance from GPS <u>antenne</u> to <u>centre of source</u>	36 m
Distance from GPS <u>antenne</u> to first active channel	136 m
Recording filter:	3Hz(18dB/octave),180Hz(72dB/octave)
Lacoste-Romberg gravity meter	
Marine proton magnetometer	

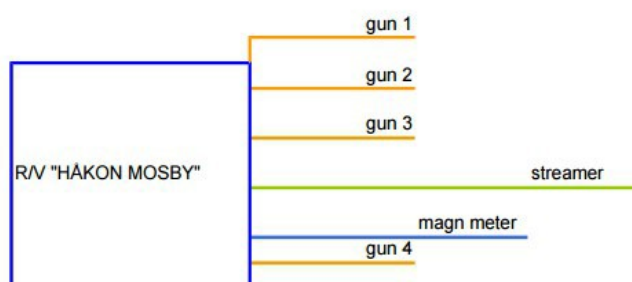


Figure 4.1: shows the source configuration of source and receivers Mjelde(2013-2014) Cruise Report.

Table 4.2: Geographical coordinates of profiles. Mjelde(2013-2014) Cruise Report.

Line	SP	DATE	TIME	UTM EAST	UTM NORTH
VMF-13-9	2894	2013.08.18	17:32:56	495706.1	8626951.5
	3415	2013.08.18	20:16:05	519401.2	8637774.4
VMF-13-11	2412	2013.08.18	14:51:17	516444.0	8637511.2
	2887	2013.08.18	17:22:59	494849.7	8627625.3
VMF-13-14	1919	2013.08.18	11:51:46	493894.6	8628874.6
	2403	2013.08.18	14:36:04	515920.5	8638899.2
VMF14-3	9	2014-08.17	15:53:28	521837.9	8635556.5
	564	2014-08.17	19:12:50	496577.8	8624076.9
VMF-14-4	1167	2014-08.18	09:56:10	497239.1	8624916.0
	1717	2014.08.18	12:59:04	522218.4	8636414.5
VMF-14-5	2263	2014.08.19	12:38:19	496090.5	8624904.1
	2835	2014.08.19	15:45:44	522096.3	8636805.8
VMF-14-6	580	2014.08.18	06:20:18	521530.9	8637081.8
	1154	2014.08.18	09:39:11	495421.8	8625165.3
VMF-14-7	1725	2014.08.19	09:27:32	519540.9	8636745.9
	2256	2014.08.19	12:28:19	495339.3	8625699.5
VMF-14-8	2848	2014.08.19	16:05:30	519981.3	8637466.9
	3396	2014.08.19	19:12:20	495039.9	8626123.6
VMF-14-10	3403	2014.08.20	06:27:03	495858.8	8627580.7
	3922	2014.08.20	09:26:18	519476.8	8638331.8

The lines are not shot in order. This is done to avoid sharp causing significant amounts of noise in the receivers when streamer is bending. Also tight turns increase the chance that the streamer comes out of position, are cut off or collide with the source.

The sources are to some extent "broad": it is not directive in the input line-level; this will to some degree reduce the energy towards the sides

Chapter 5

This chapter is about processing, sources not mentioned are taken from CGG Veritas(2008) Geocluster Release Notes.

5.1 Geocluster and Geopad(CGVeritas)

Geocluster seismic processing software consists of a set of interactive applications integrated with a processing engine. The processing nucleus contains program modules covering 2D and 3D processing. The interactive environment consists of general purpose tools (job flow building, seismic data analysis) and task specific tools (velocity analysis, refraction statics, and so on).

Main Geocluster applications used in data processing

Geopad

Geopad is a user desktop providing a working environment for Geocluster, in particular file management and application launching. Geopad is started from a text window by typing the command `geopad` and pressing enter. The following window will then appear.

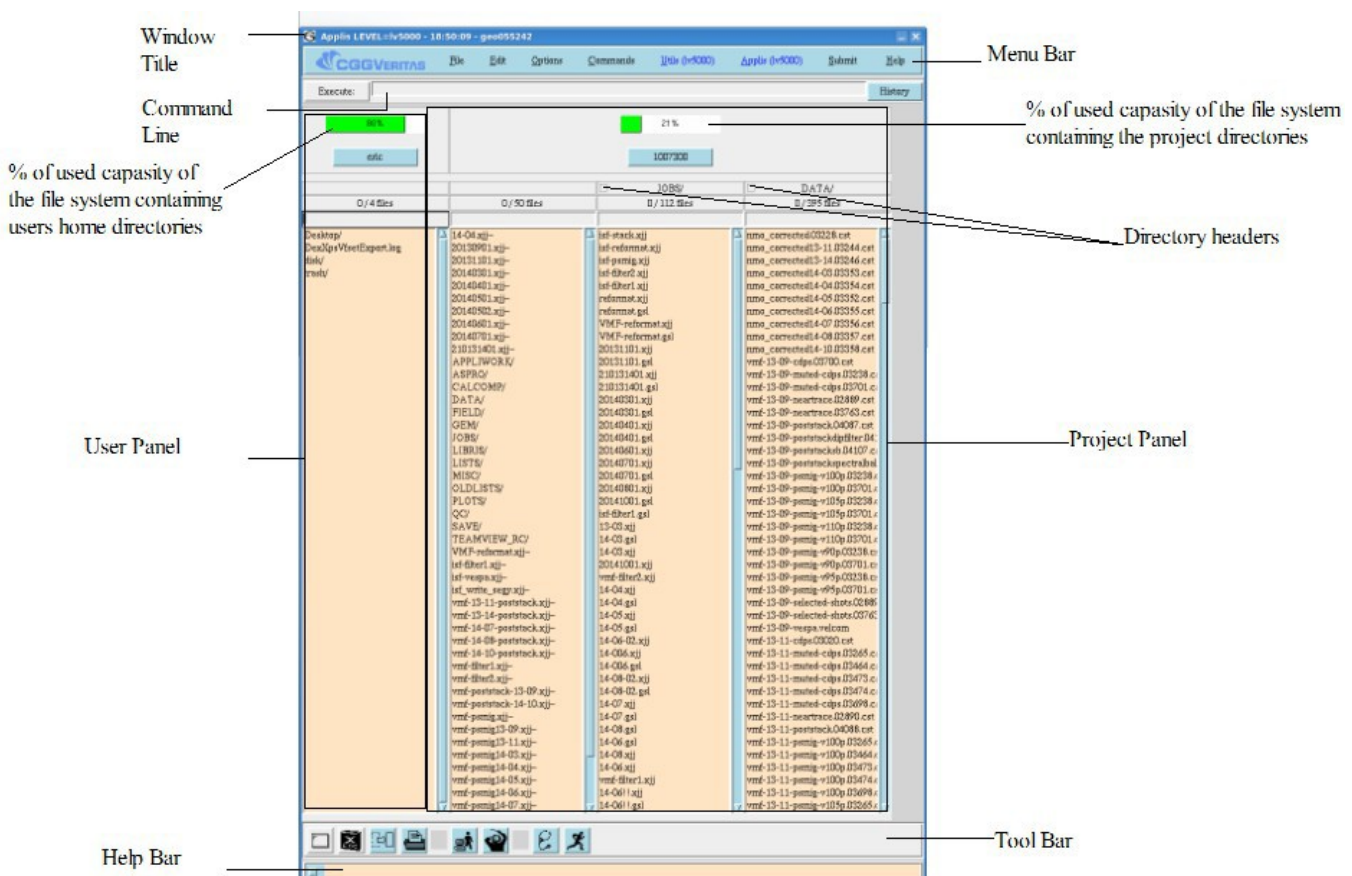


Fig 5.1: Geopad main window with different tool bars and panels.

5.1.1 XJOB

The purpose of XJOB is to create Geocluster seismic processing job flows. A job is a group of commands that are done in a particular way. It is graphically made by linking icons that symbolize Geocluster processing modules. XJob enables the user to parameterize each module using contextual screens. Then the job is compiled into a GSL procedure (GSL, Geocluster Software Language, a language that describes a seismic job flow).

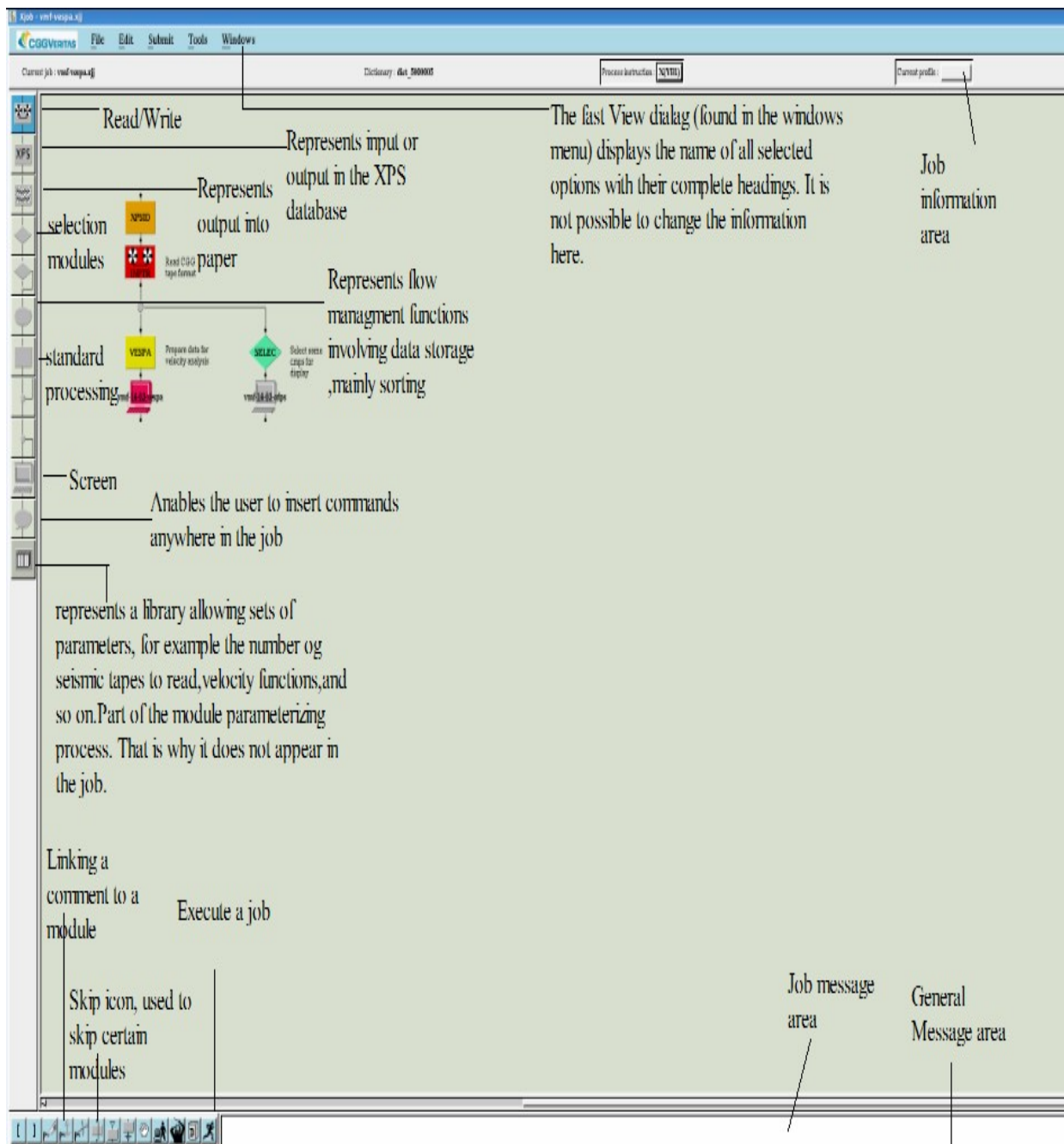


Fig 5.2 The figure shows the XJOB window

5.1.2 ChronoVista

Chrono Vista combines GeoVel, Geomig and Velpicker

The program allows the user to pick stacking velocities and horizons in the time domain, then to perform specific processing on the picked velocity.

Velocity analysis is done in a single window, characterized by a set of tracks. These tracks include the spectrum, uncorrected and corrected CMP gather, perturbed mini-stacks, and recomputed stack.

5.1.3 XPS

The XPS system (extended Processing Support) is a group of concepts and tools allowing the user to manage auxiliary data. The standard format allows data to be read by any application integrating XPS. The data is found solely in one standard location. Tools in XPS allow the user to visualize data graphically or via a spreadsheet, all auxiliary data is structured in the form of tables. Chronovista is one of the applications XPS system is implemented in.

5.1.4 Modules used in the processing

Table 5.1: Shows the different modules used and their purpose

SEGIN	SEGIN reads traces selected by LIBRI SI.
QCTRL	This module checks the content of trace header words by comparing two successive traces-
HISTA	Reduce trace length
FILTR	This program applies the filter operators stored in the filter libraries and performs time variant filtering. It also performs, if necessary, spatial interpolation between libraries.
RSAMP	RSAMP resamples traces at a different sample rate than on input using a band -limited resampling filter. The resampling phase is carried out by the program by applying an interpolation filter whose Maximum frequency can be adjusted by parameter FMAX
SPASM	Smoothing the amplitudes of the processed traces.
MODET	This module is used to modify one or more trace header words.
OUTBD	This module controls the output of seismic traces, in CGG format to tapes and disc files , based on the information in the corresponding LIBRI BD.
SELTR	This module is used to select traces to preserve or to remove. It functions by removing unwanted traces from the flow of induced traces.
REFOR	Scaling of the amplitude.
FANMO	The program uses velocity libraries and, optionally, mute and water bottom libraries. Linear interpolation is used to obtain the velocity for all points in time.
INPTR	A number representing the seismic data to be processed in the following job
DESIG	This module performs a statistical, data dependent, air-gun signature deconvolution of pre -stack data. The input to DESIG should be shot-ordered data. The output from DESIG is deconvolved traces.

SPARN	This module carries out projective filtering in the (f-x) domain. Rather than using predictive filtering, SPARN uses projective filtering. The projective filter is calculated from an auto-deconvolved prediction error filter. Besides the attenuation of random noise, there are four options *Regularization of the spatial grid before processing *Missing Trace Restoration *Impulsive Noise Attenuation *Interpolation of traces
FKFIL	This program filters a set of traces in the FK domain.
SELEC	Determination of branching conditions Modification of the flow of traces
BSORT	Selects and sorts a group of traces. The module places onto the disk the set of input traces to be sorted.
DECSC	Performs a prestack deconvolution.
RECOV	This module performs amplitude recovery .
XPSID	This module must be coded at least once prior to coding the module that call an XPS database session
VESPA	This is a module for velocity analysis. This module carry out semblance, spectrum,etc.
MUTES	This module is used to mute a trace by setting the samples to zero
STAPA	Performs stacking
MUTAN	The module MUTAN mutes input seismic traces using incidence angles as the criteria for the mute.
TIKIM	TIKIM performs a Kirchloff time migration for pre-stack data.
MNGTY	This program manages traces that belong to a same group
TRITA	This program performs a time variant predictive deconvolution.
PFILT	This program is used to convert traces to zero phases by applying a phase filter.
TVDEF	This is a spectral balancing program; it applies time-variant amplitude deconvolution, equalization and filtering.
SEGOU	This program outputs traces onto a sequential format tape.

Table 5.2.: Shows the processing workflow.

Reformatting
Read SEG-Y (SEGIN)
Check if all traces are present (QCTRL)
Reduce trace length (HISTA) Band pass
filter (FILTR)
Resample from 2 to 4 ms (RSAMP)
Remove noise burst (SPASM)
Update header words (MODET)

Filter 1
Read CGG tape format (INPTR)
Signature deconvolution (DESIG)
Remove incoherent noise (SPARN)
Spherical spreading correction (REFOR)
Spatial amplitude smoothing (SPASM)
Velocity Filtering (FKFIL)

Filter 2
XPSID (Call information from XPS database, then must be
there) Read CGG tape format (INPTR)
Sort to receiver gather (BSORT)
Velocity filtering (FKFIL)
Sort to CDP gather (BSORT)
Amplitude Recovery (RECOV)
Surface consistent predictive deconvolution (DECSC)

Migration
XPIS
Read CMP gather (INPTR)
External mute from incidence angle (MUTAN)
Internal mute from water depth (MUTES)
3D-2D scaling (REFOR)
Kirchoff time migration for pre-stack 2D data (TIKIM)
Time variant band pass filter (FILTR)

Post Stack migration with corrected velocities
MNG1Y
Dip filter (FFKFIL)
Predictive Deconvolution (TRITA)
Phase shift filter to zero phase (PFILT)
Spectral Balancing (TVDEF)
Time variant band pass (TVDEF)
Set UTM coordinates (MODET)

Table 5.3.: Shows the processing steps and their objective

No	Processing steps	Objectives
1	Reduce trace length(12844 ms to 6144 ms)	Speed up the processing
2	Bandpass filter (low frequency limit 8 Hz, high frequency limit 90 Hz)	Remove frequency of defined range(noise)
3	Resample from 2ms to 4 ms.	2 ms corresponds to max frequency 250 Hz(Not needed) 4 ms corresponds to max frequency 125 Hz
4	Signature Deconvolution	Removes the bubble pulse from the seismic trace.
5	Remove Incoherent noise	Removing random noise
6	Spherical spreading correction	
7	Spatial Amplitude smoothing	Making the amplitude of traces near each other more smooth or equal.
8	Velocity filtering (f-k) domain	Reduce Coherent noise, velocity interval (-5000 m/s -10 000 m/s)
9	Amplitude recovery	Compensate for loss of amplitude due to wave front spreading and attenuation
10	Predictive deconvolution	Removes water bottom multiples and other types of multiples.
11	Stacking	Summing traces, reducing noise that does not add constructive
12	Velocity Picking Geovel	Pick stacking velocities which corrects for NMO effect.
13	Muting	Attenuate NMO stretching effect and removes bad traces.
14	Kirchoff time migration	Corrects seismic events to the correct location
15	Time Variant Band pass filter	Energy outside the given range is removed

5.2 Reformatting

Seismic raw data are read into SEGY-format and is reformatted internally to Gecluster-format. The trace length is reduced from 12288 ms to 6144 ms, the reason for this is that the bottom half of the traces contain little information. Marine data are normally recorded with a 2 ms sampling interval. This is sufficient to record frequencies up to 250 Hz, much higher than frequencies that are actually recorded from the underground. For this reason the data are resampled to 4 ms. This is sufficient for frequencies up to 125 Hz. The resampling reduces the volume of the data by 50 % and also speeds up later processing stages. Before resampling is done a band pass filter is applied. This filter has a low frequency limit of 8 Hz and a high frequency limit of 90 Hz. By filtering frequencies over 90 Hz aliasing is not a problem. This is because the Nyquist frequency corresponding to 4 ms is 125 Hz. Since no frequency over 125 Hz is present after filtering aliasing will not occur. Also high frequency noise from the vessel or low frequencies noise from waves will not be a problem. Next the module *spasm* is replacing the amplitude at the window center by the average of the neighboring traces. Also the portions of the traces having strong amplitude values are considered noisy and therefore excluded. The module *Modet* is used at the end of this processing job to calculate the CDP number, offset, line number and CDP position to source and receivers.

Figure 5.3 shows a part of a shot gather, using the processing steps described above. The first reflection from the seabed is at approximately 0.15 seconds. The seabed multiples is shown with equal move out as the first reflection with double twt. Figure 5.4 shows a near trace gather where water depth was picked. This is done in order to remove water bottom multiples and therefore improving the quality of the data. The water bottom depths were exported to the XPS data base in order to create a water bottom library.



Figure 5.3: The seabed is the first arrow; the second arrow shows the seabed multiple. The shot points are on the x axis and twt in ms is along the y axis.

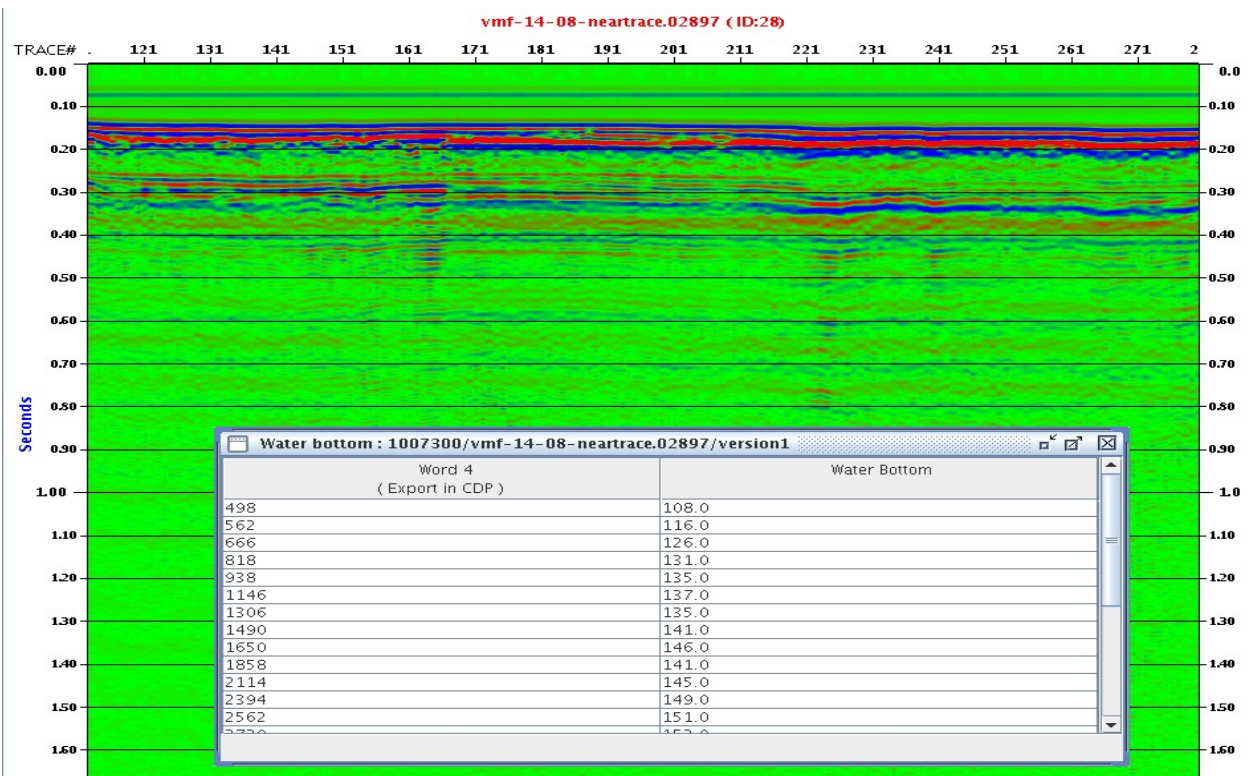


Figure 5.4: Shows a display of a near trace gather, the tables of numbers shows the time values for the picked water depth.

5.2.1 BANDPASS FILTER

The band pass filter had also the effect of attenuating noise spikes.

These noise spikes could be source generated noise. Noise spikes are a result of atmospheric discharges or piezoelectric impulses (Klemperer 1987).

However since they only occur at the end of the seismic lines they are most likely a result of bending of the streamer when the vessel is turning around (Bent Ole Ruud).

The effect this has on the shot gather is shown in Fig 5.5.

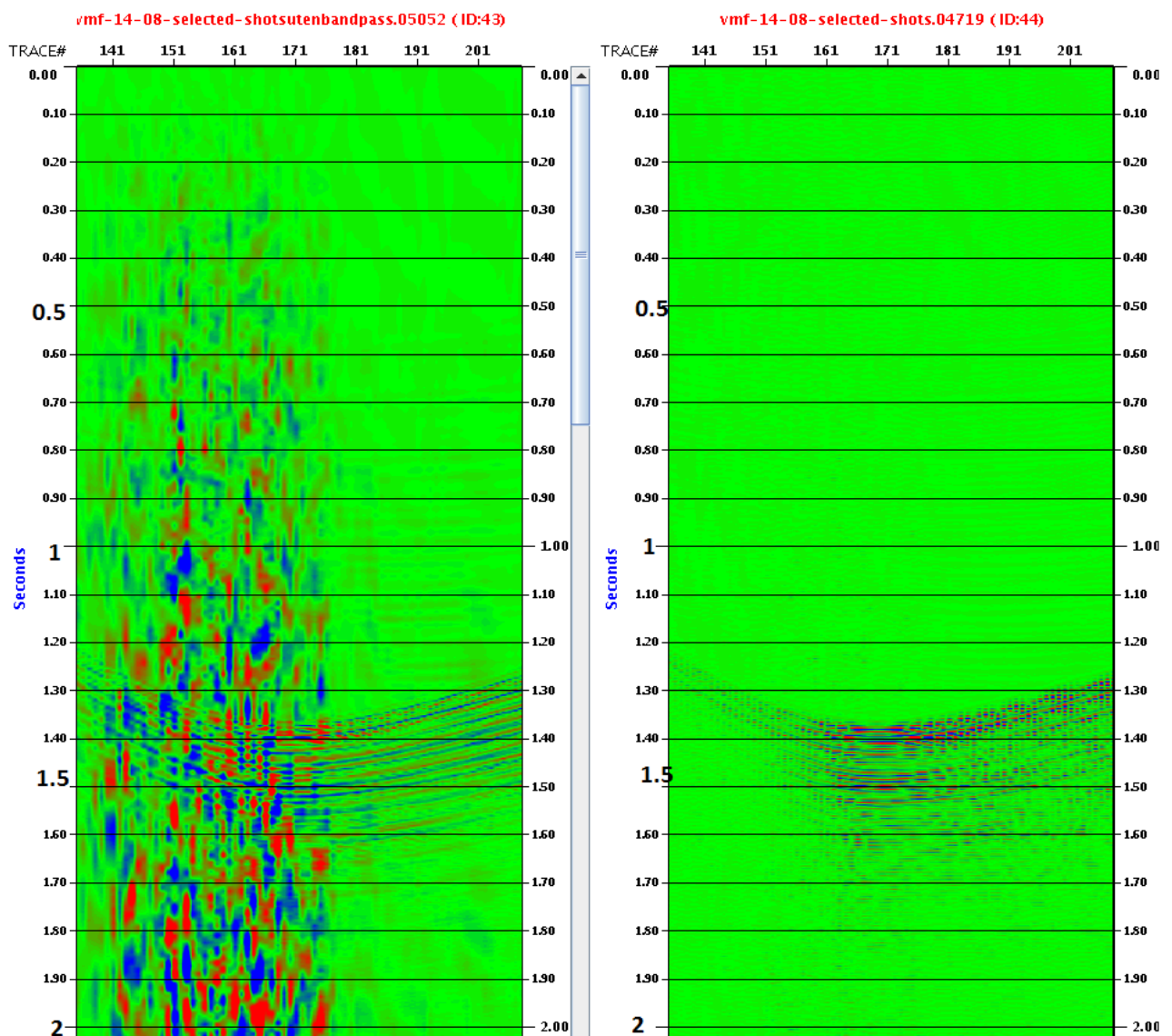


Fig 5.5.: The figure to the left shows a noise spike as a result of bending the streamer, on the figure to the right is the noise attenuated as a result of the bandpass filter

5.2.2 Removing Noise Burst

The aim of the module SPASM is to remove noise burst. This effect did not occur at the end of the seismic line and is thus not a result of bending of the streamer.

This effect is due to leakage in the streamer resulting in saltwater entering the oil filled streamer causing transmission problems (Bent Ole Ruud).

Salt water invading a channel reduces the current leakage resistance of the primary circuit in the channel. The lower resistance in the channel causes lower sensitivity as well as a loss of low frequency response and a phase shift (Brastins and Stenger Jr 1979).

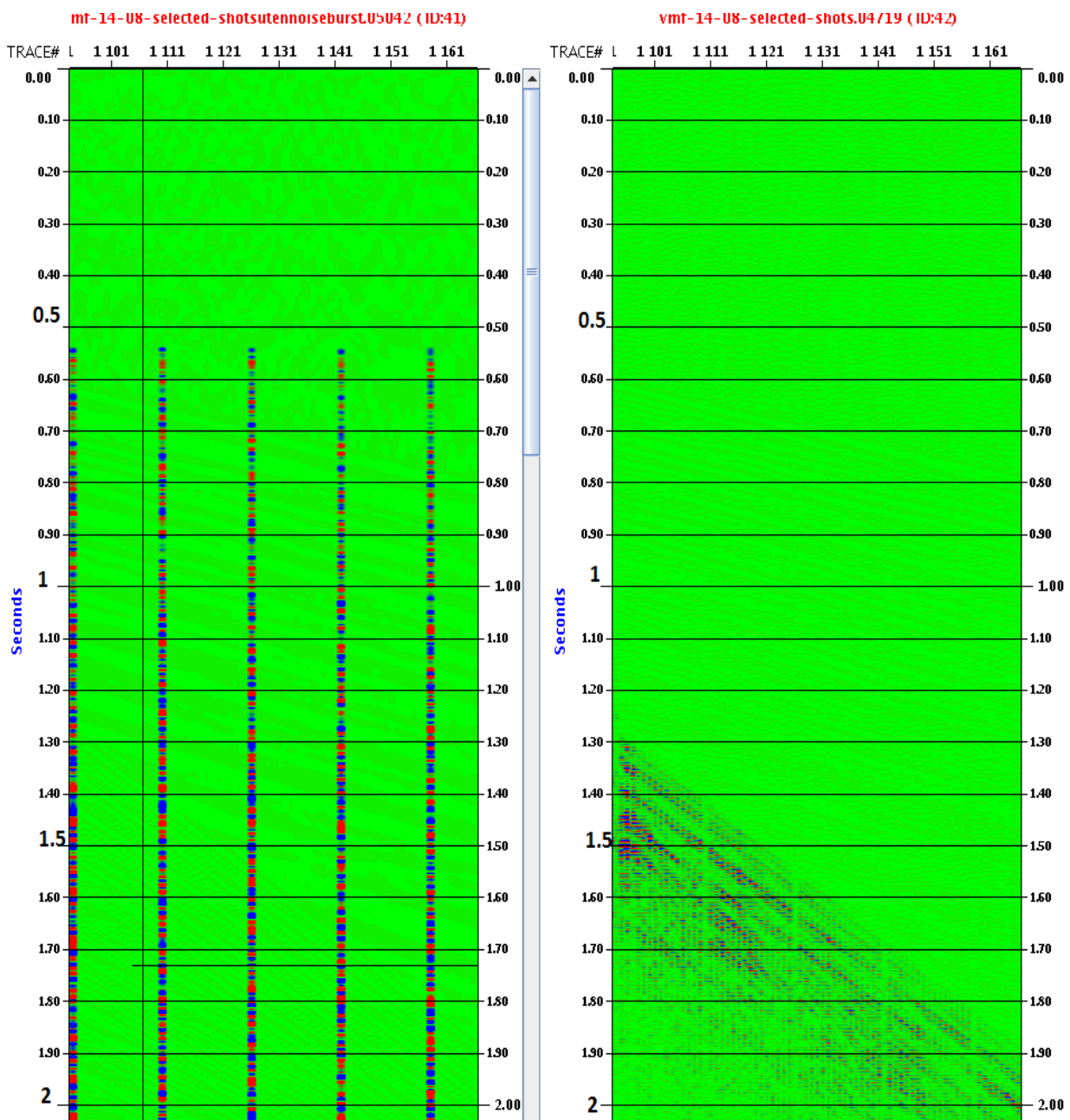


Fig 5.6.: The figure to the left shows the effect salt has on entering the streamer creating a noise burst. On the picture to the right is the noise burst removed due to the module SPASM.

5.3 Filter 1

Filter 1 job uses the output from the reformatting job as input. This job applies signature deconvolution, removal of incoherent noise, spherical spreading correction, spatial amplitude smoothing and velocity filtering. The effects of the various modules are presented.

5.3.1 Removing incoherent noise

The module SPARN has the purpose of removing incoherent noise. The module separates the signal, assumed to be predictable from the non-predictable noise. To do this the module used projective filtering. This ensures that the signal is preserved, at the same time attenuation of random noise is done. The projective filter is calculated from an auto –deconvolved prediction filter. The effect of the filter was hard to see on the near trace and the shot gather but some changes were present. Fig 5.7 shows that by applying this filter a shift in dB occurs for the same frequency indicating that noise has been removed. The blue line has SPARN applied (incoherent noise is attenuated) .Maximum frequency to be processed is set to 50 Hz and minimum frequency to be processed is set to 7. For frequencies below FMIN and above FMAX the output is identical to the input. The relationship between dB and noise is discussed in the literature by for example (Hansen 2005). He discusses shifts in dB by adding and removing incoherent noise.

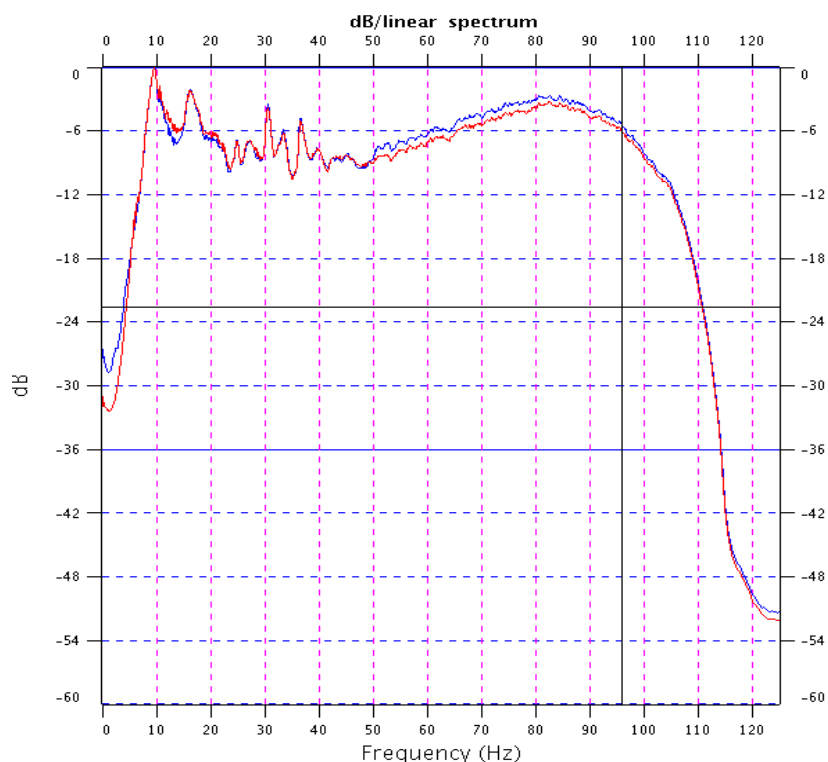


Fig 5.7: Shows a dB/frequency correlation before and after SPASM is applied. Blue graph has SPARN applied, red has no SPARN applied.

5.3.2 Signature Deconvolution

The first module used in this job is DESIG. This module performs a statistical, air-gun signature deconvolution of pre-stack data. The recorded seismic signal can be considered as the convolution of the source signal with the instrumentation, the hydrophones, and the response of the earth. When the source signature (bubble pulse) is known it can be removed from the trace data. This enhances both the vertical and lateral resolution of seismic data (Hobbs and Jakubowicz 2000). This is also shown in Fig 5.8. It should be mentioned that not all shot gathers showed as good enhanced resolution as shown in fig 5.8, but all seismic lines were improved.

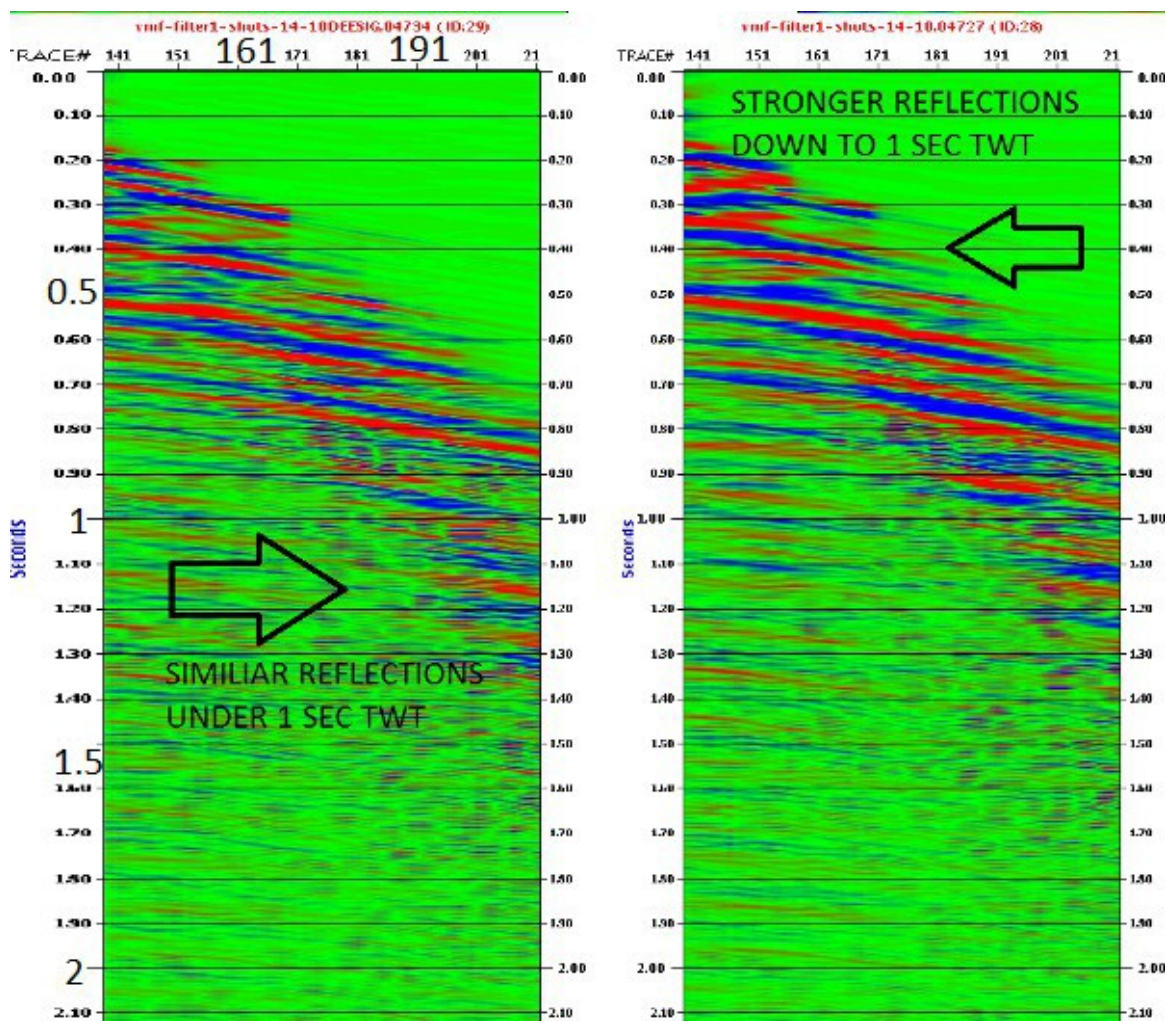


Fig 5.8: Two figures of a shot gather are shown. The picture to the right shows a shot gather with the DESIG module applied and the picture to the left shows a picture where the DESIG module is not used. The arrows show the areas of enhanced signal/noise ratio.

5.3.3 Spherical Spreading Correction.

Before the module for spherical spreading module was applied, a module which removes incoherent noise was used. The Spherical Spreading Correction is used because of loss of energy from a waveform as a consequence of geometrical spreading. This is observed as a decrease in wave amplitude. Figure 5.9 shows how the amplitude of deeper events is restored with the use of this correction.

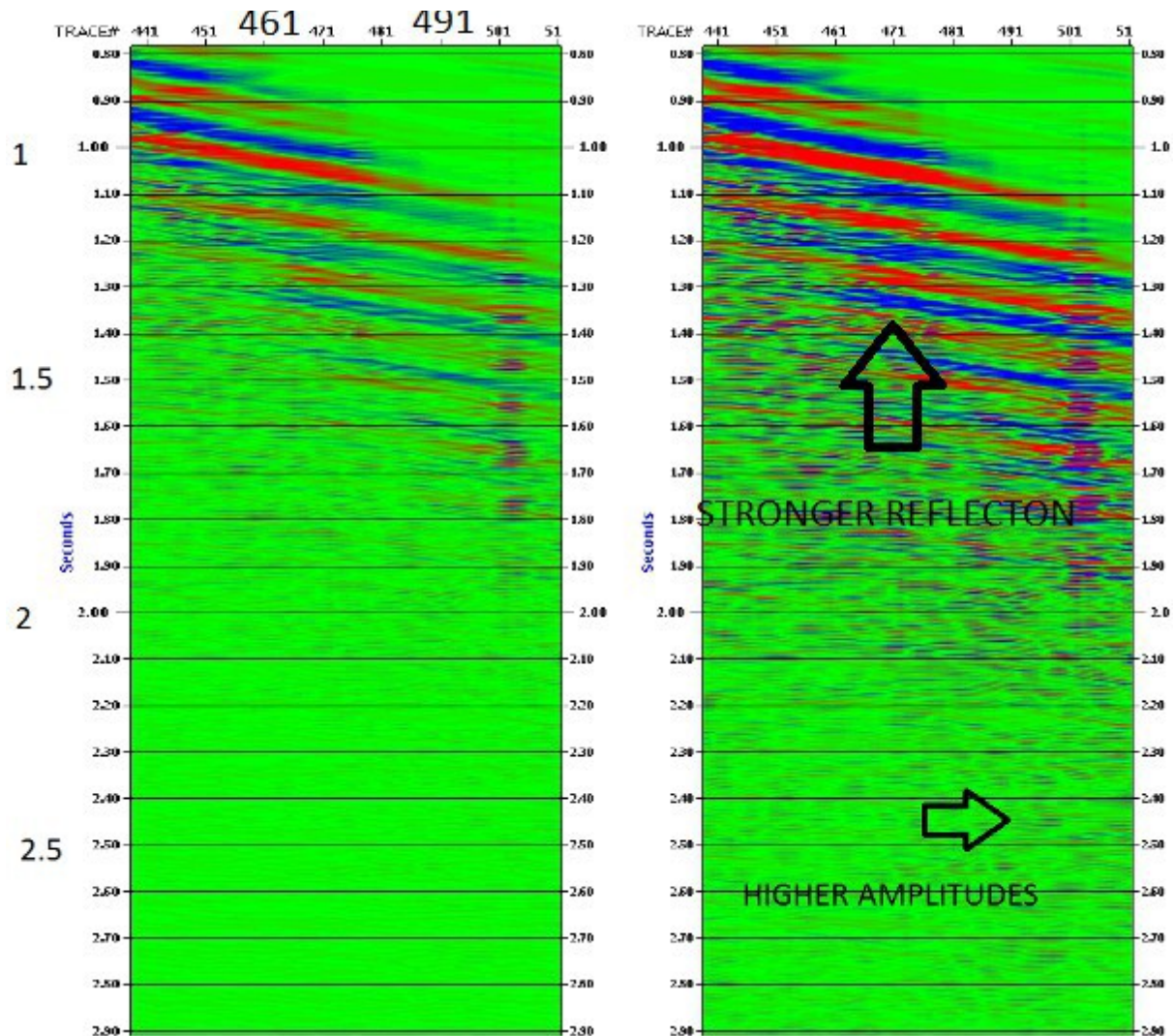


Fig 5.9: Two figures of a shot gather. The picture to the left shows a shot gather without spherical spreading correction and the picture to the right shows the recovered amplitude of the deeper reflections. The arrow points out the section where the enhanced amplitude increase is best.

5.3.4 Spatial Amplitude Smoothing.

The aim of Spatial Amplitude Smoothing is to equalize an input seismic trace with respect to its NC-1 neighboring traces. NC is the user defined number of input traces considered for amplitude comparisons (Spatial Window). The result is that the amplitudes are smoothed. The amplitude of the window center is multiplied by the coefficient M/m where M is the median or average amplitude and m is the amplitude value at the considered trace. This means that the amplitude at the window center is replaced by the median or average of the neighboring traces. The length of the spatial window is set to 11. This is the number of traces used for amplitude comparisons and smoothing. For a given input trace the program computes the average amplitude for the NC neighboring traces. The length of the window used for amplitude comparison is set to 500. MOT is set to 2, which means that processing is performed until this value changes. By looking at figure 5.10 no big changes is seen at first. The figure to the left is shown without SPASM applied and on the figure to the right SPASM is applied. By comparing different cross points on the figure it can be seen that different color and shapes appear on the different figures for the same cross point. One example is for trace number 71 at TWT=0.7 seconds. For the figure where SPASM is applied, this point corresponds to the top of a bright red reflector, whereas when SPASM is not applied this point corresponds to a blue reflector. It is clear that the amplitudes have been smoothed, but reflectors do not appear much brighter and clearer.

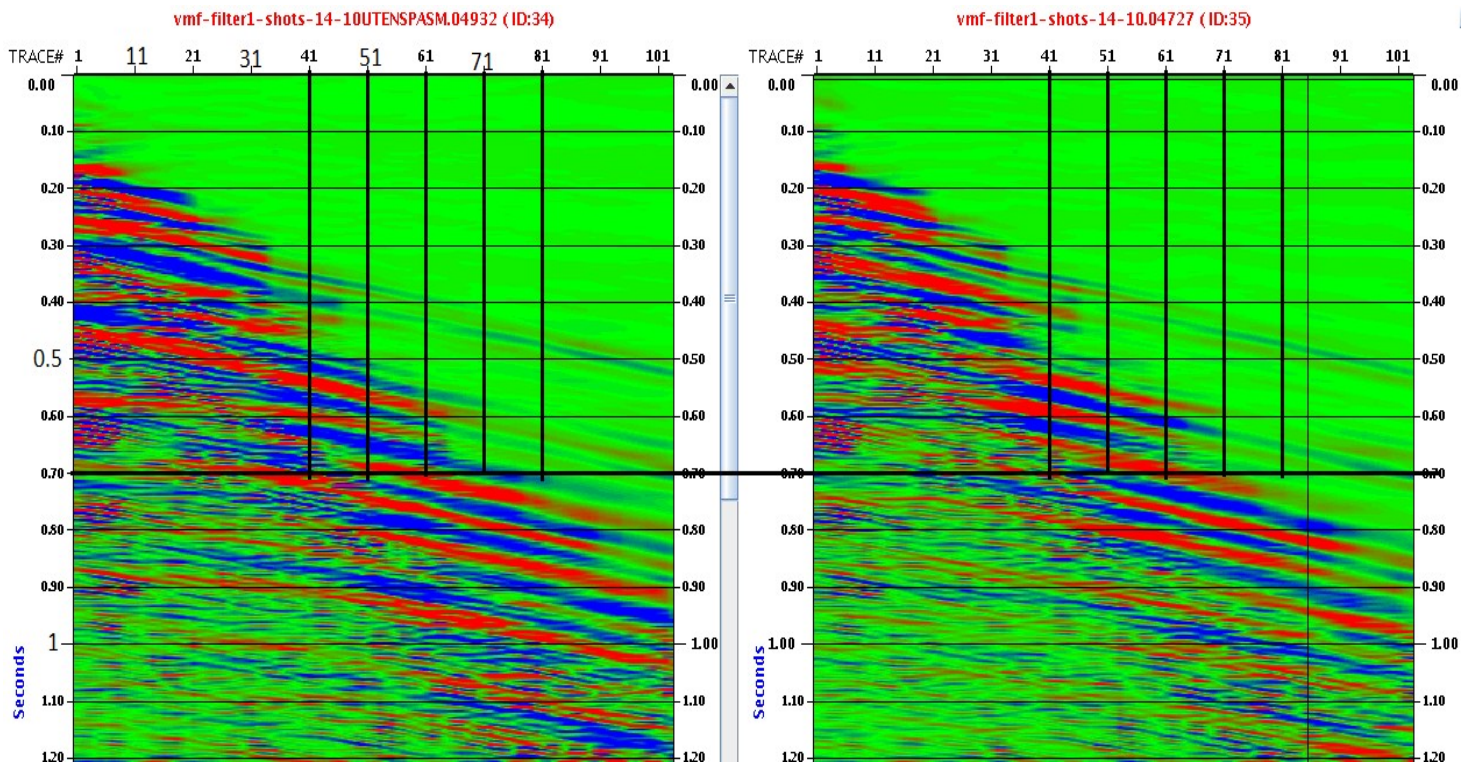


Fig 5.10: Shows the effect of SPASM module. On the figure to the right SPASM is applied.

5.3.5 Velocity Filtering (F-K) Filtering.

The theory of F-K filtering is given in 3.2.6. F-K filtering is a two dimensional filter, operating in the frequency-wavenumber domain. This filter passes or rejects data based on apparent velocity or dip. The velocity of the wave propagating along seabed in Van Mijenfjorden is estimated to be over 4000 m/s. Arrivals at lower speeds below are multiples, since they must have propagated only in the water layer. Figure 5.12 shows a plot of a fk analysis. The dip end dissipates out to the left and is folded back in the right part of the fk plot. This is due to spatial aliasing. This part is filtered away because the velocities here are higher than the upper filter limit which is defined to + 10000m/s. The velocity filter was designed such that linear events (refracted and direct waves) are attenuated.

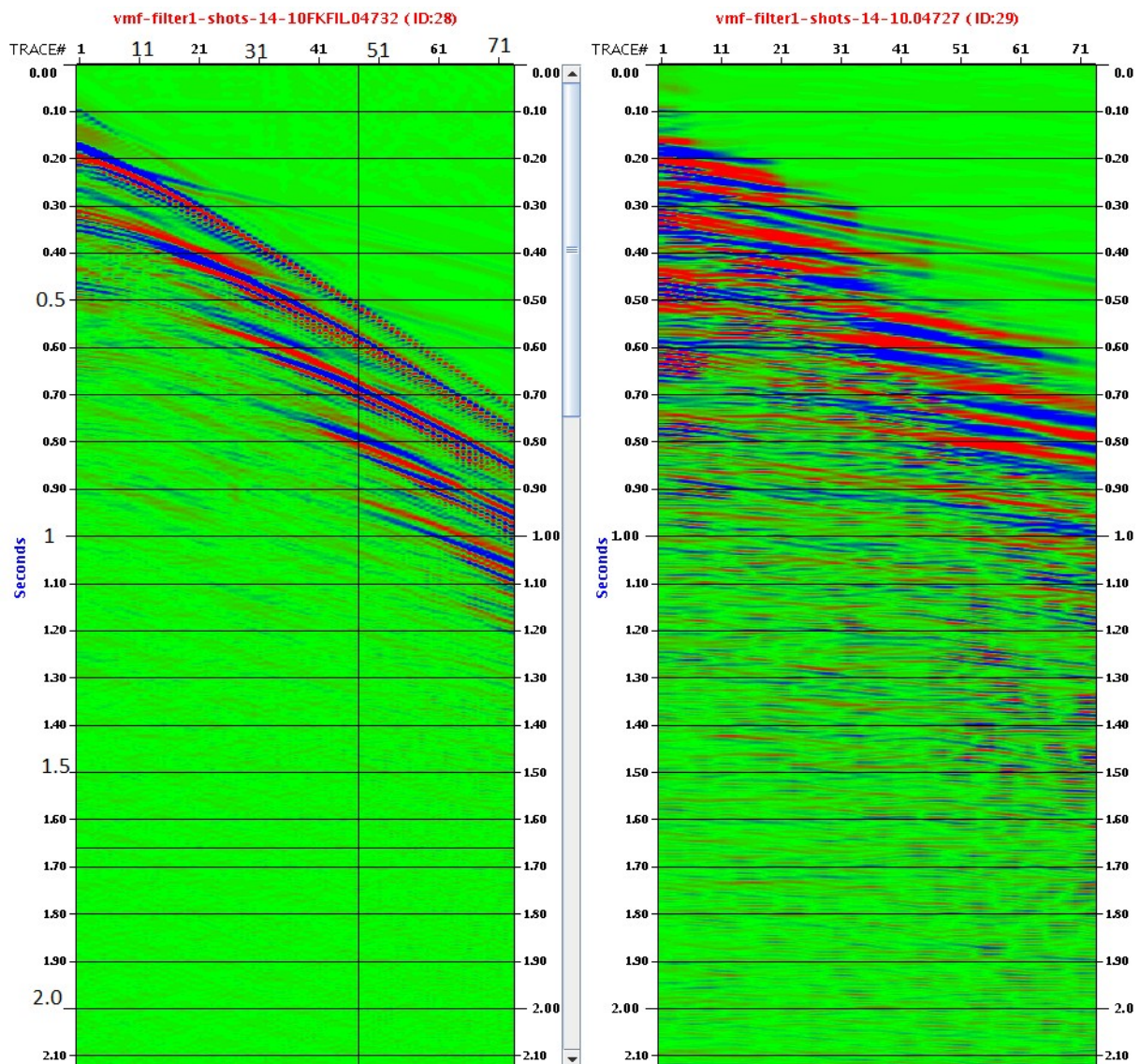


Fig 5.11: The figure to the right shows a shot gather with velocity filtering applied.

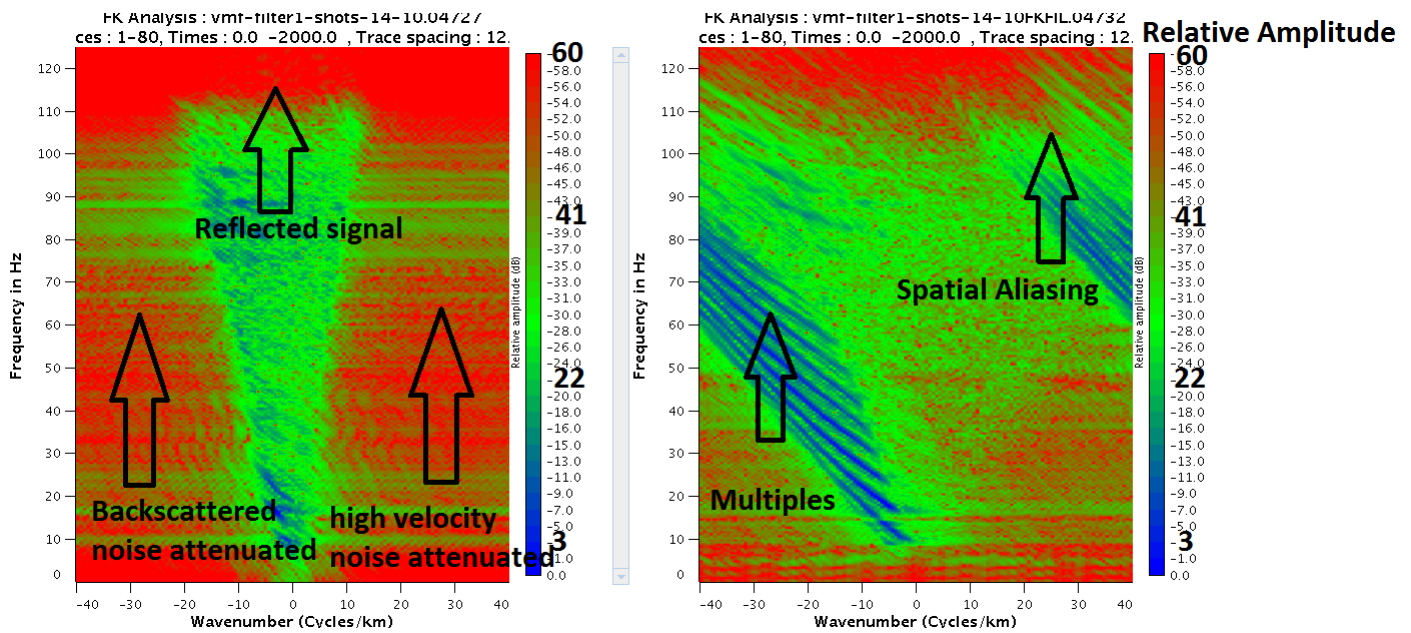


Fig 5.12: The Figure to the right shows FK analysis the shot gather without using velocity filtering. The figure to the left shows FK analysis of a shot gather where velocity filtering has been used.

Choosing the velocities to be filtered was determined at this step. It is known that multiples have lower velocities than primary reflections at the same record times because velocity increases with depth. Therefore it is necessary to check if reflectors appeared stronger by allowing lower apparent velocities. The velocity filter A has $v_1=-4000\text{m/s}$ $v_2=-5000\text{m/s}$ $v_3=8000\text{m/s}$ $v_4=10000\text{m/s}$. Velocity filter B has $v_1=-5000\text{m/s}$, $v_2=-6000\text{m/s}$, $v_3=8000\text{ m/s}$, $v_4=10000\text{m/s}$. Velocity filter C has $v_1=-6000\text{m/s}$, $v_2=-7000\text{m/s}$, $v_3=8000\text{m/s}$, $v_4=1000\text{m/s}$. The result shows that the reflections appear stronger by lower apparent velocities and weaker by allowing higher apparent velocities. The seismic velocities used further are the velocity from filter B. The reason for this is to be sure that as much multiples as possible is attenuated during processing. When these velocities are transformed into the frequency-wavenumber domain, the different areas in Fig 5.13 show which areas passes through.

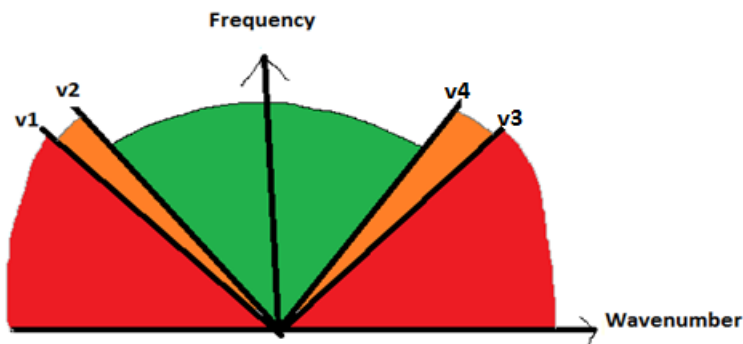


Fig 5.13: The figure shows which velocities passes (green) has interpolation filter applied (orange) And gets rejected red.

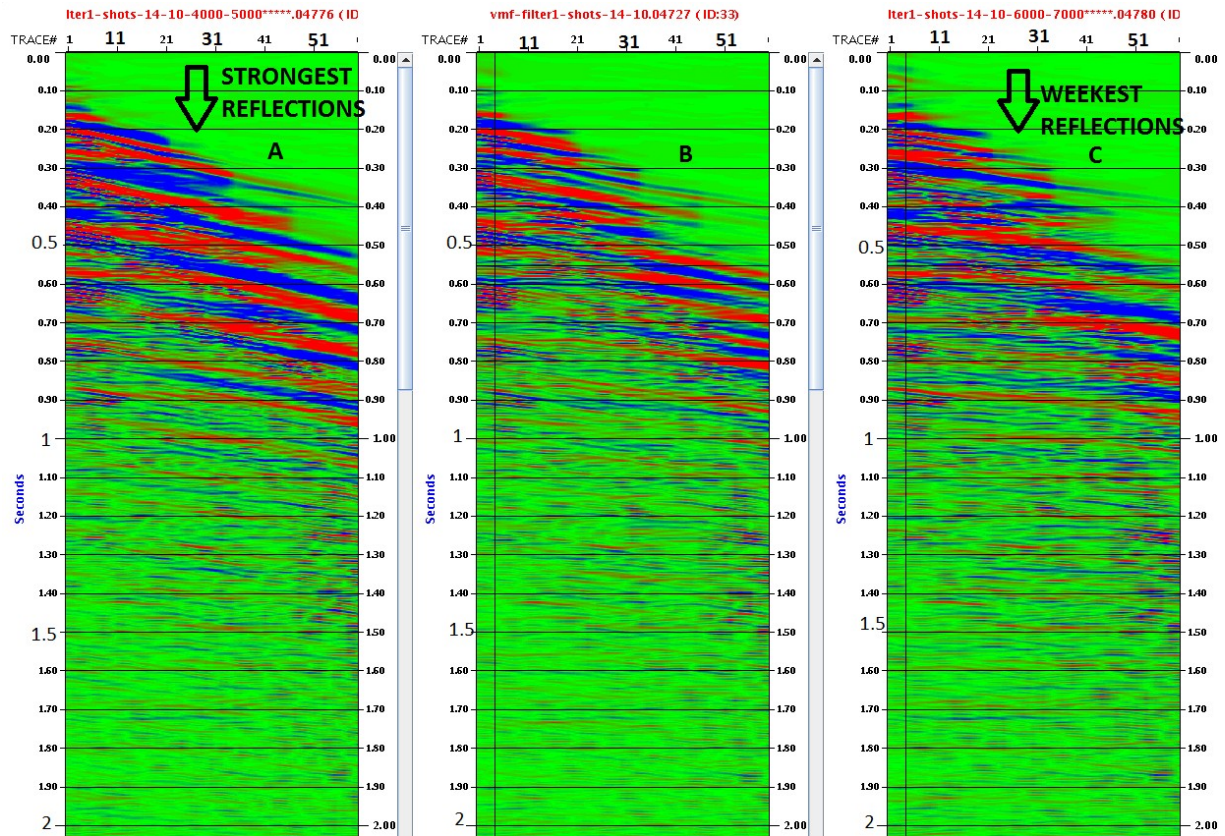


Figure 5.14: shows that reflectors appear stronger when lower velocities are allowed.

5.4 Filter 2

As in every other job, the next job used the previous job as an input. To do this, a number «Single cartridge/C» has to be set. This is done in the OUTBD module. This number corresponds to the output number of a job and is used further as an input in the INPTR module at the beginning of a job. In filter 2 job, further modules are applied to make the seismic better. The seismic are sorted to receiver gathers first. This means that one could get all the shots together in an increasing shot position, belonging to one receiver position. Then a velocity filter is applied before the data are sorted to a CMP gather. Here all traces with the same midpoint are grouped together. The sorting is done in a module called BSORT; both sorting to receiver gather and cmp gather are done in this module. At the end amplitude recovery and surface consistence deconvolution is done.

5.4.1 RESULTS OF FK FILTERING IN FILTER 2 JOB

Velocity filtering with different band pass filters as in filter 1 job was applied here. The results are shown in figure 5.15

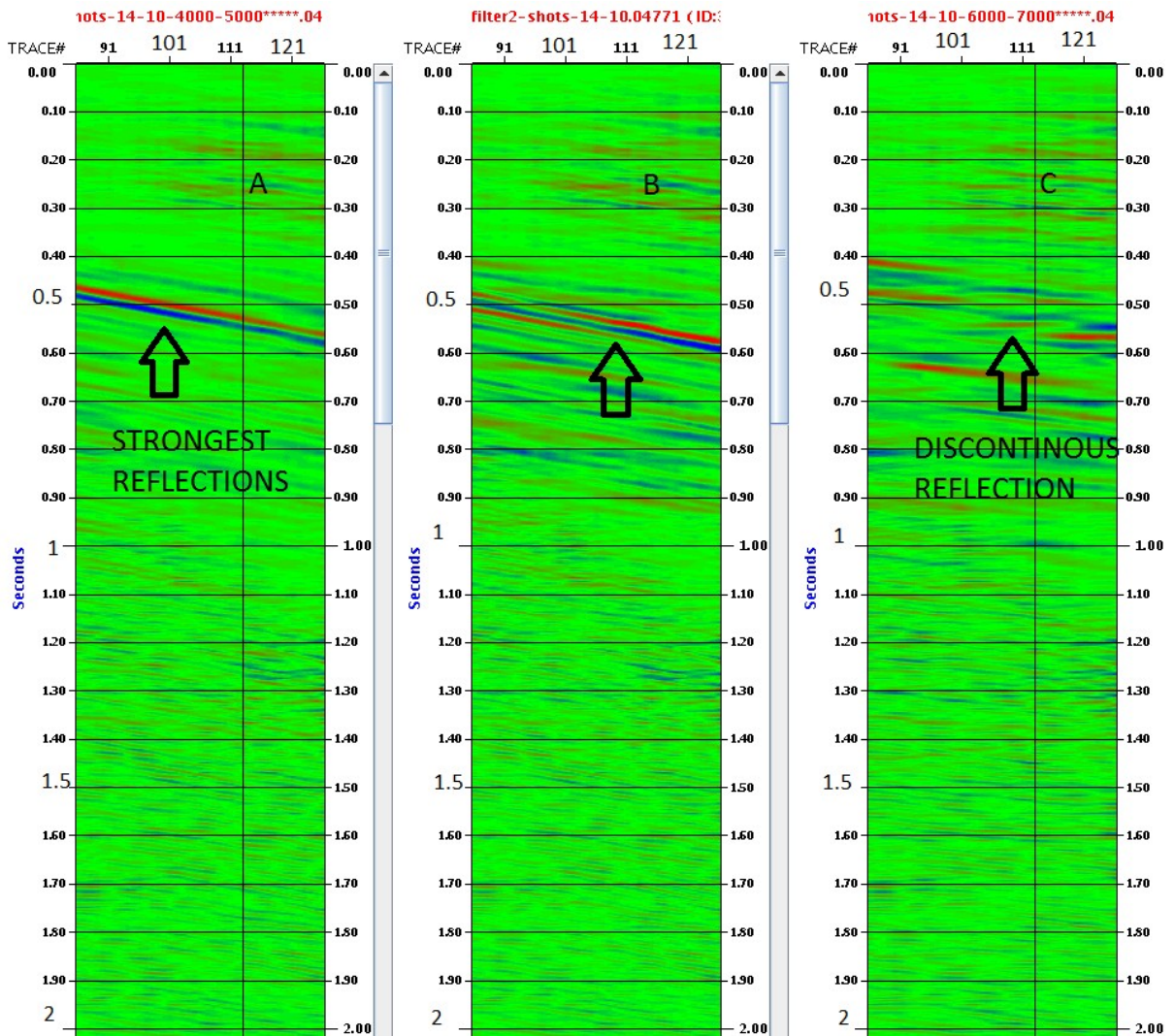


Figure 5.15: The figure shows that by allowing lower velocities stronger reflections appear. These are most likely multiples, since they have lower velocities than primaries.

5.4.2 Amplitude Recovery

“Amplitude Recovery compensates for attenuation, spherical divergence and other effects by adjusting the amplitude of the data. The goal is to get the data to a state where the reflection amplitude relate directly to the change in rock properties giving rise to them “ quote (Schlumberger , Glossary 2010).

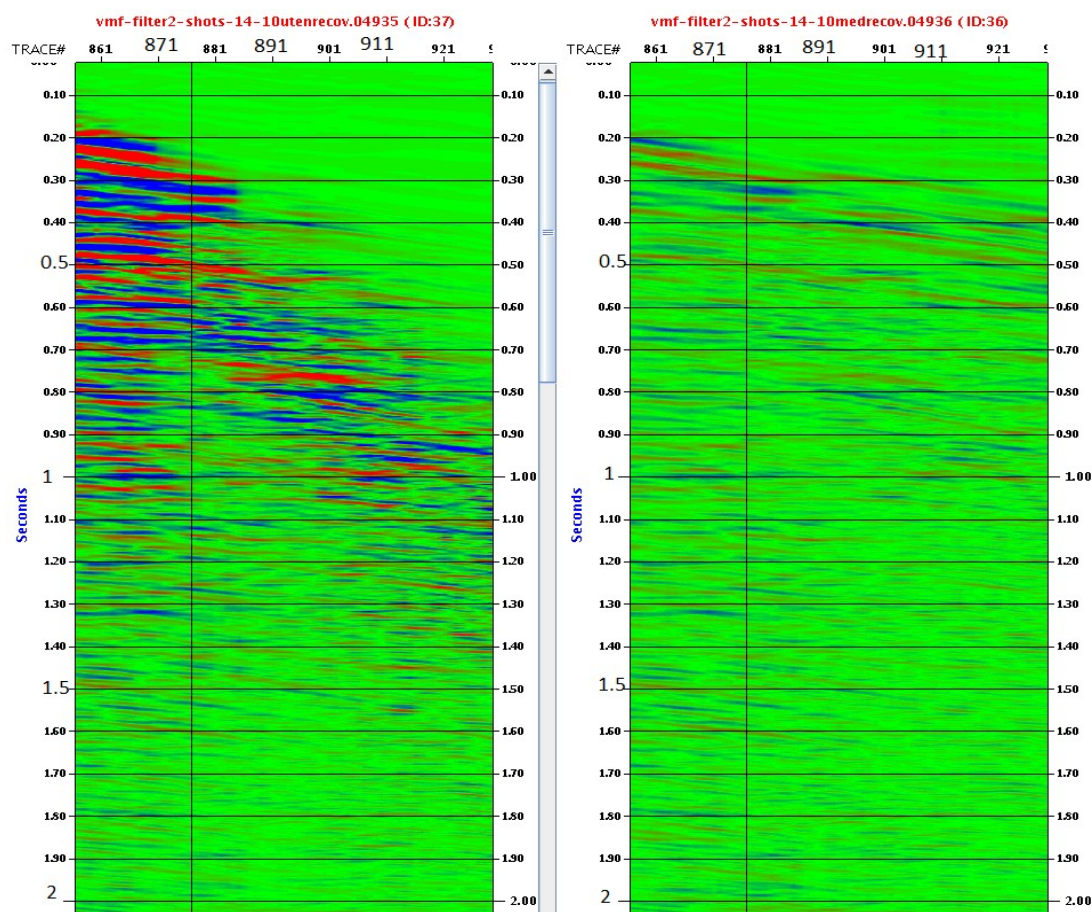


Figure 5.16: The picture to the right shows a seismic section after amplitude recovery

5.4.3 Surface Consistent Predictive Deconvolution.

Surface consistent deconvolution is based on the concept that a seismic wavelet can be broken down into its source, receiver, offset and CDP components. The seismic wavelet itself is considered as a convolution of a source signal with hydrophones and the response of the earth. The earth response includes some undesirable effects, such as reverberations, and ghosting. The objective is to cancel out these effects. The deconvolution is performed in two phases. The first phase is filter estimation, and the second phase is deconvolution of raw traces. Filters used are mean filter, receiver filter, shot-point filter and, - offset filter. Figure 5.17 shows that by applying the module DECSC reverberations are attenuated. Reverberations are rays that are repeatedly reflected at the sea bed and sea surface.

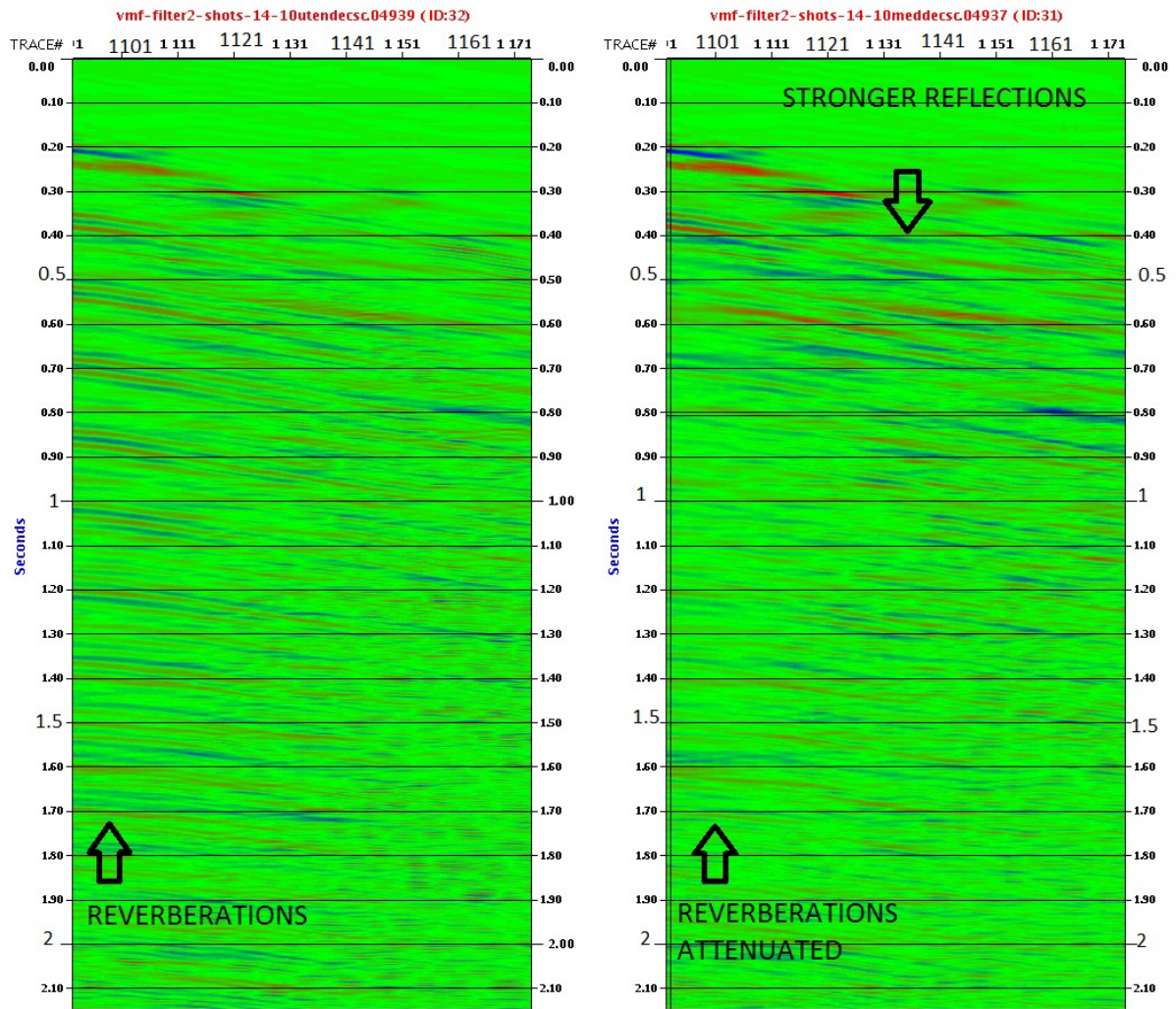


Fig 5.17: Shows the effect of Surface consistent deconvolution has on a seismic gather.

5.5 Velocity Analysis

Individual velocity analysis has been done for every seismic line. The stacking velocities are picked in a velocity spectrum window in Chronovista. Here peaks or anomalies of contoured semblance values are found. The velocities are picked for every 400 CDP (2.5 km).

Figure 5.18 shows from left : 1) a velocity spectrum with contoured semblance values showed with brighter anomalies. 2) Interval velocities, interval velocity are around 4000m/s in the upper part and increases to around 5000m/s in deeper parts. 3) CDP gather before and after NMO correction. The velocities picked in the velocity spectrum flattens the hyperbola. The mini-stack shows the pattern of velocities increasing or decreasing. As shown in figure 5.18, a frequency distortion occurs after NMO correction. Frequency distortions occur, particularly for shallow events and at large offsets. The waveform with a dominant period T is stretched so that its period T_0 after NMO correction is greater than T . Stretching is a frequency distortion in which events are shifted to lower frequencies.

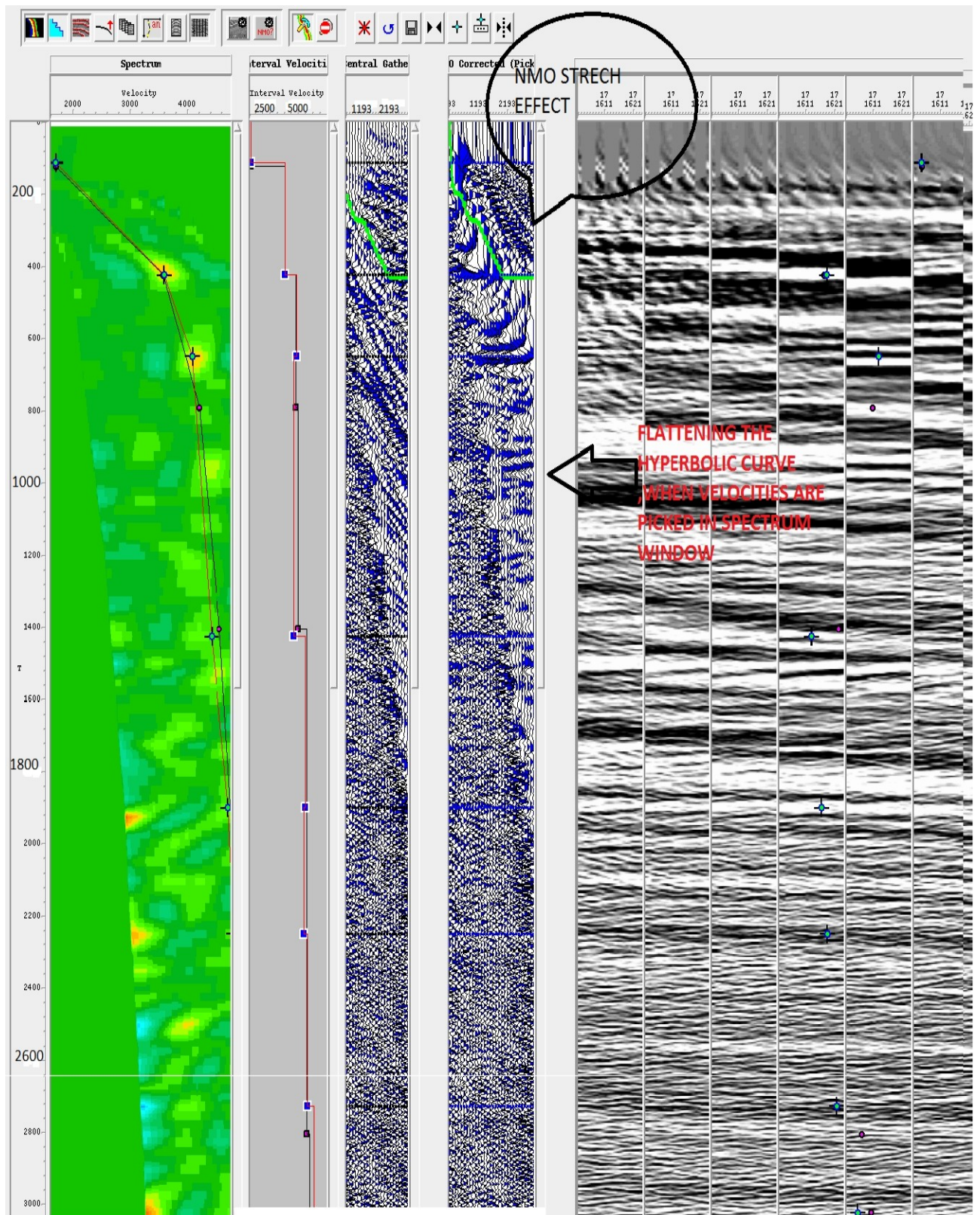


Fig 5.18: The Figure shows from left: the velocity spectrum, interval velocities, cdp gather before nmo, cdp gather after nmo and mini stacks.

5.6 Migration

The first job in the migration job is MUTAN-This module mutes input seismic traces using incidence angle as the criterion for the mute. The incidence angles are calculated using the straight-ray method. This method assumes that the event of interest is a flat interface with one layer above it, characterized by average velocity. Figure 5.19 shows a migration job with two different cases of incident muting angles. Fig 5.19 A shows MUTAN with minimum muting angle/ANGMIM=0 and maximum muting angle/ANGMAX=40. Figure 5.19 B shows with minimum muting angle/ANGMIM=20 and maximum muting angle/ANGMAX=40. The results show that for case A stronger reflections appear under 1 sec twt, but weaker reflections appear above 1 sec twt compared to figure B. Also other values for ANGMIN and ANGMAX were tried. By setting AGMIN 0 and ANGMAX 80 reflections become more transparent under 1.20 sec TWT and is not a good choice for mapping deeper seismic events. For interpreting down to 1 sec TWT the best choice would be to set ANGMIN=30 and ANGMAX=40 but as a downside, no reflections under this time is mapped. It was also tried to put ANGMIN=40 and ANGMAX=60 this mapped only the uppermost 0.6 sec TWT in the middle of the basin with some chaotic seismic characteristics. The values which are used for further processing is ANGMIN=0 and ANGMAX=40 since this gives the best picture overall.

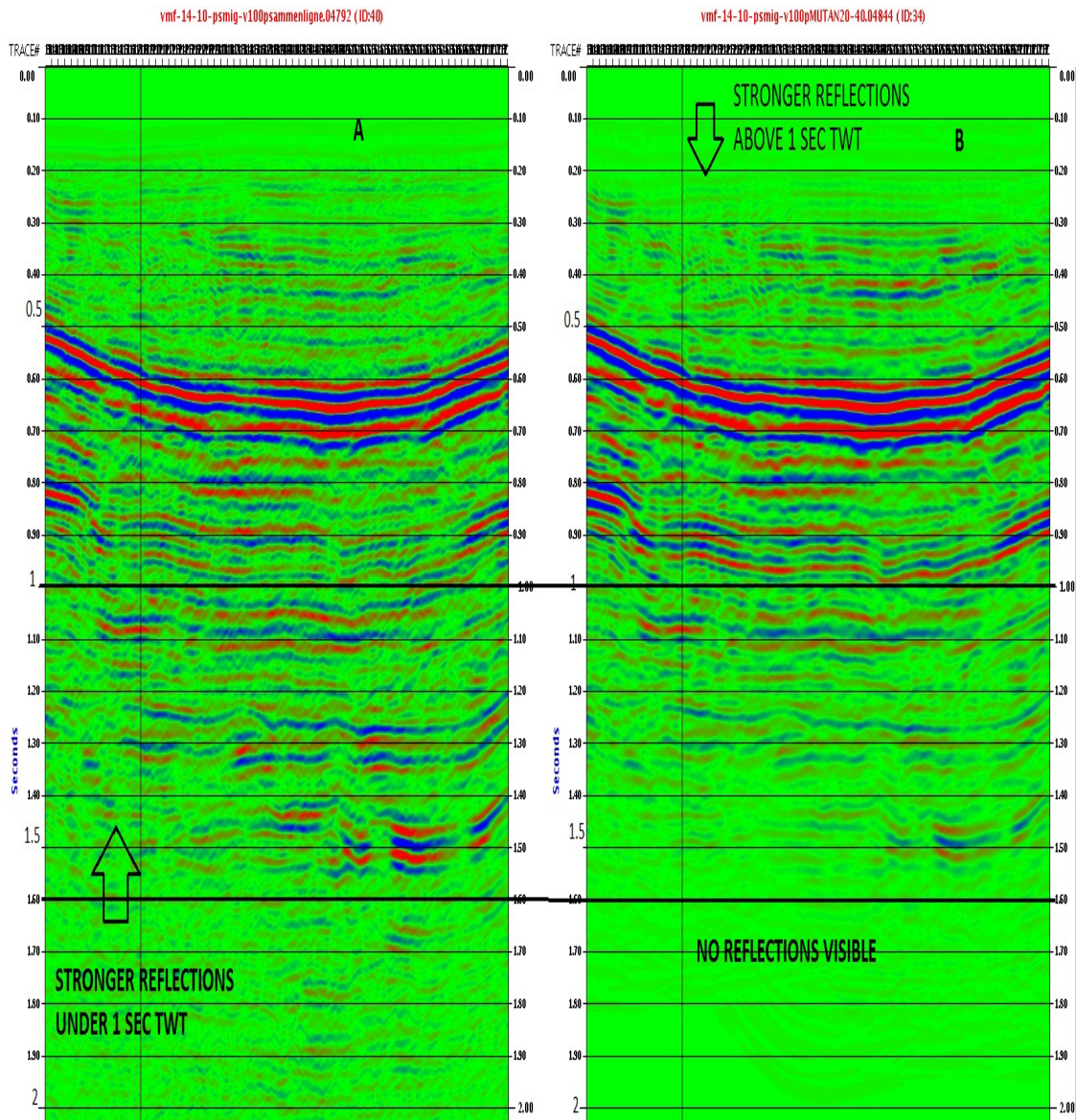


Fig 5.19: In figure A $ANGMIN=0$, $ANGMAX=40$. In figure B $ANGMIN=20$, $ANGMAX=40$.

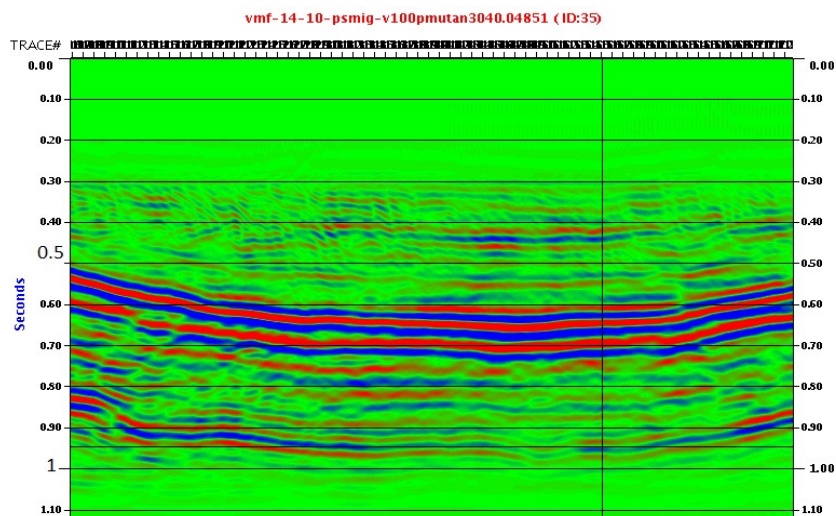


Fig5.20: In this figure $ANGMIN=30$ and $ANGMAX=40$

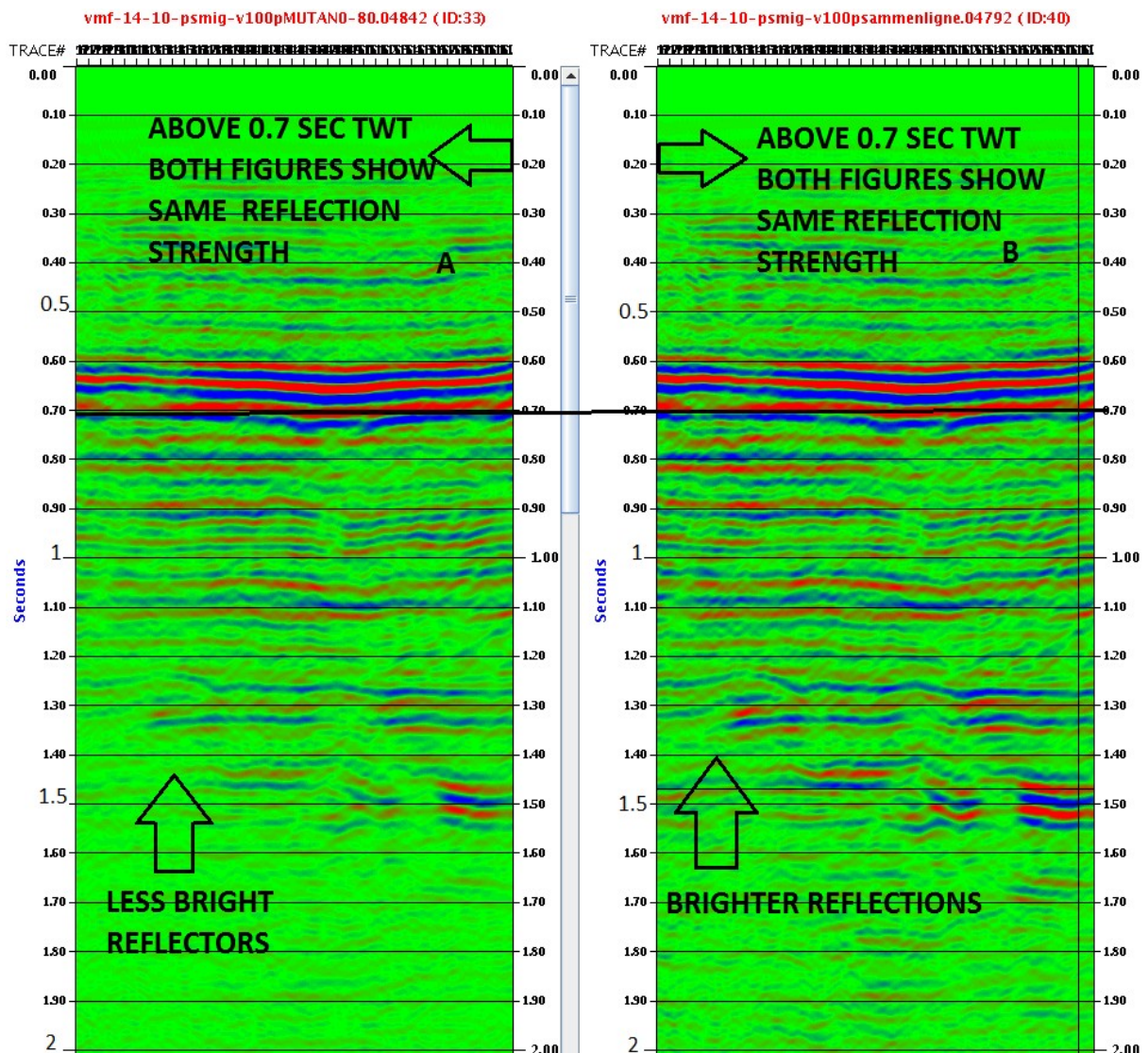


Figure 5.21: In figure A ANGMIN=0, ANGMAX=80. In figure B ANGMIN=0, ANGMAX=40

5.6.1 Kirchhoff Time Migration

Before Pre-stack time migration was performed, internal mute from water depth and 3D-2D scaling was performed. The internal mute from water depth uses a function defined by LIBRI MU to mute traces. The internal mute samples between the times defined in LIBRI MU and the end of the trace is zeroed. In the 2D-scaling an amplitude multiplication by $(T/250)^n$ is performed. T is the time of the sample in milliseconds and- n is chosen to be -0.5. This number can be chosen to be integer or real number, positive and negative.

TIKIM performs a Kirchhoff time migration for pre-stack 2D data. The Kirchhoff

algorithm is a trace by trace migration, which treats each output sample as the apex of a diffraction curve. Input samples are summed or spread along the diffraction curve, which is characterized by a locally defined 1D RMS velocity function. The reflector image is thus built by constructive interference. In this module different dip limits were chosen to evaluate which value gives the best image. Any value greater than the dip limit is muted.

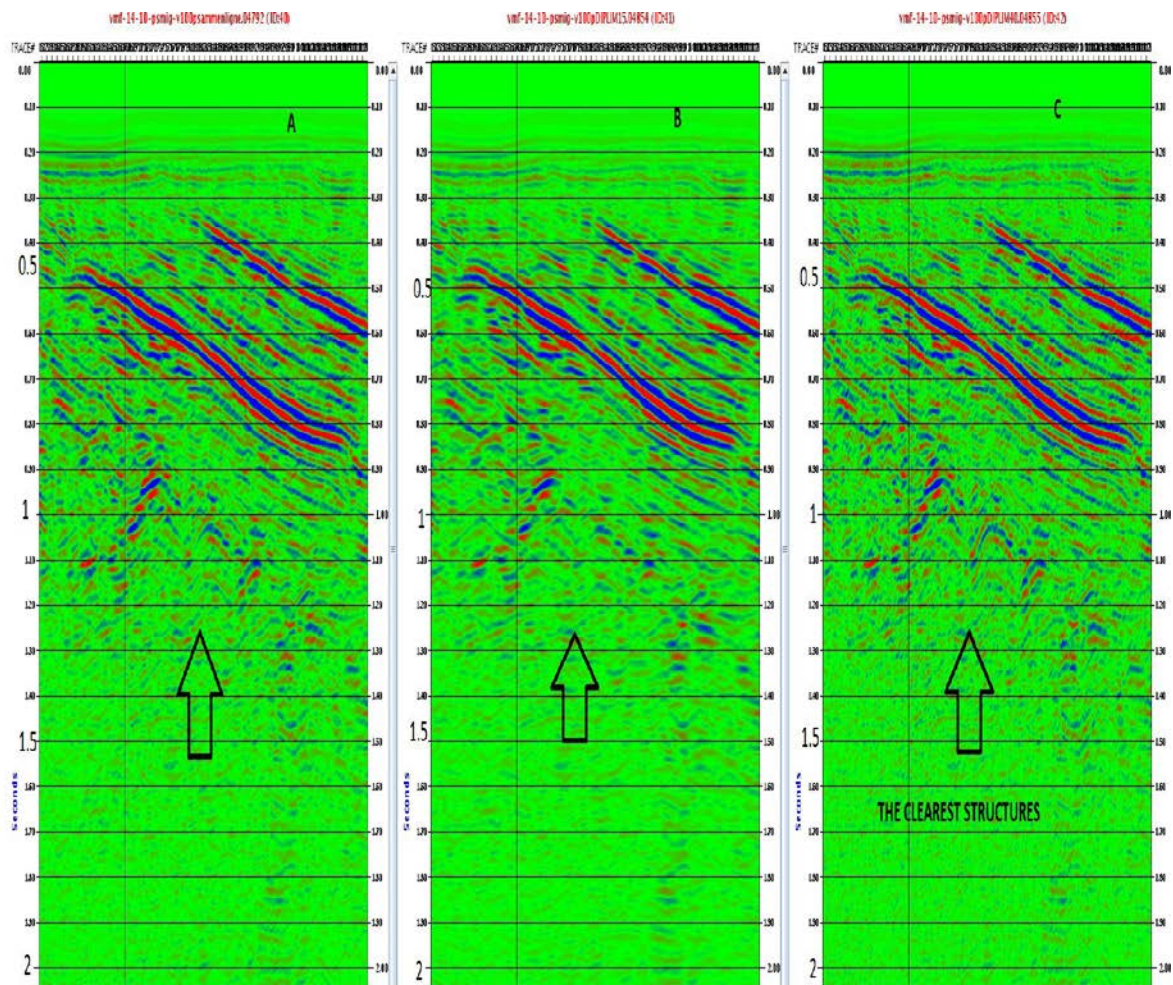


Figure 5.22: Figure A shows a DIPLIM limit of 25, B 15 and C 40. The structures were best visible with a dip limit of 40.

5.6.2 Processing the problematic area in the west

A problem in the processing is the area west of the main syncline. This area is hard to get well processed due to the presence of high dips and much folding and complex structures. The structures marked by the arrow in fig 5.23 is an area of interest for improved processing. If a dip limit under 25 was chosen these would not have appeared. As shown in fig 5.22 a dip limit of 40 gave the best picture of these structures in this area. Still these structures are not well visible. By setting maximum frequency on input to

25 Hz and using High resolution /Hr both application found in the TIKIM module a different picture of these structures are found. In HR optimal filters are used to control aliasing resulting in improved preservation of steeper dips, a reduction in high frequency noise, and a better preservation of the input signal. A problem with this is that by setting the maximum frequency on input to 25 Hz, all frequency above 25 Hz will be filtered, and as a consequence deeper events than 1,5 sec twt will not be seen at all. In the normal case the normal frequency on input is set to 100 Hz. This wider bandwidth will improve imaging of the deeper events, but if this area has much high frequency noise it will mask the primary reflections. This problem will be minimized by setting a lower value on the maximum frequency on the input data. However by setting a low frequency on input reduces the resolution and may provide an incorrect picture of the subsurface. When this picture was put into petrel, the reflectors seemed more discontinuous and it looked like many faults appeared. This was generally not the case when the input frequency was set to 100 Hz.

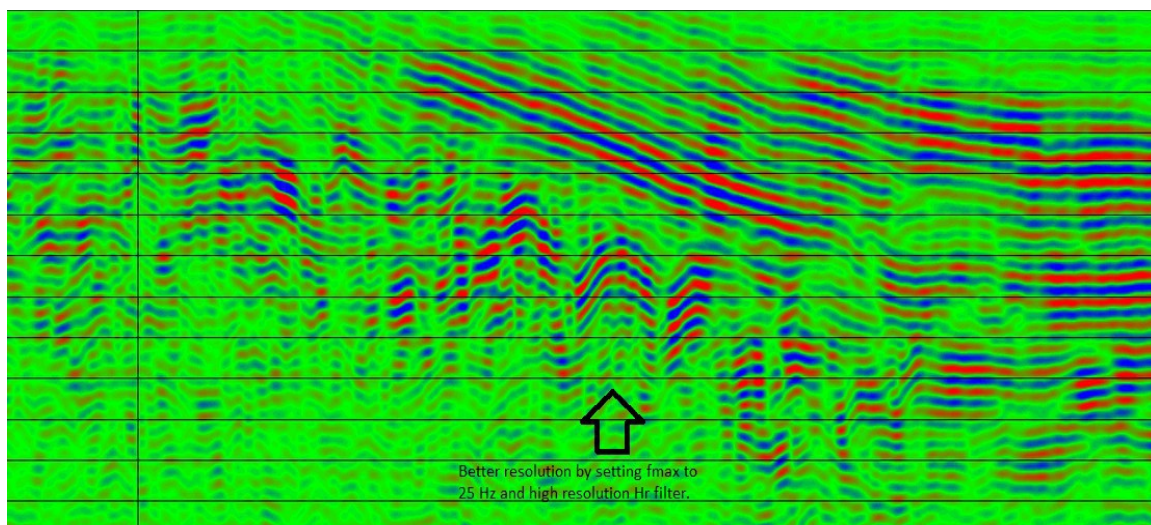


Figure 5.23 Structures in the western area appeared more visible when using maximum frequency on input data=25 Hz, high resolution/Hr and DIPLIM=40. However the maximum frequency on input data=25 Hz may have provided a wrong picture of the subsurface due to poorer resolution.

5.6.3 Time Variant Bandpass filter

Time Variant filters is used to suppress noise existing outside the frequency spectrum of the desired signal. As a result the signal.to-noise ratio is increased. The filter is necessary because the frequency of primary reflected seismic signals decreases with time, due to absorptions of higher frequencies. The bandpass filter applied is shown in the table 5.4. The filter is not defined at all intervals. In the transition zone between two filters the program performs a linear interpolation which result is a sum weighted as a function of the CDP position relative to the

two filters. This filter was also constructed for the purpose of removing low frequencies in the upper part. As stated in chapter 3.2.8, lower frequencies in the upper part are due to a frequency distortion which occurs after NMO correction where events are shifted to lower frequencies. Figure 5.24 shows that the stretch factor for the shallowest events is highly reduced after filtering these frequencies.

Window (ms) in TWT	Lower and Upper frequency limits (Hz)
0-300 ms	15-25,80-100 Hz
600-900 ms	10-25,65-85 Hz
1200-1700 ms	7.5-15,50-70 Hz
>1700	7.5-15,40-60 Hz

Table 5.4: Values used in the bandpass filter.

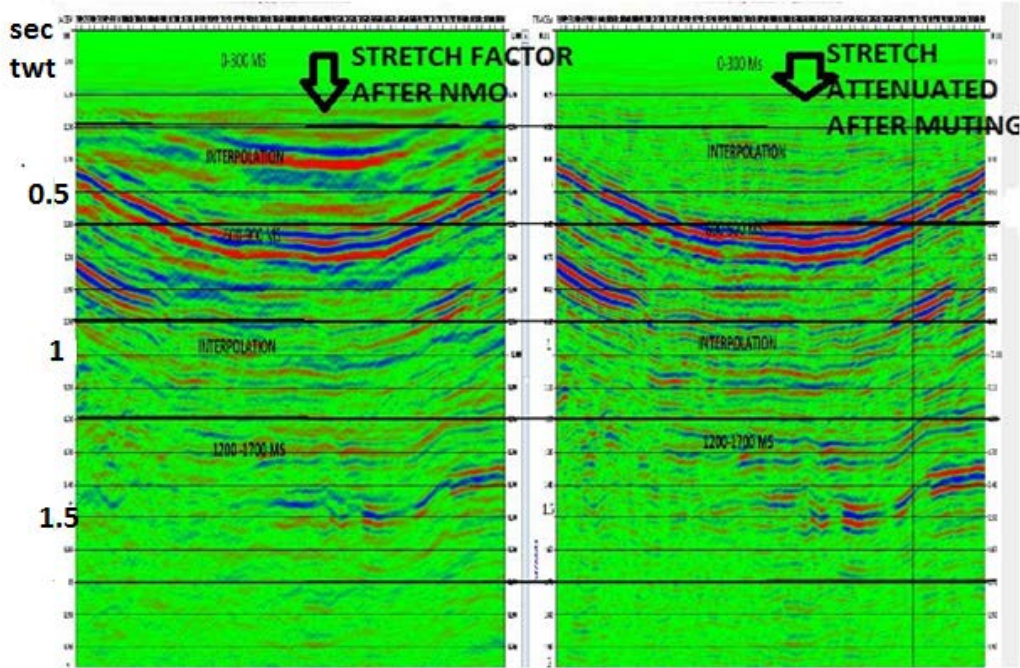


Figure 5.24. Shows the effect of a time variant bandpass filter. The filter is used on the seismic section to the right.

5.6.4 Adjusted velocities

On the end of the migration job different datasets with velocities corresponding to 90 % velocity, 95, 100,105 and 110 % were displayed. These velocities are adjusted velocities from the velocity analysis. By looking at the depth and CDP number the best reflections were picked. The adjusted velocities were further adjusted in the velocity analysis in order to optimize the seismic reflections

5.7 POSTSTACK PROCESSING

The normal post-stack job done does not apply the modules FKFIL, TRITA, TVDEF (Spectral balancing). These jobs are later turned off and on to check the effect the module have on the seismic. The other modules RECOV, PFILT, TVDEF (time variant bandpass) are checked for their effect. The first module in this job is MNGTY. This program manages traces that belong to the same group defined by the Y-flag. FK filtering was tried but no changes was possible to notice. The reason for this could be that FK filtering is done both in the filter 1 job and filter 2 job. No further filtering was thus needed. TRITA performs a time variant predictive deconvolution. The aim is generally to attenuate long period multiples. The results were poor as shown in the figure 5.25. The reason is that the method flattens out the frequency spectrum and as a result noise is strengthened in areas of low energy (Bent Ole Ruud)

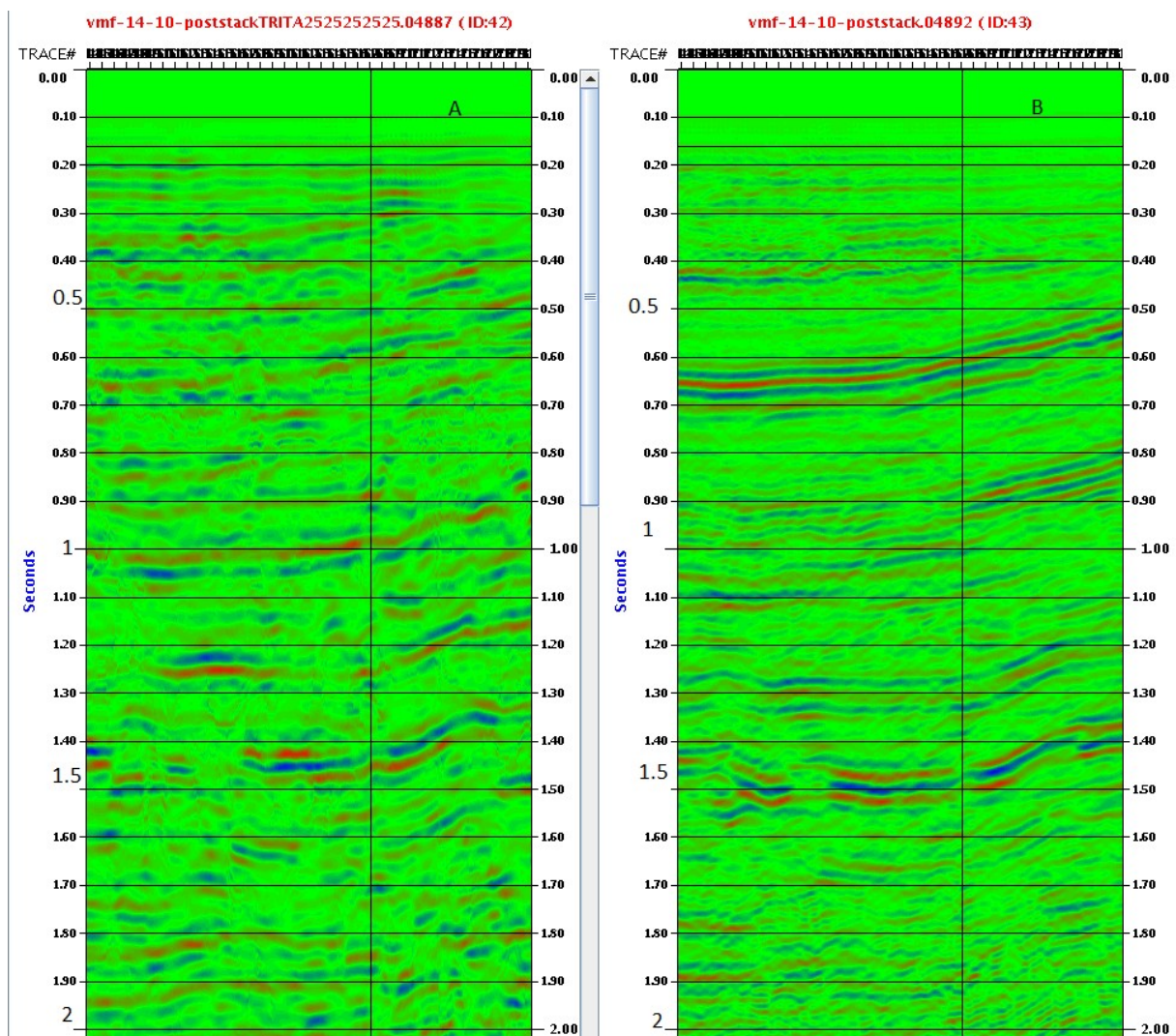


Figure 5.25 A shows a poststack where predictive deconvolution is applied. Picture B shows a case where no predictive deconvolution is applied.

RECOV performs amplitude recovery- , where the goal is to get the data to a state where the reflections amplitude relate directly to the change in rock properties giving rise to them (Glossary 2010).By looking at the figure 5.26 reflections under 1.6 sec twt would not have been visible/very transparent without applying RECOV in this stage of the processing. This method is statistical where the amplitude is related to the Reflection Coefficient (Bent Ole Ruud)

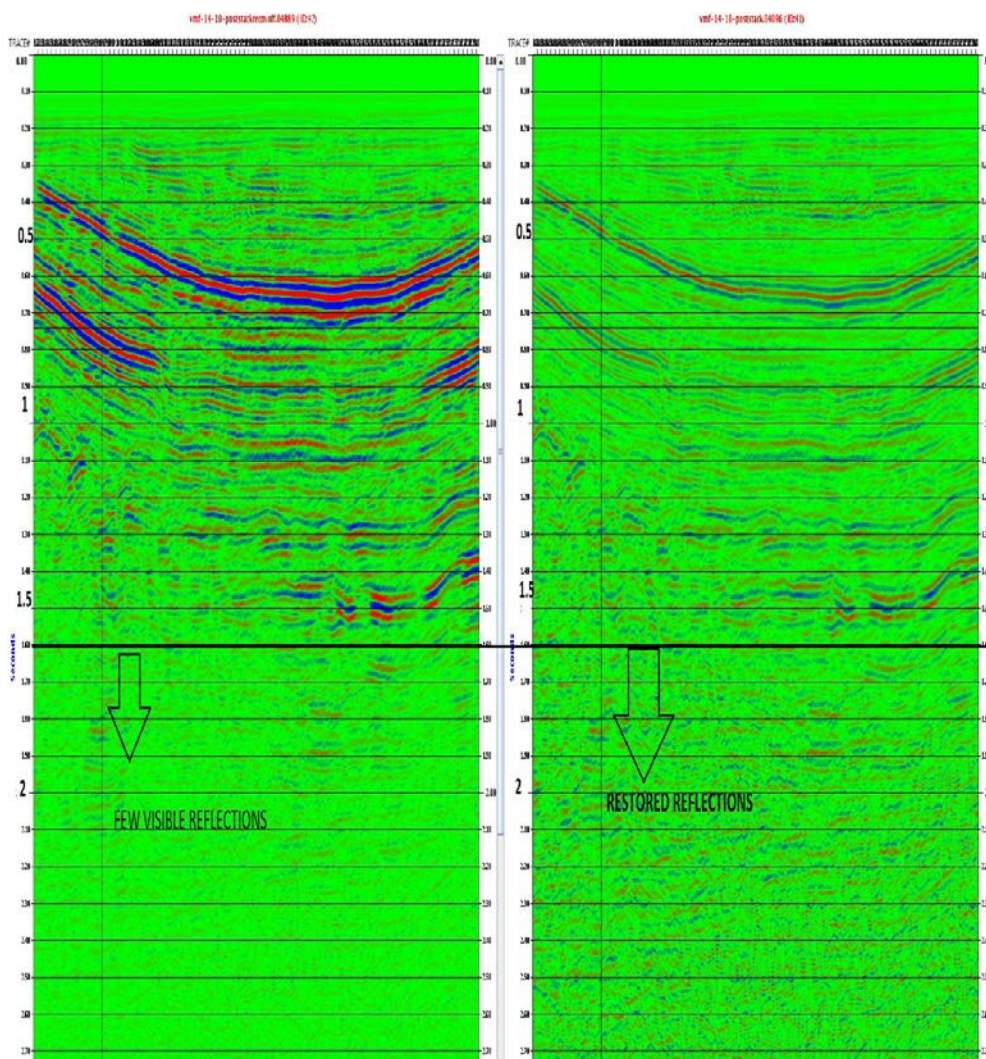


Figure 5.26: The figure shows the effect on RECOV- , the left picture has Recov applied and on the right picture no RECOV is applied.

PFILT uses a phase shift filter to convert data from mixed phase to zero phase, a phase shift of 20 degrees is used (Bent Ole Ruud).

In the zero phase the wavelet is symmetrical with a maximum at time zero. The fact that energy arrives before time zero is not physically realizable but the wavelet is useful for increased ease of picking reflection events.

Spectral balancing (TVDEF module) was tried. The objective of spectral balancing is to boost the frequencies to obtain perfect resolution. In theory this could be obtained, in practice it would likely result in the boosting of noise at low and high frequencies.

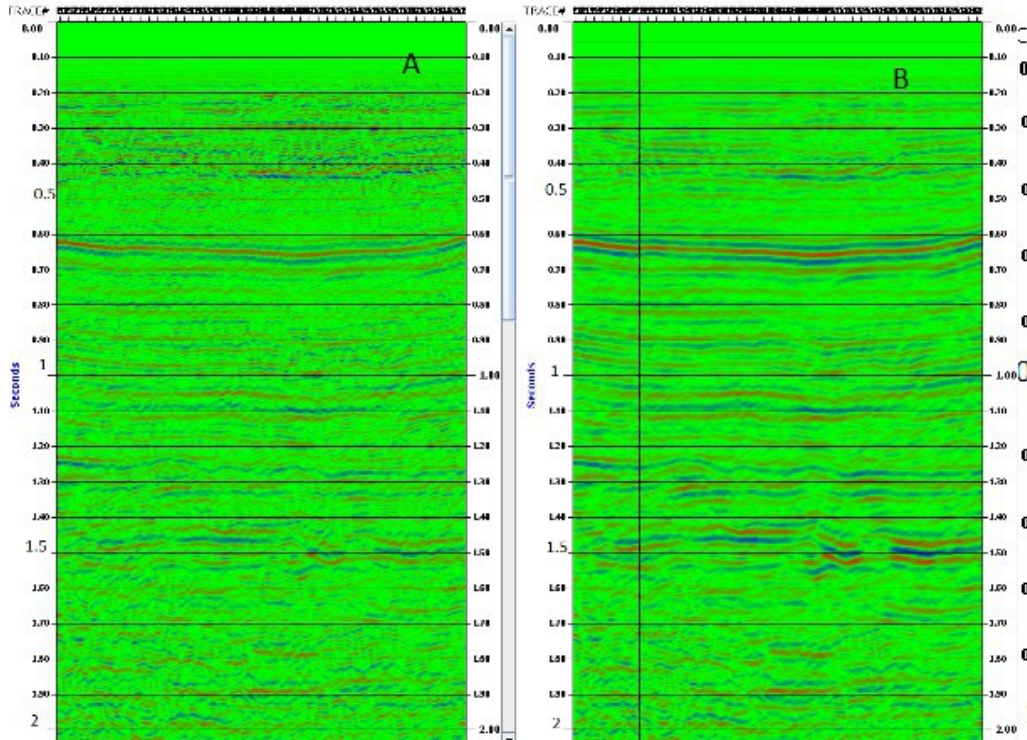


Fig 5.27: The result of spectral balancing. Picture A has spectral balancing applied. The result is that the data looks noisy. This is because high frequency noise is boosted and not the signal.

An FK analysis was performed to see the difference in this domain. Figure A on Figure 5.27 has more higher frequency signals with higher relative amplitude compared to Figure B on figure 5.27. According to Fig 5.28 no frequencies under 12 Hz are present this is because a low cut filter of 12 Hz is used. Also no frequencies over 80 Hz is present. This is not a cause of the high cut filter, since the limit is to 100 Hz. The reason is the time variant bandpass filter applied not allowing frequencies over 85 Hz

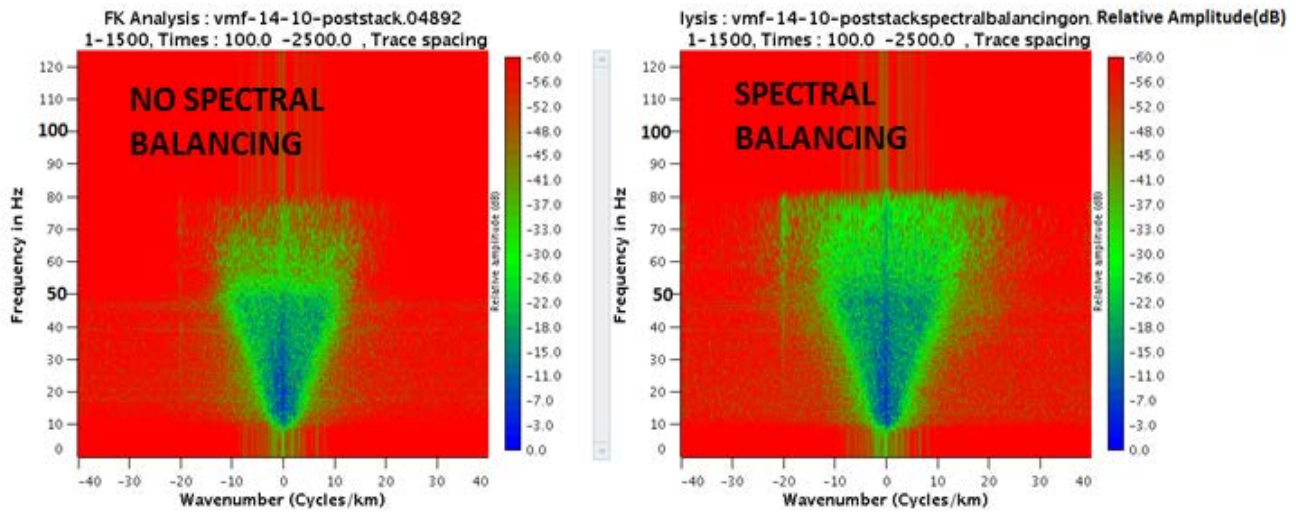


Fig 5.28: The figure to the left shows an fk plot where spectral balancing is applied. On the picture to the right no spectral balancing is applied

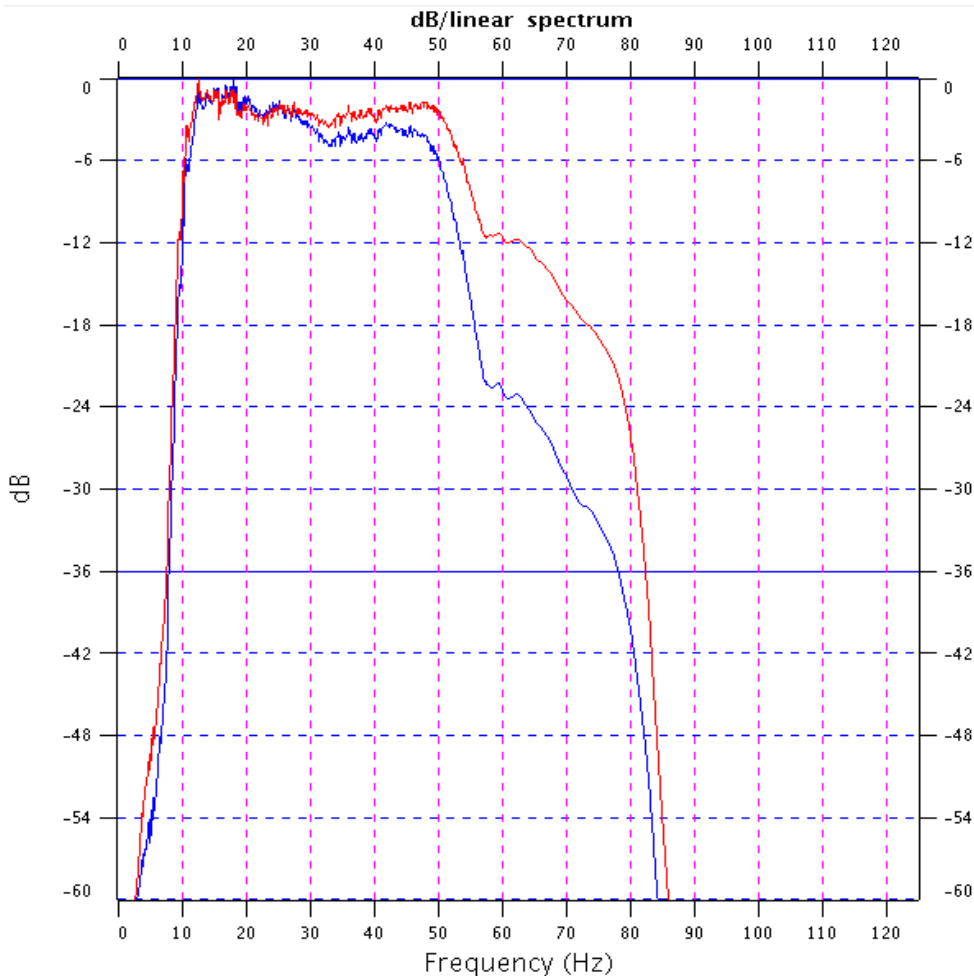


Fig 5.29: Shows a decibel /frequency spectrum. The red curve is a dB/frequency spectrum where spectral balancing is applied. As the figure indicates the frequency are boosted, where the highest boosting occurs for dB between -12 to -30 db. The blue curve shows the decibel/frequency spectrum (line 14-10) for the processed seismic used for seismic interpretation

The formula for calculating the decibel in fig 5.29 is given by

$$20 * \log_{10} \frac{A}{A_{max}}$$

Taking an example, -12 dB corresponds to an amplitude of $\frac{1}{4}$ of the maximum amplitude because $20 * \log(1/4) = -12$ Db.

-6 dB will corresponds to an amplitude of $\frac{1}{2}$ and 0 dB will correspond to maximum amplitude since $\log(1) = 0$.

Frequency is the number of oscillation's- per second and is given by

$$f = \frac{v}{\lambda}$$

Chapter 6 – Seismic interpretation

6.1 Introduction

In this chapter interpretation of the 10 lines is presented. The interpretation of the lines is correlated with data from the Ishøgda well, which was drilled in 1965-66. The well is located $77^{\circ}50'22''\text{N}$, $15^{\circ}58'00''\text{E}$ and reaches down to a depth of 3304 m, corresponding to the Lower Permian. This well was projected onto POLINV6, a seismic line across the Ess structure, see fig 6.2. The seismic line was recorded by Geco for Nordisk Polarinvest in September 1984. The correlation map for seismic horizons within this line was used as a guide for picking the different reflectors. The correlation map for the ESS structure for line POLINV6 is shown in figure 6.3. The strongest reflector in this section appears on 1.4 sec and is in good agreement with the strongest reflector appearing on the 10 seismic lines. Several anticline peaks appear in the package of the strongest reflector but only the first peak on the eastern side have reflectors dipping towards west in the above lying reflectors. The reflectors picked represent boundaries where the amplitude of the reflector changes, meaning a change in acoustic impedance has occurred.

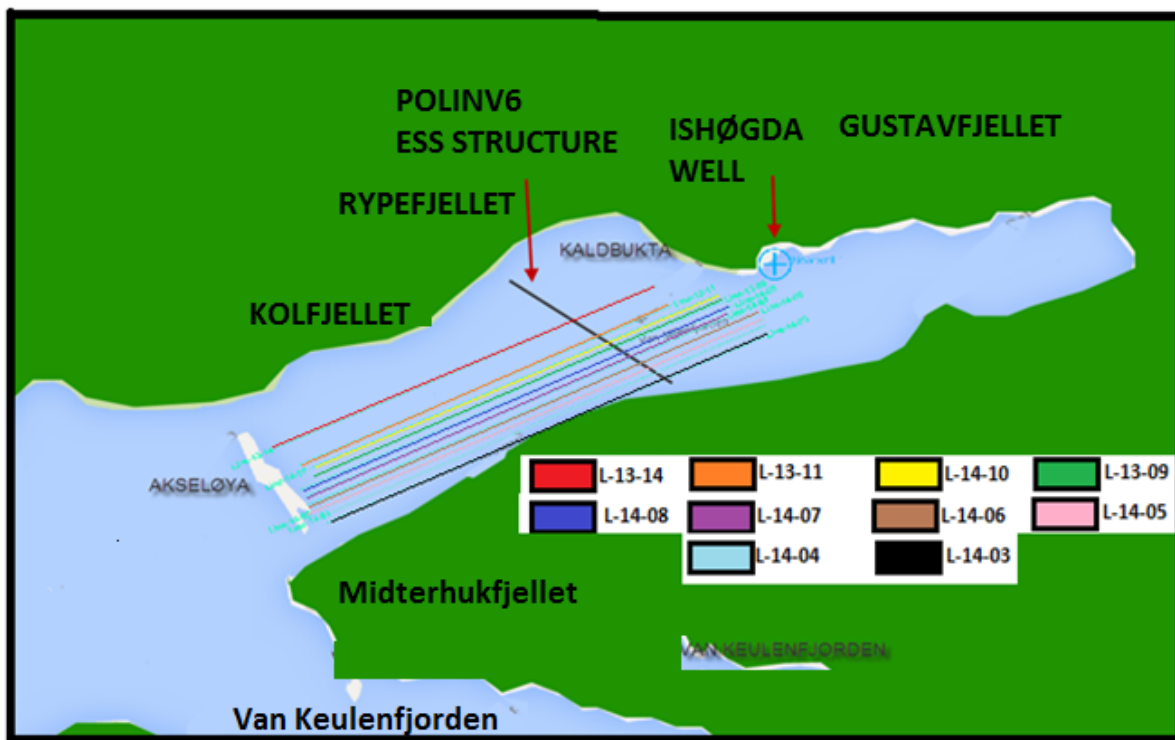


Fig 6.1: Shows the position of the seismic lines in Van Mijenfjorden and the location of the well. From line 13-14 (red color) northernmost line to line 14-13 (black color) southernmost line.

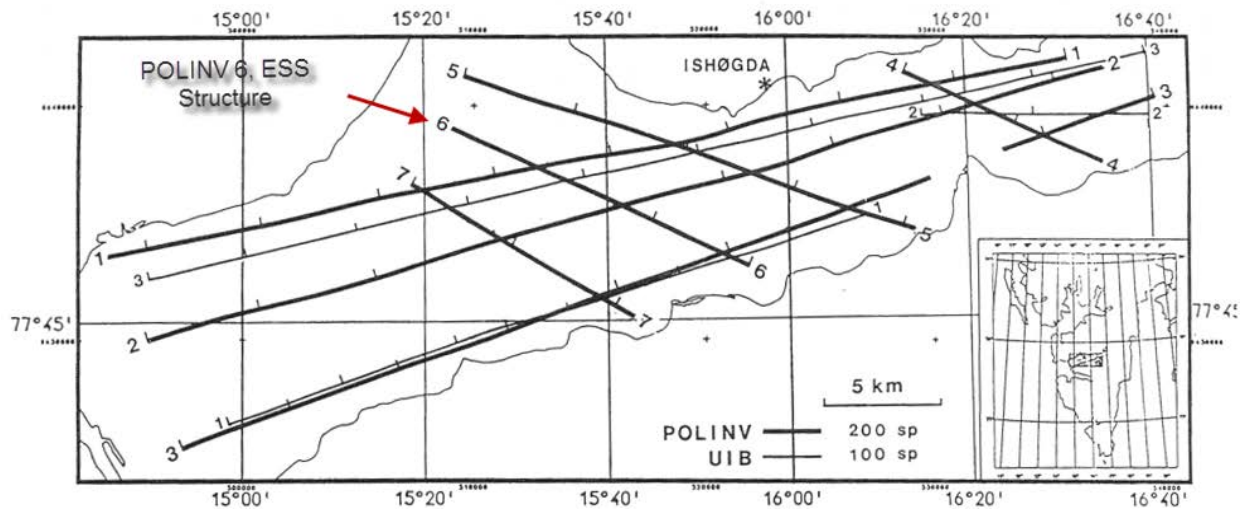


Fig 6.2: Shows the lines acquired by Geco for Nordisk Polarinvest . (Faleide and Gudlaugsson 1985)

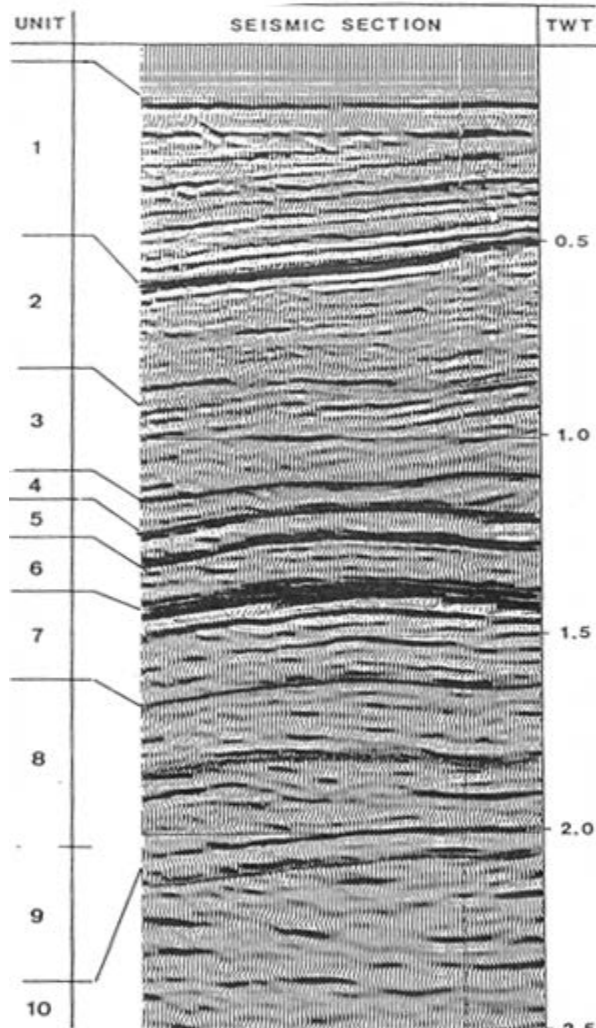


Fig 6.3: Shows the correlation of the well onto POLINV 6. See Fig 6.7 for correlation onto the 10 seismic lines.(Faleide and Gudlaugsson 1985)

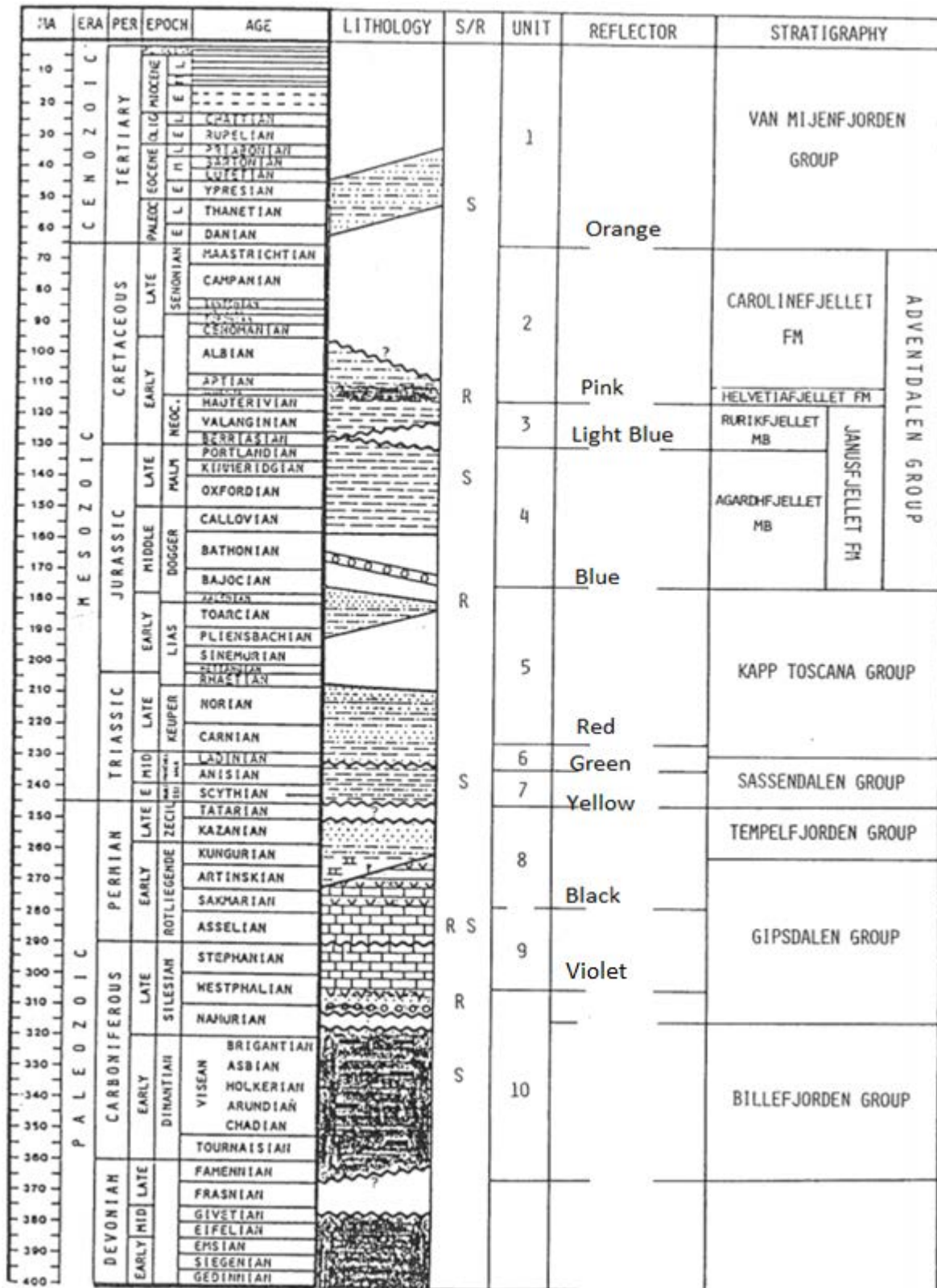


Fig 6.4 Shows the color of the horizons picked and the corresponding stratigraphy. (Faleide and Gudlaugsson 1985)

6.1.1 Data Quality

The study area is dominated by abnormally hard seabed and shallow water making the data quality poorer. Hard seabed has the effect that much of the energy will be reflected in the transition between the water layer and seabed. The result of this is that smaller amount of energy will penetrate downwards and image deeper structures. Relatively low water depth is also a problem, because short time between multiples masks the primary reflections. Multiples are removed during processing, but a consequence is attenuation of the seabed and the shallowest reflectors. In addition, several reflectors have strong amplitude affecting the degree of how well deeper events are mapped. This is because much energy is reflected on strong acoustic impedance contrast and the underlying units are not mapped as strongly until a new acoustic impedance contrast are met. A huge difference in data quality is found between the western and the eastern parts. This is to be expected as the western part could be interpreted to be a part of-, or very close to, the west Spitsbergen fold and thrust belt. This is an area of complex geometry and high degree of uncertainty is associated with the interpretation here. The continuity of reflections begins to deteriorate under 1500 ms twt and starts to be very poor below 2200 ms twt.

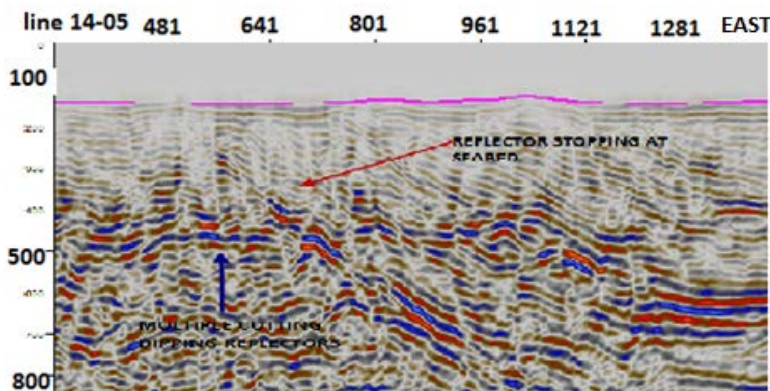


Fig 6.5: The blue arrow shows multiples cutting through dipping reflectors (red arrow)

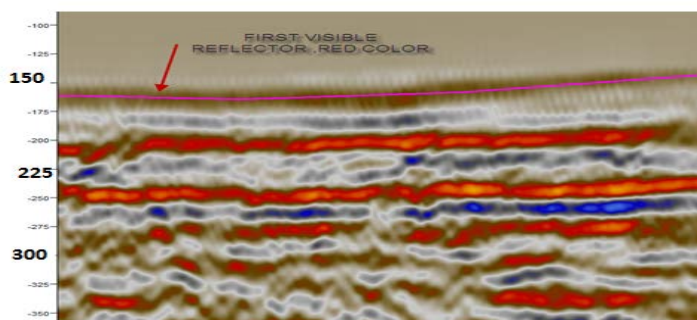


Fig 6.6: The red arrow shows the first reflection corresponding to seabed reflection.

6.1.2 Correlation map

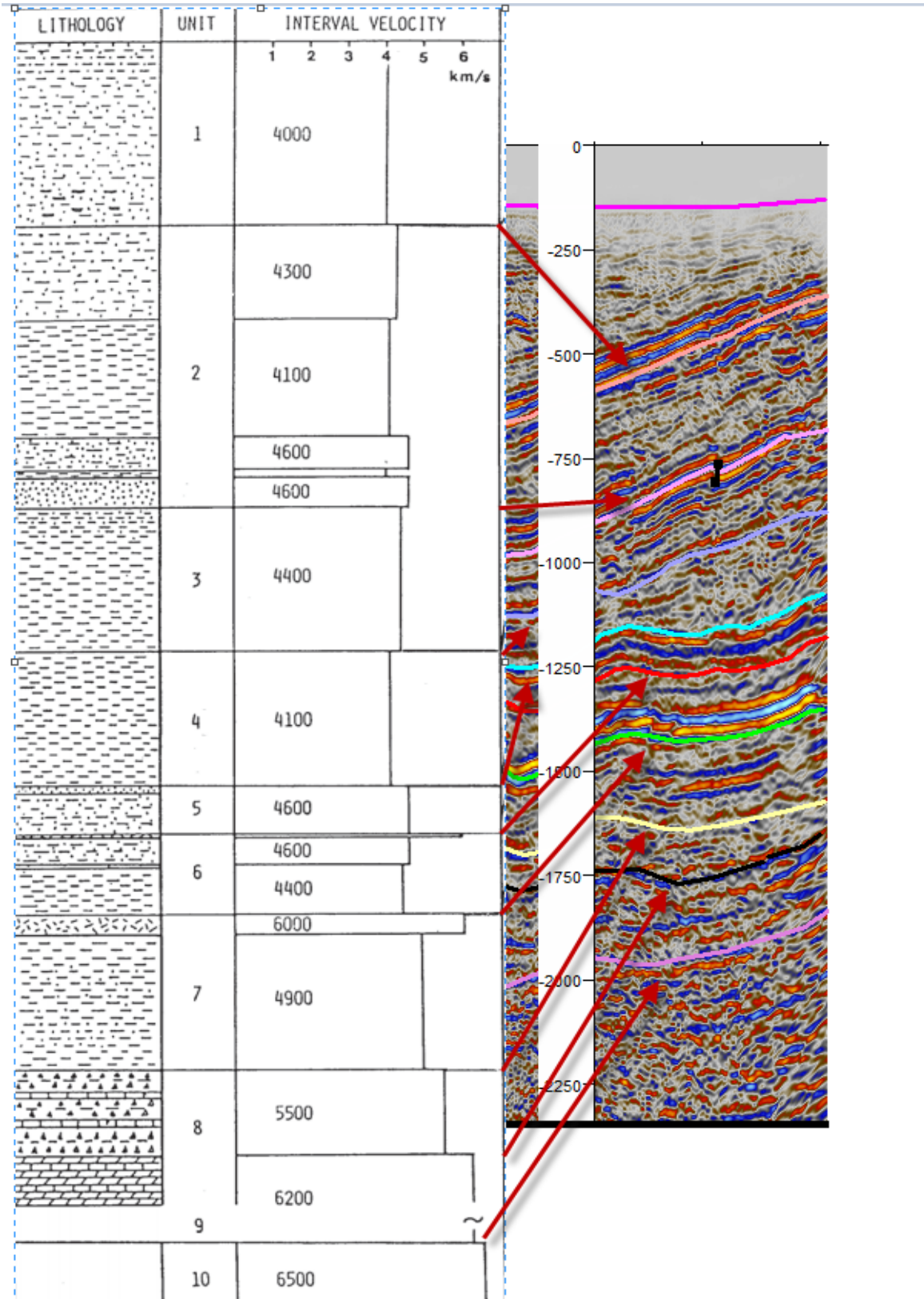


Fig 6.7: Shows the correlation map from the reflectors picked, NB: the reason for the higher dips in the Tertiary reflectors and the Cretaceous reflector compared to fig 6.3 is that the seismic is stretched in different ways. (Faleide and Gudlaugsson 1985)

6.1.3 Interpretation tool

The interpretation tool used for interpretation is Petrel (Schlumberger software) version 2013. Positive trace deflection represents an increase in acoustic impedance and is marked with red, a decrease in acoustic impedance is marked by blue. This is clearly seen on the seabed, because seabed represents an increase in acoustic impedance, see fig 6.6. A standard Zero phase pulse is also used.

6.1.4 Time Depth Conversion

Depth conversion is based on the velocity information from the well. Not all horizons represents stratigraphic boundaries as stated in figure 6.4. Unit 1-5 represents different stratigraphic layers and the thickness of the units are found using the interval velocity information between the boundaries. A thickness map representing the unit is made to give a brief overview of how the thickness changes in the layer. When the velocity varies within a unit the average velocity is used. This is found by weighting the different velocities with their lateral extent. Deeper reflectors represent horizons within units, see fig 6.4. Since the velocity varies much with depth, different average velocities are calculated to different units to give a better estimate.

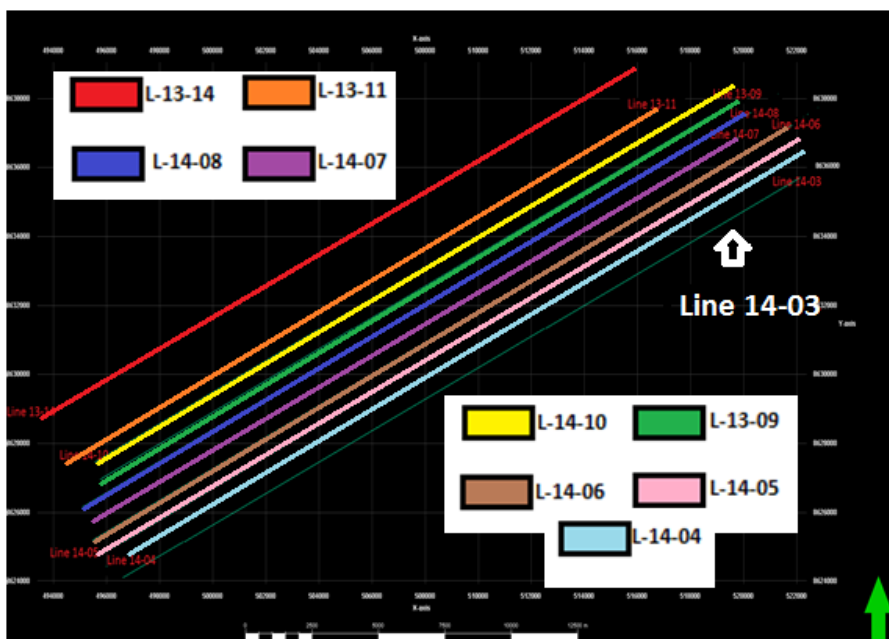


Fig 6.8 Shows the lines, and the corresponding line numbers

6.2 Interpretation of Seismic Lines

The following section describes the interpretation of line 14-08 if nothing else is stated. The profile is representative of structures that are present on all profiles. The western area differs in geometry from profile from profile and will be discussed later. The horizons in fig 6.9 are interpreted on all lines since they correlate directly with the well.

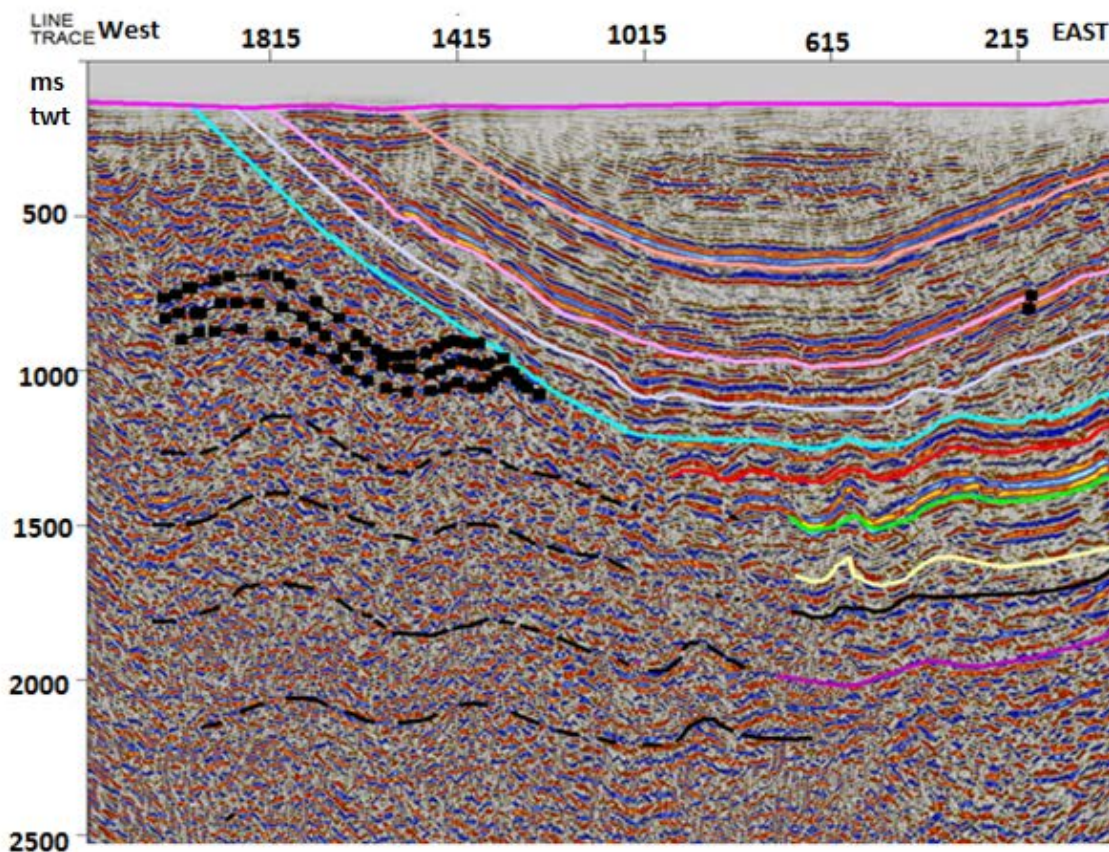
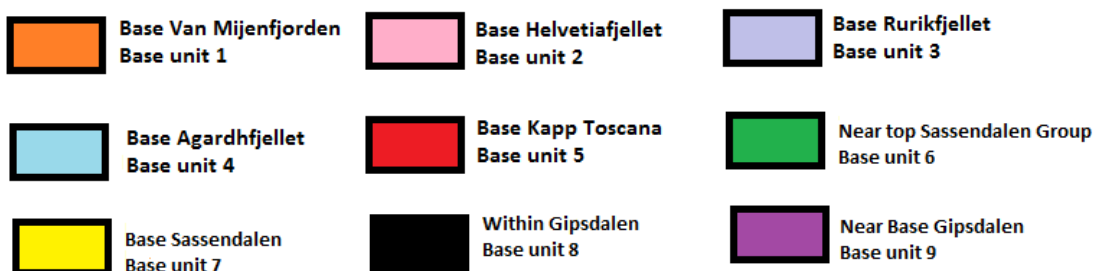


Fig 6.9: Shows the interpretation of line 14-08 . The noisy area on the western part where the asymmetrical folds are interpreted is part of the West Spitsbergen Fold and Thrust Belt.



6.2.1 Seabed

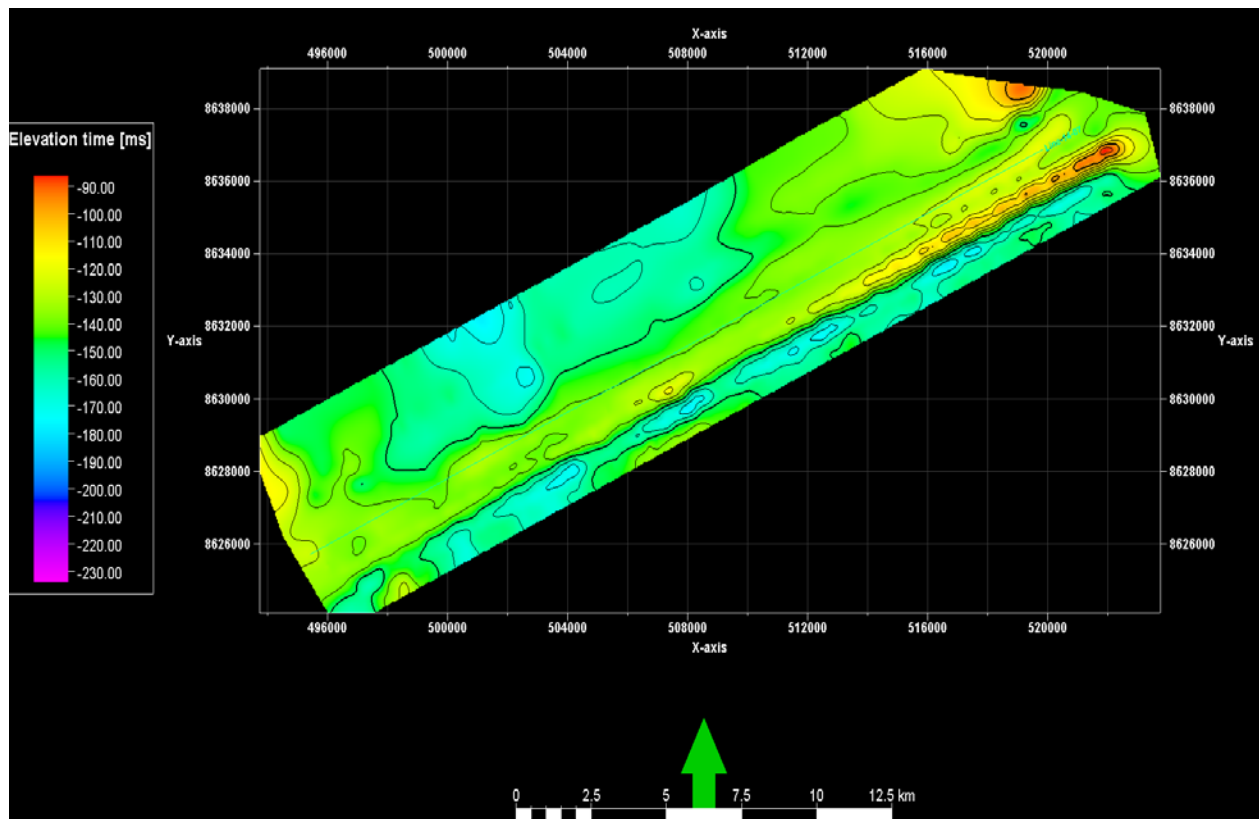


Fig.6.10: The figure shows the elevation map for the seabed.

The seabed does not follow the synclinal trend of the CSB, most likely since the seabed was extensively eroded through Quaternary. This is in agreement with Faleide and Gudlaugsson (1985) confirming that 1000-1500 m of additional Tertiary sediments were deposited, but have since been removed by erosion. The seabed was picked as the first visible reflector on every line, and they all have a red color, meaning that the seabed is marked by an increase in acoustic impedance, see fig 6.6. The elevation time varies between 140 ms in the middle of the fjord corresponding to 105 meter, and 150 ms corresponding to 112. m. The velocity used for estimating the depth is the P wave velocity in water, which is 1500 m/s. A maximum water depth of 112 meter in the outer basin is confirmed by (Hald, Dahlgren et al. 2001).

6.2.2 Base Tertiary

The reflectors within the Tertiary unit are continuous, parallel and layered. They depict a broad asymmetric syncline interpreted as central Spitsbergen basin with deposits within the Van Mijenfjorden group. Lower Tertiary is selected as the bottom of a series of strong reflections. The thickness map in fig 6.11 shows the thickness between the seabed and Base Tertiary. In the

middle of the basin is the thickness 550 ms (1100 meter), the thickness is progressively decreasing towards the western and eastern side. The uppermost part of the Tertiary basin is called Gilsonryggen, consisting of black shale with marine fossils. Generally the change in amplitude is used as a guideline in interpreting these horizons, the subgroups within the Van Mijenfjorden groups are interpreted only in one profile (fig 6.12) but the horizons shown in fig 6.9 are interpreted in all lines. This is because there is greater uncertainty in the interpretation of horizons not directly correlated with the well. The underlying formations are as follows.

Grumantbyen formation is interpreted as a series of discontinuous reflections where the amplitude is strongest in the middle of the syncline. As stated in 2.6.2 this formation consists of highly biotubated sandstone, rich in chlorite and glauconite (Dypvik, Riber et al. 2011). Below is the Basilika formation found, containing grey shales and siltstone, see section 2.6.2. The formation show quite similar seismic characteristic as the Gilsonryggen formation, see fig 6.12. Firkanten formation is a series of four continuous high amplitude reflectors. Fresh-water sandstone with shale and conglomerate dominates. Coal seams occur near the base, and shale intercalations with marine fossils appear higher in the succession (Nairn, Churkin et al. 1981).

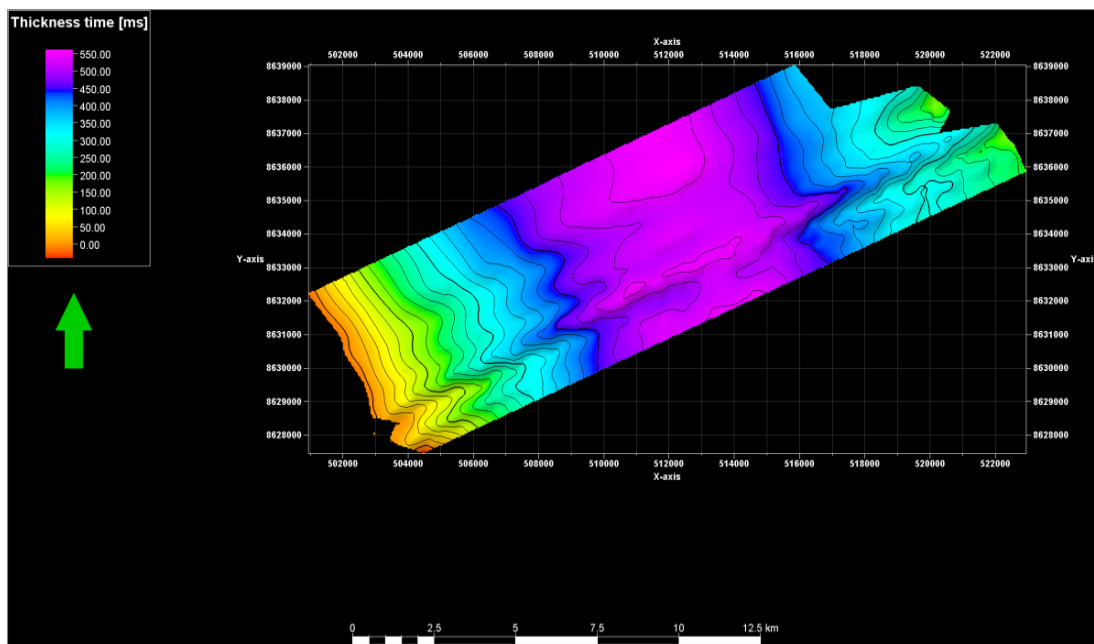


Figure 6.11 : Thickness map between seabed and Base Tertiary. Green arrow marks the north.

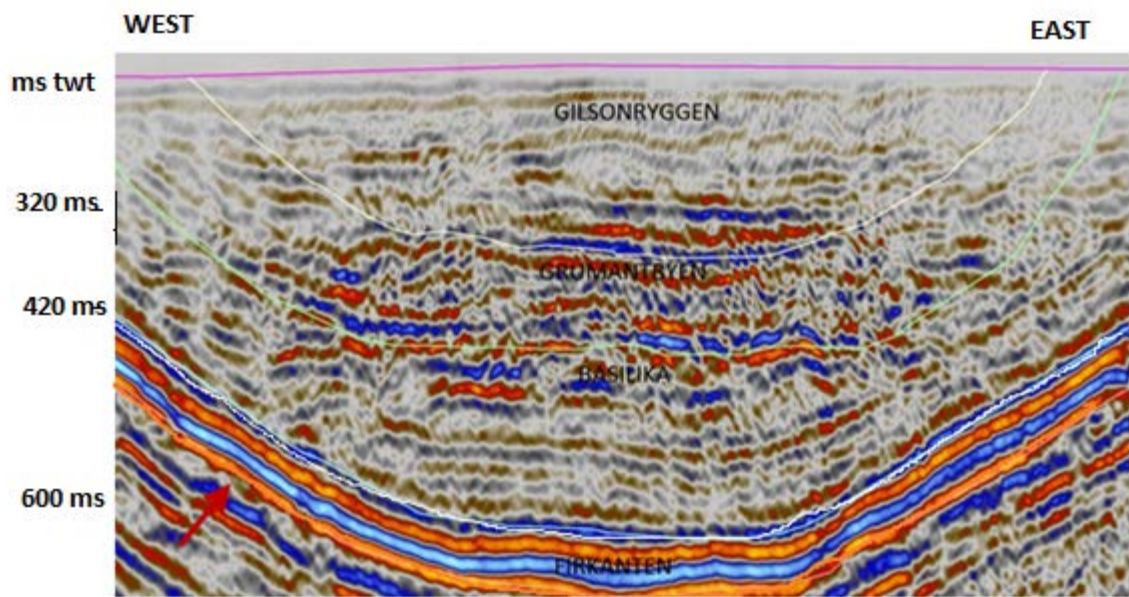


Figure 6.12 : Interpretation of various subgroups found within the Van Mijenfjorden Group. Base Gilsonryggen formation, base Grumantbyen formation, and base Basilika formation are interpreted on line 14-07 since this line has the best processing of the Van Mijenfjorden group, having few multiples.

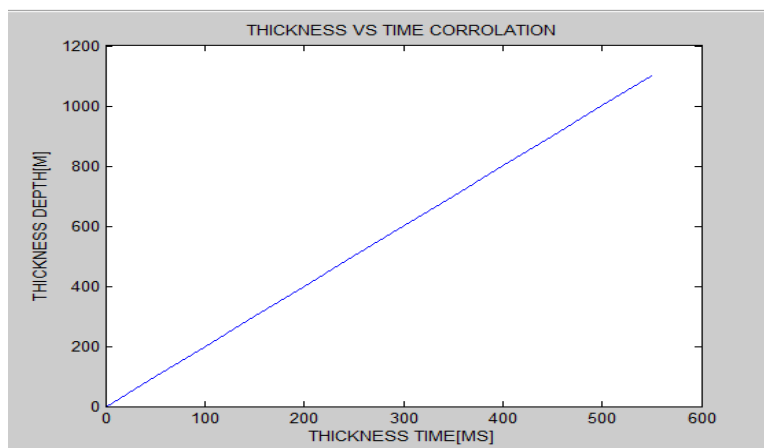


Fig 6.13 : Shows correlation between depth in meter and time for Tertiary deposits

6.2.3 Carolinefjellet and Helvetiafjellet formation

A package of strong reflectors is seen in the lower part of this formation. The reflector picked to represent the base of the Helvetiafjellet formation is the lowermost continuous strong reflector-. This reflector varies between 900 and 1000 ms in the middle of the syncline. The uppermost part of this package is interpreted to be top of the Helvetiafjellet formation, which consists deltaic sandstones (Faleide and Gudlaugsson 1985). Above this layer is a section characterized by weaker reflectors with low continuity interpreted as Carolinefjellet formation. This formation consists of sandstone silt and shales, as stated in 2.6.2.

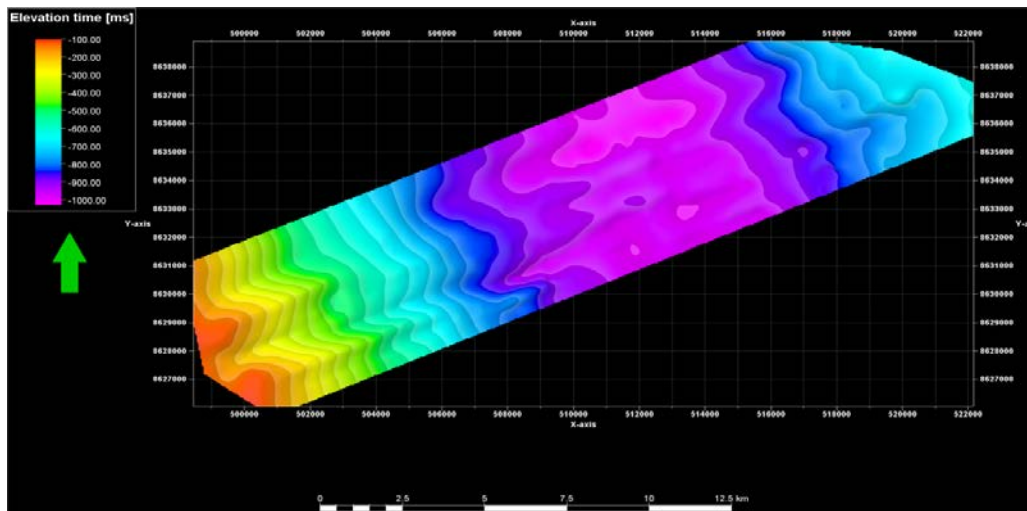


Fig 6.14: Shows the elevation time map for base of the Helvetiafjellet formation.

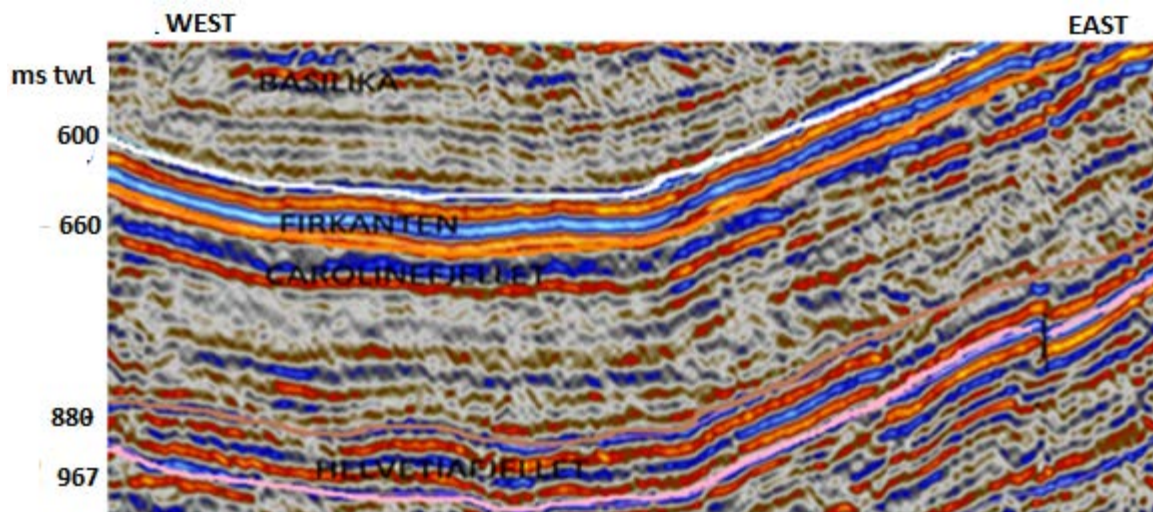
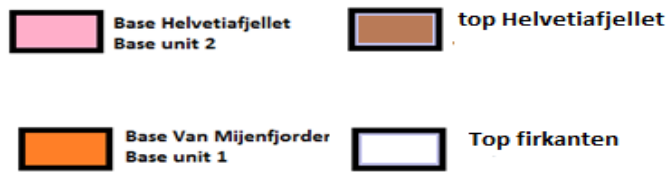


Fig 6.15 : Shows the interpretation of where Carolinefjellet and Helvetiafjellet could be located in the seismic. Carolinefjellet formation is interpreted to be the low amplitude section between Firkanten formation and Helvetiafjellet Formation.



A thickness map was made between Base Tertiary and Top Helvetiaformation corresponding to the Carolinefjellet Formation. The median velocity in this layer is 4200 m/s. Based on this information, the thickness within this layer is estimated to be roughly 570 meter in the middle of the syncline.

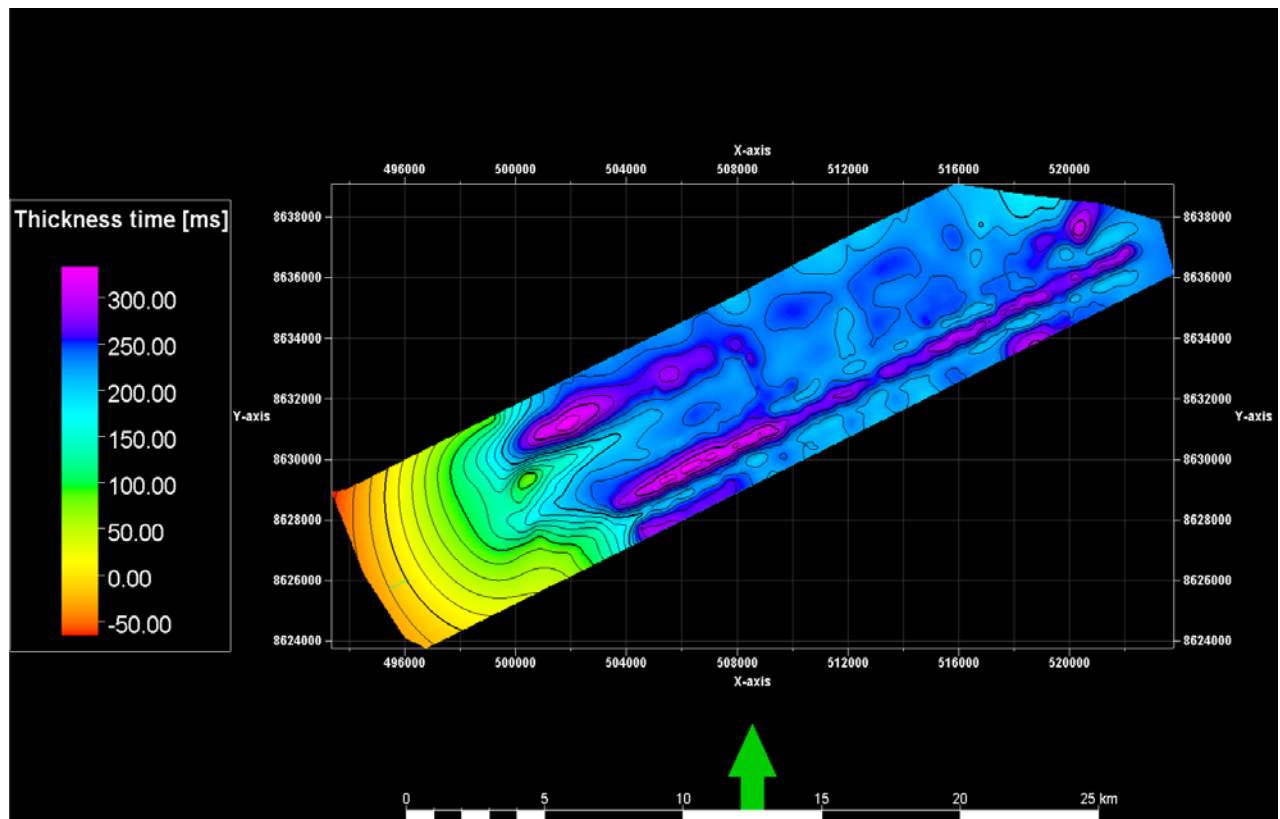


Fig 6.16: Shows a thickness map of the interpreted Carolinefjellet formation

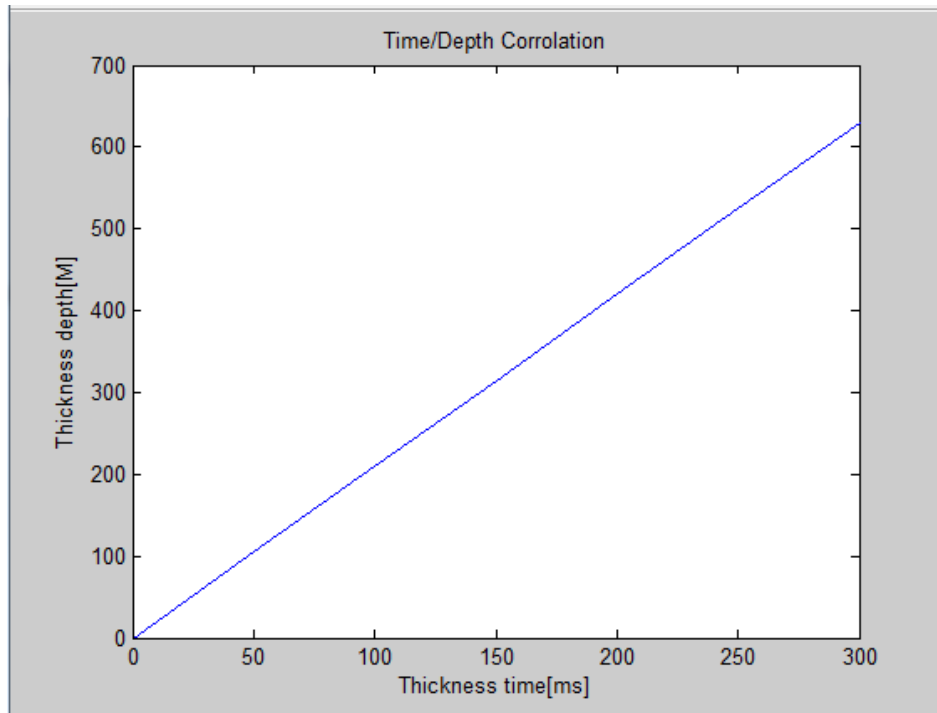


Fig 6.17: Shows the correlation between thickness time and depth for the Carolinefjellet formation

6.2.4 Base Rurikfjellet-Base Cretaceous

This reflector lies within the shales of the Janusfjellet formation. It is picked at the bottom of two strong reflectors. The amplitude of the reflector is strongest in the middle of the syncline and gets weaker towards east and west. The thickness map in fig 6.18 shows that the thickness of the Rurikfjellet MB of the Janusfjellet Formation is about 100-125 ms (220-275 meter) in the middle of the syncline. The thickness decreases towards west due to folding of the layers, as two reflectors are folded against each other. In the eastern side the thickness is increased. This must be considered with a critical sense because it represents reflections from the very edge of the seismic line. The formation is dominated by dark fracturing shale, and coarsens upwards to siltstone (Mikkelsen 2009). According to Dypvik (1984) is this formation enriched in volcanogenic components compared to the underlying Agardhfjellet Member. This may be the reason why brighter amplitude anomalies are found within this member of the Janusfjellet Formation, see fig 6.20.

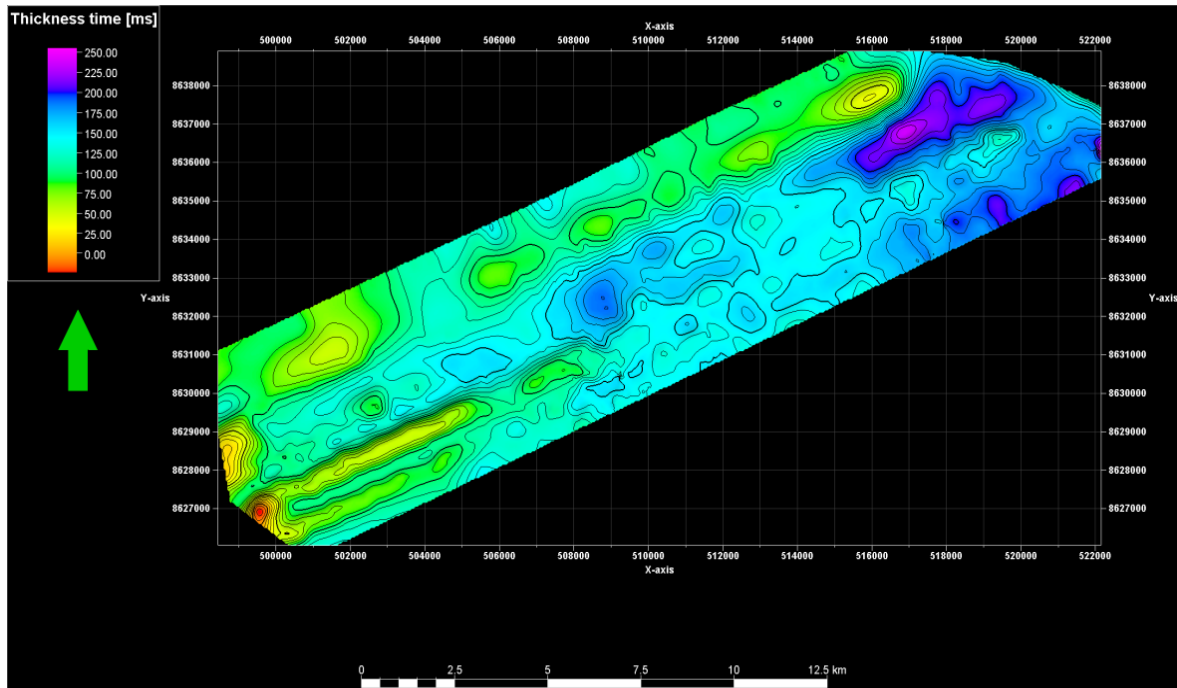


Fig 6.18:Shows a thickness map of the Rurikfjellet formation

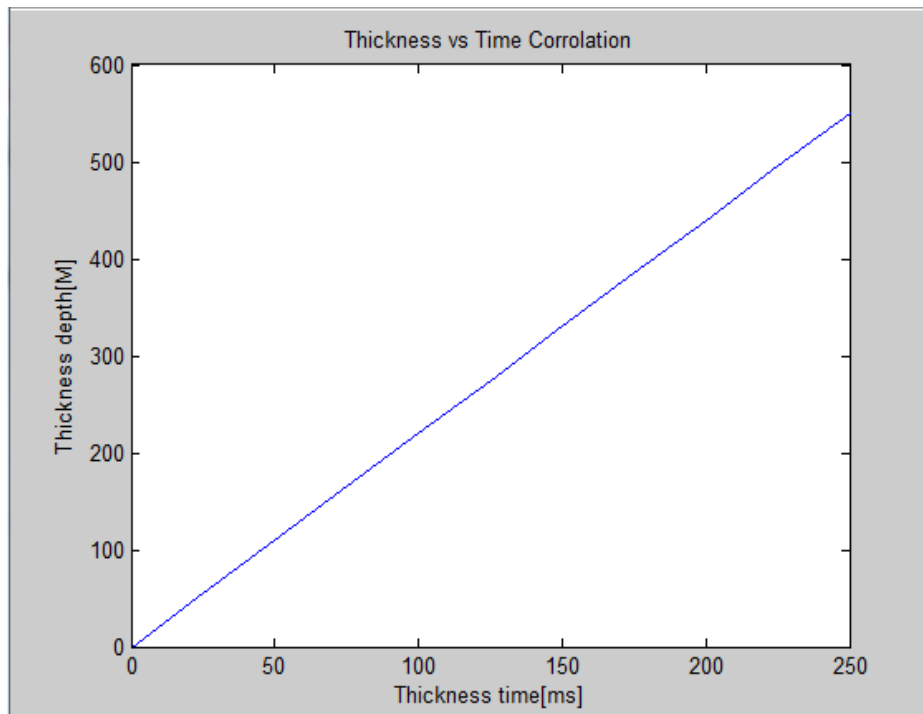


Fig 6.19:Shows correlation between thickness time and depth for the Rurikfjellet formation. An interval velocity of 4400 m/s is used from Fig 6.7.

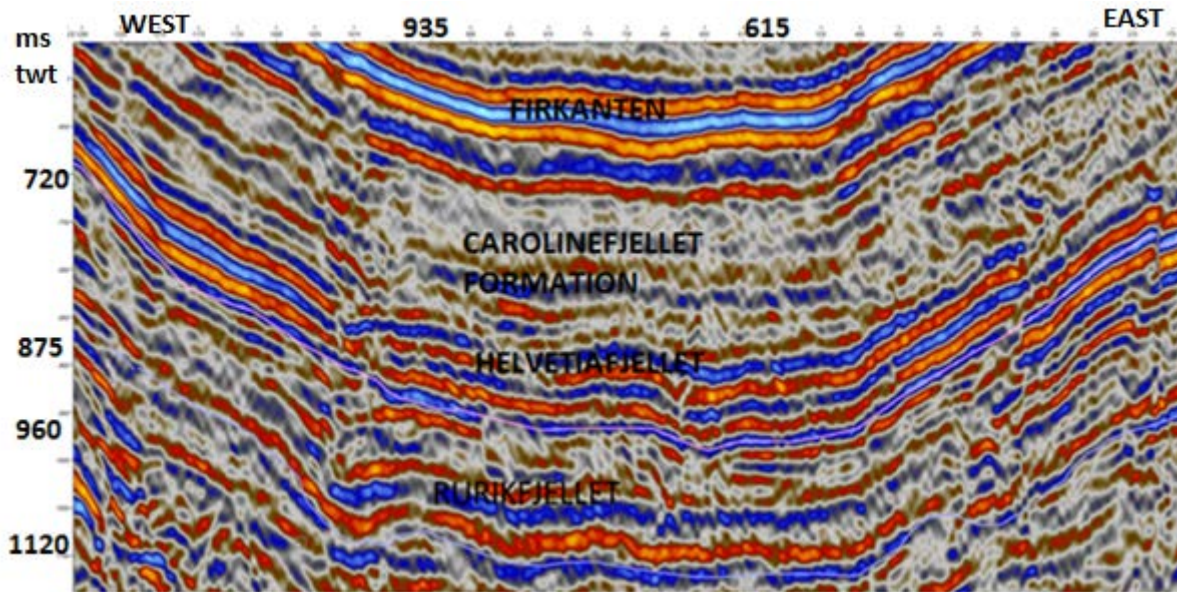


Fig 6.20 : Shows the strong amplitude reflection within the Rurikfjellet formation. The higher amplitude in Rurikfjellet formation compared to the Agardhfjellet formation could be related to an enrichment in volcanogenic components in Rurikfjellet.



6.2.5 Base Agdarfjellet Formation-Base Upper Jurassic

Base of the Agdarfjellet formation corresponds to the unconformity between the Kapp Toscana and Adventdalen group. It consists of dark shales deposited during a transgressive phase in a deep shelf environment (Faleide and Gudlaugsson 1985). Towards the western area, reflectors are seen cutting these reflectors demonstrating that it represents an unconformity, see fig 6.9. A thickness map showing the thickness between base agdarfjellet and base Rurikefjellet representing the Agardhfjellet Mb of the Janusfjellet subgroup is shown in fig 6.21. The thickness reaches up to 310 meter corresponding to 150 ms twt, see fig 6.22. This thickness is close to the thickness of the same formation in Van Keulenfjorden(fig 6.1), reported to be up to 290 m (Dypvik, Eikeland et al. 1991). Thickness variation within the Agardfjellet is also discussed by the same authors, in the seismic it can be seen that thickness variation locally is due to folding.

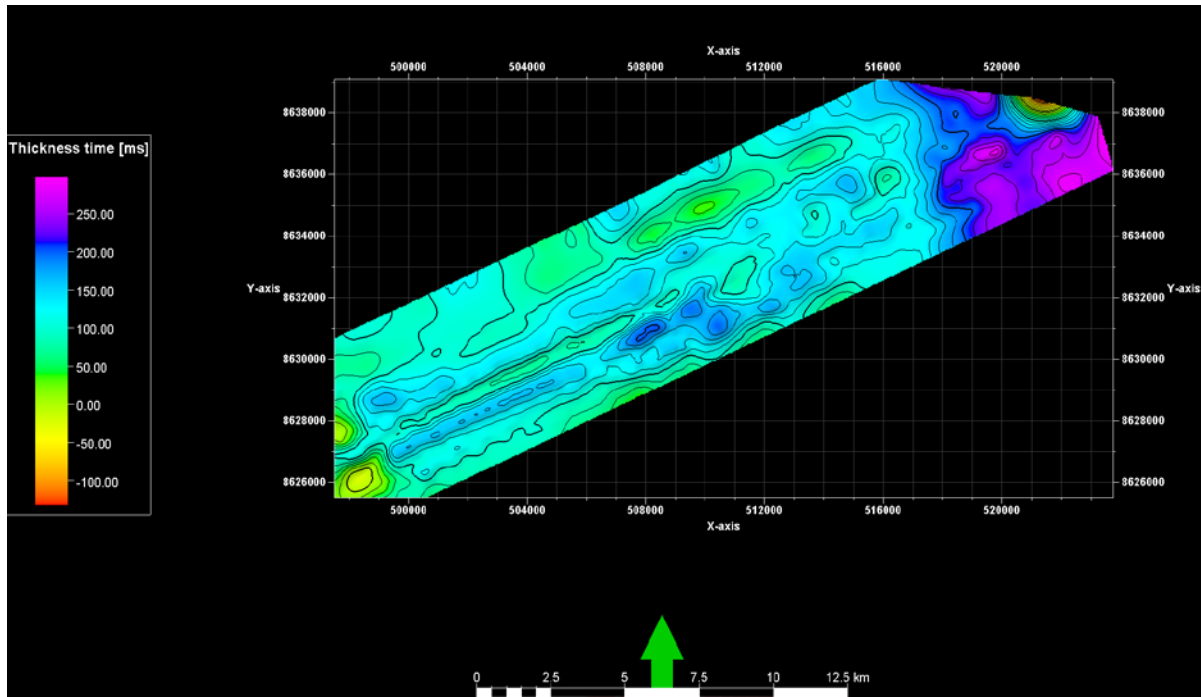


Figure 6.21: Shows a thickness map of the Agardhfjellet Formation

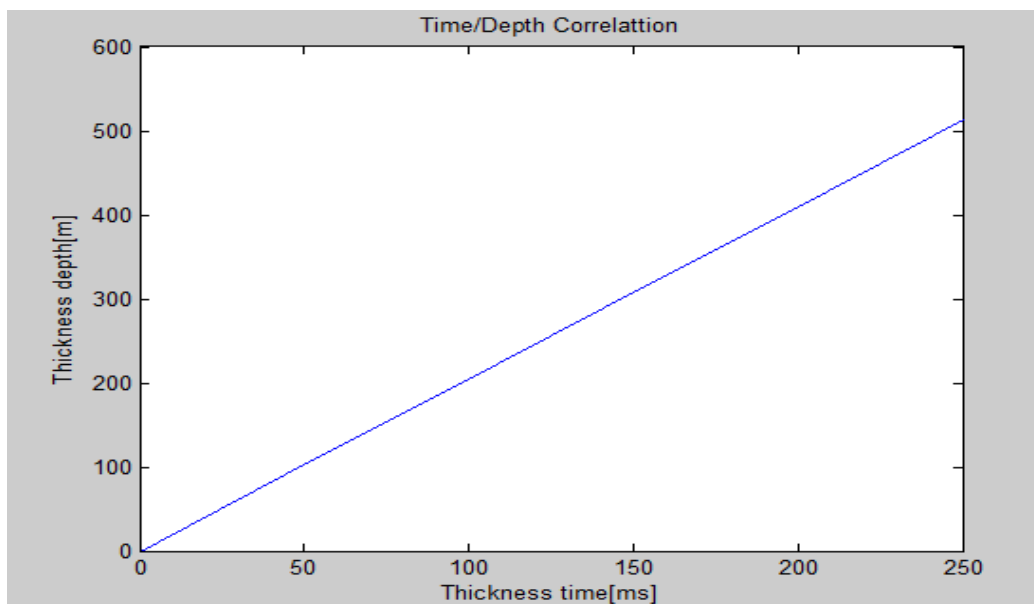


Fig 6.22: Shows the correlation between thickness time and depth for the Agardhfjellet Formation.

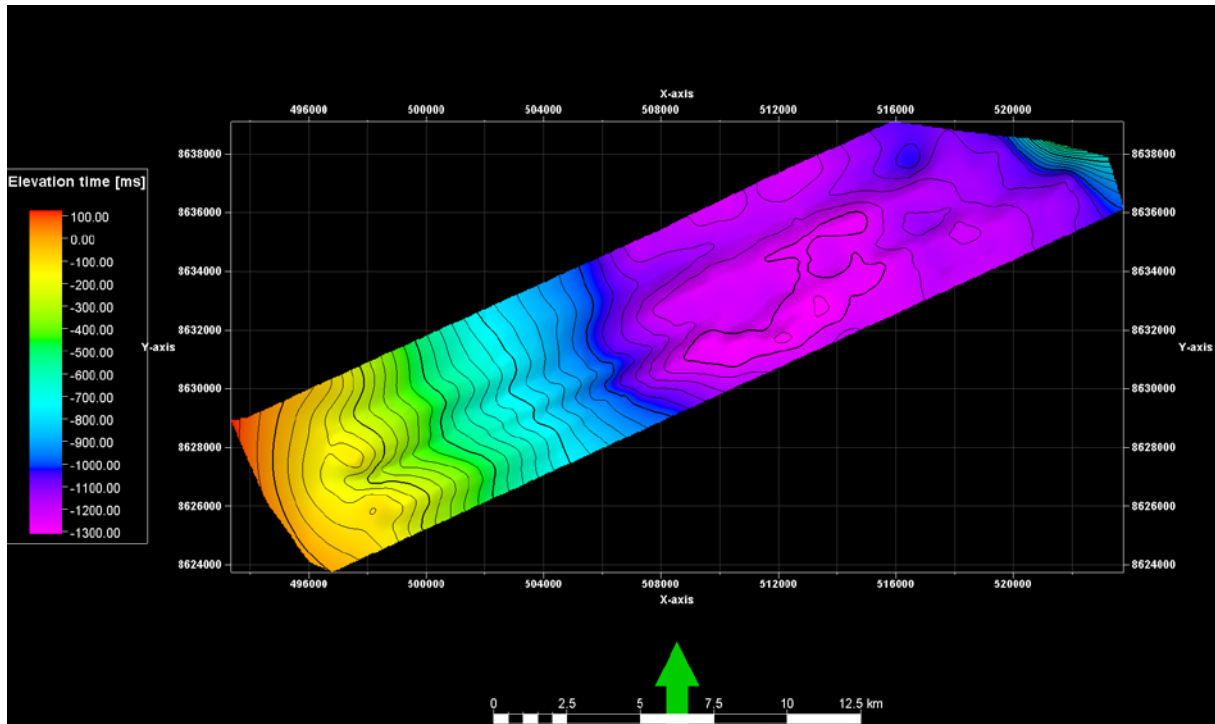


Fig 6.23:Shows the elevation time for the Agardhfjellet formation

6.2.6 Upper Triassic

This reflector is picked at the bottom of a series of reflectors with open folds. The amplitude of these reflectors are normal amplitude and does not stand out with respect to amplitude strength in any way. On the western side-the reflectors dip, while under the relatively un-deformed syncline the folding is more symmetrical. Faleide and Gudlaugsson (1985) interpreted this horizon to be a thin dolerite sill within the Kapp Toscana group. However this reflector is continuous over a larger distance than the underlying stronger reflector, positively identified as a dolerite sill. This dolerite sill cuts upper Triassic layer as figure 6.25 show.

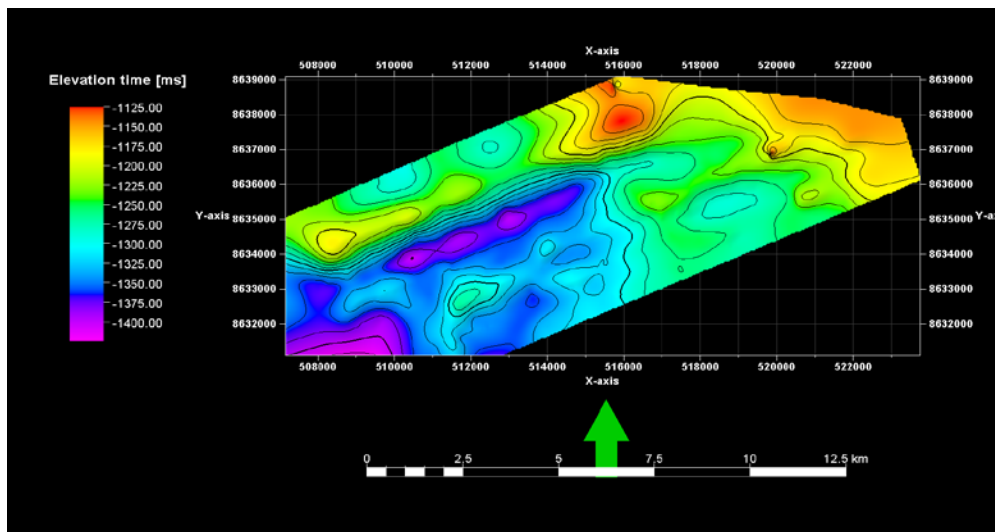


Fig 6.24: Shows the elevation time for Upper Triassic layer.

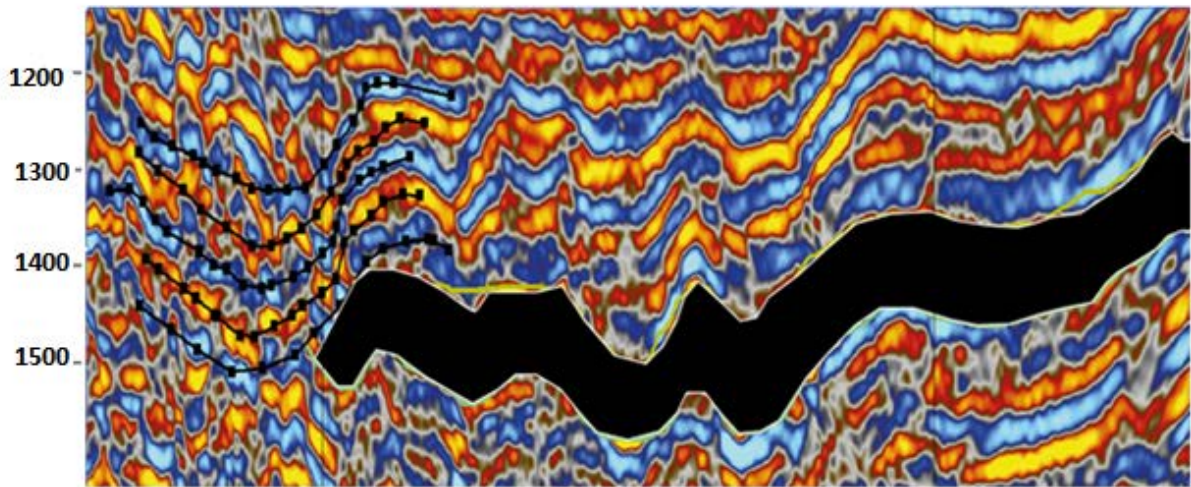


Fig.6.25: Shows the dolerite (marked by black) cutting upper Triassic layers. These layers most likely continuous upwards as shown in figure 6.9

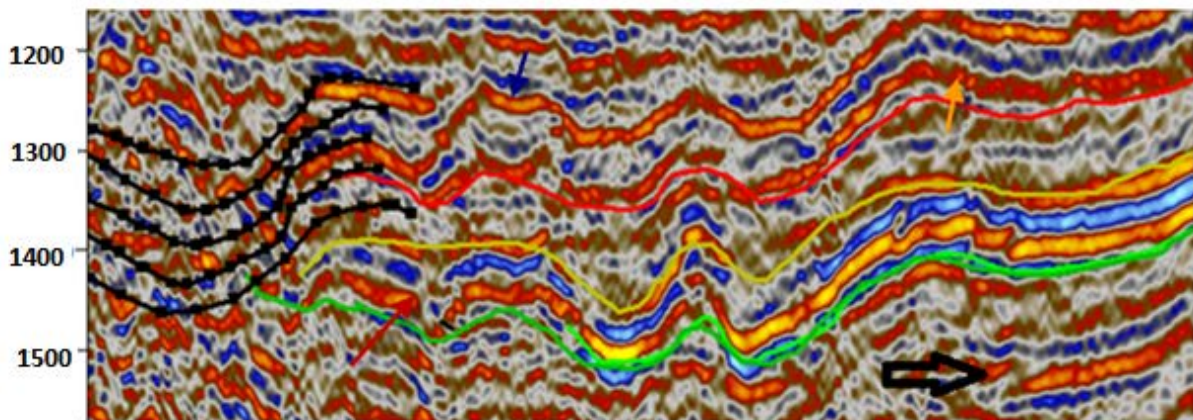
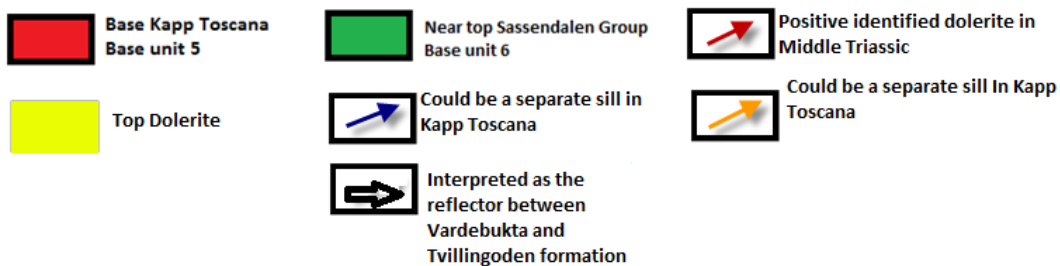


Fig 6.26: Show the same picture as in fig 6.25 without masking the dolerite.



As fig 6.26 indicate, it is possible that two dolerites intruded into Kapp Toscana, marked by the orange and blue arrow. This is because there is a reflector with very low amplitude between the two reflectors. Compared to the underlying dolerite (red arrow), no low amplitude reflectors are found in between the strong amplitudes.

6.2.7 Middle Triassic

This sequence has been positively identified as a several tens of meters thick conformable dolerite sill within the Middle Triassic shales of the Botneheia formation (Faleide and Gudlaugsson 1985). As Fig 6.26 indicates the top of the sill does not reach Base Kapp Toscana demonstrating that it does not represent the whole Middle Triassic. The Green reflector is near top Sassendalen group and probably corresponds to base Botneheia Fm since the underlying reflector marked by the black arrow in fig 6.26 is interpreted as the boundary between Tvillingoden Fm and Vardebukta Fm in Lower Triassic. As a result the dolerite nearly constitutes the whole Middle Triassic but is not a part of the very upper Botneheia Fm since it does not reach Base Kapp Toscana. The dolerites of Svalbard are mineralogical homogenous with geochemical features typical within plate tholeiites (Nejbert, Krajewski et al. 2011). The reflector represents the strongest amplitudes found in the seismic and thus differs greatly in relation to the other reflectors. Compared to the overlying succession the layers do not differ much in shape but the folds are tighter. Middle Triassic dolerite cuts the overlying reflection package on the western side. Fig 6.27 shows the elevation time from this reflector, the difference in elevation time is due to folding of the layers. The fact that the dolerite is folded means that it has intruded before the compression induced by northward movement of Greenland against Spitsbergen in Eocene.

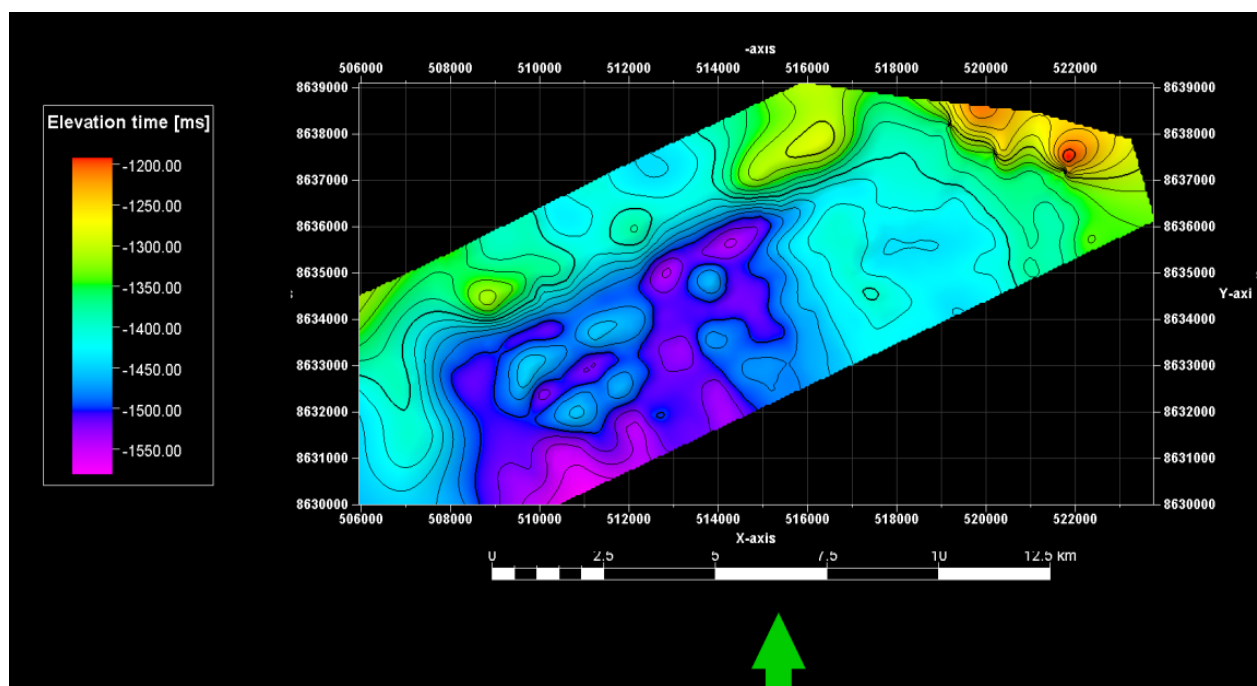


Fig 6.27: Shows the elevation time for Middle Triassic layer corresponding to the base of the dolerite

6.2.8 Top Permian

Deeper seismic events are harder to interpret because seismic resolution diminishes with depth. Top Permian is interpreted as an impedance contrast between weaker amplitude reflectors found above this reflector and stronger amplitudes below. This reflector correspond to the boundary between silicified sandstones of the Tempelfjorden group and the above lying Triassic shales (Faleide and Gudlaugsson 1985). As stated in chapter 2, sequences of extensive silica cemented reservoirs often show extremely low porosity and permeability and display a high seismic velocity. An average velocity of 4500 m/s down to the Top Permian layer gives a depth distribution for this interface as shown in fig 6.29. The Elevation time map shows that the elevation of this reflector resembles the elevation changes of the above lying reflectors. At this depth also an anticline structure appears.

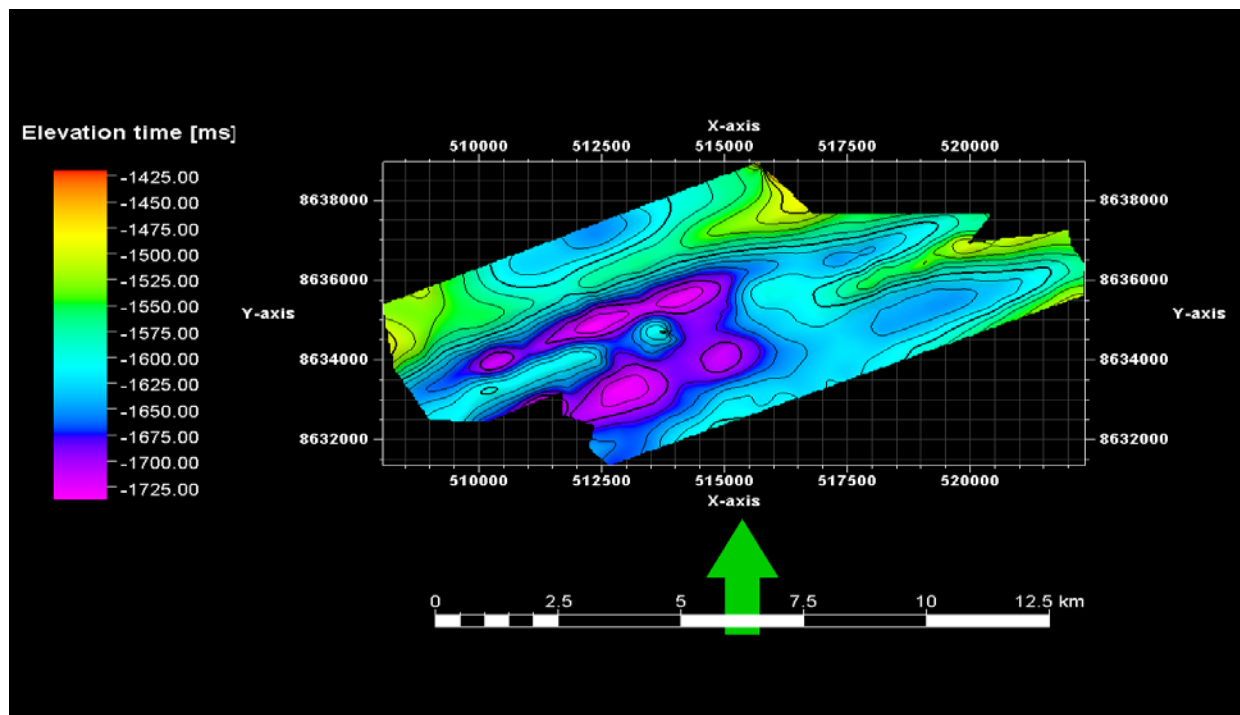


Fig 6.28: Shows the elevation time for Top Permian layer.

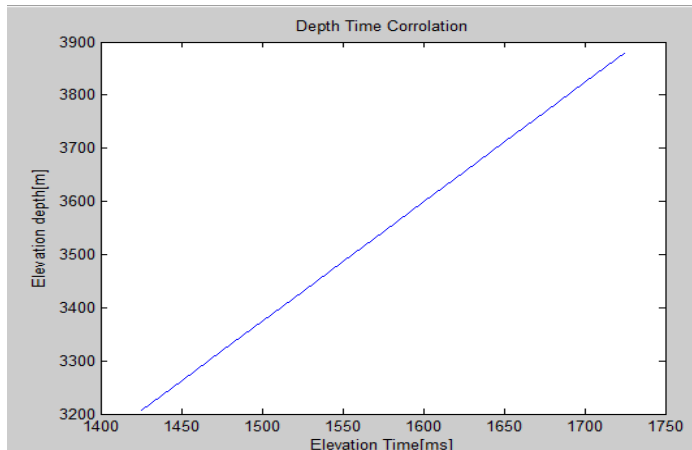


Fig 6.29: Shows time /depth conversion for Top Permian layer

6.2.9 Lower Permian

Lower Permian is within the carbonate/evaporate sequence of the Gipsdalen group close to its top. The reflector picked is representing the slight amplitude contrast found at this depth. All reflectors at this depth are more or less discontinuous, and greater uncertainty with regard to how precise the interpretation is at this depth must therefore be kept in mind. Towards the west an area of more chaotic seismic character is seen. The dotted lines in fig 6.9 show how reflectors here are thought to be propagating towards west. Relatively acoustic impedance map and amplitude smoothing map are used to better demonstrate how reflectors here propagates. The average velocity down to this interface is around 4600 m/s, giving the following elevation depth for the interface as a function of elevation time as shown in fig 6.31.

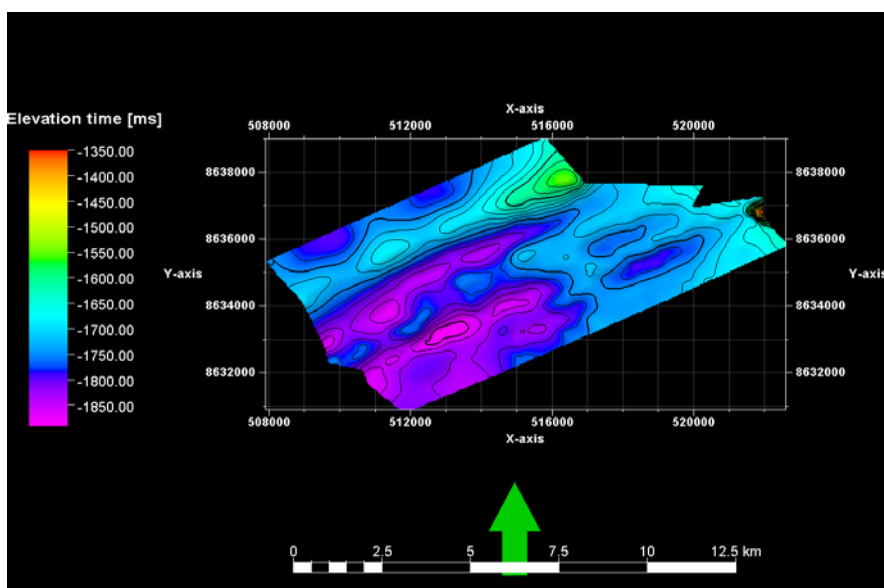


Fig 6.30:Elevationtime for Lower Permian horizon.

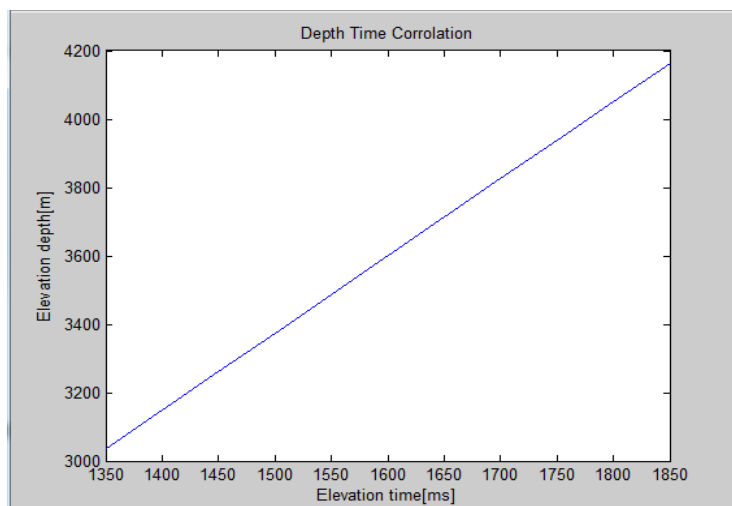


Fig 6.31: Time/Depth correlation for Lower Permian Horizon.

6.2.10 Upper Carboniferous

This reflector lies within the Gipsdalen group, and most likely corresponds to the base of the carbonate/evaporate sequence. It separates the lower amplitudes above this reflector from higher amplitudes found underneath. This reflector does not have the same anticline characteristic as the above lying reflectors. At this level the reflector is dipping towards west. The average velocity down to this reflector is estimated to be roughly 4700 m/s.

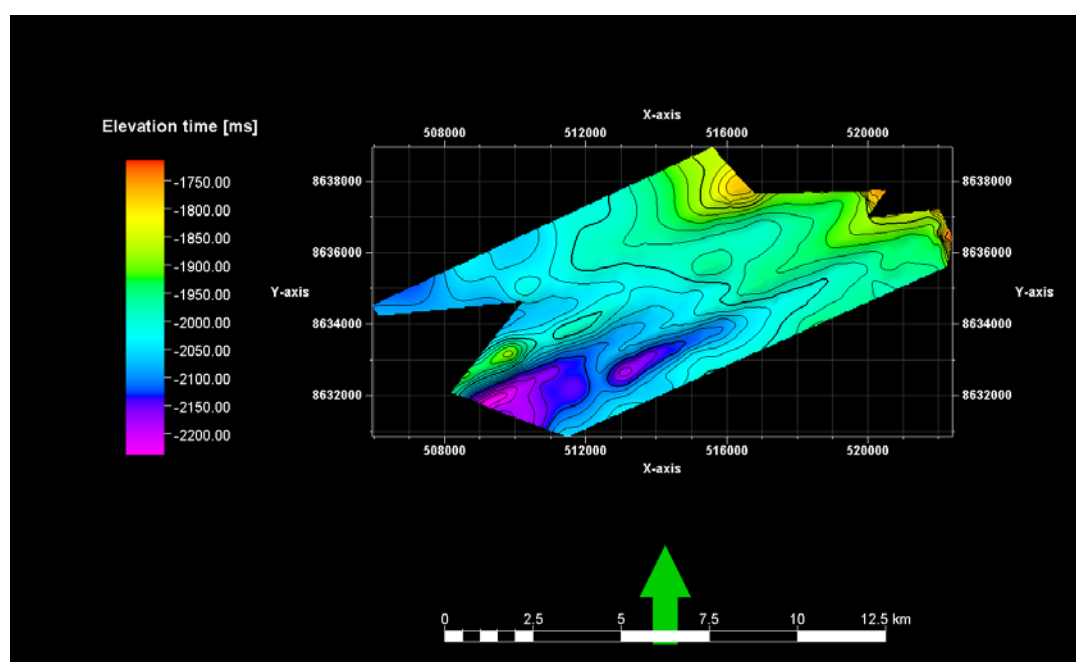


Fig 6.32: Elevation time for Upper Carboniferous.

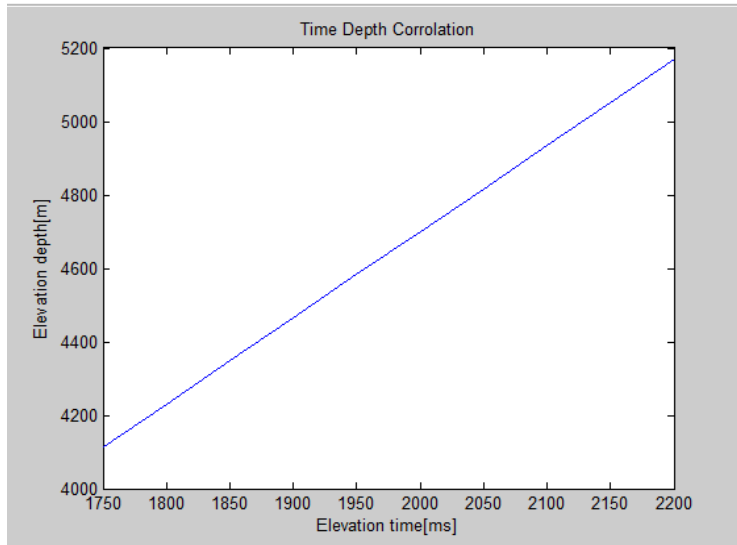


Fig 6.33: Time /Depth correlation for Upper Carboniferous

6.3 COMPLEX AREA PART OF WEST SPITSBERGEN FOLD AND THRUST BELT

The seismically complex area is part of the West Spitsbergen Fold and Thrust belt. As stated in 2.5 the west Spitsbergen fold and thrust belt is characterized by wrench faults, thrust faults and asymmetric folds. Since this is an area with complex structures due to high deformation, reflectors will frequently change direction often, due to folding. This cause a problem in the processing because it gets more difficult to migrate the traces to correct place in time and space. As a consequence, the area appears very noisy and is hard to interpret. The interpretation of this area was simplified by applying Relative Acoustic Impedance map and/or amplitude smoothing map. The structures of the eastern area vary to some degree between seismic lines. The asymmetric folds seen in the complex area between 500 and 1000ms in fig 6.34 resemble the same structures of deeper reflectors, suggesting they were formed under the same tectonic episode. The arrows in fig 6.34 show the axial plane through the asymmetric folds, and can be followed down to approximately 3000 ms twt, below which different structures appear.

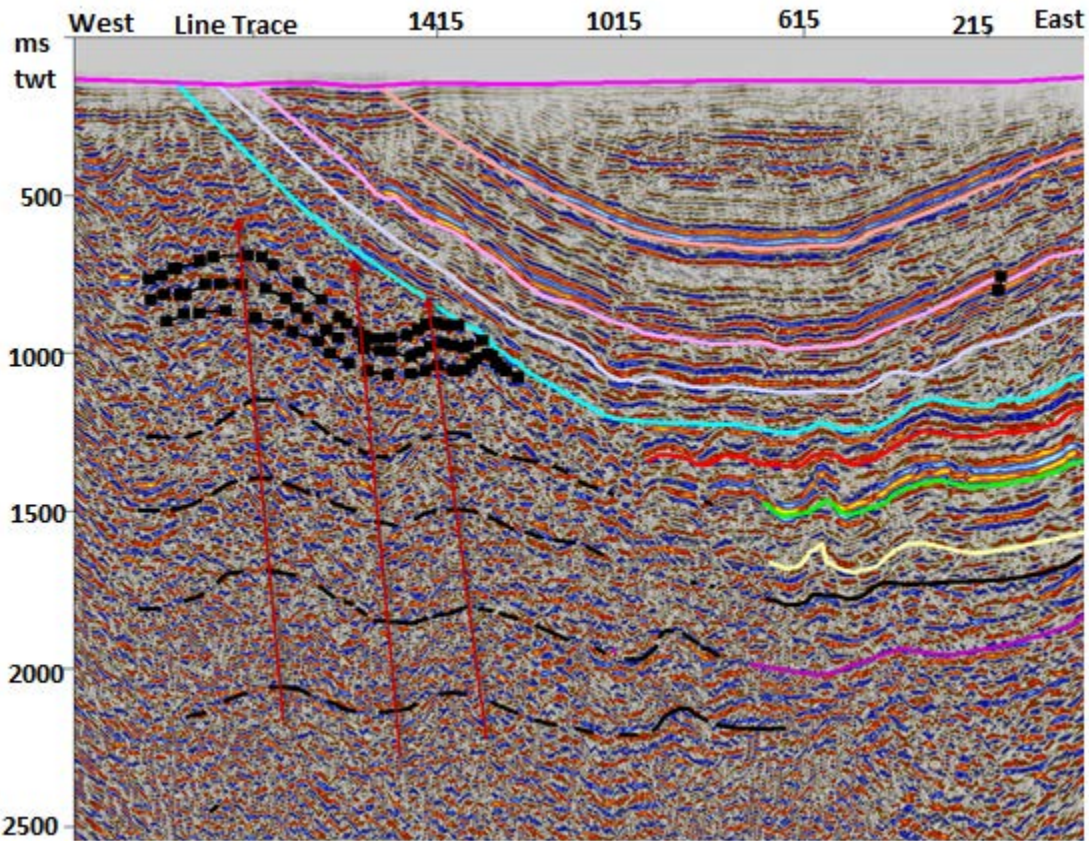
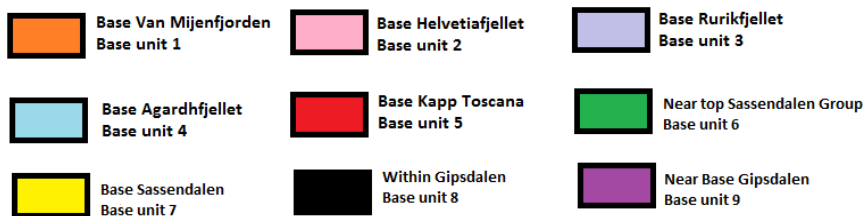


Fig 6.34: Shows the Duplex structures seen on profile 14.08. Same type of structures appear on line 14-07,14-06 and 14-03



The same type of structures are seen on the following profiles 14-07, 14-06 and 14-03, however on profile 14-03 the layers have higher dip. On profile 14-05 more symmetrical structures appear, as shown in figure 6.35. Similar structures appear on profile 13-09 and 13-14,13-11 and 14-10.

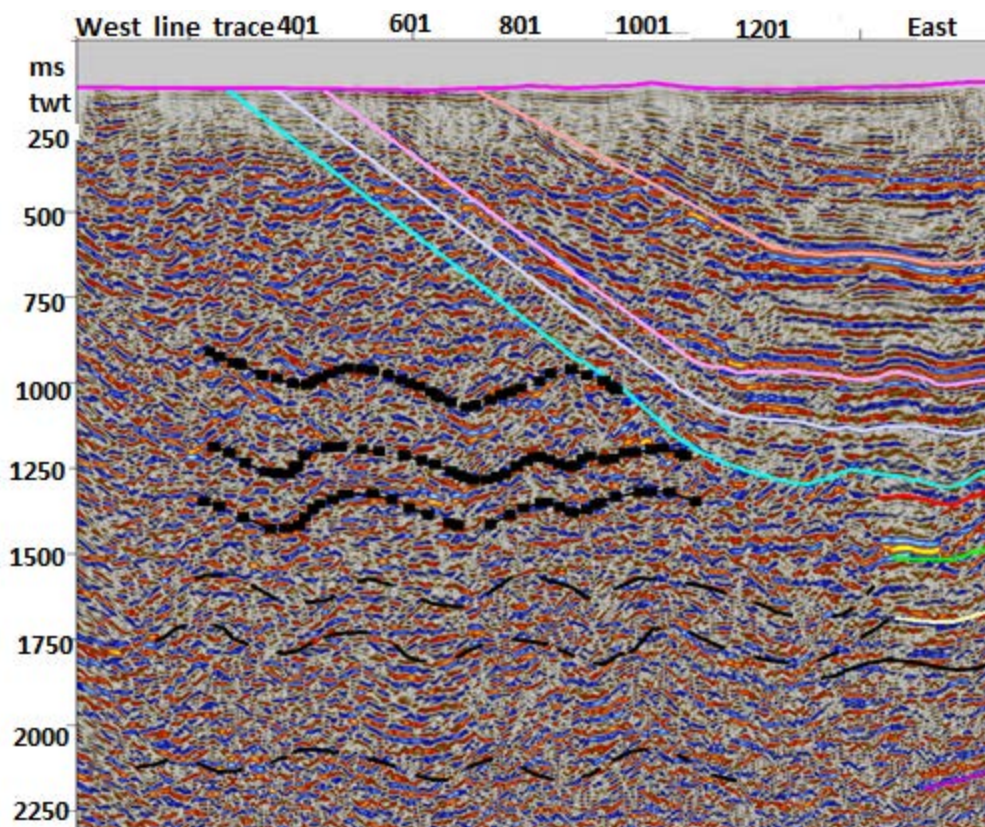


Fig 6.35: Shows the structures seen on line 14-05 .Similar structures are seen on line 13-09,13.14,13-11 and 14-10



On line 14-04 the layers are dipping towards west, see fig 6.36. This is the only line where this configuration is found. In general profiles further north show more symmetrical structures. Lines located in the middle of the study area show geometry like that on figure 6.35 and the three lines further south all three lines shows three different geometries. In line 14-03(southernmost line)-, layers are dipping towards east. On line14-04 layers are dipping towards west and on line 14-05 more symmetrical folds are found.

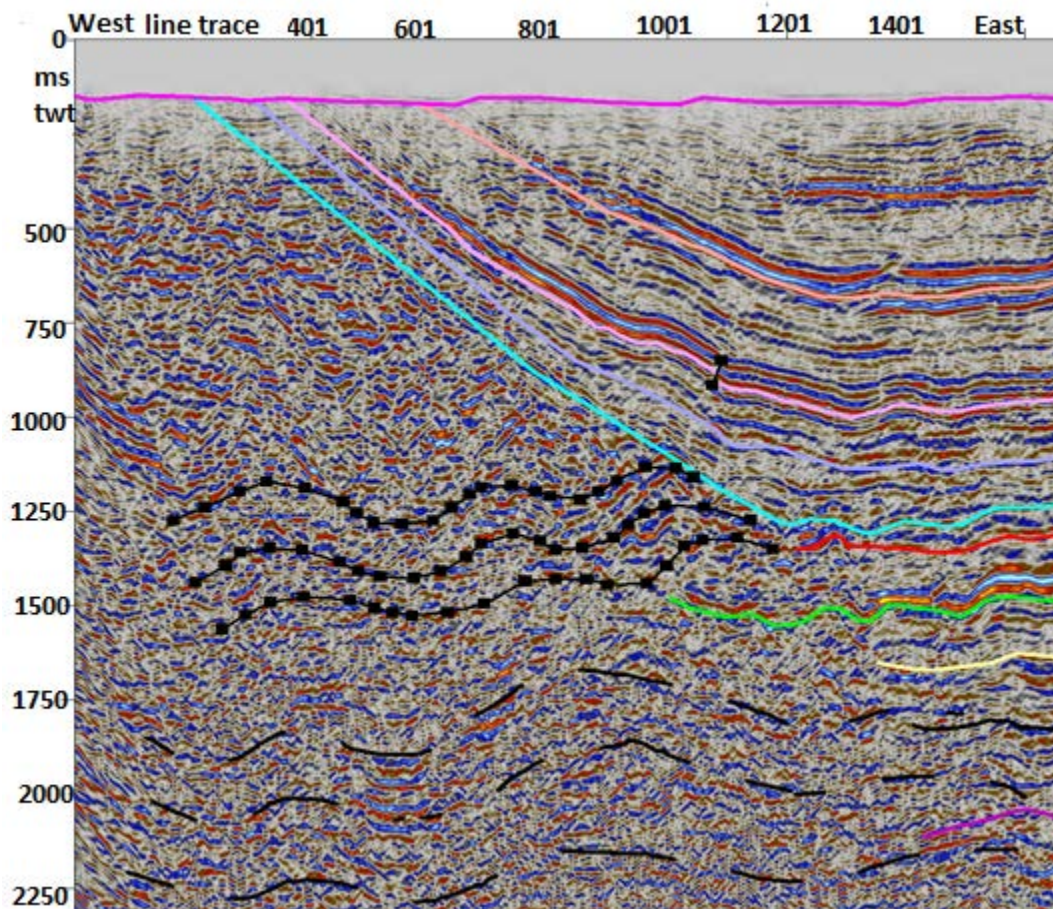
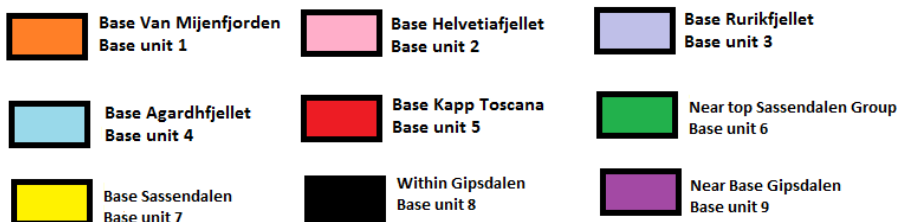


Fig 6.36: Shows that the structures of line 14-04 are dipping towards west, this is the only line where structures are dipping in this orientation.



6.4 Hecla Hoek

Finding top Hecla Hoek is difficult since the seismic is chaotic under 2400 ms twt. By applying a relative amplitude map and adjusting the amplitudes, two strong reflections are seen at 2600 ms marked by blue arrow and 2800 ms marked by red arrow. One of these reflections could be Top Hecla Hoek. Reflectors below 2600 ms are generally of higher amplitudes which could be a result of higher velocities because the density of the Hecla Hoek rocks must be high because they are located at a deeper depth. The seismic at this depth is too noisy for trying to interpret

how the horizon manifests to the west.

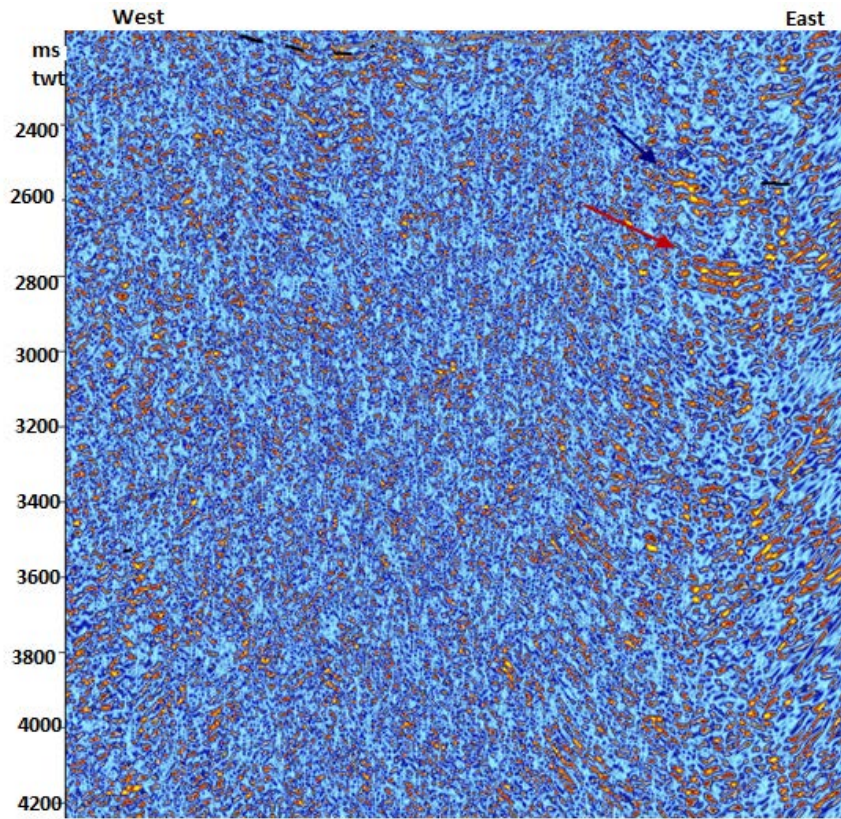


Fig 6.37: the arrows show two different locations of where Top Hecla Hoek could manifest

 Top Hecla Hoek on 2600 ms twt  Alternatively: Top Hecla Hoek on 2800 ms twt

Chapter 7

7.1 Previous studies

The following chapter compares the interpreted seismic with previously work in the study area. In the east the study area is dominated by a big syncline, Spitsbergen Central Basin (CSB), on the western side by Spitsbergen fold-and thrust belt (WSFTB). The interpreted seismic lines based on data from the Ishøgda well are compared with the following studies.

- 1) Interpretation of a 2D line from Van Mijenfjorden, interpreted by Eiken (1985).
- 2) Seismic Atlas of Western Svalbard by Eiken and Austegard (1994), which includes description of seismic profiles in the study area
- 3) Results from Bergh, Braathen et al. (1997), onshore studies in western part of Nordenskiöld Land, mainly northwest of the study area.
- 4) Results from Blinova, Thorsen et al.(2009) and Blinova, Faleide et al. (2012.), which describes studies of respectively Bellsund Graben (west of Van Mijenfjorden) and Isfjorden (north of Van Mijenfjorden), mainly based on marine seismic data.
- 5) Strømme(2010):Processing and interpretation of seismic data from Van Mijenfjorden
- 6) Nøttvedt (1994):Post Caledonian sediments on Spitsbergen

Results from previous publications, especially from sono buoy measurements from Van Mijenfjorden conducted by University of Bergen (1981) show increasing velocity with depth, (Eiken 1985). Measures from the Ishøgda well show an average increment in velocity with depth. However there exist units within the formation where the velocity decreases. This applies to upper unit 2 to middle unit 2, lower unit 2 to unit 3, unit 3 to unit 4, unit 5 to unit 6, upper unit 7 to lower unit 7, see Fig 6.5. Results from the velocity analysis also show increasing velocity with depth. Nevertheless there exist certain zones where the velocity drops, especially for the shallowest reflectors where most velocities are selected. The drop in velocity most likely responds to a velocity reduction from upper unit 2 to middle unit 2. By comparing the interval velocity information from the velocity analysis (fig 5.18) with velocity information from the well, it is possible that too high velocity is picked in the velocity analysis. The reason is that velocities are near 5000 m/s after 200 ms, interval velocities close to 5000 m/s are only present at base 6. As a consequence not all horizons marks an increase in acoustic impedance as indicated from the sono buoy. Therefore the interpretation has not focused on choosing every reflector on a positive trace deflection. The only reflector where this has been given attention is the seabed reflector, which is picked on a positive trace deflection because it represents an

increase in acoustic impedance.

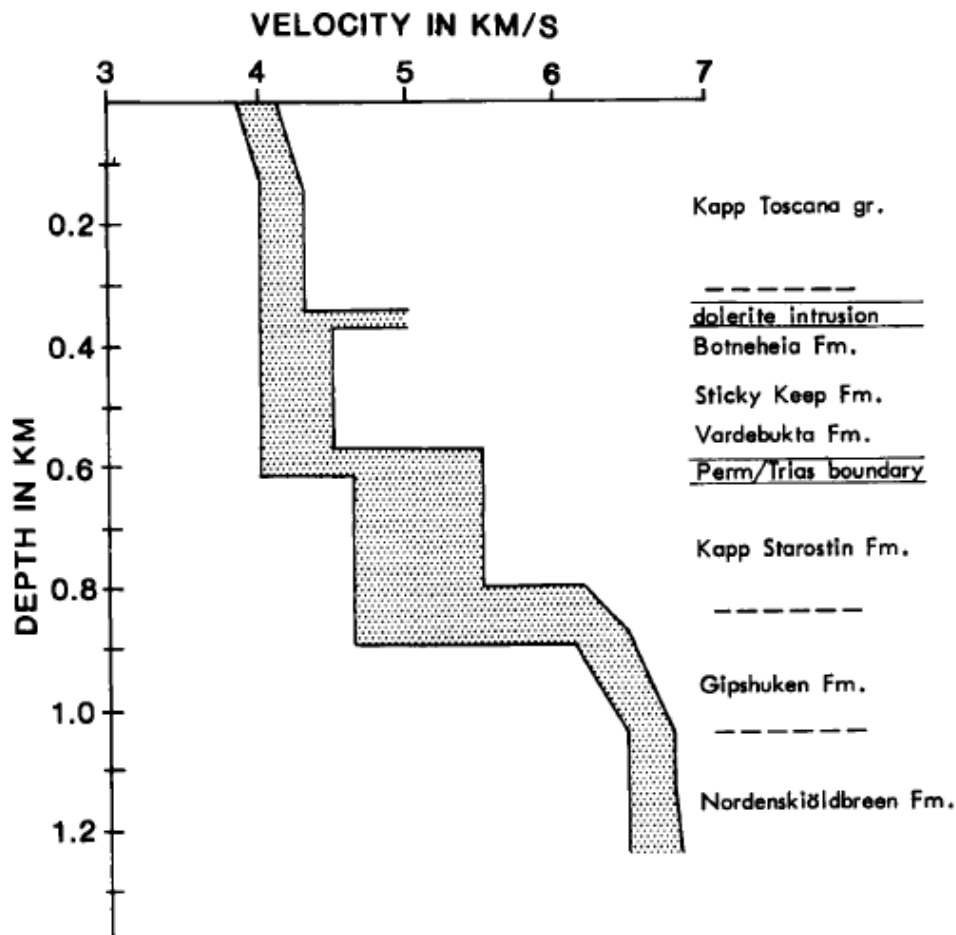


Figure 7.1: The figure shows a velocity/depth correlation from a land-seismic survey in Agardhdalen. On the right is the corresponding geological interpretation of the velocity model (Eiken 1985).

7.2 Tertiary

The Tertiary unit consists of a broad asymmetric syncline corresponding to the Spitsbergen Basin. Since Upper Cretaceous rocks are missing on Svalbard base Tertiary is an unconformity.

On the eastern side the reflector is picked at 580 ms twt, vertically above the peak anticline structure of the middle Triassic dolerite, see fig 6.3 and 6.7.

The Base Tertiary reflector is as the other reflectors based on the interpretation of POLINV 6, a cross line crossing the ten seismic lines. When this reflector is traced downwards to the east, it ends up at the bottom of a series of strong reflections. This corresponds to the

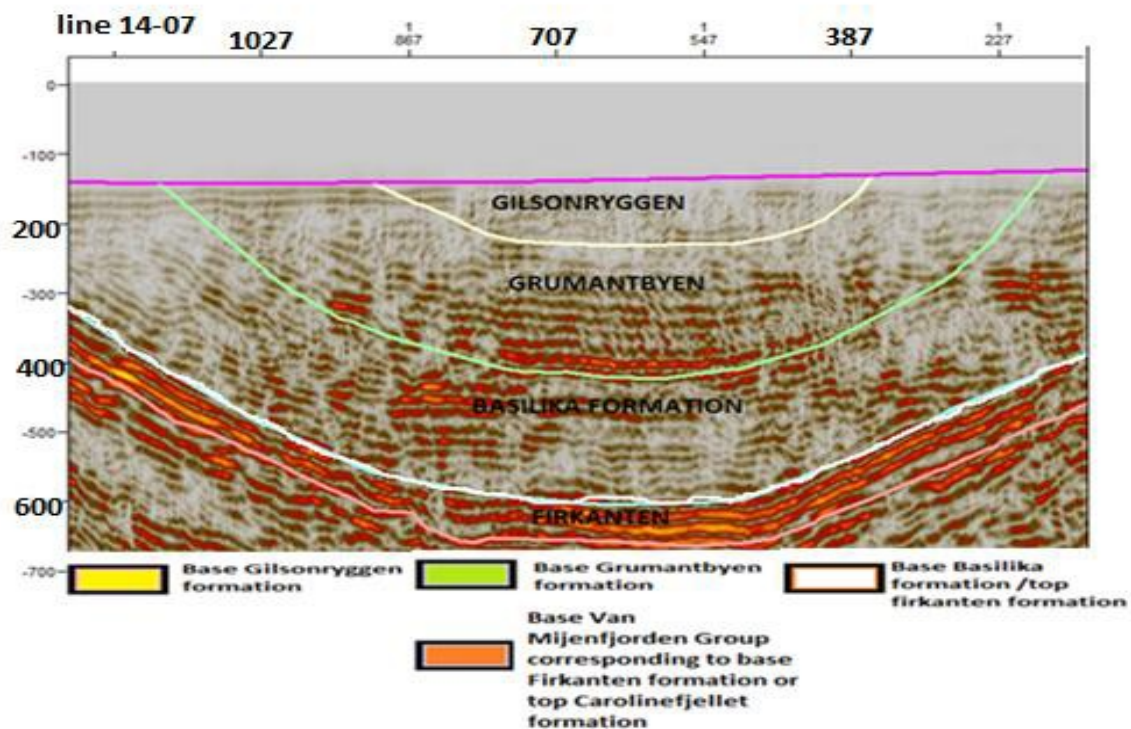
seismostratigraphic definition of Eiken and Austegard (1994). However, Base Tertiary is in several studies from Isfjorden defined as a transparent zone within a series of strong reflections (Bergh, Braathen et al. 1997). It is therefore possible that base Tertiary can be located deeper. The thickness in the middle of the basin is estimated to be 1030 meter, which is slightly smaller than the thickness of 1.1-1.2 km estimated by Eiken(1985).

The interpretation of Gilsonryggen, Grumantbyen, and Basilika were not interpreted on POLINV 6, and the interpretation of these formations were based on variations in acoustic impedance. Base Gilsonryggen formation is interpreted to be located at 320 ms and is within a series of weak reflectors. Based on the Seismic stratigraphic map by Nøttvedt (1994), base Gilsonryggen is at the bottom of a strong reflector at 200 ms depth. No noteworthy impedance contrast at 200 ms is seen at line-14-07. The cause for the different seismic configurations is either processing related or associated with regional differences in geology.

Grumantbyen formation is within a series of stronger reflectors and is picked at 500 ms in the middle of the syncline. In the interpretation performed by Nøttvedt (1994), base Grumantbyen formation consists of two strong reflectors at 420 ms and the reflection amplitude decreases gradually upwards into a transparent zone.

The Basilika formation is within a package of weak reflectors, the base of the formation is picked at 600 ms on the top of a series of strong reflectors. These observations are consistent with the seismic stratigraphic diagram of Nøttvedt (1994). In addition, base Tertiary (base Firkanten formation) is interpreted to be at the bottom of a series of strong reflectors. Since the same seismic characteristic is detected on the ten seismic lines, it is likely that base Tertiary is picked correctly.

By adjusting for the depths of Gilsonryggen and Grumantbyen by assuming the interpretation performed by Nøttvedt (1994) is more realistic, a modified interpretation of Van Mijenfjorden group is given in fig 7.2



Fig

7.2: Shows an alternative interpretation of the various formations in Van Mijenfjorden Group on line 14-07 compared to fig 6.12.

The high continuity and amplitude in the Firkanten formation is possibly related to coal seams near the base of the formation see section, table 3.1. Coal in the Firkanten formation is also reported by various authors including Manum and Throndsen (1978), Marshall, Ugunaa et al. The thickness in Firkanten formation is estimated to be 120 meter (60 ms twt between base Van Mijenfjorden Group and Top Firkanten, interval velocity of 4000 m/s). On Spitsbergen the thickness of this formation ranges from 100 to 170 meter and the thickness of 120 meter is thus in the correct thickness range (Orheim, Bieg et al.2007).

Following, the thickness between Base Basilika formation and Base Grumantbyen is 360 m (180 ms twt, interval velocity of 4000 m/s). A thickness of 350 m is estimated for the Basilika formation in Van Keulenfjorden according to (Dypvik and Nagy 1978).

Furthermore, a thickness of 400 meter is the estimated thickness of Grumantbyen formation (200 ms twt, 4000m/s). According to Livsic (1992) the thickness of Grumantbyen formation in Western Spitsbergen is in the range of 160 to 240 meter, as a consequence a thickness of 400 is overestimated.

A correction for this is done by adjusting base Gilsonryggen down to the impedance contrast, and as a result a thickness of 240 meter is obtained. Now is also the thickness Gilsonryggen consistent with the thickness of Frysjaodden Formation ranging in thickness from 200 m in northern Spitsbergen, to more than 400 meter towards the southern and

southwestern parts (Svinth 2013). By adjusting for these observations the following interpretation of the formations within the Van Mijenfjorden group is given in fig 7.3. The sum of the various depths in the Van Mijenfjorden group gives:

$$320+240+350+120=1030\text{m}$$

The reason Eiken (1985) got a higher thickness in the Tertiary unit is that slightly higher velocity is used, see fig 7.1.

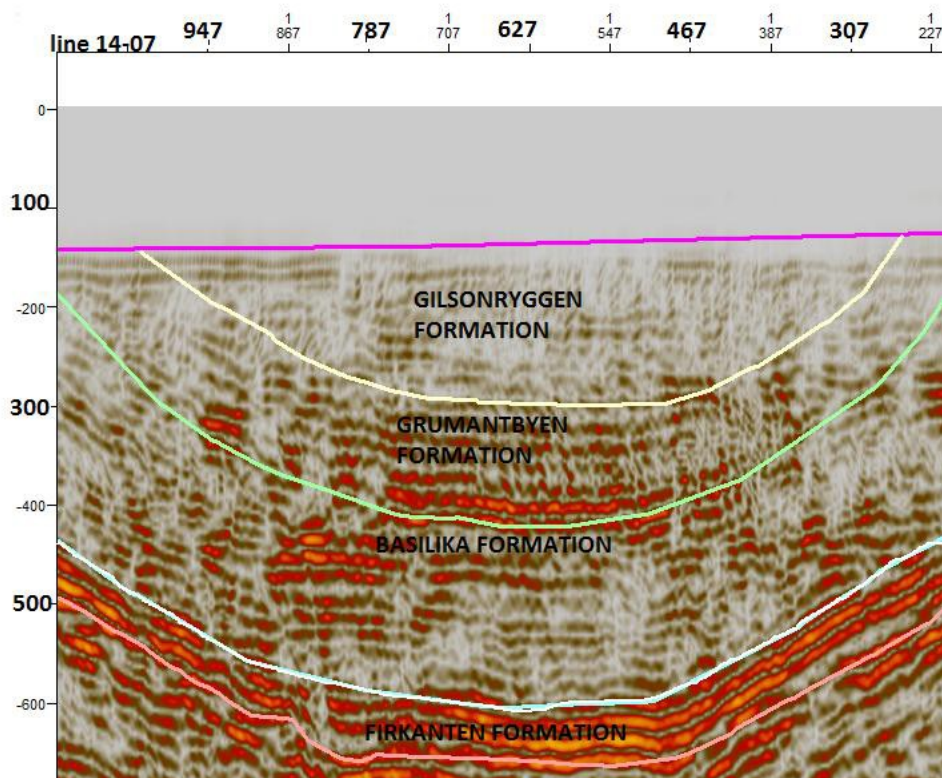


Fig 7.3: Shows the formations within the Tertiary units after correction for depth errors in fig 7.2.



7.3 Cretaceous Unit

Carolinefjellet formation, Helvetiafjellet formation and Rurikfjellet formation are all part of the Cretaceous unit. The two reflectors in the Cretaceous unit directly correlated to the well are base Rurikfjellet and base Helvetiafjellet formations, see fig 6.4. Base Helvetiafjellet is picked at 880 ms twt; vertically above the peak anticline structure of the middle Triassic dolerite, see Fig 6.3 and 6.7. This reflector can be followed down to 950 ms in the middle of the syncline. As seen in figure 6.15, the Helvetiafjellet formation has stronger amplitude than the overlying Carolinefjellet formation but the amplitude and continuity as well as reflector spacing are variable

The highest amplitude showing the most continuous reflector with the least reflector spacing is found on the dipping layers towards the west, although it stops at approximately 400 ms due to reflectors cutting into multiples, see fig 6.5 (blue arrow). In the middle of the syncline reflectors show smaller amplitude, less continuity and higher reflector spacing, see fig 7.6. The larger reflector spacing with depth is most likely caused by gradual loss of higher frequencies with depth.

According to Faleide and Gudlaugsson (1985) this formation consists of deltaic sandstone. Continuous reflectors are characteristics of deep water environments Badley and Gibson (1987). Since this reflector does not show high continuity, it makes the interpretation of deltaic sandstone more realistic since reflectors having low continuity are not representative of deep water environments. Subsequently, variable amplitude and continuity is typical for deltaic deposits according to Sheriff and Geldart (1985), see table 3.1.

The depth of the Helvetiafjellet corresponds to the depth interpreted by Nøttvedt (1994) and the Helvetiafjellet formation is in his interpretation similarly within a zone of more discontinuous reflectors. It is worth noticing that Nøttvedt (1994) interpreted base Helvetiafjellet as intra lower Cretaceous.

Bergh, Braathen et al. (1997) described the base of the Helvetiafjellet as a sharp contrast between the Janusfjellet Formation subgroup and the Helvetiafjellet Formation, see fig 7.6. The interval velocity within the Helvetiafjellet is 4600 m/s, and the underlying shales of the Rurikfjellet formation have velocities of 4400 m/s. This is consistent with Eiken (1985) and Flood, Nagy et al. (1971), stating there exist a very small velocity contrasts both below and above this unit.

Eiken (1985) interpreted the depth to intra Lower Cretaceous to be 2 km. By calculating the average velocity down to the base of the Helvetiafjellet (4250m/s) and using the depth down to the interface (950 ms twt) a depth of 2020 m is obtained which is close to his estimate.

The overlying Carolinefjellet formation is interpreted to be within a package of reflectors showing low amplitude, see fig 7.6. According to Krajewski and Luks (2003), a section of the Carolinefjellet Formation in coastal cliffs at Kapp Morton in Van Mijenfjorden shows a wide range of deposits ranging from shales, silt, sandstones to “cannon ball carbonate concretions”.

The thickness of the Carolinefjellet formation was estimated to be roughly 570 meter, see fig 6.16 and 6.17. Investigations done in the area on land adjacent to Van Mijenfjorden shows that the thickness of the Carolinefjellet formation reaches up to 600 meter, more than twice the thickness of the same formation in the Longyear area (Hars, Maher et al.2001)



Fig 7.4: Shows the area where the thickness of Carolinefjellet was measured (Hays, Maher et al.2001)

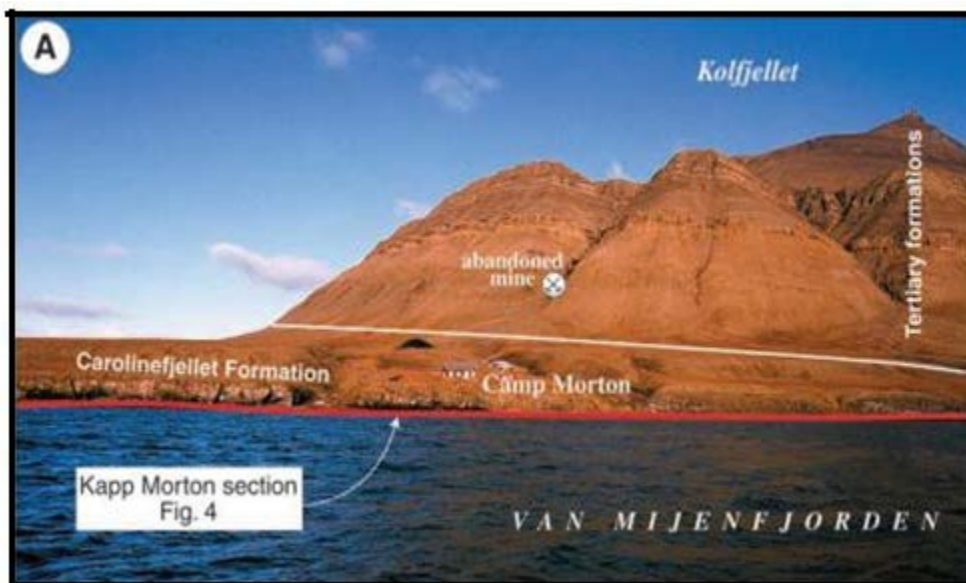


Fig7.5: Shows the location of Carolinefjellet formation on Camp Norton, adjacent to Kolfjellet (Krajewski and Luks 2003).

Base Rurikfjellet formation is picked at 1100 ms. This depth is 100 ms deeper than the depth picked by Nøttvedt (1994). A thickness map was created showing that the thickness is 220-275 meter. According to Dypvik, Eikeland et al. (1991) the thickness of Rurikfjellet formation in central Spitsbergen reaches up to 226 meter. The high thickness of 275 meter interpreted at the very edge of the seismic could then be seen as thickness distortions, due to seismic waves coming from the sides.

Base Agardfjellet is picked at 1180 ms on the eastern side where the anticline structures are located, see Fig 6.3 and 6.7.

By following the reflector down to the the middle of the syncline the elevation time for this reflector reaches the deepest point on 1280ms twt, which corresponds to the depth interpreted by Nøttvedt (1994).

Although the top of the formation in his study is picked at 1000 ms twt compared to 1100 ms twt. The shallowest point of this reflector is located at 1200 ms twt; this reflector corresponds to Upper Triassic and is described by Bergh, Braathen et al. (1997) as representing a velocity contrast between the Kapp Toscana Group (sandstones) and overlying low velocity shales of the Janusfjellet Subgroup.

According to the same authors higher amplitudes are found below this reflector and weaker amplitudes above. This is consistent both with (Strømme 2010), who interpreted upper Triassic at 1200 ms in the middle of the basin, and the seismic lines in this thesis.

By comparing the statement by Bergh, Braathen et al.(1997) with velocity information from the well, we see that the Agardfjellet member of the Jansufjellet fm has an interval velocity of 4100 m/s and the underlying Kapp Toscana has interval velocity of 4600 m/s, validating the claim.

The interval between 1200 ms twt and 1100 ms twt (Agardhfjellet) is in the interpretation by Nøttvedt (1999) an area of low amplitude, the amplitudes in the Rurikfjellet formation is considerably higher.

The same type of seismic characteristics is found in this survey, see fig 7.6. In chapter 6 Base Agardhfjellet Fm was interpreted as an unconformity, likewise in Isfjorden there is an unconformity at the Triassic/Jurassic boundary (Blinova et al., 2012)

Thickness estimation was done where the estimated thickness reaches up to 310 meter. The cause for the bigger thickness variation in Agardhfjellet formation compared to Rurikfjellet formation is due to more extensive folding of the layers.

Thickness variation in the Janusfjellet subgroup is also mentioned by Dypvik, Eikeland et al. (1991). Different causes for thickness variation is mentioned :

1. several episodes of syndepositional movement,
2. differences in sediment accumulation,
3. Mesozoic normal faulting,
4. extensive erosion.

However, a recent investigation has shown that most of the thickness variations found within the Janusfjellet subgroup can be explained by Tertiary compressional tectonics (Dypvik, Eikeland et al. 1991). This is in agreement with the seismic, since within this subgroup-, layers are extensively folded, especially in the Agardhfjellet Fm, see fig 7.6. The thickness of the group is also mentioned by Dypvik, Eikeland et al. (1991) confirming a thickness up to 290 m in central Spitsbergen. This is close to the thickness estimated in this survey reaching up to 310 meter.

According to Faleide and Gudlaugsson (1985) late Jurassic shales in the Janusfjellet formation played a key role in the deformation of the above lying layers. The shales were mobilized and started to flow, differential loading was probably the most important factor contributing to the mobilization.

According to the seismic, it becomes clear that thickness variation in Agardhfjellet formation is due to folding, caused by compression, see fig 7.6. Layers within the Rurikfjellet are less folded. It is not sure that the small anticline structures marked by the arrow in fig 7.6 within the Rurikfjellet formation and Helvetiafjellet formation is caused by compression, inducing small anticline structures within the layers of the syncline. Or if the cause is mobilization of the shales from the Agardhfjellet formation as stated by Faleide and Gudlaugsson (1985).

As seen on fig 7.6, the base of the Agardhfjellet formation has a folded characteristic but the package within this formation is less folded. As a consequence the folded layers within the Rurikfjellet and Helvetiafjellet is likely to be caused by mobilization

of the shales, since this explains the amplitude differences marked by the red and green arrows in fig 7.6.

It is also likely that the differences in folding are due to different rock properties causing rocks to fold differently under same amount of pressure. The induced pressure could also vary with depth causing different geometries of folds.

If the theory concerning mobilization of the shales is correct, it caused deformation up to the Carolinefjellet formation in all the 7 northernmost lines as no anticline structure is seen within these formation or the above lying formations.

However in the 3 southernmost lines, from 14-03 to 14-05, an anticline structure is seen in the Van Mijenfjorden group, see fig 7.15. The anticline structures gets progressively bigger and more complex towards north, reaching its most complex structure at line 14-05.

No anticline structure in the Tertiary unit is seen from line 14-06 and further north. It is not sure if these structures are related to compressional forces or if they are related to mobilization of the shales, because as fig 7.6 indicate the amplitude in the Carolinefjellet formation is low and only limited information is possible to get out concerning folding of the layers.

However, since the anticline structure in line 14-05 is broader than the anticline structures within the underlying Helvetiafjellet, it is likely that these structures are related to compression, since we would assume the same width in the underlying formation, but this is not observed, see fig 7.16.

The only line showing signs of anticline structures within the Carolinefjellet formation is on line 14-04, as a consequence, mobilization of the underlying shales could play some role in the deformation of structures within Lower Van Mijenfjorden group, since the anticline structure seen within lower Tertiary resembles the anticline structures in Carolinefjellet and Helvetiafjellet.

No anticline structures are seen above Firkanten formation in any lines.

It should be mentioned that the vertical resolution is 50 m, therefore minor folds and structures could occur in the seismic, however none bigger than 50 meter.

The thickness of the Jurassic-Cretaceous sequence has been discussed in the literature.

Eiken (1985) estimated a thickness of 1500-2000 meter which is much more than the 750-900 m suggested by Flood, Nagy et al. (1971).

By summing the three thickness found within the Jurassic-Cretaceous sequence (310+570+226) and estimating the thickness of the Helvetiafjellet formation using 70 ms twt two-way travel time in the formation and an interval velocity of 4600 m/s, a thickness of 161m is obtained.

Adding this onto the three thicknesses gives a thickness of 1270m, which is somewhere in between of the two estimates.

This thickness is close to the thickness of 1350 m measured in the Grumantbyen borehole

about 40 km north of van Mijenfjorden (Skol et al.1980 rendered by Eiken 1985).

It should be mentioned that the thickness will vary somewhat because of the folding of the deeper events and that the thickness corresponds to the thickness in the middle of the basin.

According to Faleide and Gudlaugsson (1985) the Helvetiafjellet formation consist of fluvio deltaic sandstones, dark shales and some coal. The fluvial dominated sequence is sourced mainly from an uplifted region in northern Spitsbergen.

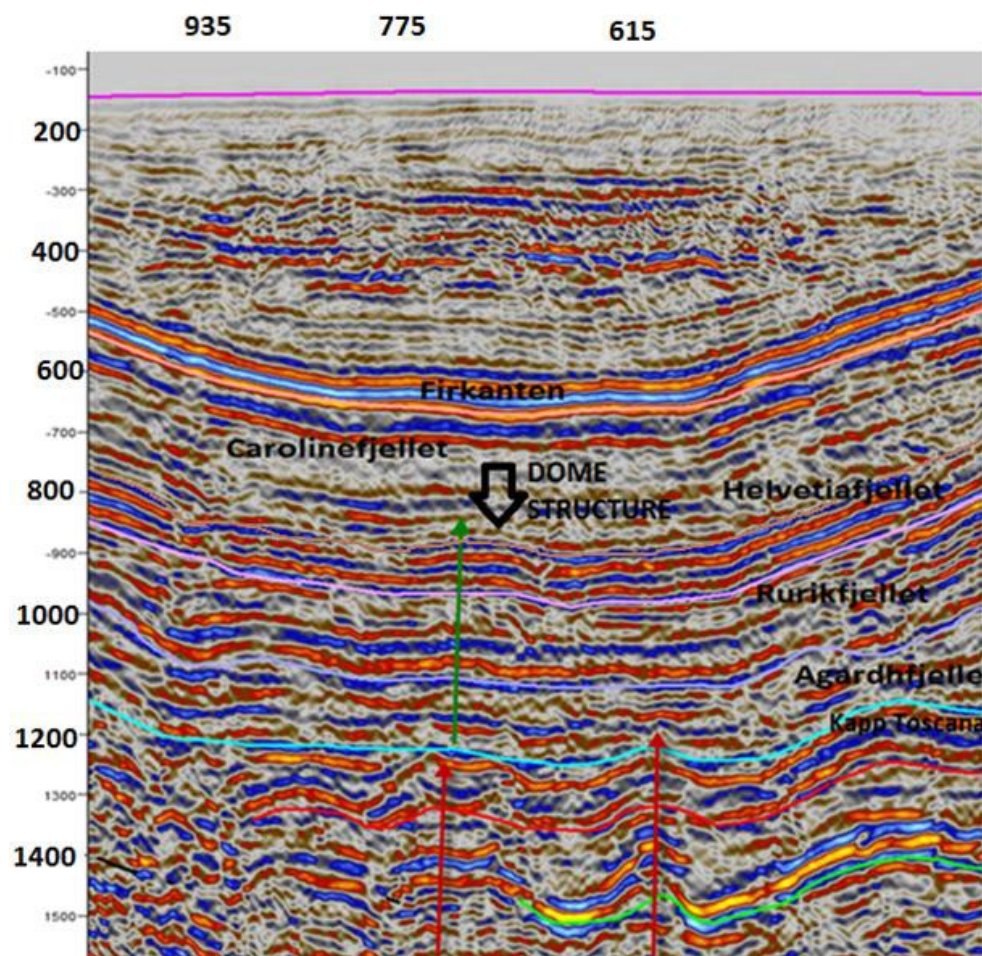


Fig 7.6: Green arrow points out the dome structure seen in the Rurikfjellet and Helvetiafjellet, which are caused by mobilization of the Late Jurassic black shales



7.4 Triassic unit

The Kapp Toscana Group and the Sassendalen Group are both part of the Triassic unit. Base unit 5 (red reflector) is close to base of the Kapp Toscana, see Fig 6.4.

The upper part of Kapp Toscana group is called Wilhelmøya formation. According to Faleide and Gudlaugsson (1985) this is a thin marginal unit representing sporadic sedimentation from later Triassic into Middle Jurassic times. Faleide interpreted this horizon to be a sill within the Kapp Toscana group.

However this is uncertain, as Fig 7.6 shows the relative amplitude strength between the positive identified sill between 1300 and 1500 ms differs greatly compared to the amplitude between 1200 and 1300 ms. Also the package within the Kapp Toscana (between red and blue reflector) is possibly continuous over a greater distance by following the direction of the duplex structures, see fig 7.8.

The underlying dolerite between green and yellow reflector are in this model cutting into the duplex structures which are a continuation of the Upper Triassic shales, see fig 7.8. A model where a single, thick dolerite occurs, is proposed in Fig 7.9; here the dolerite intrudes in both the Kapp Toscana Group of upper Triassic and the upper part of Sassendalen group in the middle Triassic.

As figure 7.9 indicates both the reflectors in the Kapp Toscana and the reflectors corresponding to Upper Triassic stops by the black line indicating a polarity shift, which could specify where the dolerite stops, since different colors indicating differences in acoustic impedance are found on both sides of this line.

However, since the relative amplitude strength between the upper and lower part are large this is not likely to occur, because the dolerite would normally not have a lower amplitude anomaly in its upper part and bigger in its lower part, see fig 7.7.

If two dolerite intrusions exists, one intruding into the Kapp Toscana and one intruding into the Middle Triassic, a question worth answering is: why the relative amplitudes between the two dolerites differs?

The amplitude strength could differ if the two dolerites have different thickness, see fig 7.6 for amplitude differences. However, since the upper Triassic layers can be followed in the direction marked by the black horizon in fig 7.8, a model with two different dolerites is unsure. Nevertheless, it is possible because according to velocity information from the well the interval velocity in Kapp Toscana and the area where the dolerite is located both show the same velocity of 6000 m/s, and this kind of velocity is normal for dolerite intrusions.

The most realistic model would then be a smaller dolerite intrusion in the Kapp Toscana and a bigger dolerite in Botneheia Fm of the Sassendalen Group. As fig 6.26 shows it is possible

that there are two small dolerites in Kapp Toscana, because the reflector spacing is bigger compared to the underlying dolerite.

Fig 7.7 shows a different extension of the Kapp Toscana package compared to fig 7.8.

Here the extended horizons follow the small syncline structure of the overlying Agardfjellet formation marked by the purple arrow; the end of the arrow shows the same doming as the beginning of the arrow in fig 7.7.

This doming is not shown above base Helvetiafjellet formation, indicating that the structure could be caused by differential loading of the overlying sediments. Furthermore, the lateral extent of the dolerite intrusion (between the green and yellow horizon)-is uncertain. The dolerite could stop by 1; blue arrow marking the end of the bright amplitude, 2; the red arrow allowing smaller amplitude laterally, 3; by the black duplex structures.

The package between green and yellow reflector is also interpreted by Nøttvedt (1994) to be a dolerite intrusion and is interpreted at the same depth as the reflector in this thesis. However Eiken (1985) suggested two different interpretations of the reflector, either the Permian/Triassic boundary or a sill in the middle Triassic, but favored the sill interpretation. Work done by Faleide and Gudlaugsson (1985) confirms the sill conclusion.

According to Eiken (1985) sill intrusions are common in middle Triassic around Storfjorden.

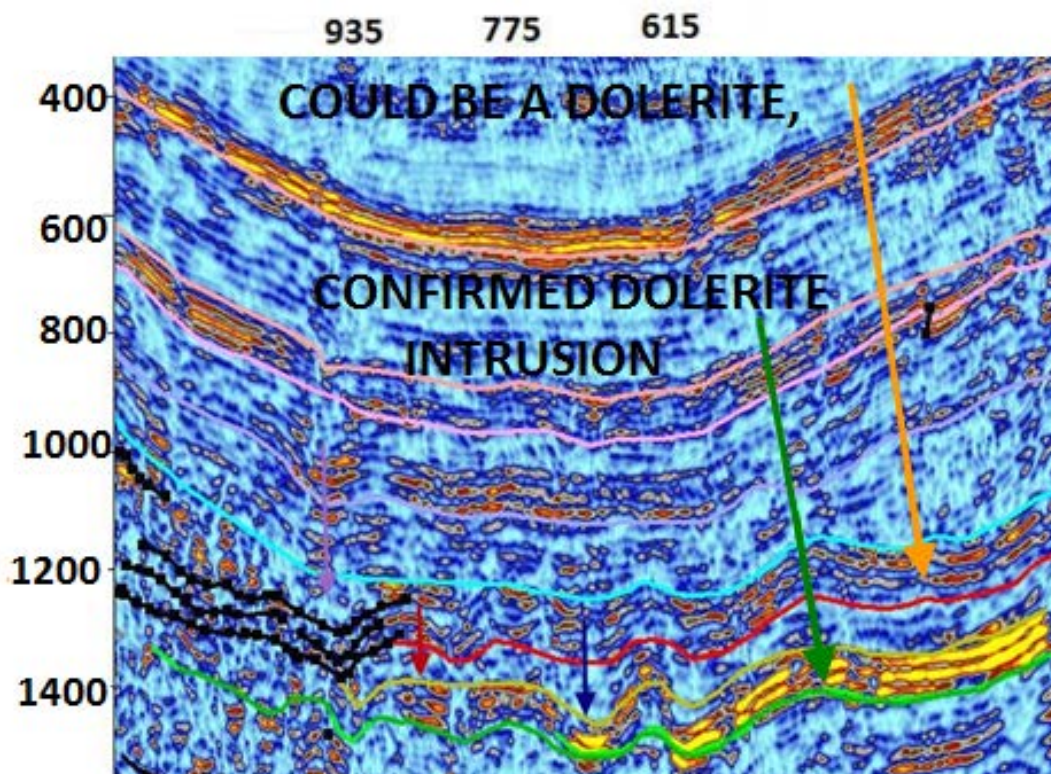


Fig 7.7: Figure points out where the dolerite intrusion might stop. The black structures under purple arrow is an alternative interpretation of the horizon in the area compared to fig 7.8

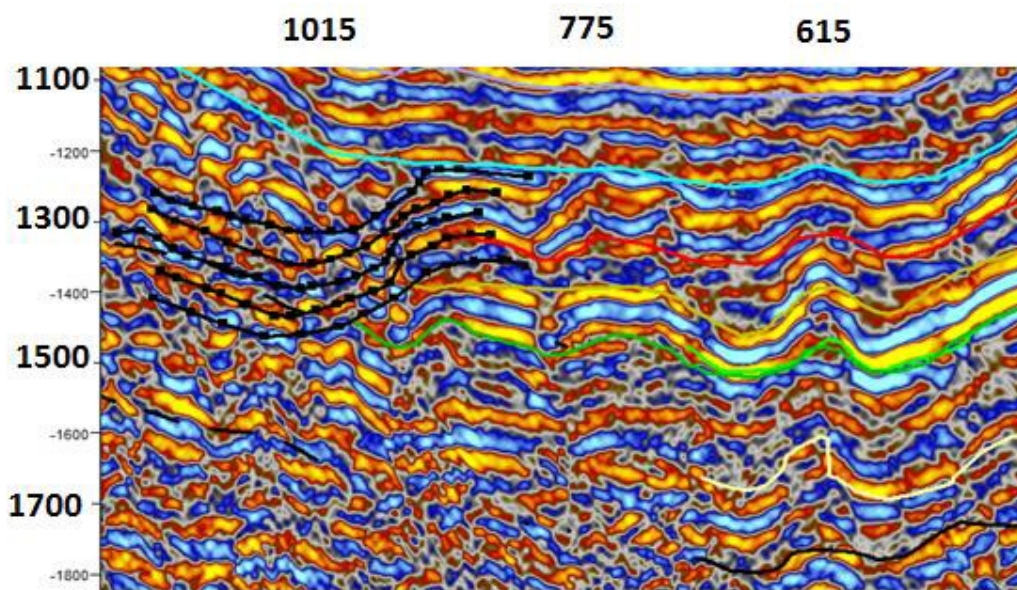


Fig 7.8: Figure shows that at the end of the dolerite different kinds of polarity appear. Another interpretation is a fault.



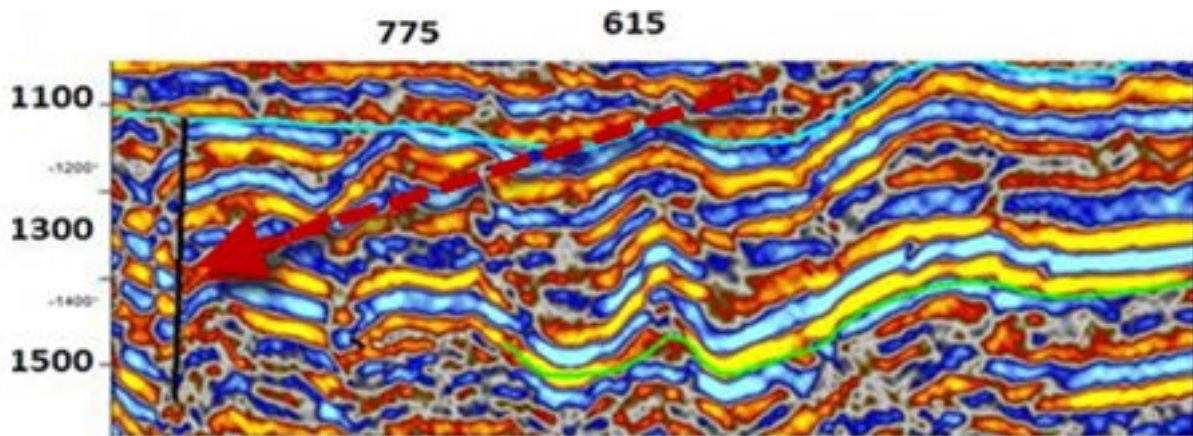


Fig 7.9: Figure shows that at the end of the dolerite. Different kinds of polarity appear this could be where the dolerite ends. Another interpretation is a fault.



Table 7.1: Show that the dolerite is deformed differently on one line to another.

Line	
14-03	Dolerite dips towards west, anticline structure appear in the dolerite.
14-04	Shows a clearer anticline structure,
14-05	Tighter anticlinal compared to that on 14-04
14-06	Even tighter anticlinal compared to 14-05
14-07	Fold appearing here is similar to than on 14-06
14-08	Similar to the fold on 14-07(is clearer)
13-09	Similar to than on 14 -07 (not as clear as 14-07)
14-10	Anticline structure is smaller.
13-11	Similar to 14-10
13-14	The strong amplitude appearing between 1400 and 1500 ms twt does not show at this line. Probably no dolerite in this line.

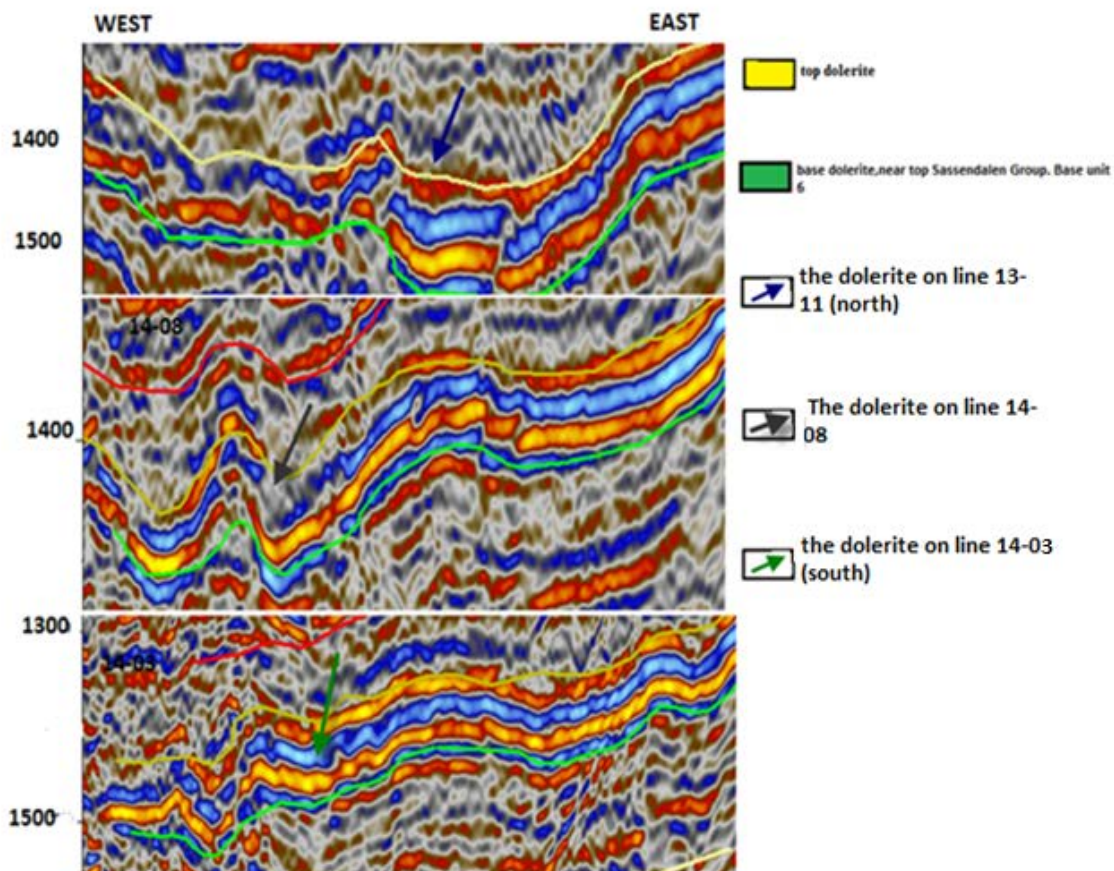


Fig 7.10: The figure shows that the geometry of the dolerite varies from one line to another.

The main observation in the seismic is that the dolerite show higher degree of folding in the lines located in the southern and middle part of the survey, whereas line 14-10 and 13-11 show much weaker, or non-existing anticline structure. This could be caused by less induced stress into the lines further north. The age of the dolerite is probably of Early Cretaceous age since the presence of Cretaceous igneous intrusions is well documented throughout Svalbard (Senger et al., 2011)

7.5 Permian unit

Top Permian reflector is picked at 1600 ms in the anticline structures seen on the eastern side. The reflector is interpreted based on the depth and the geometry of the reflectors seen in Fig 6.3 and 6.7.

Following the reflector to the middle of the basin it reaches a depth of 1700 ms.

This is consistent with Nøttvedt (1994).

The depth of the top Permian reflection is also interpreted at approximately the same depth as

Strømme (2010), where the horizon is near 1700 ms in the middle of the profile (under the middle of the syncline).

According to Bergh, Braathen et al,(1997) the top Permian reflection is identified as a strong impedance contrast between the high velocity silicified carbonates of the Kapp Starostin formation and overlying low velocity in Sassendalen Group (weak discontinuous reflections). This statement is consistent with the seismic interpreted by Strømme (2010) and the seismic lines in this thesis, see fig 7.11.

Similarly, in the interpretation done by Nøttvedt (1994) the area between the top Permian unit and the base of the dolerite intrusion is characterized by low seismic amplitude, see fig 7.11. This package corresponds to Vardebukta Fm (lower part of Lower Triassic), and Tvillingodden Fm (upper part of Lower Triassic).

A strong reflection is seen in the middle of the package and is interpreted to represent- the boundary between the Vardebukta Formation and Tvillingodden Formation, see the red arrow in fig 7.11.

Silicified cemented reservoirs often show very low porosity and permeability, and as a consequence increase the seismic velocity. This is confirmed by the well, showing velocities of 5500m/s in the Tempelfjorden group. The same velocity is measured in the Agardhdalen at this depth by Eiken (1985), see Fig 7.1.

The difference between the velocity measurements is that according to the sonoboy the velocity increases from 4500 m/s to 5500 m/s at the Permian /Triassic boundary, and according to the well it increases from 4900 m/s to 5500 m/s at the same horizon .

The variance is probably related to regional differences in geology. An unconformity between Permian and Triassic layers occurs in Isfjorden according to Blinova et al, (2012).

However, no indication of unconformity is observed near yellow reflector in fig 7.11 corresponding to the boundary between Permian/Triassic

The depth to the top Permian reflector is given in Fig 6.29, according to the figure 1700 ms corresponds to a depth of approximately 3.8 km.

A depth of 3.8 km is consistent with Eiken (1985), by following the Top Permian horizon in his depth-converted geo-seismic section to the middle of the basin, assuming the horizon dips as the overlying horizons.

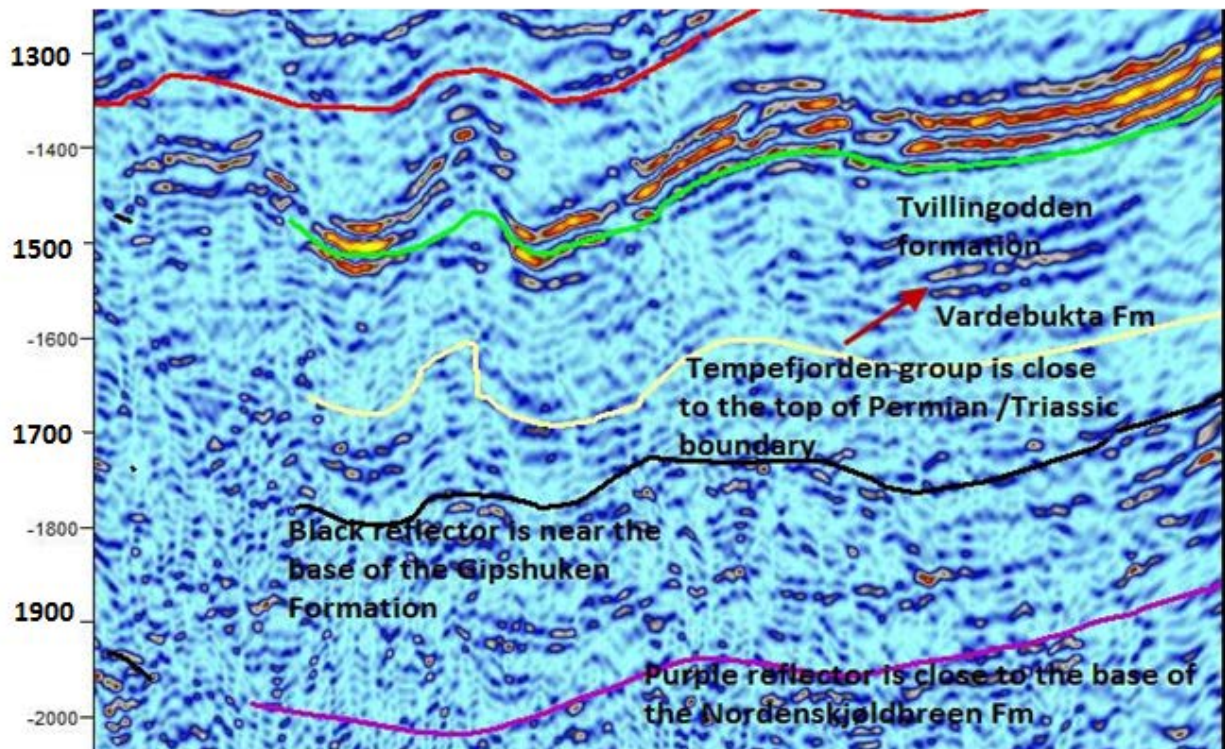


Fig 7.11: The figure shows deeper reflectors with a relative amplitude map.



The black reflector is within the carbonate /evaporates sequence of the Gipsdalen group close to its top (Faleide and Gudlaugsson 1985).

As Fig 7.11 indicates the reflector separates lower amplitudes above the reflector from higher amplitudes underneath.

As a consequence, the black reflector possibly represents the base of the Gipshuken formation since it represents an acoustic impedance contrast.

According to Bergh, Braathen et al. (1997) there exists a strong double reflection at this depth which may reflect the transition from low- velocity porous evaporates of the Gipshuken formation to underlying higher velocity dolomites of the Nordenskioldbreen formation.

However, no reflection package at this depth in Van Mijenfjorden stands out as representing a strong double reflection.

According to velocity information from the well, the interval where the velocity increases is from middle unit 7 (approximately from 1550 ms)- ,and the

amplitude gets progressively higher until about 2600 ms twt. At this depth a bright reflector anomaly is found with a different orientation than the above lying reflectors, probably representing top Hecla Hoek. The reflector could correspond to the clear reflection interpreted by Bergh, Braathen et al. (1997) which occurs in an interval between 2 and 3 s twt. Based on estimations from aeromagnetic and gravity data the reflector is confirmed as top Hecla Hoek (Bergh, Braathen et al.1997).

7.6 Carboniferous unit

The purple reflector is close to lower Carboniferous or base Nordenskjøldbreen Fm and reaches down to a depth of 2000 ms twt under the middle of the syncline. This is consistent with Nøttvedt (1994) who interpreted base Nordenskjøldbreen Fm at 2200 ms twt in the middle of the profile.

According to Faleide and Gudlaugsson (1985) there exists an unconformity between Billefjorden and Gippsdalen. At 2200 ms where the green arrows in Fig 7.12 are pointing, a contrast between the overlying and underlying geology is seen. Below the black reflector in fig 7.12 reflectors are dipping in the direction indicated by the red arrows. Above they dip in the direction indicated by the blue arrow.

Since reflectors are dipping differently above and below the black reflector, the horizon could indicate an unconformity. An unconformity at base Gippsdalen group in Isfjorden is also reported by (Blinova, Faleide et al. 2012).

Furthermore, Bergh, Braathen et al. (1997) described the Devonian sediments as having a distinct seismic signature from the overlying layers as shown in fig 7.12.

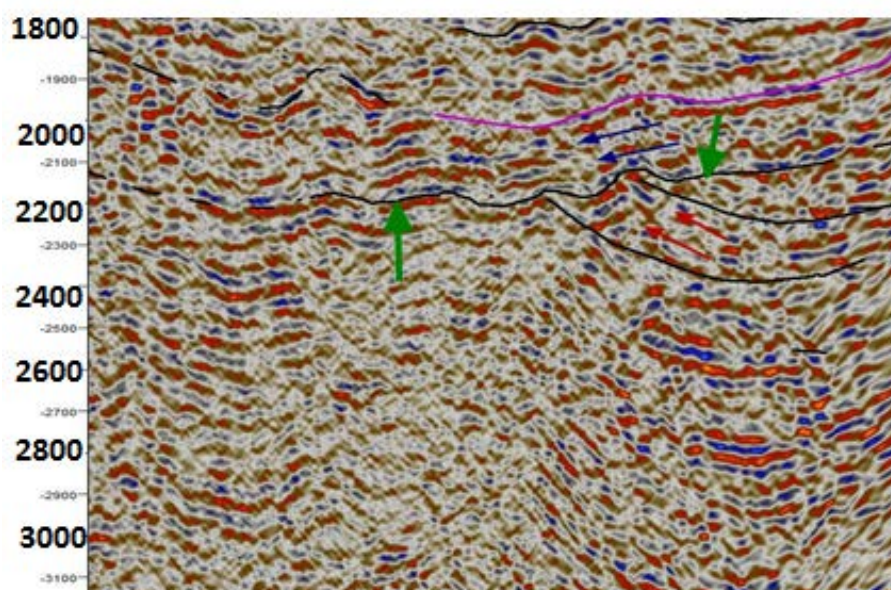
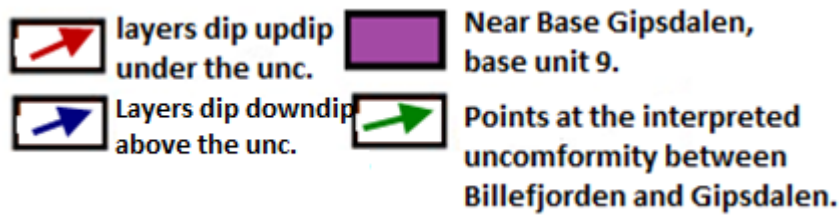


Fig 7.12: The figure shows a possible unconformity at base Carboniferous.



7.7 Hecla Hoek

The top of the Hecla Hoek could be located at 2600 ms twt or 2800 ms twt. According to Bergh, Braathen et al.(1997) a clear reflection occur in Isfjorden, between 2 and 3 s and is interpreted at top Hecla Hoek. Since the strongest reflection between 2 and 3 s twt in Van Mijenfjorden occur at 2600 or 2800 ms twt, the top of the Hecla Hoek is interpreted to be at this depth. According to fig 7.13, the first reflector dipping up with strong amplitude is located at 2600 ms twt. The statement that Hecla Hoek is located between 2 and 3 s twt is confirmed by estimated depth to basement from aeromagnetic and gravity data (Bergh, Braathen et al.1997). The reflector at 2600 ms and 2800 ms are interpreted to evaluate whether the geometry of the reflections are different, fig 7.14 shows the results. As indicated by the figure, reflections less than 2800 ms twt show layers with steeper dips. In the package between 2600 and 2800 ms (indicated by green arrows), layers are dipping with the same dip as the overlying units up to 2200 ms twt where the unconformity at base Gipsdalen is interpreted to be located. Since the geometry of the reflections begins to dip much steeper below 2800 ms twt compared to the overlying units, this is the depth where top Hecla Hoek is interpreted.

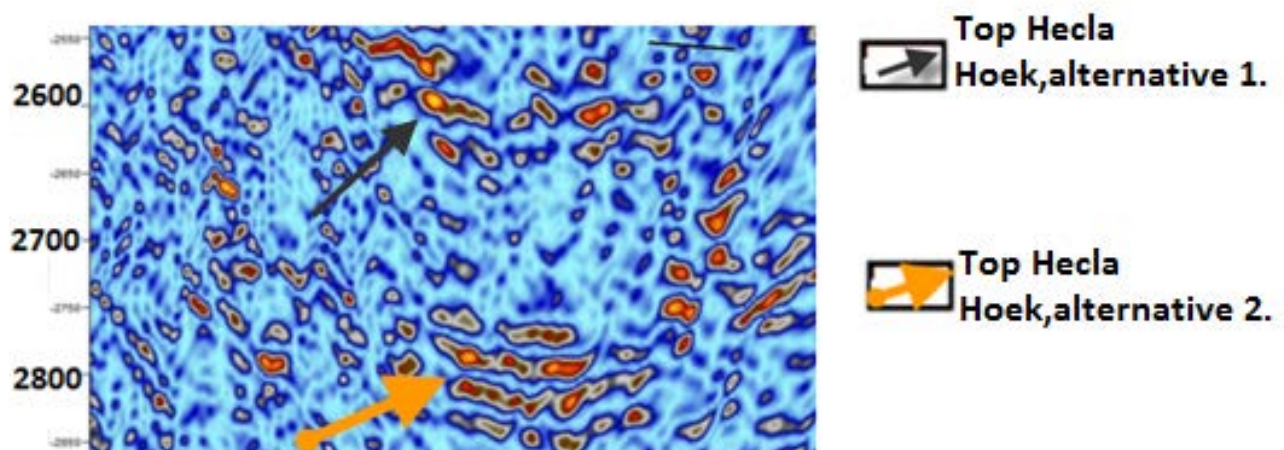
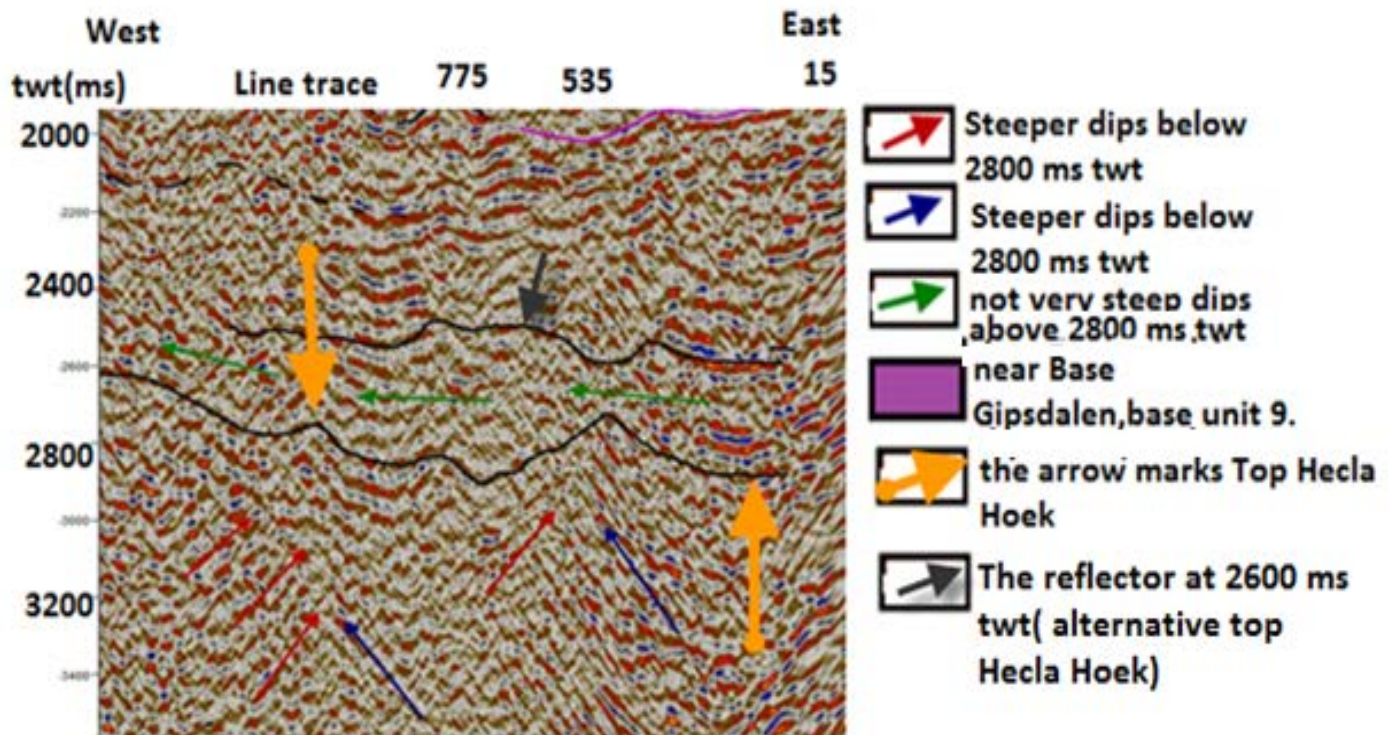


Fig .7.13: The figure show two strong amplitudes at 2600 and 2800 ms twt



7.14: The figure shows that the dip in reflectors increases below about 2800 ms interpreted to be Hecla Hoek .

The rocks between 2200 ms twt and 2800 ms twt can thus be interpreted to be Devonian sediments, since as stated in chapter 2 , Hecla Hoek is a term used for rocks from Riphean to Silurian age. The reflector at 2800 ms twt is as a consequence close to top Silurian. The reason higher dipping layers are found under 2800 ms twt could be because the main Caledonian orogeny ended at the transition from Silurian to Devonian as stated in 2.3.

7.8 West Spitsbergen Fold and Thrust belt.

In chapter 6 the different geometries in West Spitsbergen Fold and Thrust belt in Van Mijenfjorden were described.

The cause for the different configurations could be related to different stress in different directions .Towards north structures are more symmetrical, indicating that the stress could have been lower compared to lines in the middle of the survey. This is because lines located in the middle of the survey show more asymmetrical folds. In the southern part all lines show different configurations, line 14-03 and 14-04 show higher dipping layers and more deformed structures indicating higher stress. Line 14-05 shows more symmetrical folds, which might indicate that the stress acting here would be lower and similar to the stress acting further north. Higher deformed structures in the southernmost lines are shown in the syncline. Only in the three southernmost lines small anticline structure

appear in the lower Tertiary unit, see fig 7.17. Furthermore, there are none or very small anticline structures within the syncline from base Rurikfjellet up to seabed in the three northernmost lines, compared to the seven lines further south, where line 13-14 show the least deformation, see fig 7.15. Lines located in the middle of the survey (line 14-06, 14-07 and 14-08) show no anticline structures in lower Tertiary, but have signs of anticline structures within the Helvetiaformation in the middle of the basin.

The West Spitsbergen Fold and Thrust belt is considered to have been formed due to a dextral transpression in response to the opening of the North Atlantic Ocean and separation of Greenland and Svalbard during Eocene (Saalman and Thiedig 2000). In this period a strike slip movement occurred between Svalbard and Greenland (Faleide and Gudlaugsson 1985).

The asymmetrical folds in Van Mijenfjorden and especially those located in the middle of the lines are S shaped and asymmetrical. Asymmetrical folds are common in fold and thrust belts as stated in 3.3.3.

The asymmetric folds are not interpreted to be parasite folds since they are not related to a bigger structure. Since this is the case, the asymmetry could have been formed in the middle of a shear zone and the asymmetry could provide information on the direction of stress during deformation (Fossen 2010).

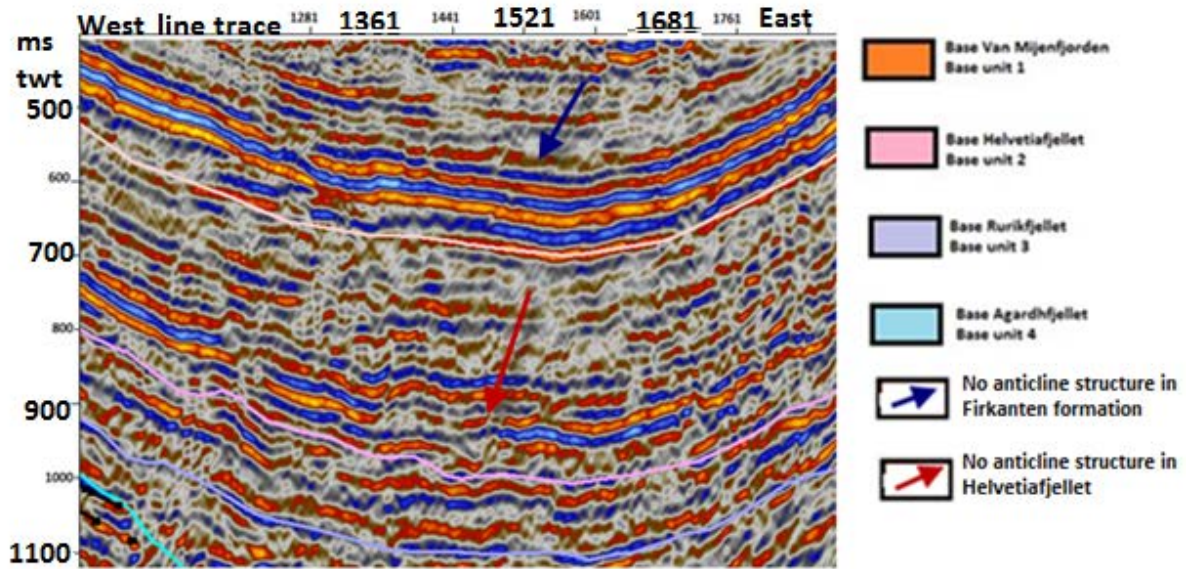
These folds could then have been formed in Paleocene when a strike slip movement occurred between Svalbard and Greenland.

In Eocene the same folds could have been compressed resulting in tighter folds since the tectonic regime changed at this stage resulting in crustal shortening.

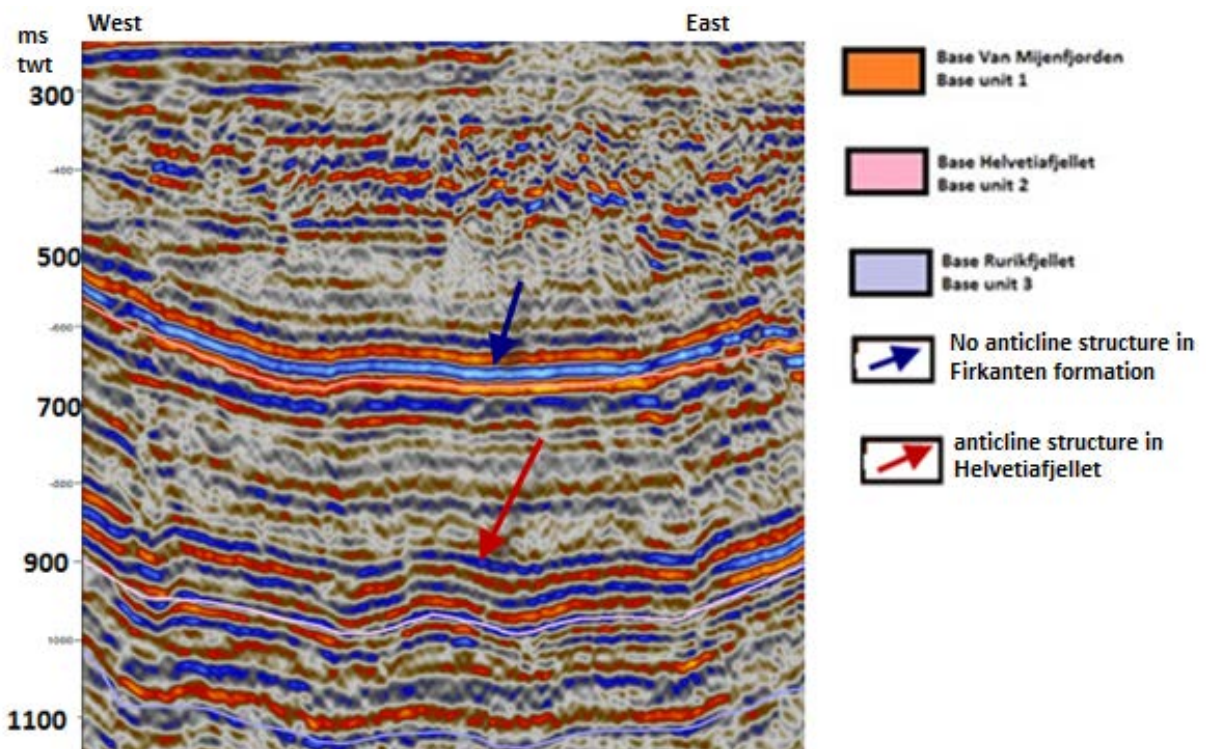
The formation of S folds is discussed in the literature. A two-step deformation process is proposed in which compression is followed by shear stress. This could be the case for the S like folds in Van Mijenfjorden, but the difference is that shear stress occurred before compression. Asymmetric S folds can also occur if the compressional direction was non-coaxial and the intensities varied (asymmetrical compression) (Wang, Deng et al. 2011). The compression intensity could vary in Van Mijenfjorden since different structures are seen at different lines in the fjord.

A reason for the more symmetrical folds further north could then be explained by lower induced stress in this area. Another cause for the different geometries in different places could be caused by different rock properties at different locations. As a consequence the rocks will deform differently under same amount of stress. Normal faulting and partial collapse of the compressional structures in the West Spitsbergen Fold and Thrust Belt could be a reality. This is because Greenland was attached to the North American plate in Oligocene and Greenland thusly moved WNW relative to Eurasia. As

a result, seafloor spreading started between Greenland and Svalbard and caused oblique extension (Blinova 2011). However, no normal faults are observed in this study, but this could be due to noisy seismic.



7.15. Figure shows that no anticline structures appear in the syncline for line 13-14. Same type of characteristics is seen on line 13-11, 14-10, and 13-09 (4 northernmost lines)



7.16 The figure shows that no significant anticline structure is seen within lower tertiary for line 14-06, line 14-07 and 14-08 (lines in the middle of the survey), but anticline structures appear in the Helvetiafjellet and underlying units.

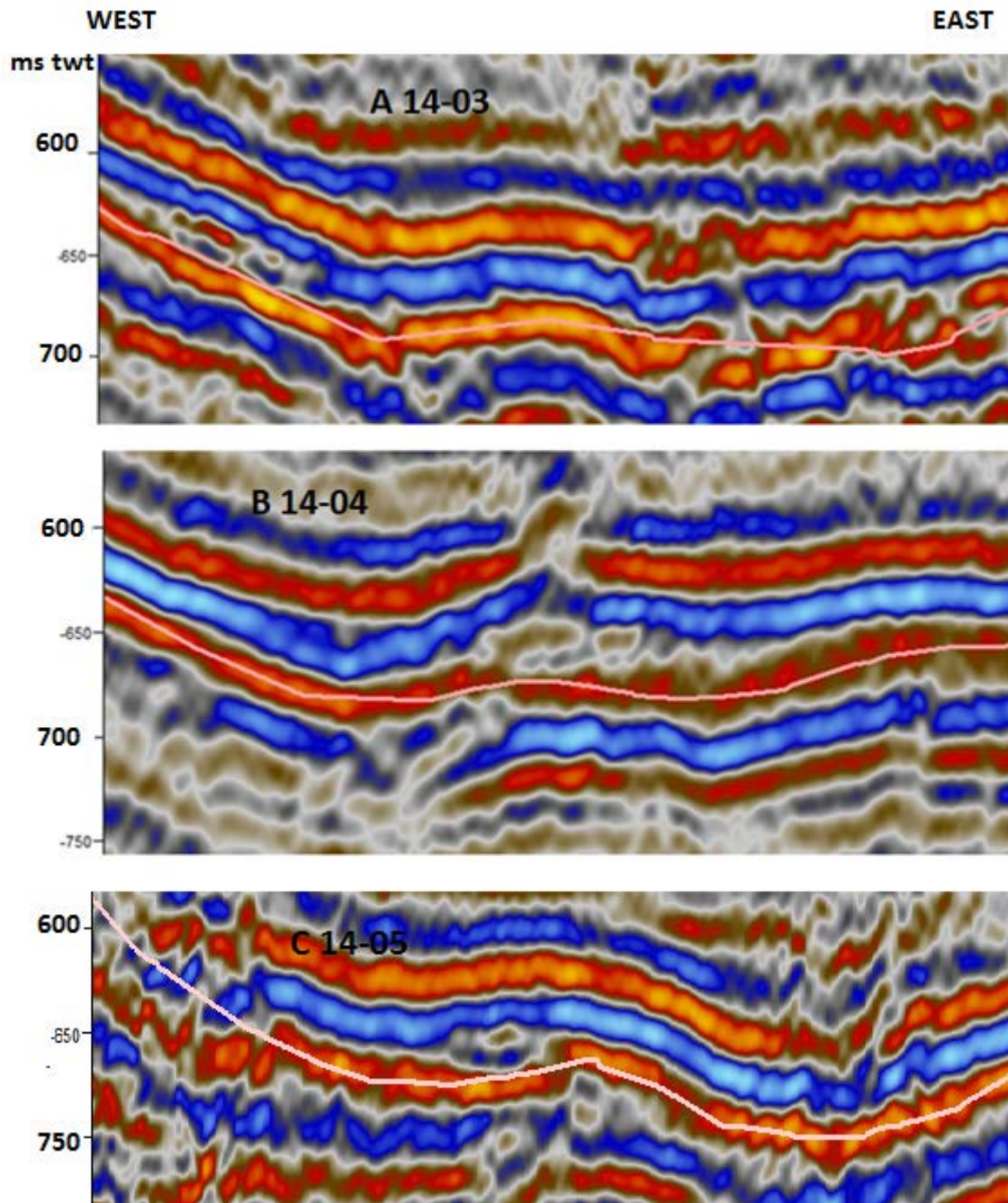
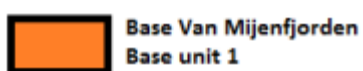


Fig 7.17: The figure shows that anticline structures are found within the lower Tertiary unit at only the 3 southernmost lines



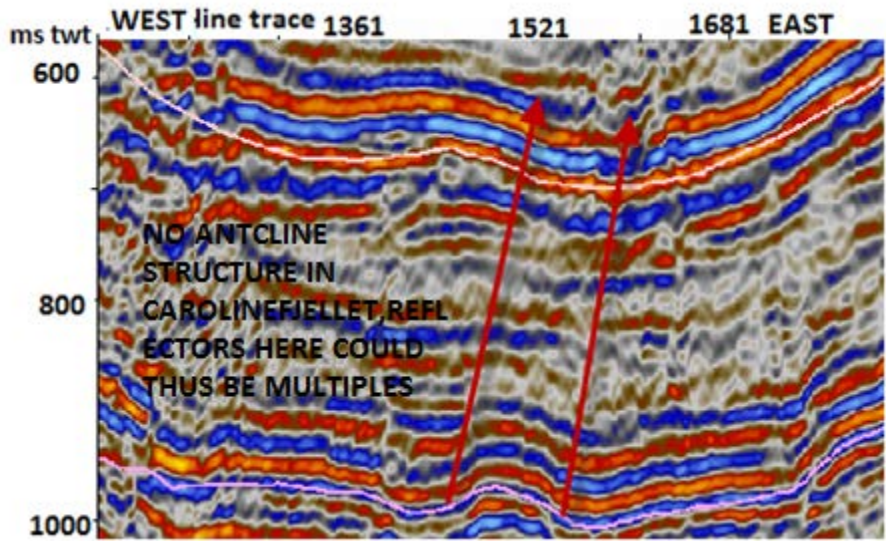


Fig 7.18: The figure shows that the anticline structure within lower Tertiary in line 14-05 is in a different location and has larger width than the anticline structure in Helvetiafjellet.

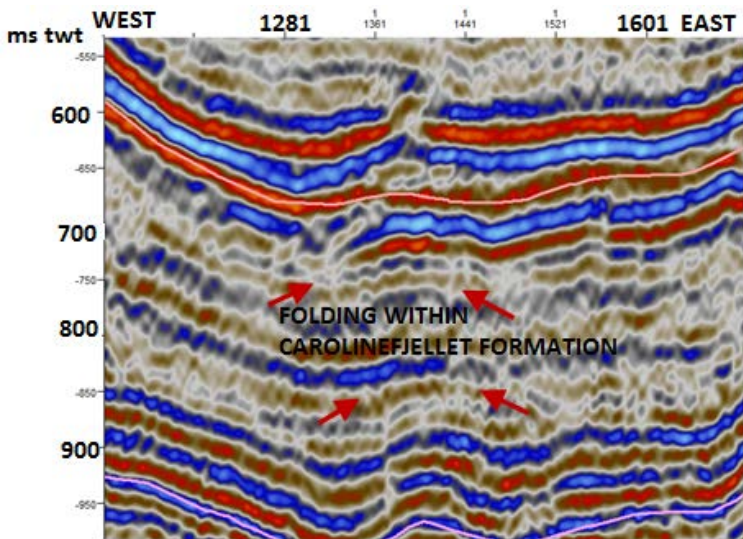
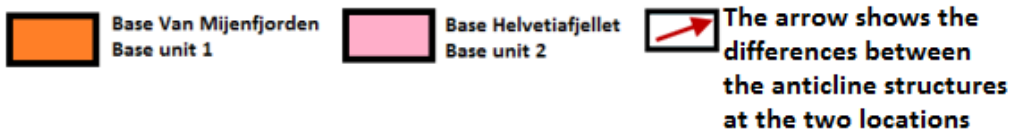
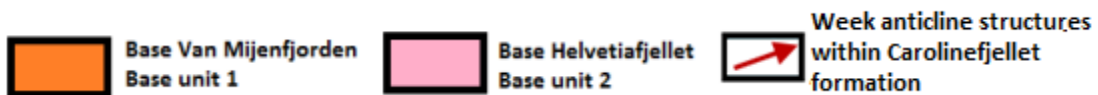


Fig 7.19: The figure shows that the anticline structure in lower Tertiary in line 14-04 is different from the anticline structure in line 14-05. Notice that the anticline structure within Helvetiafjellet is similar, but the anticline structure within lower Tertiary differs. It appears more asymmetrical on line 14-05 within the lower Tertiary unit, see fig 7.18 for comparison.



Conclusions: Processing

- The main focus of the processing has been removal of multiples; they are a problem in the data because of hard seabed and low water depth. Attenuation of multiples has been done by applying f-k filtering and surface consistent deconvolution. Lower values of v_1 and v_2 (under 4000m/s) resulted in more multiples, whereas higher values for v_1 and v_2 resulted in less multiples. Surface consistent deconvolution was especially good for attenuation of reverberations, which are multiples that reflect many times between seabed and seafloor.
- Under 900 ms the vertical resolution is 25 m; the vertical resolution for the upper 900 ms is 12.5 meter.
- By applying Signature Deconvolution increased resolution of the data was obtained.
- Muting the seismic data based on incident angles affect how strong reflections appear at different depths. Setting $ANGMIN=20$ and $ANGMIN=40$ gives clearer reflections down to 1 sec twt compared to putting $ANGMIN=0$ and $ANGMIN=40$. A side effect is that by not allowing incident angles below 20 degrees, deeper reflections than 1 sec twt are mapped very poorly. Also by choosing a too high value for $ANGMAX$ reflections become more transparent with depth and are then not a good choice for mapping deeper structures. The overall best values was setting $ANGMIN=0$ and $ANGMAX=40$.
- $DIPLIM$ of 40 degrees gave the best result for mapping structures in the complex area. If too small $DIPLIM$ values are picked, layers showing high dip will not be seen on the seismic. The interpretation of the seismic in the complex area depends on the value of maximum frequency of input data. In the normal case 100 Hz is used. By setting the maximum frequency on input data lower, the seismic appears less noisy, but as a consequence the resolution is poorer. In the general case it looked like more faults appeared by setting this value lower. The interpretation of the complex area is highly dependent on what value this frequency is set to.
- Time Variant Bandpass filter has a huge effect of how noisy the seismic appear. This filter highly attenuated the NMO stretch effect which occurs for the shallowest events.
- Spherical Spreading correction had a good effect of restoring the amplitudes of deeper reflections.
- Spectral balancing resulted in noisy seismic because it boosted high frequency noise.

Conclusions: Seismic interpretation

- The Tertiary unit consists of a broad asymmetric syncline corresponding to the Spitsbergen Basin. The thickness between the seabed and Base Tertiary is 1100 m. Gilsonryggen formation corresponds to the uppermost package of weak reflections. Grumantbyen formation is within a package of stronger reflections and corresponds to the first package of strong reflections in the seismic. Basilika formation is within a package of weak reflections. Base Tertiary corresponds to base Firkanten Formation at the end of a series of strong reflections.
- Base Helvetiafjellet is located at 950 ms in the middle of the syncline; the Helvetiafjellet has stronger amplitudes than the overlying weak reflections seen in the Carolinefjellet formation. The depth down Helvetiafjellet is roughly 2 km.
- Thickness of the Carolinefjellet formation is 570 meter, which is close to the thickness of this formation measured on land (600 m).
- Thickness of the Rurikfjellet resembles the thickness of the Rurikfjellet found on land adjacent to the fjord.
- Folded dome structures up to the Helvetiafjellet formation could be caused by mobilization of shales from the Agardfjellet formation; the thickness of this formation varies due to folding of the layers. Base Agardhfjellet formation corresponds to an unconformity.
- Two sills occur in Van Mijenfjorden, one in Kapp Toscana and another one in the upper Sassendalen group. The dolerites are more deformed in the southern parts, compared with the northernmost lines.
- Top Permian layer is located at 1700 ms under the middle of the overlying asymmetric syncline; the reflector is marked by a strong acoustic impedance contrast between high velocity silicified carbonates of the Kapp Starostin Formation and overlying low velocity Triassic shales in the Sassendalen formation. The depth down to Top Permian is 3.8 km.
- Purple reflector is close to lower Permian or base Nordenskjøldbreen Fm. At 2200 ms an angular unconformity is located and interpreted as base Carboniferous.
- Top of Hecla Hoek is interpreted to be located at 2800 ms twt.

- Different stress has acted differently on various locations in the Van Mijenfjorden area, causing more deformed structures in the lines located to the south, compared with the lines further north.
- The Asymmetrical folds in Van Mijenfjorden are a result of Early Tertiary shear stress and compression.

REFERENCES:

- Abay, T. B., D. A. Karlsen, and J. H. Pedersen, Source Rocks at Svalbard: An Overview of Jurassic and Triassic Formations and Comparison with Offshore Barents Sea Time Equivalent Source Rock Formations.
- Al-Shuhail, A. A., 2013, Estimation of velocity function parameters in unconsolidated sands using semblance velocity analysis: *Arabian Journal of Geosciences*, v. 6, p. 549-556.
- Al-Yahya, K., 1989, Velocity analysis by iterative profile migration: *Geophysics*, v. 54, p. 718-729.
- Bacon, M., R. Simm, and T. Redshaw, 2007, 3-D seismic interpretation, Cambridge University Press.
- Badley, M. E., and B. Gibson, 1987, Practical Seismic Interpretation by Michael E. Badley: *The Journal of the Acoustical Society of America*, v. 82, p. 1100-1100.
- Bergh, S. G., A. Braathen, and A. Andresen, 1997, Interaction of basement-involved and thin-skinned tectonism in the Tertiary fold-thrust belt of central Spitsbergen, Svalbard: *AAPG bulletin*, v. 81, p. 637-661.
- Bergh, S. G., and P. Grogan, 2003, Tertiary structure of the Sorkapp-Hornsund region, south Spitsbergen, and implications for the offshore southern extension of the fold-thrust belt: *Norsk Geologisk Tidsskrift*, v. 83, p. 43-60.
- Blinova, M., 2011, Seismic study along the west Spitsbergen continental margin and adjacent area of the West Spitsbergen Fold and Thrust Belt (Isfjorden). PHD Thesis
- Blinova, M., J. I. Faleide, R. H. Gabrielsen, and R. Mjelde, 2012, Seafloor expression and shallow structure of a fold-and-thrust system, Isfjorden, west Spitsbergen: *Polar Research*, v. 31.
- Blinova, M., Thorsen, R., Mjelde, R. & Faleide, J. I. (2009). Structure and evolution of the Bellsund Graben between Forlandsundet and Bellsund (Spitsbergen) based on marine seismic data. *Norwegian journal of Geology*, 89, 215-228.
- Brastins, A., and R. L. Stenger Jr, 1979, Testing of seismic streamers, Google Patents.
- Brown, A. R., 2013, What Is Seismic Interpretation?, AAPG EXPLORER.
- CGG Veritas (2008). Geocluster Release Notes.
- Claerbout, J. F., 1985, Fundamentals of geophysical data processing. Pennwell Books, Tulsa, OK
- Croxton, C., and C. Pickton, 1976, The Van Mijenfjorden Group (Tertiary) of South-West Nordenskiöld Land: Spitsbergen. *Nor. Polarinst. Skr*, v. 164, p. 29-46.
- Czuba, W., O. Ritzmann, Y. Nishimura, M. Grad, R. Mjelde, A. Guterch, and W. Jokat, 2004, Crustal structure of the continent–ocean transition zone along two deep seismic transects in north– western Spitsbergen: *Polish Polar Res*, v. 25, p. 205-221.
- Dallmann, W. K., 1999, Lithostratigraphic lexicon of Svalbard: review and recommendations for nomenclature use: Upper Palaeozoic to Quaternary bedrock, Norsk Polarinstitut.
- Drijkoningen, G., and D. Versuur, 2003, TA3600 TG001. Lecture notes
- Dypvik, H., 1984, Jurassic and Cretaceous black shales of the Janusfjellet formation,










- Svalbard, Norway: *Sedimentary Geology*, v. 41, p. 235-248.
- Dypvik, H., T. Eikeland, K. BACKER-OWE, A. Andresen, H. Johansen, A. Elverhøi, J. Nagy, P. Haremo, and T. Biærke, 1991, The Janusfjellet Subgroup (Bathonian to Hauterivian) on central Spitsbergen: a revised lithostratigraphy: *Polar Research*, v. 9, p. 21-44.
- Dypvik, H., and J. Nagy, 1978, Early Tertiary bentonites from Svalbard; a preliminary report: *Polarforschung*, v. 48, p. 139-150.
- Dypvik, H., L. Riber, F. Burca, D. Rütger, D. Jargvoll, J. Nagy, and M. Jochmann, 2011, The Paleocene–Eocene thermal maximum (PETM) in Svalbard—clay mineral and geochemical signals: *Palaeogeography, Palaeoclimatology, Palaeoecology*, v. 302, p. 156-169.
- Eiken, O., 1985, Seismic mapping of the post-Caledonian strata in Svalbard: *Polar research*, v. 3, p. 167-176.
- Eiken, O., and A. Austegard, 1994, Seismic atlas of Western Svalbard: a selection of regional seismic transects, Norsk polarinstitutt.
- Faleide, J. I., and S. T. Gudlaugsson, 1985, Van Mijenfjorden Svalbard, Geology and Petroleum Potential. Unpublished (restricted distribution)
- Faleide, J. I., A. Solheim, A. Fiedler, B. O. Hjelstuen, E. S. Andersen, and K. Vanneste, 1996, Late Cenozoic evolution of the western Barents Sea-Svalbard continental margin: *Global and Planetary Change*, v. 12, p. 53-74.
- Flood, B., J. Nagy, T. S. Winsnes, and N. Polarinstitutt, 1971, Geological Map of Svalbard 1: 500 000: Sheet 1G, Spitsbergen, Southern Part, Norsk Polarinstitutt.
- Fossen, H., 2010, *Structural geology*, Cambridge University Press.
- Gadallah, M. R., and R. L. Fisher, 2005, *Applied seismology: A comprehensive guide to seismic theory and application*, PennWell Books.
- Gee, D. G., L. Björklund, and L.-K. Stølen, 1994, Early Proterozoic basement in Ny Friesland—implications for the Caledonian tectonics of Svalbard: *Tectonophysics*, v. 231, p. 171-182.
- Ghosh, G., and D. Saha, 2005, Kinematics of large scale asymmetric folds and associated smaller scale brittle—Ductile structures in the proterozoic somnur formation, pranhita—Godavari Valley, South India: *Journal of earth system science*, v. 114, p. 125-142.
- Gjelberg, H. K., 2010, Facies Analysis and Sandbody Geometry of the Paleogene Battfjellet Formation, Central Western Nordenskiöld Land, Spitsbergen.
- Gjelberg, J., and R. J. Steel, 1995, Helvetiafjellet Formation (Barremian-Aptian), Spitsbergen: characteristics of a transgressive succession: *Norwegian Petroleum Society Special Publications*, v. 5, p. 571-593.
- Glossary2015, Schlumberger: Retrieved from the internet < URL <http://www.glossary.oilfield.slb.com>>
- Hald, M., T. Dahlgren, T. E. Olsen, and E. Lebesbye, 2001, Late Holocene palaeoceanography in Van Mijenfjorden, Svalbard: *Polar Research*, v. 20, p. 23-35.
- Hansen, C., 2005, *Noise control: from concept to application*, CRC Press.
- Hautus, M., 1980, *The Fourier transform and its applications*: Ronald N. BRACEWELL

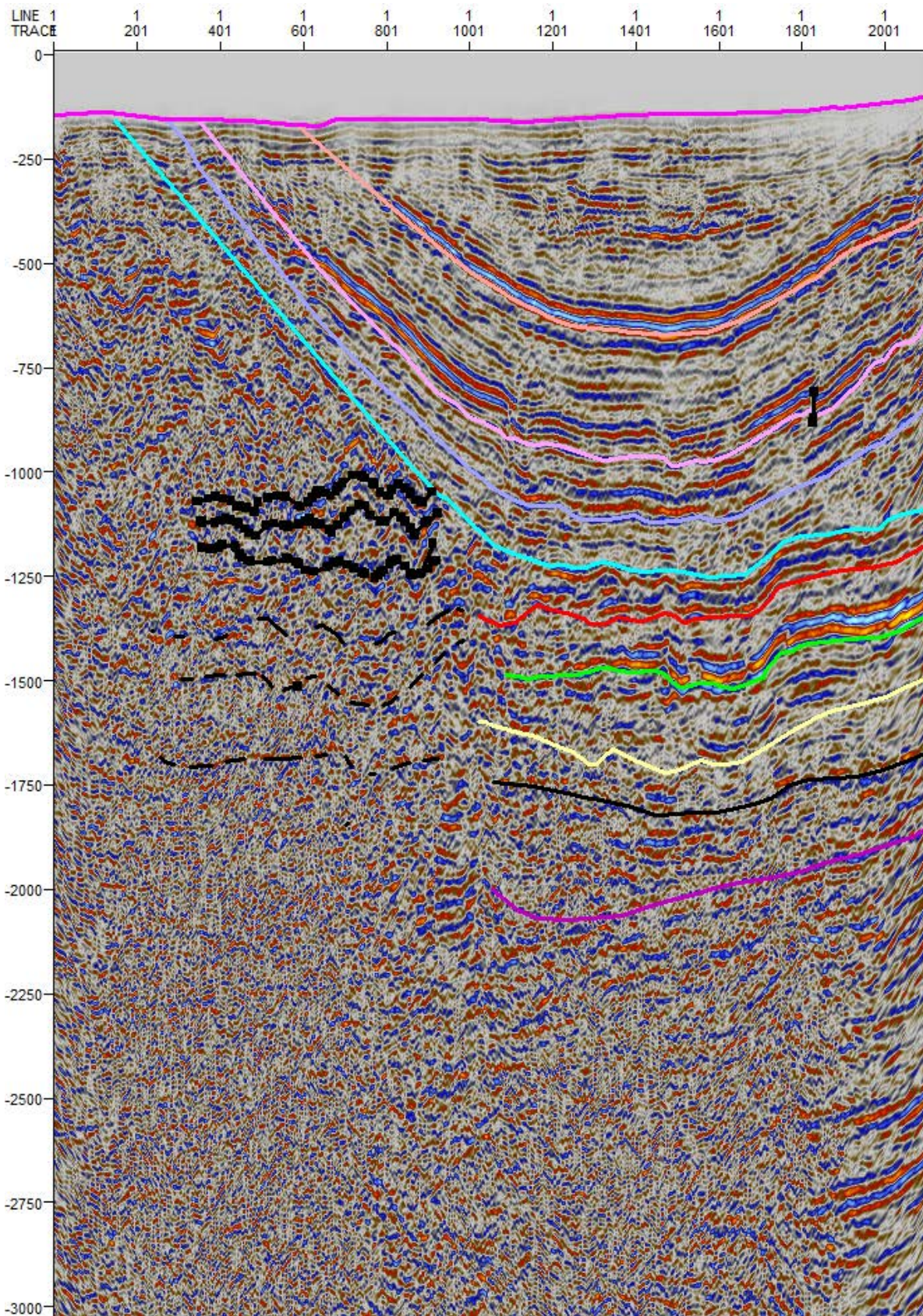
- McGraw-Hill, New York, 1978, xvi+ 444 pages, Dfl. 79, 85, North-Holland.
- Hays, T., H. Maher, and R. Shuster, 2001, Investigation of the manifestation of the Cretaceous High Arctic Large Igneous Province on Svalbard.
- Hjelle, A., 1993, Svalbards geologi, Norsk Polarinstitutt.
- Hobbs, R., and H. Jakubowicz, 2000, Marine source signature measurement using a reference seismic source: Expanded Abstracts, SEG Annual Meeting, Calgary, p. 57-60.
- Hynne, I. B., 2010, Depositional environment on eastern Svalbard and central Spitsbergen during Carnian time (Late Triassic): A sedimentological investigation of the De Geerdalen Formation. Master thesis
- Johnsen, S. O., A. Mørk, H. Dypvik, and J. Nagy, 2001, Outline of the geology of Svalbard: 7th ESF IMPACT Workshop.
- Kearey, P., M. Brooks, and I. Hill, 2013, An introduction to geophysical exploration, John Wiley & Sons.
- Klemperer, S. L., 1987, Seismic noise-reduction techniques for use with vertical stacking: An empirical comparison: *Geophysics*, v. 52, p. 322-334.
- Krajewski, K. P., 2008, The Botneheia Formation (Middle Triassic) in Edgeøya and Barentsøya, Svalbard: lithostratigraphy, facies, phosphogenesis, paleoenvironment: *Polish Polar Research*, v. 29, p. 319-364.
- Krajewski, K. P., and B. Luks, 2003, Origin of “cannon-ball” concretions in the Carolinefjellet Formation (Lower Cretaceous), Spitsbergen: *Polish Polar Res*, v. 24, p. 217-242.
- Landrø, M., L. Amundsen, and D. Barker, 2011, High-frequency signals from air-gun arrays: *Geophysics*, v. 76, p. Q19-Q27.
- Lauritzen, O., 1981, The development of the Gipshuken Formation (Lower Permian) at Trollfuglfjella in Central Spitsbergen, Svalbard: *Norsk Polarinst. Skr.*, v. 176, p. 1-23.
- Leever, K. A., R. H. Gabrielsen, J. I. Faleide, and A. Braathen, 2011, A transpressional origin for the West Spitsbergen fold-and-thrust belt: Insight from analog modeling: *Tectonics*, v. 30.
- Livsic, J., 1992, Tectonic history of Tertiary sedimentation of Svalbard: *Norsk geologisk tidsskrift*, v. 72, p. 121-127.
- Lundin, E., and A. Doré, 2002, Mid-Cenozoic post-breakup deformation in the ‘passive’ margins bordering the Norwegian–Greenland Sea: *Marine and Petroleum Geology*, v. 19, p. 79-93.
- Lydersen, C., B. A. Krafft, M. Andersen, and K. M. Kovacs, 2002, Marine mammals in the Bellsund–Van Mijenfjorden–Van Keulenfjorden area: new investigations and status of knowledge.
- Maher Jr, H. D., 2001, Manifestations of the Cretaceous high Arctic large igneous province in Svalbard: *The Journal of Geology*, v. 109, p. 91-104.
- Marshalla, C., J. Ugunaa, D. J. Largea, W. Mereditha, M. Jochmannb, B. Friisb, C. H. Vanec, B. F. Spirod, C. E. Snapea, and A. Orheime, Maturity Issues within Palaeocene Coal, Spitsbergen: Implications for local 1 and regional burial and uplift models 2. Year not stated .
- Mikkelsen, E. R., 2009, Monitoring of CO2 Sequestration at the Longyearbyen CO2 Lab by Time-lapse Seismic: An Interdisciplinary Rock Physics Study.

- Miller, R. D., 1992, Normal moveout stretch mute on shallow-reflection data: *Geophysics*, v. 57, p. 1502-1507.
- Mjelde, R. (2013) Cruise report, Svalex (unpublished)
- Mjelde, R. (2014) Cruise report, Svalex (unpublished)
- Myhre, A. M., and O. Eldholm, 1988, The western Svalbard margin (74–80 N): *Marine and Petroleum Geology*, v. 5, p. 134-156.
- Müller, R. D., and R. F. Spielhagen, 1990, Evolution of the Central Tertiary Basin of Spitsbergen: towards a synthesis of sediment and plate tectonic history: *Palaeogeography, Palaeoclimatology, Palaeoecology*, v. 80, p. 153-172.
- Mørk, A., G. Elvebakk, A. W. Forsberg, J. O. VIGRAN, and W. WEITSCHAT, 1999, The type section of the Vikinghogda Formation: a new Lower Triassic unit in central and eastern Svalbard: *Polar Research*, v. 18, p. 51-82.
- Nairn, A., M. Churkin, and F. G. Stehli, 1981, *The Ocean Basins and Margins*, p. 631.
- Nejbert, K., K. P. Krajewski, E. Dubińska, and Z. Pécskay, 2011, Dolerites of Svalbard, north-west Barents Sea Shelf: age, tectonic setting and significance for geotectonic interpretation of the High-Arctic Large Igneous Province: *Polar Research*, v. 30.
- Nøttvedt, A., 1994, Post Caledonian sediments on Spitsbergen: *Seismic atlas of western Svalbard. Norsk Polarinstitutt Meddelelser*, v. 130, p. 40-48.
- Ohta, Y., 1994, Caledonian and Precambrian history in Svalbard: a review, and an implication of escape tectonics: *Tectonophysics*, v. 231, p. 183-194.
- Orheim, A., G. Bieg, T. Brekke, V. Horseide, and J. Stenvold, 2007, Petrography and geochemical affinities of Spitsbergen Paleocene coals, Norway: *International Journal of Coal Geology*, v. 70, p. 116-136.
- Reynolds, J. M., 2011, *An introduction to applied and environmental geophysics*, John Wiley & Sons.
- Robinson, E. A., and S. Treitel, 1980, *Geophysical signal analysis*, v. 263, Prentice-Hall New Jersey.
- Roksandić, M., 1978, Seismic facies analysis concepts: *Geophysical Prospecting*, v. 26, p. 383-398.
- Ruud, B. O. (2015), personal communication.
- Saalmann, K., and F. Thiedig, 2000, Structural Evolution of the Tertiary West Spitsbergen Fold-and-Thrust Belt on Broggerhalvoya, NW-Spitsbergen: *Polarforschung*, v. 68, p. 111-119.
- Schlumberger.Glossary <http://www.glossary.oilfield.slb.com/en/Terms.aspx?LookIn=term%20Name&filter=NMO> 31.05.2015 (NMO picture)
- Schlumberger.Glossary http://www.glossary.oilfield.slb.com/en/Terms/t/true-amplitude_recovery.aspx 31.05.2015 (Amplitude recovery)
- Senger, K., S. Roy, K. Ogata, K. Bælum, A. Braathen, R. Noormets, S. Olaussen, and J. Tveranger, 2011, Exploring for saucer-shaped igneous intrusions on Spitsbergen, Svalbard: 2nd International Geosciences Student Conference, 9/7-12/7 2011.
- Senger, K., S. Roy, J. Tveranger, S. Planke, S. Buckley, K. Ogata, A. Braathen, S. Olaussen,

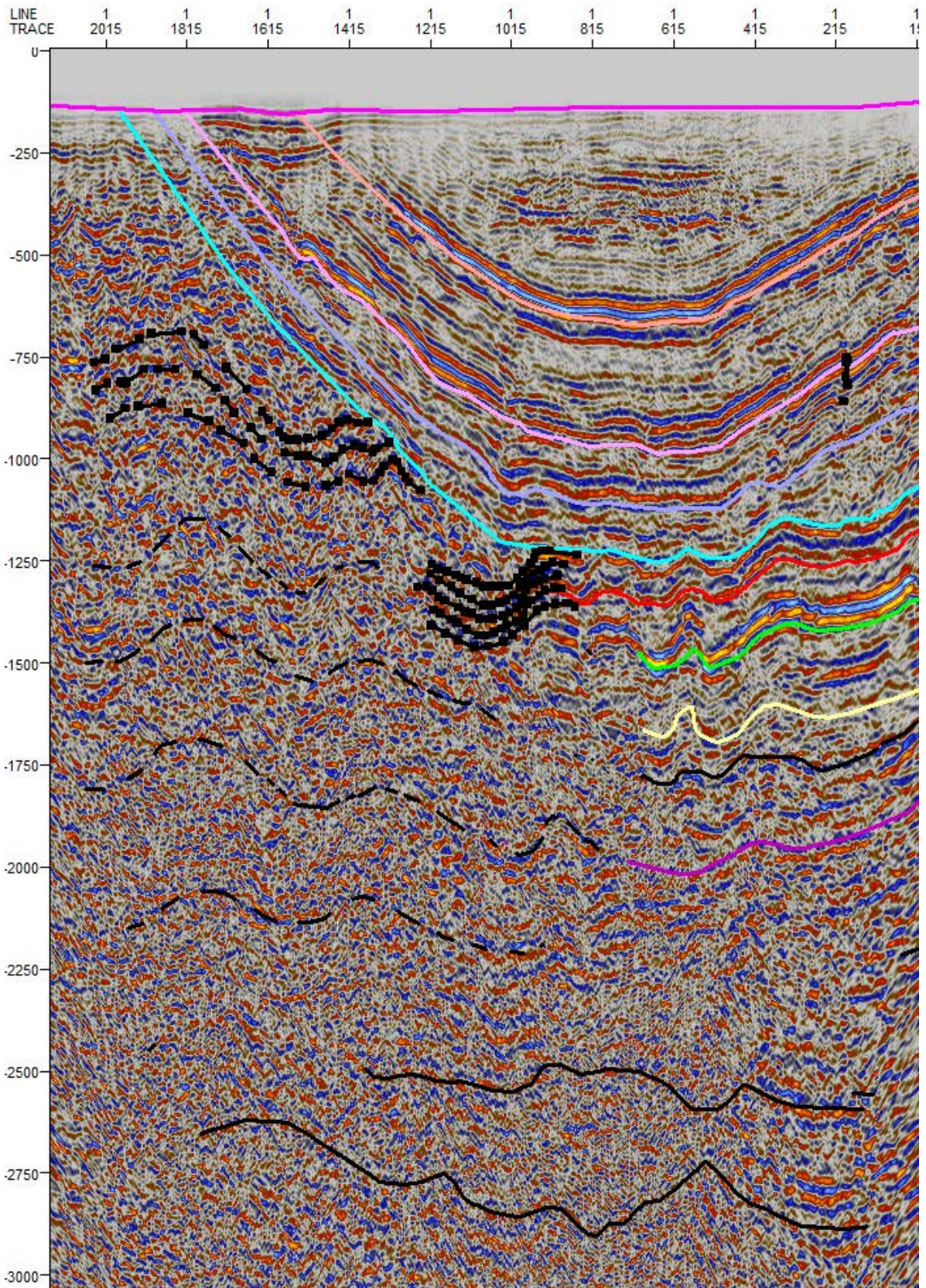
- R. Noormets, and R. Mjelde, 2012, Geometries of igneous intrusions in Inner Isfjorden, Svalbard: implications for fluid flow and CO₂ storage: Proceeding, LASI 5 Conference, Port Elizabeth, South Africa, p. 29-30.
- Senger, K., J. Tveranger, K. Ogata, A. Braathen, and S. Planke, 2014, Late Mesozoic magmatism in Svalbard: A review: *Earth-Science Reviews*, v. 139, p. 123-144.
- Shen, S.-Z., J.-I. Tazawa, and G. R. Shi, 2005, Carboniferous and Permian Rugosochonetidae (Brachiopoda) from West Spitsbergen: *Alcheringa*, v. 29, p. 241-256.
- Sheriff, R. E., and L. P. Geldart, 1995, *Exploration seismology*, Cambridge university press.
- Steel, R., 1985, The Tertiary strike-slip basins and orogenic belt of Spitsbergen.
- Strømme, M. L., 2010, Prosessering og tolkning av refleksjonsseismiske data fra Van Mijenfjorden, Svalbard. Master Thesis
- Svinth, A. A. G., 2013, A Sedimentological and Petrographical Investigation of the Todalen Member and the Boundary Beds of the Endalen Member.: Within the Firkanten Formation (Paleocene) in the Central Basin of Spitsbergen, Svalbard.
- Talwani, M., and O. Eldholm, 1977, Evolution of the Norwegian-Greenland sea: *Geological Society of America Bulletin*, v. 88, p. 969-999.
- Wang, Q., J. Deng, D. Huang, C. Xiao, L. Yang, and Y. Wang, 2011, Deformation model for the Tongling ore cluster region, east-central China: *International Geology Review*, v. 53, p. 562-579.
- Worsley, D., O. Aga, A. Dalland, A. ElverhØi, and A. Thon, 1986, Evolution of an Arctic archipelago. *The Geological History of Svalbard: Statoil, Norway*, v. 121.
- Yilmaz, Ö., 2001, *Seismic data analysis*, v. 1, Society of exploration geophysicists Tulsa.

Appendix Seismic profiles.

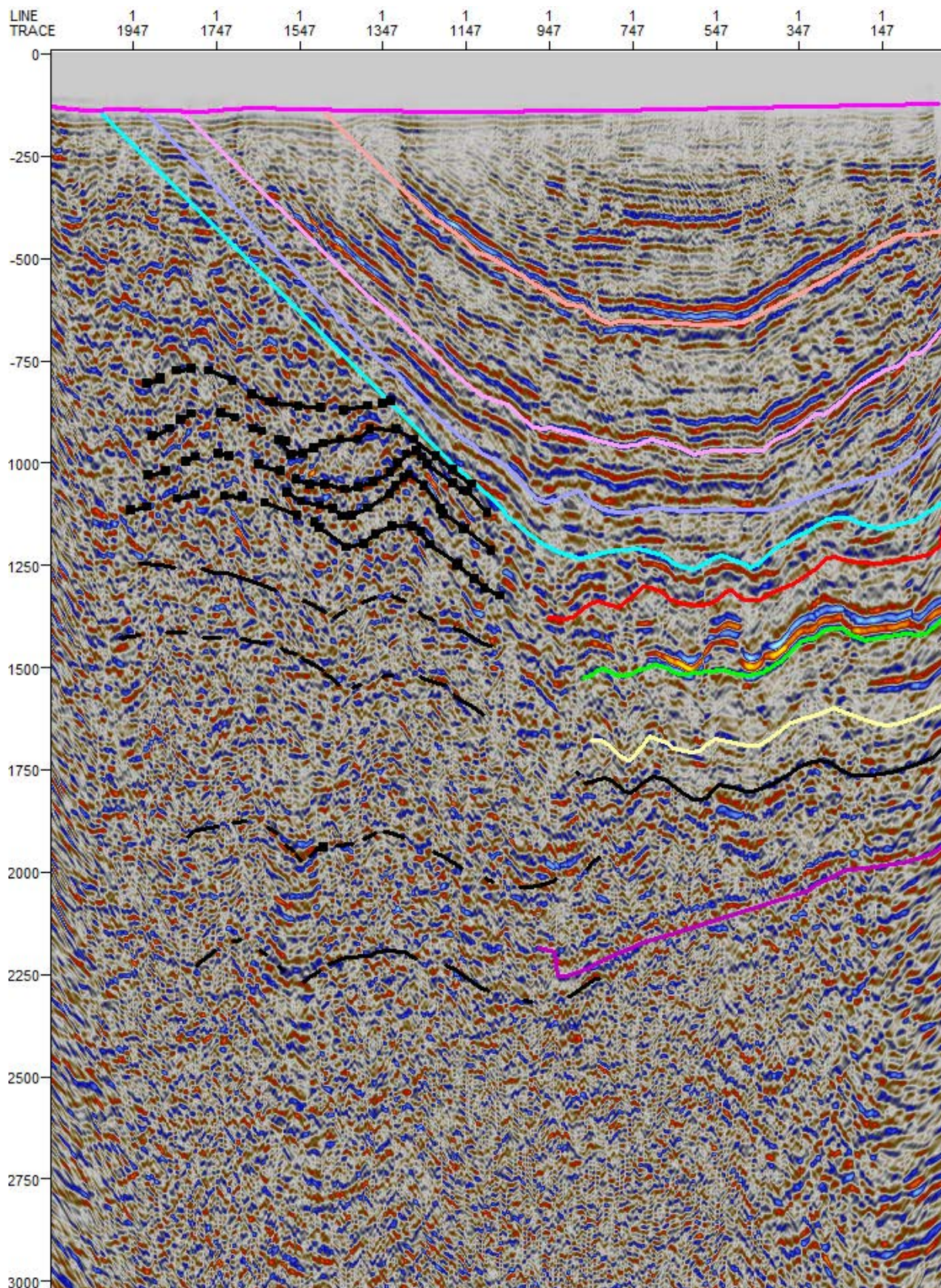
 Base Van Mijenfjorden Base unit 1	 Base Helvetiafjellet Base unit 2	 Base Rurikfjellet Base unit 3
 Base Agardhfjellet Base unit 4	 Base Kapp Toscana Base unit 5	 Near top Sassendalen Group Base unit 6
 Base Sassendalen Base unit 7	 Within Gipsdalen Base unit 8	 Near Base Gipsdalen Base unit 9



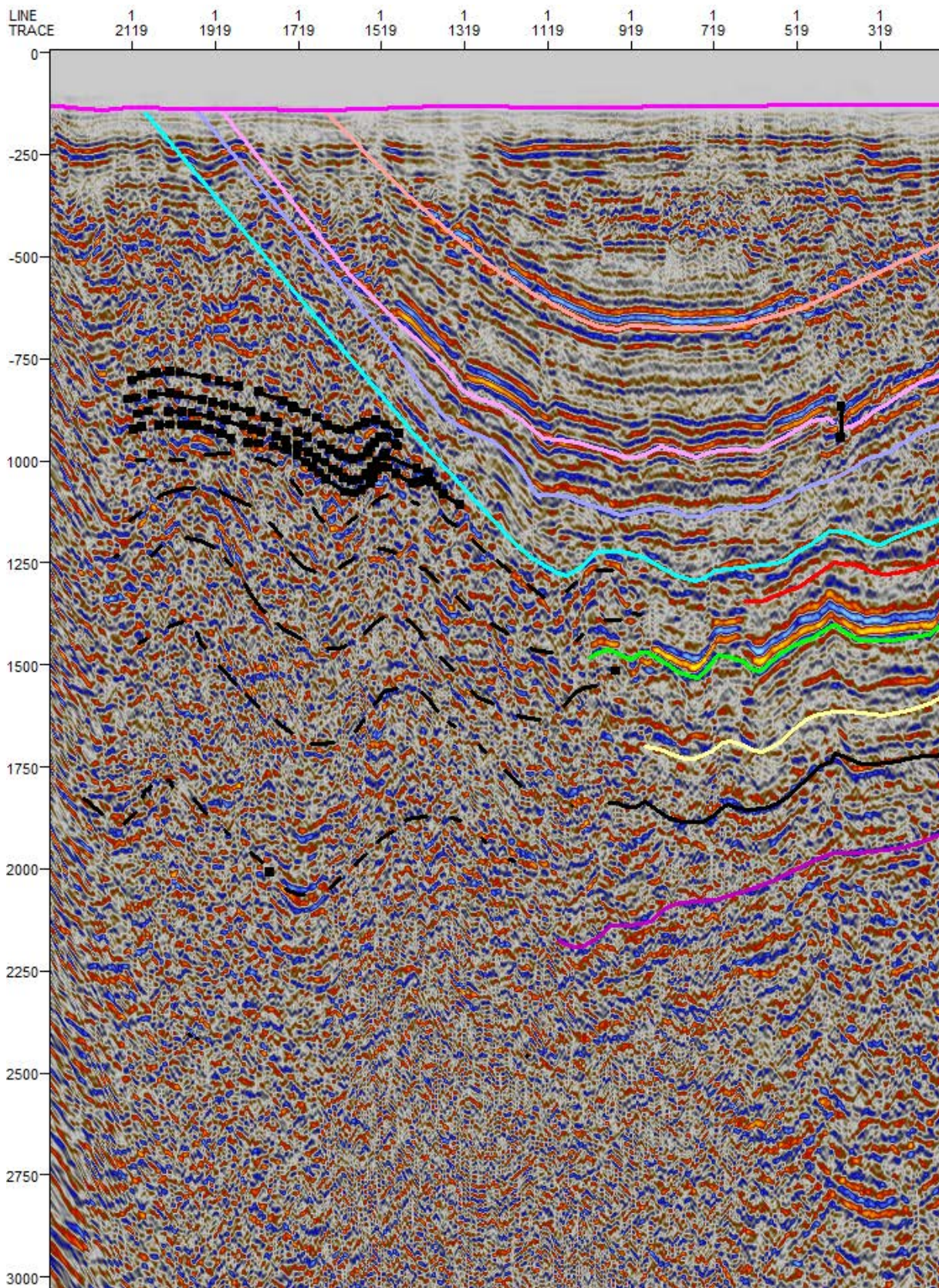
14-10



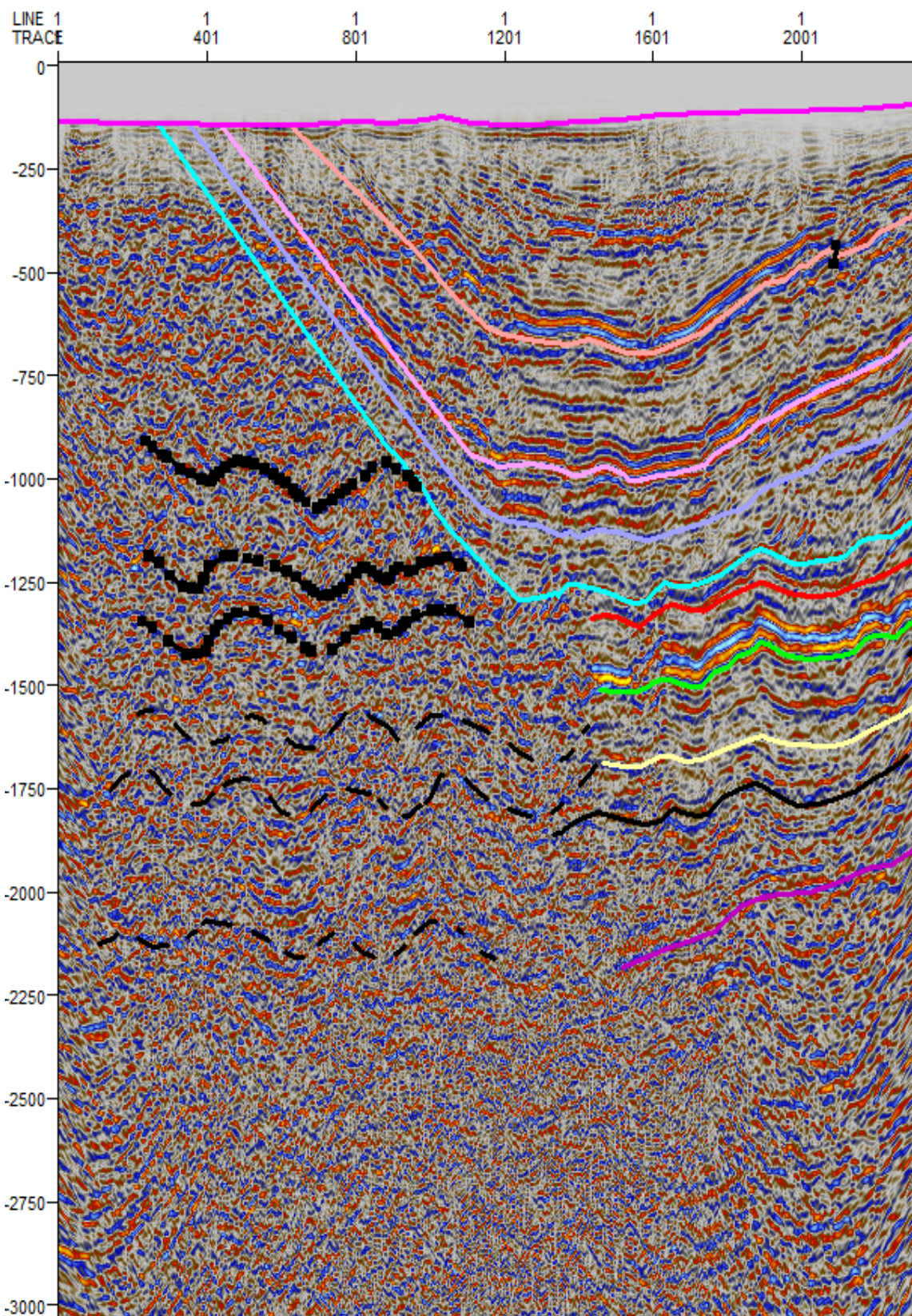
14-08



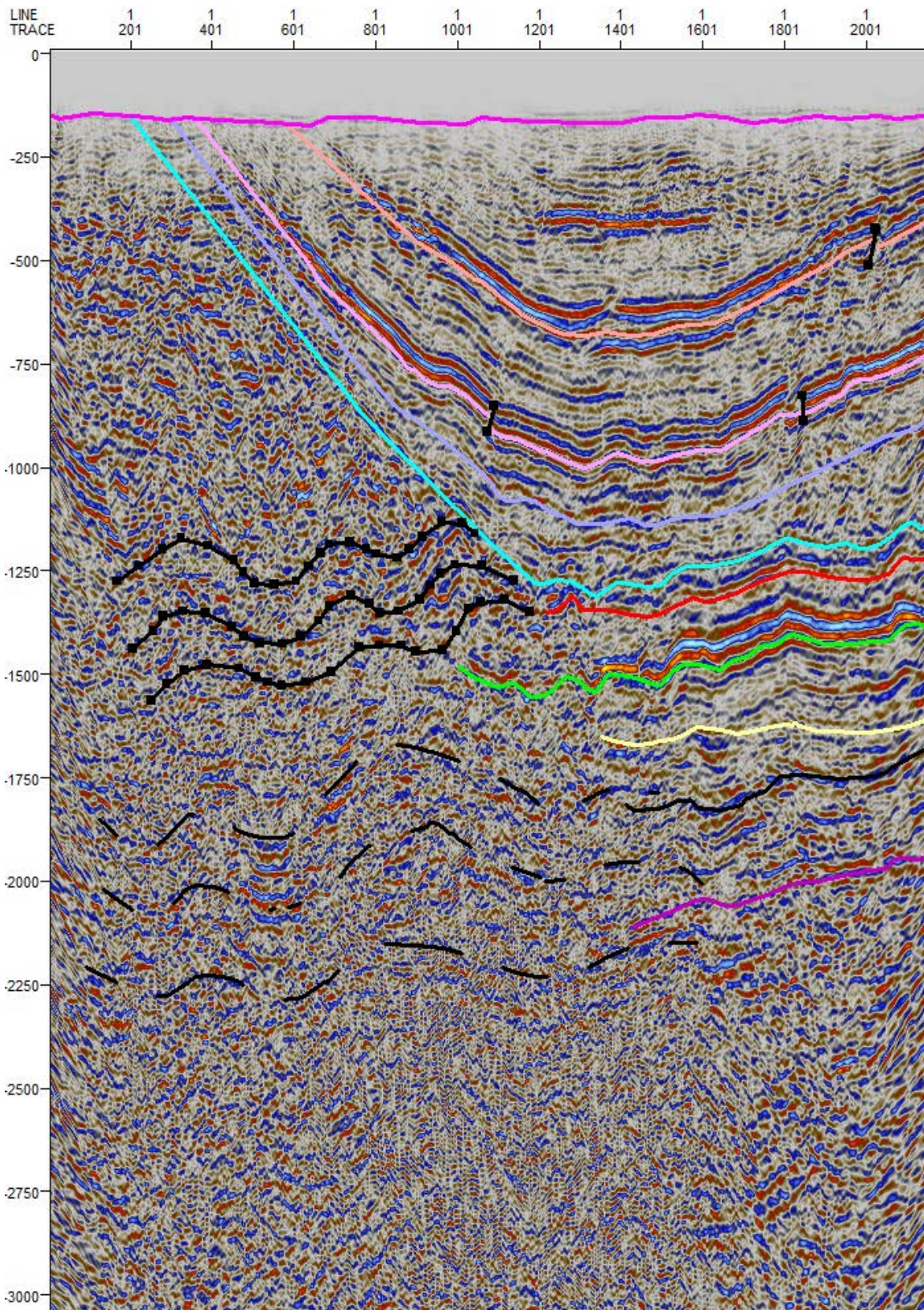
14-07



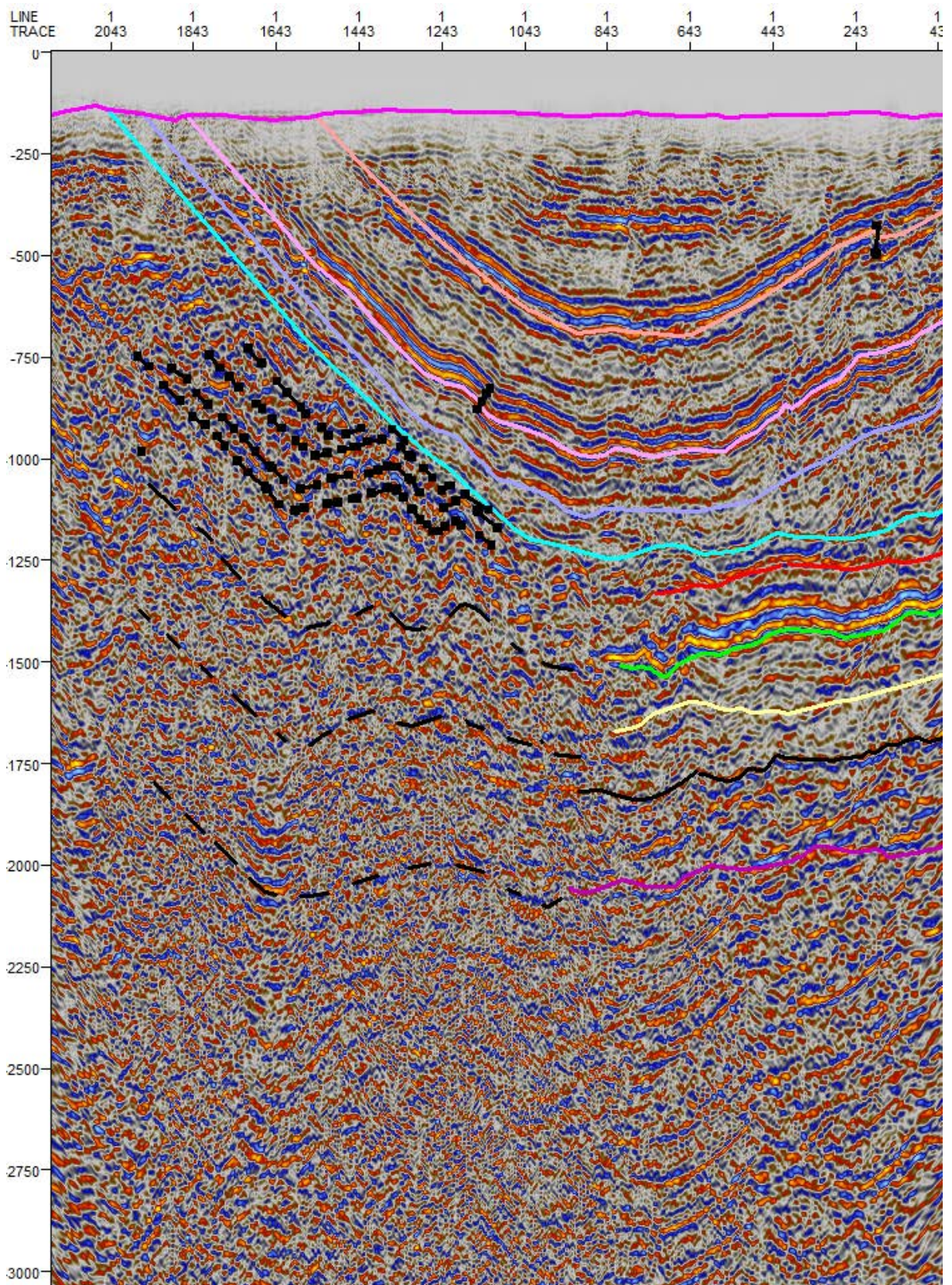
14-06



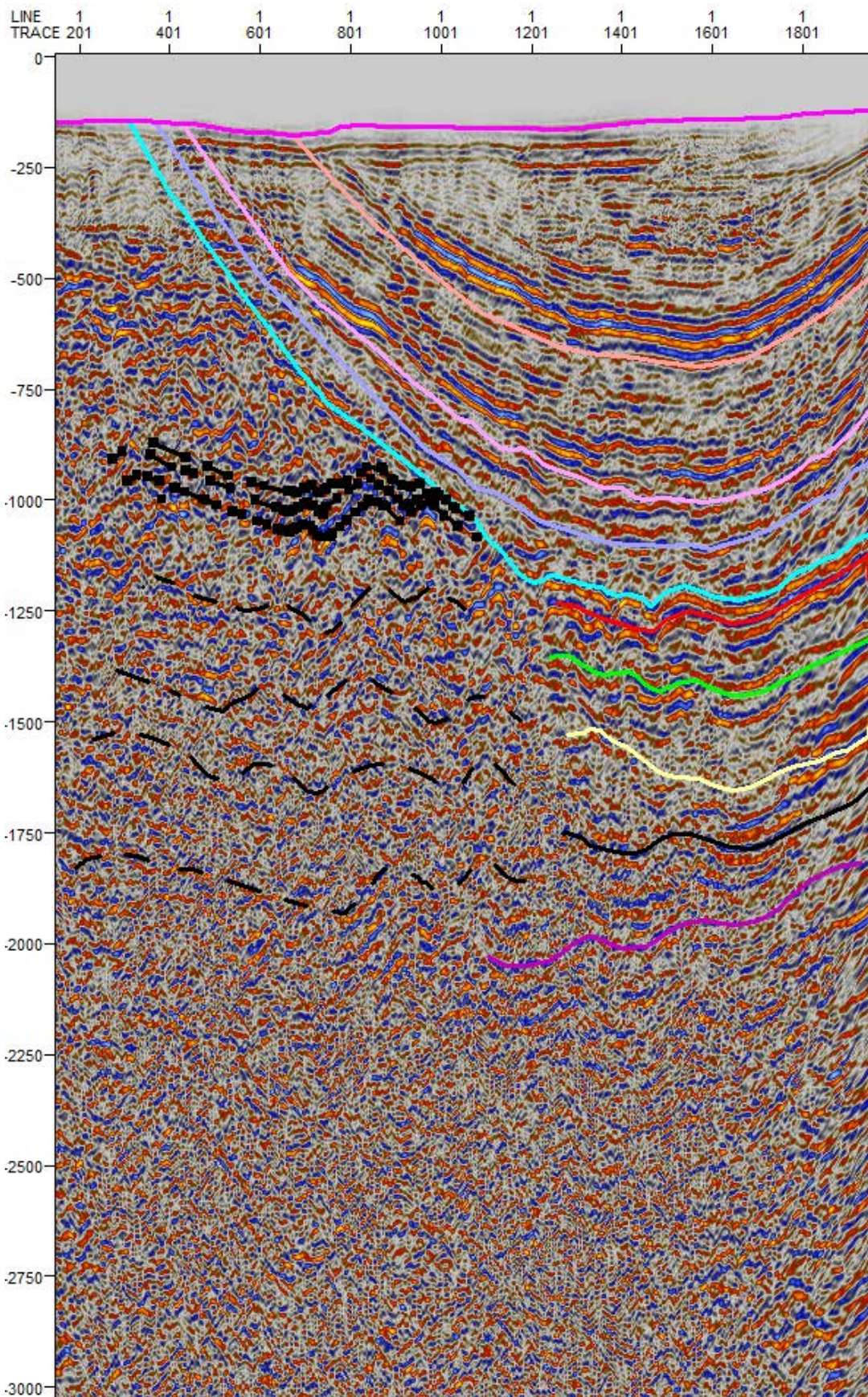
14-05



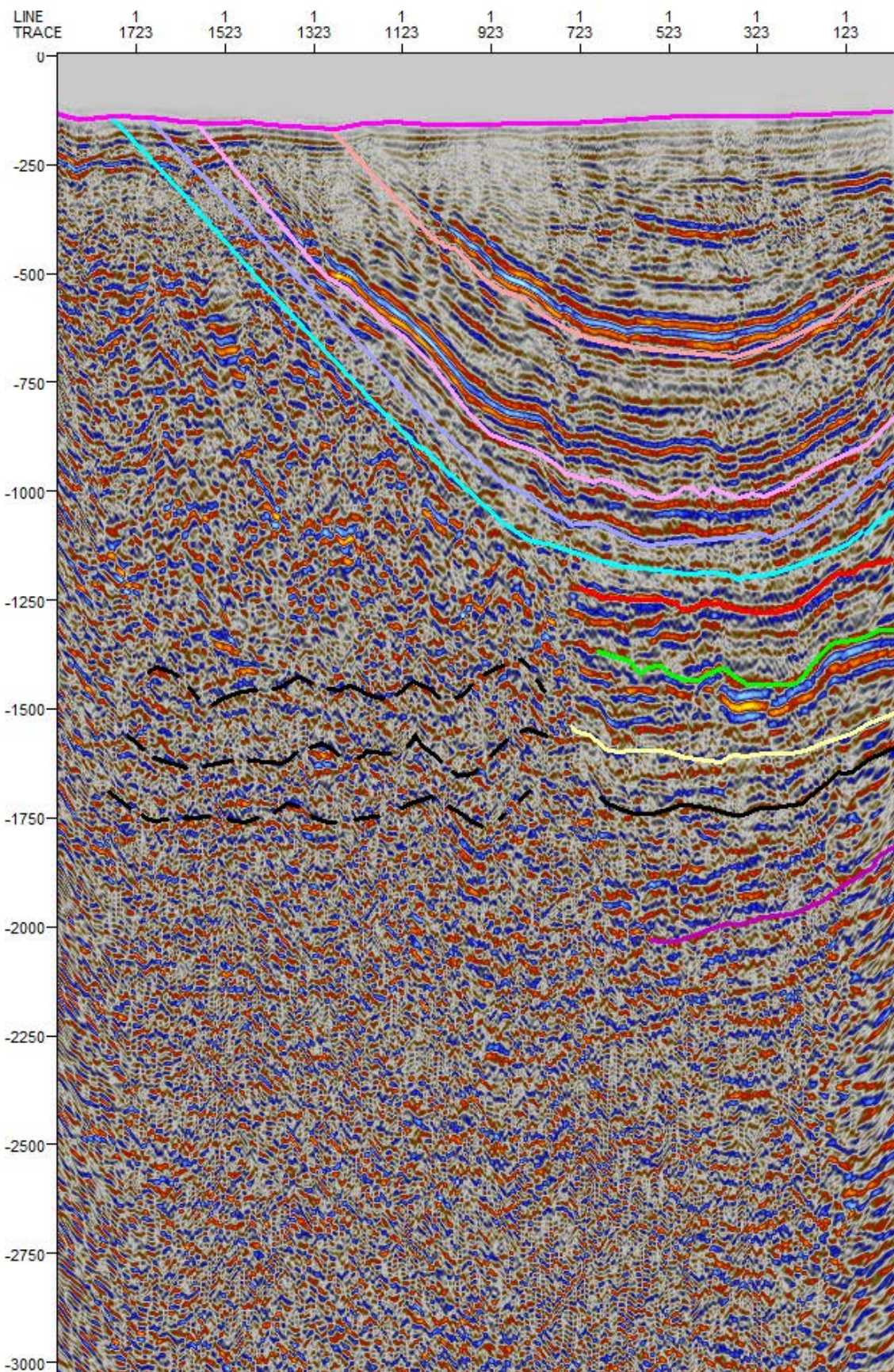
14-04



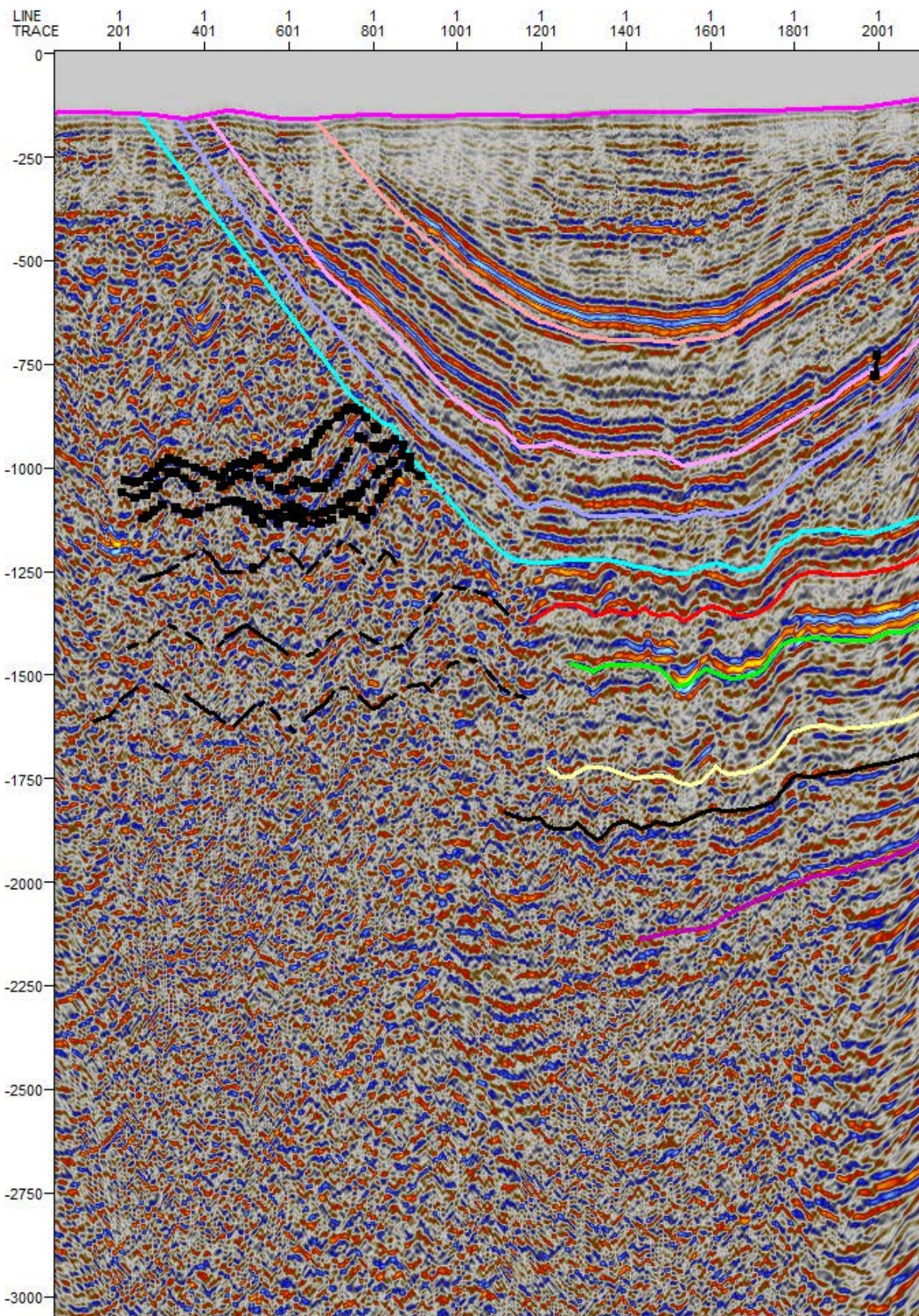
14-03



13-14



13-11



13-09